PSL★
UNIVERSITÉ PARIS

THÈSE DE DOCTORAT
DE L'UNIVERSITÉ PSL

Préparée à École normale supérieure - PSL

Méthode bootstrap en physique théorique
Bootstrap Method in Theoretical Physics

Soutenue par
Zechuan Zheng
Le 15/09/2023

École doctorale n°564
Physique en Île-de-France

Spécialité
Physique des hautes énergies - Théorie

Composition du jury :

Alice GUIONNET	*Président*
Directeur de recherche, École normale supérieure de Lyon	
Alexander ZHIBOEDOV	*Rapporteur*
Chercheur permanent senior, CERN-Organisation européenne pour la recherche nucléaire	
Agnese BISSI	*Rapporteur*
Associate professor, Uppsala University	
Alexander MIGDAL	*Examinateur*
Professeur, New York University	
Miguel PAULOS	*CoDirecteur de thèse*
Chargé de recherche, École Normale Supérieure	
Vladimir KAZAKOV	*Directeur de thèse*
Professeur, École Normale Supérieure	

ENS
ÉCOLE NORMALE SUPÉRIEURE

PSL★
RESEARCH UNIVERSITY PARIS

Acknowledgement

Acknowledgement

I would like to express my deepest gratitude and appreciation to my supervisor, Vladimir Kazakov, for his invaluable guidance, unwavering support, and encouragement throughout the course of my PhD journey. His knowledge and experience in the field, combined with his patience, have been instrumental in the completion of this work. I am privileged to have been one of his students, and his mentorship has not only shaped this thesis but has also significantly impacted my personal and professional development. I have learned so much from his wisdom, and his intellectual rigor has pushed me to broaden my thinking and approach to research.

In the same vein, I would also like to express my sincere thanks to my co-supervisor, Miguel Paulos. His insightful comments, constructive criticisms, and detailed feedback have greatly enhanced the quality of this thesis. His unwavering faith in my abilities even during tough times has been a constant source of motivation. His enthusiasm for research and dedication to teaching have left an indelible impression on me.

In addition, I would like to express my profound gratitude to Edouard Brézin, Davide Gaiotto, Slava Rychkov, Pedro Vieira and Xi Yin. I am deeply appreciative of the essential role they have played in the progression of my academic journey, particularly their assistance and guidance during various application processes. Their faith in my potential and their willingness to support my professional endeavors have been a significant contribution to the progression of my academic journey.

I am sincerely thankful to Agnese Bissi, Alice Guionnet, Alexander Migdal, and Alexander Zhiboedov for accepting the responsibility of being part of the jury for my thesis defense. Their presence and valuable insights added significant depth to my work and their constructive feedback has contributed to the quality of this thesis.

I would also like to express my sincere gratitude to my esteemed colleagues in the global physics research community. Your guidance, collaborations, and shared intellectual curiosity have significantly enriched my research journey. Specifically, I would like to acknowledge António Antunes, Camille Aron, Avik Banerjee, Benjamin Basso, Lior Benizri, Antoine Bourget, Xiangyu Cao, Xiaowen Chen, Zhongwu Chen, Sihao Cheng, Minjae Cho, Zhihao Duan, David Jaramillo Duque, Manuel Díaz, Nikolay Ebel, Rajeev Erramilli, Farah El Fakih, Lucija Farkaš, Barak Gabai, Kausik Ghosh, Gabriel Gouraud, Yinchen He, Yifei He, Aditya Hebbar, Ludwig Hruza, Hongye Hu, Yangrui Hu, Amir-Kian Kashani-Poor, Apratim Kaviraj, Arthur Klemenchuk Sueiro, Ivan Kostov, Werner Krauth, Augustin Lafay, Ho Tat Lam, Bingxin Lao, Nat Levine, Songyuan Li, Wenliang Li, Yuezhou Li, Zhijin Li, Henry Lin, Ying-Hsuan Lin, Ruochen Ma, Marina Krstic Marinkovic, Dalimil Mazac, Maria Neuzil, Colin Oscar Nancarrow, Enrico Olivucci, Vassilis Papadopoulos, Sabrina Pasterski, Joao Penedones, Eric Perlmutter, Giuseppe

Policastro, Jiaxin Qiao, Mingfeng Qiu, Marten Reehorst, Balt van Rees, Victor Rodriguez, Junchen Rong, Joshua Sandor, Didina Serban, Benoit Sirois, Evgeny Sobko, Xueyang Song, Ning Su, Tin Sulejmanpasic, Zimo Sun, Petar Tadić, Emilio Trevisani, Jan Troost, Alexander Tumanov, Alessandro Vichi, Xing Wang, Chong Wang, Zixia Wei, Yuan Xin, Hari Yadalam, Kang Yang, Weicheng Ye, Zahra Zahraee, Bernardo Zan, Yi Zhang, Xiang Zhao, Deliang Zhong, and Liujun Zou. Your contributions to the academic community, intellectual discussions, and encouragement have played a crucial role in my growth as a researcher. I am truly grateful for your support and am excited about our continued collaboration in furthering the frontiers of physics.

To my friends at École Normale Supérieure, I owe a deep sense of gratitude. Your support, companionship, and the shared experiences have been pivotal in this journey. Specifically, I would like to acknowledge Yawen Chen, Qiyuan Chen, Jinhui Cheng, Senwen Deng, Wenshuo Fan, Jiahui Feng, Hao Fu, Tiancheng He, Yue Hong, Chuhao Huang, Mengzi Huang, Yulai Huang, Gang Lin, Haohao Liu, Youmin Liu, Daheng Min, Junhui Qin, Liang Qin, Yue Qi, Yi Shan, Qing Wang, Songbo Wang, Yitong Wang, Keyu Wang, Zhenhong Wang, Ziao Wang, Yijun Wan, Shiyi Wei, Baojun Wu, Yuxiao Xie, Minchen Xia, Ziyu You, Yilin Ye, Yiwei Zhang, Chao Zhang, Yiru Zheng, Qimeng Zhu and Zhaoxuan Zhu. Despite my attempt to be comprehensive, I apologize if anyone has been inadvertently left out. Know that your influence and contribution to my life and work at ENS are deeply appreciated.

Lastly, and most importantly, I would like to express my deepest gratitude to my parents, who are thousands of miles away in China. Despite the distance and the challenges posed by the COVID-19 pandemic which has kept us apart, their unwavering support, encouragement, and love have been my source of strength and resilience. The pandemic has reminded us of the fragility of life and the importance of family. Even though I have been unable to return home and see them, their constant care, understanding, and faith in my abilities have been a comforting presence throughout this journey. They have been my rock, providing me with the courage and determination to overcome the obstacles I have faced.

Résumé

Dans le domaine de la physique contemporaine, la méthode bootstrap est généralement associée à une approche basée sur l'optimisation pour résoudre des problèmes. Cette méthode exploite notre compréhension d'un problème physique spécifique, utilisée comme les contraintes pour le problème d'optimisation, afin de délimiter la région autorisée de notre théorie physique. Notamment, cette méthode donne souvent non seulement des limites numériques précises pour les quantités physiques mais offre également des perspectives théoriques sur la nature du problème en question. La méthode numérique bootstrap moderne a connu son plus grand succès dans les domaines de la théorie des champs conformes (via le bootstrap conforme) et de l'amplitude de dispersion (à travers le bootstrap de la matrice S). Cette thèse présente l'application de la méthode bootstrap aux modèles matriciels (matrices aléatoires), à la théorie de Yang-Mills et à la théorie des champs conformes. Nous commencerons par un examen des éléments fondamentaux de ces théories. Ensuite, nous nous plongerons dans les études bootstrap de ces modèles.

Nous proposons une méthode bootstrap de relaxation améliorée pour la résolution numérique de modèles multi-matriciels à la limite de N grand. Cette méthode fournit des inégalités rigoureuses sur les moments de trace simple des matrices jusqu'à un ordre "coupure" spécifié des moments. Nous avons une preuve rigoureuse de l'applicabilité de cette méthode dans le cas du modèle à une matrice. Nous démontrons l'efficacité numérique de notre méthode en résolvant le modèle à deux matrices analytiquement "insolvable" avec une interaction $\mathrm{tr}[A, B]^2$ et des potentiels quartiques. Nous étendons ensuite notre étude à la théorie de Yang-Mills sur réseau aux dimensions 2, 3 et 4 en utilisant la méthode numérique bootstrap. Notre approche combine des équations de boucle, avec une coupure sur la longueur maximale des boucles, et des conditions de positivité sur certaines matrices de moyennes de boucles de Wilson. Nos résultats suggèrent que cette approche bootstrap peut offrir une alternative tangible à l'approche de Monte Carlo, jusqu'à présent incontestée.

Nous explorons le problème de la mise en limite des corrélateurs CFT dans la section euclidienne. En reformulant la question comme un problème d'optimisation, nous construisons numériquement des fonctionnelles qui déterminent des limites supérieures et inférieures sur les corrélateurs dans plusieurs circonstances. Notre analyse révèle que le corrélateur d'Ising 3d prend les valeurs minimales possibles autorisées dans la section euclidienne. Nous découvrons également un intrigant CFT 3d qui sature les limites de l'écart, de la maximisation OPE et des valeurs des corrélateurs.

Abstract

In the realm of contemporary physics, the bootstrap method is typically associated with an optimization-based approach to problem-solving. This method leverages our understanding of a specific physical problem, which is used as the constraints for the optimization problem, to carve out the allowed region of our physical theory. Notably, this method often yields not only precise numerical bounds for physical quantities but also offers theoretical insights into the nature of the problem at hand. The modern numerical bootstrap method has seen its greatest success in the fields of conformal field theory (via the conformal bootstrap) and Scattering amplitude (through the S-matrix bootstrap). This dissertation presents the application of the bootstrap method to matrix models (random matrices), Yang-Mills theory, and conformal field theory. We will commence with a review of the fundamental elements of these theories. Following this, we will delve into the bootstrap studies of these models.

We propose an enhanced relaxation bootstrap method for the numerical resolution of multi-matrix models in the large N limit. This method provides rigorous inequalities on the single trace moments of the matrices up to a specified "cutoff" order of the moments. We have rigorous proof of the applicability of this method in the case of the one-matrix model. We demonstrate the numerical efficiency of our method by solving the analytically "unsolvable" two-matrix model with tr[A, B]² interaction and quartic potentials. We further extend our study to the lattice Yang-Mills theory at dimensions 2, 3, and 4 using the numerical bootstrap method. Our approach combines loop equations, with a cutoff on the maximal length of loops, and positivity conditions on certain matrices of Wilson loop averages. Our results suggest that this bootstrap approach can provide a tangible alternative to the, so far uncontested, Monte Carlo approach.

We explore the problem of bounding CFT correlators in the Euclidean section. By reformulating the question as an optimization problem, we construct functionals numerically which determine upper and lower bounds on correlators under several circumstances. Our analysis reveals that the 3d Ising correlator takes the minimal possible allowed values on the Euclidean section. We also uncover an intriguing 3d CFT that saturates gap, OPE maximization, and correlator value bounds.

Contents

Contents

Chapter 1

Introduction

1 Background

In the realm of modern quantum field theory (QFT), the importance of symmetry cannot be overstated. Our progressive understanding of QFT has invariably been coupled with insights gleaned from symmetries, whether assumed (like Poincaré symmetry and the constraining power of anomalies), or spontaneously broken.
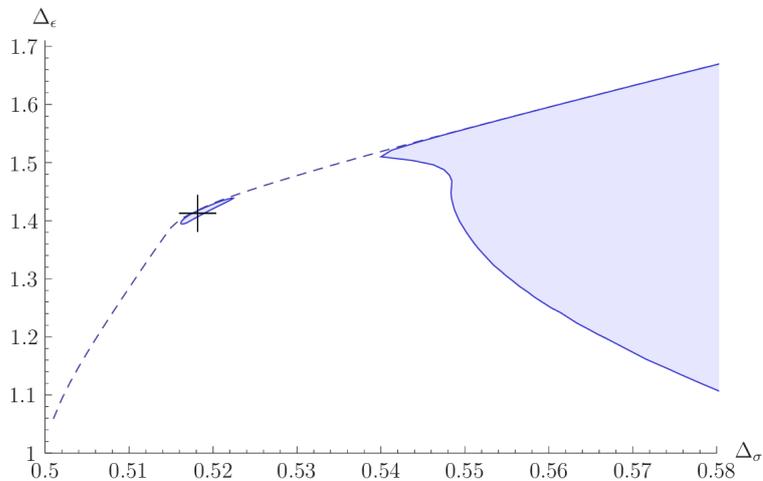

Figure 1.1: The depicted region corresponds to the parameter space allowed by the $3d$ Ising model. It is defined by the constraints from three distinct four-point correlators, under the assumption that there is only a single relevant $\mathbb{Z}_2$-odd operator present. The plot has been adapted from the work by Kos et al. [Kos, 2014].

The bootstrap philosophy in physics embodies a methodology that aims to exploit the potential power of symmetry to its utmost limit. The approach seeks to solve problems primarily using the assumption of symmetry, along with other generic constraints such as unitarity and locality. This method eschews reliance on the microscopic details of the problem at hand. Although this perspective was initially proposed in the 1960s within the context of the S-matrix [Chew, 1961], it was largely overshadowed due to the subsequent successes in Quantum Chro-

modynamics (QCD).

The first significant outcome following the bootstrap philosophy did not materialize until the 1980s, when Belavin, Polyakov, and Zamolodchikov (BPZ) used the "conformal bootstrap" to solve minimal models with $c < 1$ [Belavin, 1984]. Their solution relied heavily on the infinite symmetries present in $2d$ conformal field theory, a feature absent in other dimensions.

The 21st century has seen an unprecedented surge in the development of mathematical optimization theory, largely spurred by the rapid expansion of the machine learning industry, which had a significant breakthrough in 2006 [Hinton, 2006]. Around the same period, a seminal work emerged, which used optimization theory to bound the dynamics of $4d$ conformal field theory (CFT) [Rattazzi, 2008]. This method, known as the "bootstrap method," sparked renewed interest in the application of optimization theory to tackle problems in theoretical physics [Ferrara, 1973; Polyakov, 1974]. Despite its numerical nature, the bootstrap method has proven successful in generating rigorous bounds for dynamical quantities. The approach has seen particularly noteworthy success within the context of CFT [1], demonstrating that very accurate numerical results can be obtained solely from assumptions of CFT axioms, unitarity, and global symmetries.

Conformal invariance and the operator product expansion led to the so-called bootstrap equation:

$$\sum_{\Delta} a_\Delta^2 F_\Delta(z, \bar{z}) = 0, \quad (z, \bar{z}) \in (\mathbb{C} \backslash (-\infty, 0) \cup (1, \infty))^2 \tag{1.1}$$

Here, conformal invariance helps us determine $F_\Delta[z, \bar{z}]$ (either analytically or numerically), and unitarity gives us the reality and potential Δ region in Eq. (5.4).

The aforementioned situation embodies an infinite generalization of linear programming. From this, we can obtain bounds for intriguing dynamical quantities such as the dimension gap above the identity operator. For instance, consider a functional Λ acting on F_Δ, where $\Lambda(F_\Delta) \geq 0$ for $\Delta \geq \Delta_{\text{gap}}$ and $\Lambda(F_0) > 0$. The existence of such a functional, coupled with Eq. (5.4), implies that there must be at least one operator in the region $0 < \Delta < \Delta_{\text{gap}}$. By searching for Λ across all possible Δ_{gap}, we can obtain an optimal bound for the dimension gap.

Numerous subsequent studies utilizing the bootstrap approach have yielded compelling results, showcasing the effectiveness of this methodology. One of the most significant achievements in this vein has been the determination of the operator dimensions in the 3D Critical Ising model with unprecedented precision [El-Showk, 2012; El-Showk, 2014; Kos, 2014]. As depicted in Fig. 5.1, the $3d$ critical Ising model, as determined by the conformal bootstrap, resides within a minuscule island in the parameter space.

The successful execution of the bootstrap method, showcased in Figure 5.2, is a testament to the essential interplay between physics, mathematics, and computer science:

- On the physics front, a comprehensive understanding of the underlying principles is key for devising effective constraints. Notable instances of this include the application of the conformal block expansion[Dolan, 2004] of the four-point correlator in conformal field

---

[1]Comprehensive reviews of these advancements can be found in [Poland, 2019; Bissi, 2022]. See also [Poland, 2022; Hartman, 2022] for more recent updates.
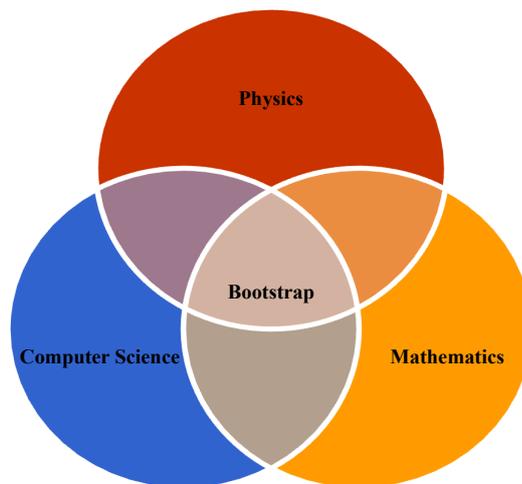
Figure 1.2: The bootstrap method.

theory, and the usage of Makeenko-Migdal loop equations[Makeenko, 1979] in gauge theory as non-trivial constraints within bootstrap calculations.

- Mathematics lends the necessary toolset to interpret and validate the constraints associated with the physical model. For instance, solid mathematical analysis is required to ascertain the numerical veracity of the conformal bootstrap [Pappadopulo, 2012].

- In the sphere of computer science, robust techniques are vital for the practical implementation of the bootstrap method. Proficiency in programming is necessitated for the development of specialized optimization solvers, such as *SDPB* [Simmons-Duffin, 2015; Reehorst, 2021; Liu, 2023], *JuliBoots* [Paulos, 2014], *PyCFTBoot*[Behan, 2017] and *Fun-Boot* [Ghosh, 2023b], which are designed specifically to tackle bootstrap problems. It is also noteworthy that substantial numerical outcomes from the bootstrap method are typically generated using supercomputing resources [Chester, 2020].

Despite the impressive advancements in conformal bootstrap, the application of the bootstrap method to systems devoid of the benefit of conformal symmetry remains a challenging problem. A potential area of exploration is the S-matrix bootstrap [Homrich, 2019; Kruczenski, 2022; Paulos, 2017a; Paulos, 2017b; Paulos, 2019], where the author embarked on some preliminary investigation into this area during his master's studies [Paulos, 2020c]. However, the progress in the field of S-matrix bootstrap has largely been confined to the establishment of broad bounds on the parameters of the theory. As of now, it is not feasible to effectively incorporate information or constraints derived from the ultraviolet (UV) theory into the S-matrix bootstrap framework.

In light of recent advancements [Anderson, 2017; Lin, 2020; Han, 2020b], a novel bootstrap approach has emerged for investigating matrix models. This method is characterized by not only adhering to general assumptions such as unitarity and global symmetries but also by incorporating relations among physical observables imposed by the equations of motion.[2] Its wide

---

[2]For a detailed study on the mathematical convergences of this method, readers are directed to [Guionnet,

applicability has been quickly demonstrated in lattice field theories [Anderson, 2017; Anderson, 2018; Cho, 2022; Kazakov, 2023], matrix models [Han, 2020b; Jevicki, 1983; Jevicki, 1984; Koch, 2022; Lin, 2020; Lin, 2023; Mathaba, 2023], quantum systems[Aikawa, 2022a; Aikawa, 2022b; Bai, 2022; Berenstein, 2021; Berenstein, 2022b; Berenstein, 2023b; Berenstein, 2022a; Berenstein, 2023a; Bhattacharya, 2021; Blacker, 2022; Ding, 2023; Du, 2022; Eisert, 2023; Fawzi, 2023; Han, 2020a; Hastings, 2022b; Hastings, 2022a; Hessam, 2022; Hu, 2022; Khan, 2022; Kull, 2022; Li, 2022; Li, 2023b; Morita, 2023; Nakayama, 2022; Nancarrow, 2022; Tavakoli, 2023; Tchoumakov, 2021; Fan, 2023b; Fan, 2023a; John, 2023; Li, 2023a; Zeng, 2023], and even classical dynamical systems [Goluskin, 2018; Goluskin, 2020; Tobasco, 2018; Cho, 2023a].

The initial part of this thesis discusses our application of this novel bootstrap method to matrix models [Kazakov, 2022] and large N lattice gauge theories [Kazakov, 2023]. In our first publication, we rigorously justified the bootstrap approach within the context of a one-matrix model and introduce a relaxation on the quadratic terms in the loop equations, thereby attaining unprecedented precision in an unsolvable two-matrix model. In our second publication, we further expand the application of this bootstrap method (along with the relevant relaxation) to the large N lattice gauge theory. Remarkably, this approach yielded excellent results in the estimation (or more precisely, the bounding) of the plaquette average of the lattice gauge theory.

The latter portion of this thesis delves into the author's collaborative work with Miguel Paulos, focusing on bounding correlation functions via the conformal bootstrap[Paulos, 2022]. Given the unique exponential behavior of the target function in this specific bootstrap problem, the traditional polynomial approximation used in *SDPB*[Simmons-Duffin, 2015] is unsuitable. We demonstrated that the solution for maximizing the gap usually saturates the minimization of the correlator. Meanwhile, the maximization of the correlator, subject to additional constraints, effectively reproduces the Mean-field theory.

In the final chapter of this thesis, we consolidate our findings, offering a concise summary and implications of our work. Moreover, we suggest a variety of promising directions for future research and exploration.

2   Main results

2.1   Matrix bootstrap

A major portion of my research agenda revolves around the matrix bootstrap [Kazakov, 2022]. This endeavor includes two crucial components: a solid justification of the bootstrap method for the one-matrix model using the results of the Hamburger moment problem, and a noteworthy advancement of this method for bootstrapping large N matrix models via convex relaxation.

More specifically, the justification process, capitalizing on the results of the Hamburger moment problem, rigorously affirms that the positivity of the correlation matrix implies the positivity of the resolvent, and vice versa:

$$\textit{Positivity of correlation matrix} \Leftrightarrow \textit{Positivity of Resolvent} \tag{1.2}$$
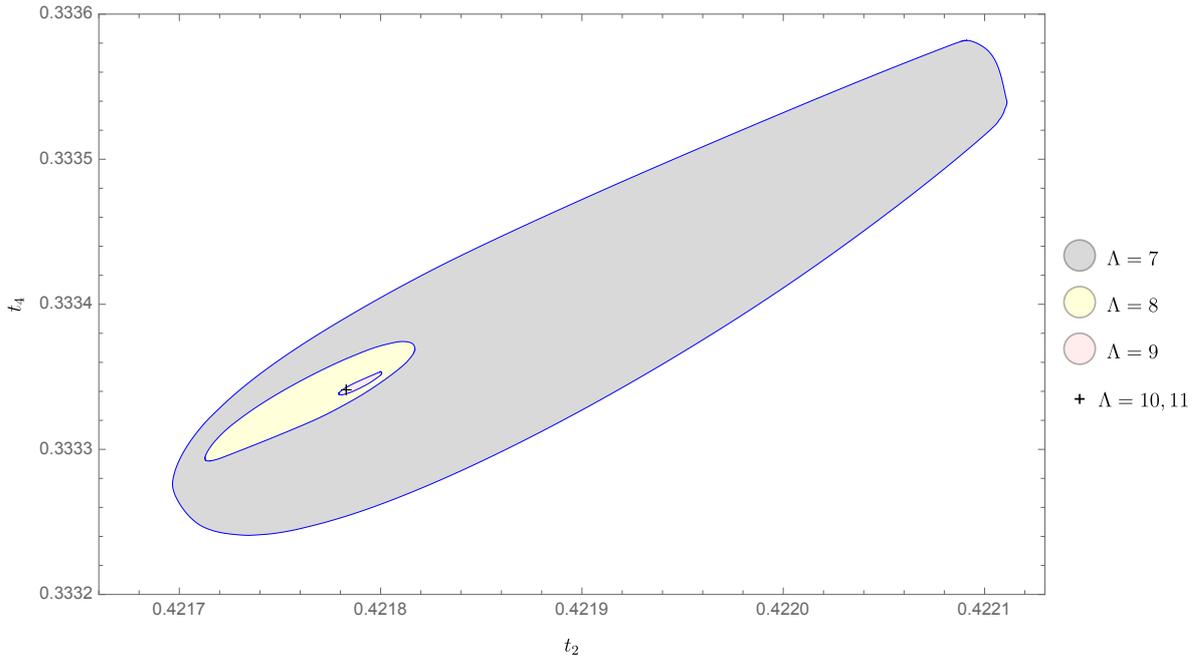
2022; Kazakov, 2022; Cho, 2023b].

Figure 1.3: The allowed region of $t_2 - t_4$ of model (5.7) with parameter $g = 1, h = 1$ for the cutoff $\Lambda = 7, 8, 9, 10, 11$. We recall the definition of Λ: the longest operators in the correlation matrix and in the loop equations have the length 2Λ.

This equivalence was employed in conjunction with the loop equations to analytically and exhaustively categorize the solutions of the large N matrix model specified below:

$$Z_N = \int d^{N^2} M \, e^{-N \text{tr} V(M)}, \quad V(x) = \frac{1}{2}\mu x^2 + \frac{1}{4}g x^4 \tag{1.3}$$

The latter half of the paper focuses on the resolution of the subsequent model:

$$Z = \lim_{N \to \infty} \int d^{N^2} A, d^{N^2} B, e^{-N\text{tr}\left(-h[A,B]^2/2 + A^2/2 + gA^4/4 + B^2/2 + gB^4/4\right)} \tag{1.4}$$

Given our existing methodologies, this model lacks an analytical solution. To bootstrap this model, we employed a relaxation method as follows:

$$Q = xx^{\text{T}} \Rightarrow \mathcal{R} = \begin{pmatrix} 1 & x^{\text{T}} \\ x & Q \end{pmatrix} \succeq 0. \tag{1.5}$$

In the above, Q represents the quadratic terms in the loop equations, derived from the large N factorization. The vector x refers to the column vector of single trace variables. The results obtained from the relaxed bootstrap problem considerably outshine the precision and efficiency of the conventional numerical method for large N matrix models, the Monte Carlo (MC) method [Jha, 2022]. For $g = h = 1$, we achieved a 6-digit precision result:

$$\begin{cases} 0.421783612 \leq t_2 \leq 0.421784687 \\ 0.333341358 \leq t_4 \leq 0.333342131 \end{cases} \tag{1.6}$$

5

The illustration of the contraction of the permissible domain as a function of the corresponding bootstrap cutoff is visually demonstrated in Figure 5.3.

2.2 Bootstrapping the Lattice Yang-Mills Theory

Another project [Kazakov, 2023] involved using this method to bootstrap the single plaquette Wilson loop average in large N lattice Yang-Mills theory.[3] The results are encouraging when compared with the MC method, especially considering that the MC method for lattice QCD has undergone intense investigation over several decades.
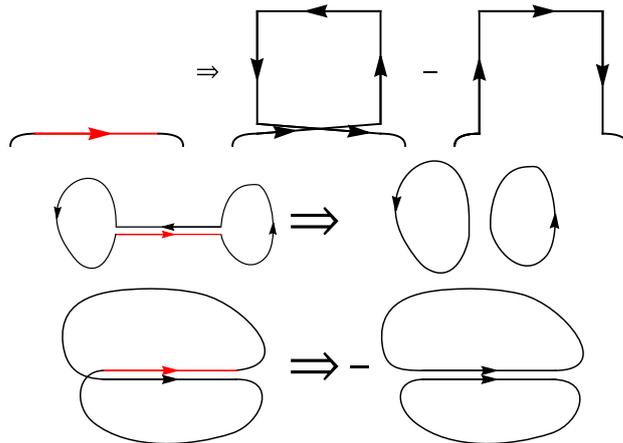

Figure 1.4: Schematic representation of LEs: The first line shows the variation of a link of Wilson loop in the LHS of Eq.(5.10). The 2nd and 3rd lines show the splitting of the contour along the varied line into two sub-contours, for two different orientations of coinciding links in the RHS of Eq.(5.10).

We analyze the Wilson-action-based Large Gauge Theory (LGT) [Wilson, 1974] represented by $S = -\frac{N_c}{\lambda} \sum_P \operatorname{Re} \operatorname{tr} U_P$, with U_P denoting the product of four unitary link variables around the plaquette P. Considering the 't Hooft limit ($N_c \to \infty$), the primary focus lies on the Wilson loop Averages (WAs): $W[C] = \langle \frac{\operatorname{tr}}{N_c} \prod_{l \in C} U_l \rangle$, where the matrix product traverses link variables within the lattice loop C. WAs adhere to Makeenko-Migdal Loop Equations (LEs)[Makeenko, 1979], or Schwinger-Dyson equations, which encapsulate the measure invariance concerning group shifts, such that $U_l \to U_l(1 + i\epsilon)$.[4] The LEs are represented schematically:

$$\sum_{\nu \perp \mu} \left(W[C_{l_\mu} \cdot \overrightarrow{\delta C_{l_\mu}^\nu}] - W[C_{l_\mu} \cdot \overleftarrow{\delta C_{l_\mu}^\nu}] \right) = \lambda \sum_{\substack{l' \in C \\ l' \sim l}} \epsilon_{ll'} W[C_{ll'}] \, W[C_{l'l}] \tag{1.7}$$

with the LHS indicating the loop operator's action on the link l_μ, and the RHS signifying the contour splitting $C \to C_{ll'} \cdot C_{l'l}$, as shown in Figure 5.4.

---

[3]For other bootstrap studies of the gauge theory or QCD, the reader could refer to [Nakayama, 2015; Albert, 2022; Albert, 2023; Fernandez, 2023; Guerrieri, 2019; He, 2023; Caron-Huot, 2023b; Ma, 2023]. It is a widespread belief that large N Yang-Mills is equivalent to large N QCD because of the suppression of the fermionic component in the planar limit. However, recent evidence suggests that this assumption may be more nuanced [Cherman, 2023].

[4]The recent advancement involves utilizing loop equations to address issues in turbulence.[Migdal, 2023a; Migdal, 2023b].
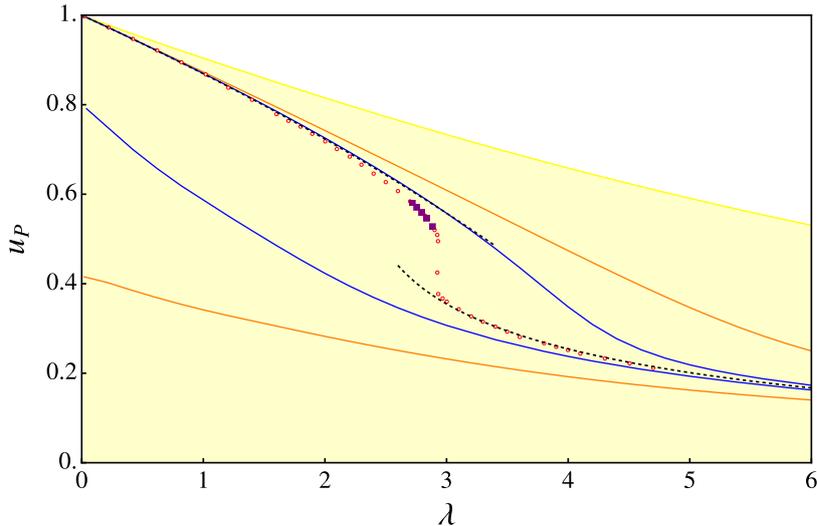
Figure 1.5: The figure presents our bootstrap results for upper and lower bounds on the plaquette average in $4D$ LGT. The domains for $L_{\max} = 8, 12, 16$ are respectively depicted in yellow, orange, and blue. Red circles represent the Monte Carlo (MC) data for $SU(10)$ LGT, with 5 purple squares indicating the results for $SU(12)$. The upper and lower dashed lines signify the 3-loop perturbation theory [Alles, 1998] and strong coupling expansion [Drouffe, 1983], respectively.

In most cases, the system of loop equations (5.10) yields more loop variables than independent loop equations. As suggested by Anderson et al. [Anderson, 2017], the positivity of $\langle \mathcal{O}^\dagger \mathcal{O} \rangle$ can be utilized to constrain the relevant dynamical quantities. We have significantly advanced this method by incorporating the following enhancements:

1. We take into account the Back-track loop equations, which will be discussed in more detail later.

2. The reflection positivity of the lattice system is considered.

3. Lattice symmetry is utilized to reduce the positivity conditions.

4. We employ the large N relaxation method proposed by the previous results [Kazakov, 2022].

These improvements have allowed us to derive an impressive numerical bound on the one plaquette average $u_P = \frac{1}{N_c} \langle \mathrm{tr} U_P \rangle$. As shown in Fig. 5.5, the bootstrap bounds for u_P for $L_{\max} = 8, 12, 16$ demonstrate rapid refinement as the cutoffs increase. The upper bound effectively encapsulates the physically significant Wilson loop phase and reliably replicates the 3-loop Perturbation Theory over an extensive coupling range, even exceeding the phase transition point. A comparison with Monte Carlo data, however, indicates room for improvement, especially in the (2.4, 2.8) interval where the data diverges from the Perturbation Theory. This interval, sourced from [Athenodorou, 2021], was used to compute masses and the string tension. A notable enhancement is anticipated upon reaching $L_{\max} = 20$ or 24, although this will necessitate substantial computational resources.

7

2.3   Conformal bootstrap

The author's scholarly pursuits during the PhD career also extend to the conformal bootstrap.

Recent studies have underscored the stringent constraints CFT data, defining local operator correlators, must adhere to [Poland, 2019]. These restrictions not only bound the CFT theory space but also intriguingly position salient theories at the edge of the allowable domain [El-Showk, 2012]. The conformal bootstrap community has so far investigated this space, mainly probing two directions of constraints on a specific set of four-point correlators. First, we maximize the gap in scaling dimensions of the first operator in the Operator Product Expansion (OPE) [Rattazzi, 2008]. Second, we bound the OPE coefficient of specific operators within these correlators [Rattazzi, 2011]. These bounds are established using numerical or analytical functionals, offering dual perspectives on the CFT landscape. This work proposed new directions by bounding CFT correlator values, a natural yet unexplored problem. This approach, similar to the method of minimizing or maximizing S-matrix values, is expected to reveal uncharted territories in the CFT space. The S-matrix problem, known to yield bounds saturable by exciting theories, is closely tied to (limits of) CFT correlators [Paulos, 2017b], suggesting equal potential for the corresponding CFT problem.
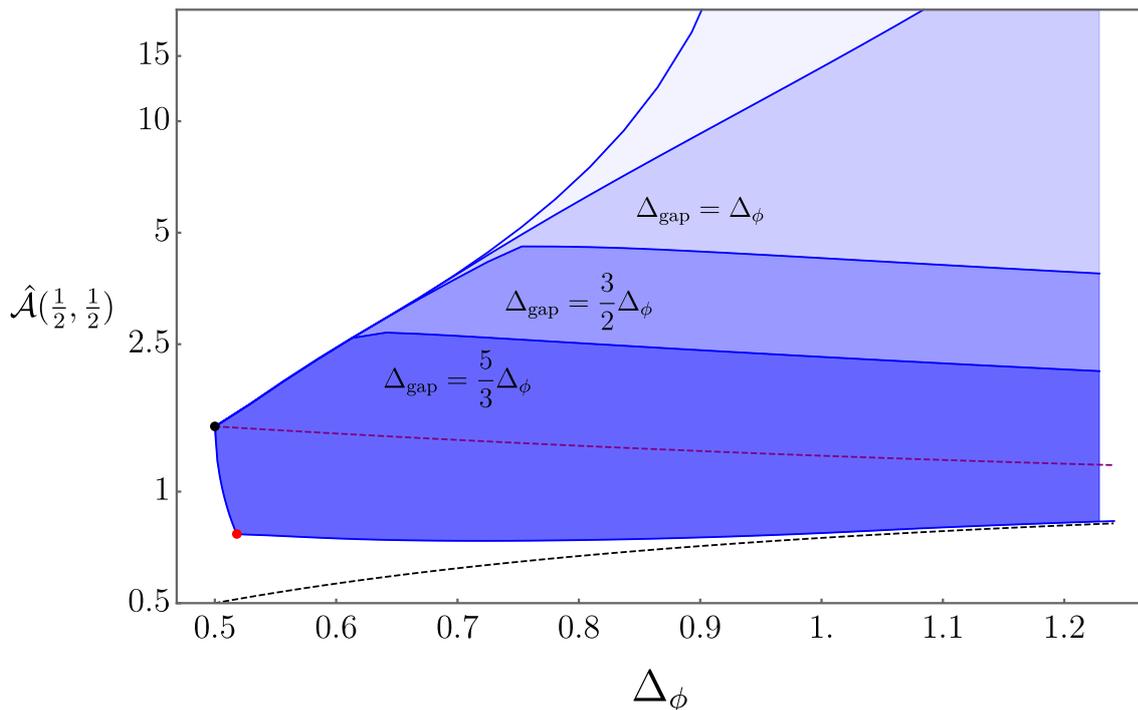
Figure 1.6: Bounds on 3d CFT correlator values, with $\hat{\mathcal{A}}(z, \bar{z}) = (z\bar{z})^{\Delta_\phi} \mathcal{G}(z, \bar{z}) - 1$. The shaded region represents the values such a correlator may take at the crossing symmetric point $z = \bar{z} = \frac{1}{2}$. The dashed lines inside the allowed region correspond to maximal allowed values assuming a gap. The upper bound goes to ∞ close to $\Delta_\phi = 1$. The dashed line outside the allowed region is the 1d generalized free fermion correlator, which provides a (suboptimal) lower bound. The dashed line inside the allowed region is the generalized free boson correlator, which provides an upper bound for $\Delta_{\text{gap}} = 2\Delta_\phi$. The black and red dots are the free theory and 3d Ising values respectively.

Our numerical findings, captured in Figures 5.6, depict the four-point correlator's allowed range at the crossing symmetric point $z = \bar{z} = \frac{1}{2}$ as a function of Δ_ϕ, and bounds along $z = \bar{z}$ for varied Δ_ϕ values, respectively.

Figure 5.6 reveals an upper correlator bound for some Δ_ϕ range, irrespective of spectrum assumptions. Imposing gaps in the scalar sector refines this bound, with the generalized free boson correlator closely saturating the upper bound for a $2\Delta_\phi$ gap, aligning with the exact bound in [Paulos, 2021][5]. For $\Delta_\phi = 1$, the bound diverges due to the unitary crossing equation solution devoid of identity for $\Delta_\phi \geq d - 2$. This leads to no bound without a spectrum gap assumption, requiring the gap $\Delta_g > \Delta_\phi/2$.

At $\Delta_\phi = 1/2$, the free theory point, the upper and lower bounds converge with the free theory value, as expected for the single CFT correlator with that dimension. The lower bound is also congruent with the exact bound determined by the 1d generalized free fermion solution, albeit stronger due to the 3d crossing equation constraints.

The lower bound displays a pronounced kink at $\Delta_\phi \sim 0.518149$, the spin field dimension in the 3d Ising CFT. This reinforces our argument linking correlator minimization with gap maximization, as the latter leads to the 3d Ising model at the precise Δ_ϕ value:

$$\Delta_g^{\min} \sim \Delta_{\text{gapmax}} \tag{1.8}$$

---

[5]The argument draws upon the analytic functional, a specific theoretical construct in conformal field theory with an extensive historical foundation [Afkhami-Jeddi, 2020; Carmi, 2020; Caron-Huot, 2021; Caron-Huot, 2023a; Dey, 2017; Dey, 2018; El-Showk, 2013; El-Showk, 2018; Ferrero, 2020; Ghosh, 2021; Ghosh, 2023a; Ghosh, 2023b; Giombi, 2020; Gopakumar, 2017a; Gopakumar, 2017b; Gopakumar, 2021; Hartman, 2019; Hartman, 2022; Kaviraj, 2020; Kaviraj, 2022; Li, 2023c; Mazac, 2017; Mazáč, 2019; Mazac, 2019a; Mazac, 2019b; Mazáč, 2021; Paulos, 2020b; Paulos, 2020a; Paulos, 2021; Qiao, 2017; Trinh, 2022].

Chapter 2

Matrix Bootstrap and Lattice Bootstrap

1 Matrix model and Lattice gauge theory

Matrix models, primarily renowned for their role in the study of quantum gravity and string theory, serve as a powerful tool for the analytic investigation of numerous complex systems. Large N lattice Yang-Mills theory, on the other hand, is instrumental in our understanding of non-perturbative aspects of quantum chromodynamics (QCD).

In this section, we provide an introductory overview of matrix models and large N lattice Yang-Mills theory, restricting our focus to aspects pertinent to our ensuing bootstrap problem formulation.

1.1 Matrix Models and the Loop Equations

Matrix models, including the matrix integrals, are of considerable interest in a multitude of physical and mathematical domains such as multi-component quantum field theory [t Hooft, 1974] (see [Migdal, 1983] for the review), two-dimensional quantum gravity and string theory [David, 1985; Kazakov, 1985b; Kazakov, 1985a; Kazakov, 1987], mesoscopic physics [Bohigas, 1984], algebraic geometry [Dijkgraaf, 2002; Dijkgraaf, 2003; Eynard, 2007; Kontsevich, 1992], and number theory [Montgomery, 1973]. A subcategory of matrix models, known as random matrices, have been substantially studied due to their propensity for capturing the statistical behavior of intricate quantum systems.

We focus our attention on one of the principal categories of random matrix models, namely the Hermitian matrix models. A typical $N \times N$ Hermitian one-matrix model can be defined via its probability measure, often represented in the form of a partition function Z_N:

$$Z_N = \int d^{N^2}M \, \mathrm{e}^{-N\mathrm{tr}V(M)} \tag{2.1}$$

where $d^{N^2}M = \prod_{i,j1}^{N} dM_{ij}$ serves as the invariant Hermitian measure. The potential is custom-

arily chosen to be a polynomial:

$$V(x) = \sum_{k=2}^{d+1} \frac{g_k}{k} M^k. \tag{2.2}$$

The significant "physical observable" in this context is the k-th moment:

$$\mathcal{W}_k = \langle \mathrm{Tr} M^k \rangle = \int \frac{d^{N^2} M}{Z_N} \frac{1}{N} \mathrm{tr} M^k \, \mathrm{e}^{-N \mathrm{tr} V(M)}. \tag{2.3}$$

This model, in the planar limit, is solvable for arbitrary polynomial potentials [Brezin, 1978]. Several methods, including direct recursion relations for planar graphs, orthogonal polynomials, the saddle point approximation for the eigenvalue distribution, and loop equations, have been developed to that effect.

In the context of our bootstrap problem, the loop equations derived using the Schwinger-Dyson method assume critical importance. Utilizing the normalized trace $\mathrm{Tr} = \frac{1}{N} \mathrm{tr}$, we express the loop equation in terms of the moments:

$$\langle \mathrm{Tr} V'(M) M^k \rangle = \sum_{l=0}^{k-1} \langle \mathrm{Tr} M^l \mathrm{Tr} M^{k-l-1} \rangle. \tag{2.4}$$

In the $N \to \infty$ limit, we employ the factorization property:

$$\langle \mathrm{Tr} M^l \mathrm{Tr} M^m \rangle = \langle \mathrm{Tr} M^l \rangle \langle \mathrm{Tr} M^m \rangle + \mathcal{O}(1/N^2). \tag{2.5}$$

The loop equation then simplifies to:

$$\sum_{j=1}^{d} g_j \, \mathcal{W}_{k+j} = \sum_{l=0}^{k-1} \mathcal{W}_l \, \mathcal{W}_{k-l+1}. \tag{2.6}$$

While these loop equations constitute a set of coupled nonlinear equations and are generally complex, they simplify in the large N limit and are amenable to solving using techniques such as orthogonal polynomials or topological recursion. The solutions deliver expectation values of the traces of powers of M, which encapsulate crucial information regarding physical quantities in the theory, including the free energy and correlators.

In summary, despite the inherent complexity of loop equations, their solutions afford valuable physical insights, underlining the power of matrix models as analytical tools in the study of complex quantum systems.

1.2 Large N Lattice Yang-Mills Theory

Quantum Chromodynamics (QCD), the theory of strong interactions, is an example of a non-Abelian gauge theory (a Yang-Mills theory) based on the $SU(3)$ gauge group. Generalizing this to an $SU(N)$ gauge group allows us to study the theory in the large N limit, which provides both conceptual and computational simplifications. However, direct analytical treatment of large N QCD, or any non-Abelian gauge theory, is challenging due to the strong coupling at low

energies. A common approach to overcome this issue is to put the theory on a lattice, leading to the so-called Lattice Gauge Theory [Wilson, 1974][1]:

$$S = -\frac{N_c}{\lambda} \sum_P \operatorname{Re} \operatorname{tr} U_P \tag{2.7}$$

Lattice Gauge Theory provides a non-perturbative formulation of Yang-Mills theory where spacetime is discretized to a lattice of points. On this lattice, the gauge fields are defined on the links connecting the points and the fermion fields at the sites.

In the large N limit, Lattice Gauge Theory simplifies significantly. This limit suppresses quantum fluctuations, allowing a semi-classical treatment[Gopakumar, 1995]. Moreover, it provides a systematic $1/N$ expansion where each order corresponds to a specific class of Feynman diagrams (planar diagrams at leading order).

In practice, Lattice Gauge Theory, especially in the large N limit, is often studied using numerical simulations. The path integral is evaluated stochastically using techniques such as Monte Carlo sampling[Creutz, 1980]. Large N reduces the sign problem, making these simulations more feasible.

The large N limit of Lattice Gauge Theories also has a deep connection to Matrix Models. This limit simplifies the Lattice Gauge Theory to a Matrix Model, where the degrees of freedom are matrices rather than fields[Bhanot, 1982; Eguchi, 1982; Gonzalez-Arroyo, 2010]. This opens the way to study non-perturbative aspects of gauge theories using the powerful methods developed in the context of Matrix Models.

In conclusion, the large N Lattice Yang-Mills theory provides a unique window to non-perturbative aspects of gauge theories. It is a broad and active field of research, with connections to areas as diverse as String Theory and Statistical Mechanics.

2   Bootstrapping a toy model

To be concrete, here we briefly illustrate "Bootstrap by equations of motion" by a toy model: 0-dimensional φ^4 model. Consider the model defined by the following partition function:

$$Z = \int_{-\infty}^{\infty} \exp(-\frac{x^2}{2} - g\frac{x^4}{4})\mathrm{d}x, \ \ g > 0, \tag{2.8}$$

and our goal here is solving the observables:

$$\mathcal{W}_k = \frac{1}{Z} \int_{-\infty}^{\infty} x^k \exp(-\frac{x^2}{2} - g\frac{x^4}{4})\mathrm{d}x. \tag{2.9}$$

Due to the simplicity of the model, we have a lot of available method to solve the model. For a closed-form solution, we have:

---

[1]For a review of other realization and generalization of the lattice Yang-Mills theory, the reader could refer to [Cao, 2023].

$$\mathcal{W}_2 = \frac{\pi \left(-I_{-\frac{1}{4}}\left(\frac{1}{8g}\right) + (4g+1)I_{\frac{1}{4}}\left(\frac{1}{8g}\right) - I_{\frac{3}{4}}\left(\frac{1}{8g}\right) + I_{\frac{5}{4}}\left(\frac{1}{8g}\right)\right)}{2\sqrt{2}g K_{\frac{1}{4}}\left(\frac{1}{8g}\right)} \tag{2.10}$$
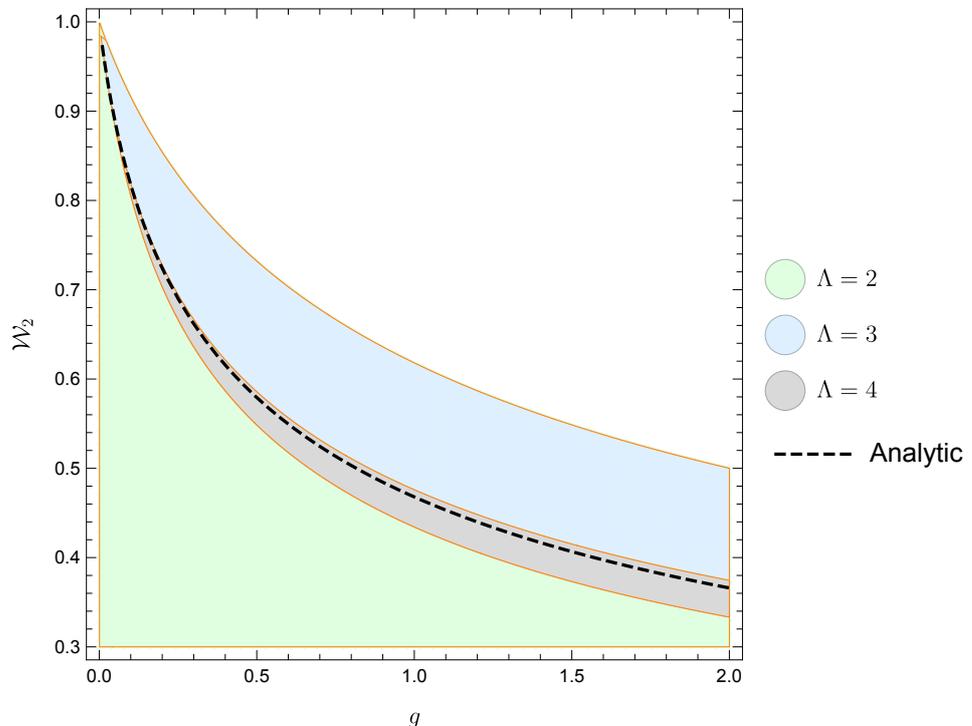

Figure 2.1: The shrinking of the allowed region for the toy model.

The bootstrap method starts by considering the Dyson-Schwinger equations (or by integration by part):

$$(k+1)\mathcal{W}_k = \mathcal{W}_{k+2} + g\mathcal{W}_{k+4} \tag{2.11}$$

and global symmetry:

$$\mathcal{W}_k = 0, \text{ for odd } k \tag{2.12}$$

to solve all the higher moments in terms of $\mathcal{W}_2$. To formulate the problem as an optimization problem, a crucial step is considering the expectations of square of polynomials are always positive semi-definite:

$$\frac{1}{Z}\int_{-\infty}^{\infty}\left(\sum \alpha_i x^i\right)^2 \exp\left(-\frac{x^2}{2} - g\frac{x^4}{4}\right) \geq 0, \ \forall \alpha \tag{2.13}$$

This is a quadratic form in α, so its positivity is equivalent to:

$$\mathbb{W} = \begin{pmatrix} \mathcal{W}_0 & \mathcal{W}_1 & \mathcal{W}_2 & \dots \\ \mathcal{W}_1 & \mathcal{W}_2 & \mathcal{W}_3 & \dots \\ \mathcal{W}_2 & \mathcal{W}_3 & \mathcal{W}_4 & \dots \\ \vdots & \vdots & \vdots & \ddots \end{pmatrix} \succeq 0 \tag{2.14}$$

13

We can solve the Semi-Definite Programming(SDP) maximizing or minimizing $\mathcal{W}_2$ constrained by a truncation of the matrix $\mathbb{W}$:

$$\min \text{ or } \max \ \mathcal{W}_2 \tag{2.15}$$

$$\mathbb{W}_\Lambda \succeq 0 \tag{2.16}$$

Here $\mathbb{W}_\Lambda$ is the top $(\Lambda + 1) \times (\Lambda + 1)$ sub-matrix of $\mathbb{W}$.

For $g = 1$, $\Lambda = 10$, we can get the numerical bootstrap result (5.5 digits):

$$0.4679137 \leq \mathcal{W}_2 = 0.4679199170 \leq 0.4679214 \tag{2.17}$$

The value in the middle is from the closed-form solution Eq 2.10 (exact value). The l.h.s and r.h.s is the bootstrap result maximizing and minimizing $\mathcal{W}_2$.

This simple toy model (cannot be even simpler) is actually the prototype of the bootstrap implementations fall in the category of "Bootstrap by Equations of Motion". We see that it could be fairly general, i.e. this method can potentially work for any system defined by a measure satisfy certain positivity conditions.

Paper I

Analytic and Numerical Bootstrap for One-Matrix Model and "Unsolvable" Two-Matrix Model

Vladimir Kazakov *and* **Zechuan Zheng**

Laboratoire de Physique de l'École Normale Supérieure,
CNRS, Université PSL, Sorbonne Universités,
24 rue Lhomond, 75005 Paris, France

We propose the *relaxation* bootstrap method for the numerical solution of multi-matrix models in the large N limit, developing and improving the recent proposal of H.Lin. It gives rigorous inequalities on the single trace moments of the matrices up to a given "cutoff" order (length) of the moments. The method combines usual loop equations on the moments and the positivity constraint on the correlation matrix of the moments. We have a rigorous proof of applicability of this method in the case of the one-matrix model where the condition of positivity of the saddle point solution appears to be equivalent to the presence of supports of the eigenvalue distribution only on the real axis and only with positive weight. We demonstrate the numerical efficiency of our method by solving the analytically "unsolvable" two-matrix model with $\mathrm{tr}[A, B]^2$ interaction and quartic potentials, even for solutions with spontaneously broken discrete symmetry. The region of values for computed moments allowed by inequalities quickly shrinks with the increase of the cutoff, allowing the precision of about 6 digits for generic values of couplings in the case of $\mathbb{Z}_2$ symmetric solutions. Our numerical data are checked against the known analytic results for particular values of parameters.

Contents

1   Introduction

Matrix integrals play an important role in numerous physical and mathematical subjects, such as multi-component quantum field theory [1] (see [2] for the review), two-dimensional quantum gravity and string theory [3–6], mesoscopic physics [7], algebraic geometry [8–11], number theory [12], etc. A rather general class of matrix integrals has the form

$$Z = \int d^{N^2}A \, d^{N^2}B \, d^{N^2}C \ldots e^{-\mathrm{tr}\mathcal{V}(A,B,C,\ldots)} \tag{1.1}$$

where $A, B, C, \ldots$ are Hermitian $N \times N$ matrices with $U(N)$ invariant integration measure and the potential $\mathcal{V}(x, y, z, \ldots)$ is an analytic function (often a polynomial) of the variables $x, y, z, \ldots$. The partition function Z is a function of parameters (couplings) of the potential. The typical "physical" quantities to study are various correlators of traces of "words" built out of products of matrices $A, B, C, \ldots$, computed w.r.t. the measure represented by the expression under the integral:

$$\Big\langle \frac{\mathrm{tr}}{N}(A^k B^l C^m \ldots) \frac{\mathrm{tr}}{N}(A^n B^p C^q \ldots) \ldots \Big\rangle. \tag{1.2}$$

The $N \to \infty$ limit, with the appropriately adjusted parameters of the potential and of the averaged quantity, is of a special importance in multiple applications since it describes the thermodynamical limit of macroscopically many degrees of freedom for various physical systems. Such a limit deals with the infinite number of integrals, thus the matrix integral becomes a functional integral.

A particularly interesting $N \to \infty$ limit, for the potential scaled as $\mathcal{V}(x, y, z, \ldots) = N\, V(x, y, z, \ldots)$, where the function $V(x, y, z, \ldots)$ contains only finite, N-independent parameters, is usually called the 't Hooft, or planar limit. Among many important matrix models of this kind there is the so called Eguchi-Kawai d-matrix integral equivalent, in the 't Hooft limit, to the multicolor Quantum Chromodynamics [13]. The 't Hooft limit is characterized by the perturbative expansions given in terms of planar Feynman graphs ($1/N$-expansion appears to be a topological expansion: the "fat" graphs of a given genus g are weighted with the factor N^{2-2g}). This allows the counting of such planar graphs [14–16] and enables the introduction and exact solution of statistical mechanical models on random planar dynamical lattices – Ising model on random triangulations [17, 18] and various generalizations [6, 19–21].

The direct analytic computation of a majority of such multi-matrix integrals is virtually impossible, apart from some trivial, albeit important, cases, such as the quadratic potential $V(x, y, z, \dots)$ leading to the gaussian integral.[1]

For a sub-class of such integrals with specific potentials the problem can be reduced to integrations over a smaller number of variables than $\sim N^2$. For example, sometimes the problem can be reduced to the integrations or summation only over $\sim N$ variables, such as eigenvalues of the matrices. Then, in the large N limit, the problem can be reduced to the saddle point calculation, significantly simplifying the problem of computation of that functional integral.[2] The basic example of such a simplification is the one matrix model

$$Z = \int d^{N^2} A \, \mathrm{e}^{-\mathrm{tr} \mathcal{V}(A)} \tag{1.3}$$

solvable for any potential $\mathcal{V}(x)$. Once we have two or more matrix integration variables in (1.1) the problem usually gets much more complicated. Generically, such models are unsolvable, i.e. the number of degrees of freedom cannot be efficiently reduced, and the saddle point approximation is inappropriate since the characteristic "energy" and entropy of the integration variables are both of the order $\sim N^2$. Here comes the question whether we can study these integrals at least numerically.

Virtually the only universal general method of numerical computation of functional integrals is the Monte-Carlo method. It has been applied to some matrix integrals with more or less of success. Its main drawbacks are well known: i) the result comes with a statistical error; ii) it is sometimes difficult to reach the numerical equilibrium state in a reasonable time; iii) MC is bad for the systems with sign-changing Boltzmann weights or non-local interactions; iv) the size of the system (the number of integrals) is limited by computational facilities v) The precision is usually rather modest, maximum about 3-4 digits.

Do we have any alternative?

In the 1980's, in a series of papers [23–25], the authors formulated the problem of large N matrix integral and large N quantum mechanics in the loop space (space of moments). The authors attempted the numerical study for the loop variables by minimizing an effective action. They were the first to stress the importance of positive semi-definiteness conditions for certain matrices of loop variables in getting physically meaningful results.

Recently, an important progress has been made in the computations of multi-point correlators in conformal field theories in various dimensions, due to the conformal bootstrap method [26]. The method uses various properties of correlators, such as crossing and positivity, to "bootstrap" numerically their values and the values of the critical exponents. It appeared to be far more efficient and precise then other numerical approaches, giving the critical exponents of 3d Ising model with the record 6-digits precision [27]. An appealing property of this method is the absence of any statistical error in the results, which are given within rigorously established margins.

---

[1]Expansions w.r.t. parameters around the gaussian point lead in the 't Hooft limit to the perturbation theory formulated in terms of planar Feynman graphs. It can help to study the model in a specific, narrow domain of the parameter space.

[2]An (incomplete) review of such *solvable* matrix models can be found in [22].

Inspired by this success a few authors applied the philosophy of the numerical bootstrap to the computations of various matrix integrals [28, 29] and even of the lattice multi-color QCD and $\mathcal{N} = 4$ SYM theory [30]. Instead of the direct study of the matrix integrals they proposed to study the large N Schwinger-Dyson equations which are often also called loop equations, in analogy with their applications to QCD [31]. They are easily obtained by the obvious Ward identities resulting from insertion of the full matrix derivative under the matrix integral:

$$0 = \int d^{N^2}A \, d^{N^2}B \, d^{N^2}C \dots \frac{\text{tr}}{N}(\frac{\partial}{\partial A}A^m B^n C^k \dots)\text{e}^{-\text{tr}\mathcal{V}(A,B,C,\dots)} \qquad (1.4)$$

where the matrix derivative inside the trace $\frac{\partial}{\partial A}$ acts on all A-matrices, including the potential. All other loop equations correspond to all possible "words" of matrices under the trace and to all insertions of various matrix derivatives at any place in the "words".[3] Then the positivity conditions are imposed stating that the inner product[4] of any operator with itself is positive. Rigorous bounds on the dynamical quantities of the theory can be derived from these positivity conditions and loop equations.

This new approach, compared to the previous work of loop variables [23–25], imposes the large N Schwinger-Dyson equations (loop equations) explicitly, rather than getting loop equations as a result of effective action minimization. In parallel with the philosophy of conformal bootstrap, this approach focuses more on the geometry of the space of loop variables under sensible physical constraints, which guarantees the rigorousness of the bounds on physical quantities.

In the inspiring work of Lin [28] the method was rather successfully applied to the one-matrix model mentioned above, to the exactly solvable two-matrix model with $\text{tr}(AB)$ interaction [15, 16] describing the Ising model on planar graphs [17] as well as to the model with $\text{tr}(AB^2 + A^2B)$ interaction, presented there as a case of "unsolvable" matrix model [5]. Lin uses the non-linear equations (1.4) to bootstrap the loop averages up to the positive semi-definite matrix of size 45.

This new approach has, in our opinion, a great potential for the precision computations of physically important matrix integrals in the 't Hooft limit. But at the same time it is very much perfectible at this stage.

Firstly, the numerical matrix bootstrap approach of [28–30], based on the loop equations and positivity constraint, is not well understood analytically. Its efficiency, and the power of positivity, still looks quite mysterious. It is not even fully understood why we need the positivity condition. Secondly, the matrix bootstrap has a very distinguished feature comparing to most of the other bootstrap problems we dealt with so far: it is in general non-convex. The non-convexity comes from the quadratic terms in the loop equation, which is a result of large N factorization. In optimization theory, this is called Nonlinear SDP

---

[3]In the 't Hooft limit, the single trace "words" are enough due to the factorization property which we will describe in the next section.

[4]Here inner product of an operator $\mathcal{O}$ means $\langle \text{tr}\mathcal{O}^{\dagger}\mathcal{O} \rangle$.

[5]We will demonstrate in the Appendix A that, in fact, all two-matrix models with cubic interactions, including this one, are solvable in the above-mentioned sense.

(semi-definite programing) and all the solvers for it are not mature enough compared with the highly developed SDP solvers dealing with linear problems. In [28–30], the authors tried to bootstrap the matrix models by the Nonlinear SDP directly, and this non-linearity limited the bootstrap capabilities to very simple models, or to more complex models but only up to very small lengths of operators.

1.1 Main results

In this work, we advance the matrix bootstrap approach trying, on the one hand, to understand analytically the role of positivity conditions, and on the other hand, to overcome, at least partially, the above-mentioned limitations of the method.

First, we derive a necessary and sufficient condition for the positivity of bootstrap for large N one-matrix model, to clarify how this method is working. Namely, we show that the positivity is equivalent to the condition for the resolvent to have the cuts only on the real axis, with the positive imaginary part corresponding to the positive density of eigenvalue distribution. This condition actually enables us, in principle, to analytically solve the bootstrap problem for any one-matrix model. For the illustrative purposes, we will apply the new positivity condition to the one-matrix model with quartic potential:

$$V'(x) = \frac{\mu}{2}x^2 + \frac{g}{4}x^4, \qquad (\mu = \pm 1) \tag{1.5}$$

where we normalized the quadratic term to ± 1. We will use the analytic bootstrap to completely classify the admissible set of solutions of the loop equations and positivity conditions, and to locate the critical value of $\mathbb{Z}_2$ symmetry breaking.

So far, we could solve exactly a very limited set of bootstrap problems, and most of them correspond to very simple theories, such as Sine-Gordon theory in S-matrix bootstrap [32] and 1d mean field theory in conformal bootstrap [33]. Since this method appears to be applicable to any one-matrix model and generalized to some solvable multi-matrix models, it provides us with a big new family of exactly solvable bootstrap problems. Hopefully these solvable bootstrap models will give us more of intuition about the way the bootstrap method works.

The other new result of this work is a new bootstrap scheme for the study of nonlinear SDP for multi-matrix integrals, which appears to be numerically much more efficient than those proposed in the past. The main ingredient of the method is the introduction of relaxation matrix in the place of non-linearity of the loop equation. Namely, we treat the quadratic terms as independent variables and impose the positivity condition on these variables. Surprisingly, it seems enough to bootstrap the region of admissible values of the computed quantity that is quickly shrinking with the increase of the "cutoff" – the maximal length of "words" in the involved operators.

As a particular example of analytically unsolvable matrix integral we will study by this method the following two-matrix model

$$Z = \lim_{N \to \infty} \int d^{N^2}A \, d^{N^2}B \, \mathrm{e}^{-N\mathrm{tr}\left(-h[A,B]^2/2 + A^2/2 + gA^4/4 + B^2/2 + gB^4/4\right)}. \tag{1.6}$$

21

Various versions of this model have been studied in the past in connection to certain $\mathcal{N} = 1$ supersymmetric Yang-Mills theories [34]. In the particular case $g = 0$ the model is solvable and it will serve us as an important check of applicability and efficiency of our relaxation bootstrap method. Our results show a very good precision: up to 6 digits with the maximal cutoff equal to 22 for the words under averages. We were also able to establish with a reasonable accuracy the phase structure of the model in the g, h coupling space, i.e. the positions of critical lines corresponding to the convergence radius of planar perturbative expansion, as well as to the spontaneous $\mathbb{Z}_2$ symmetry breaking.

The two-matrix model (1.6) considered in this paper serves mostly for the illustration of the power of our method, though it could have in principal some physical applications, such as the statistical mechanics on dynamical planar graphs, in the spirit of [35–37].

This article is organized as follows. The next Section 2 serves as a retrospect of the Hemitian matrix integral and the numerical bootstrap technique developed for it so far. Then in Section 3 we propose our equivalent condition for the positivity condition described in Section 2. This condition will justify the numerical bootstrap method and enable us to analytically solve the corresponding bootstrap problem. in Section 4, we will describe the way our relaxation method works for analytically unsolvable large N multi-matrix integrals. We test this relaxation method in Section 5 on the concrete unsolvable model (1.6). We will see that our relaxation method is able to largely meet our expectations, with remarkable precision. In the last section, after short conclusions, we will briefly discuss possible applications of our method to some more physical problems, such as the multicolor lattice Yang-Mills theory.

Note: The main results of this work are compared with the later Monte Carlo(MC) results [38]. This comparison convinces us that the bootstrap method is more efficient than MC regarding the large N two-matrix model calculation.

2 Hermitian one-matrix model bootstrap

In this section we will revisit several basic facts about large N limit Hermitian one-matrix model and the related numerical bootstrap proposed in [28]. We will be mainly focused here on the aspects of this model which are crucial for the theoretical development in the next section and provide us with important intuition. The reader can refer to numerous works and reviews, some already cited above (see e.g. [39] for a good state-of-art description of results on Hermitian one-matrix model).

2.1 Hermitian one-matrix model in the planar limit and loop equations

The Hermitian one-matrix model is defined by matrix integral:

$$Z_N = \int d^{N^2} M \, e^{-N \mathrm{tr} V(M)} \tag{2.1}$$

where the invariant Hermitian measure is $d^{N^2}M = \prod_{i,j1}^{N} dM_{ij}$. The potential is usually taken polynomial [6]:

$$V(x) = \sum_{k=2}^{d+1} \frac{g_k}{k} M^k. \tag{2.2}$$

The main "physical observable" is the k-th moment:

$$\mathcal{W}_k = \langle \text{Tr} M^k \rangle = \int \frac{d^{N^2}M}{Z_N} \frac{1}{N} \text{tr} M^k e^{-N \text{tr} V(M)}. \tag{2.3}$$

This model is solvable in the planar limit for arbitrary polynomial potentials [14]. There exist several methods for that: direct recursion relations for planar graphs, orthogonal polynomials, saddle point approximation for the eigenvalue distribution, loop equations (see [2, 40] for a review). The loop equations will play the crucial role in our bootstrap method.

To derive them we simply use the Schwinger-Dyson method by writing

$$0 = \int d^{N^2}M \, \frac{\text{tr}}{N} \left(\frac{\partial}{\partial M} M^k \right) e^{-N \text{tr} V(M)} \tag{2.4}$$

since the expression under the integral is a total derivative. The boundary terms are absent assuming that the highest power $d+1$ of the potential is even and its coefficient is positive $t_{d+1} > 0$. [7]

Applying explicitly the matrix derivative in (2.4) we write the loop equation in terms of the moments:[8]

$$\langle \text{Tr} V'(M) M^k \rangle = \sum_{l=0}^{k-1} \langle \text{Tr} M^l \text{Tr} M^{k-l-1} \rangle. \tag{2.5}$$

In the $N \to \infty$ limit we can use the factorization property:

$$\langle \text{Tr} M^l \text{Tr} M^m \rangle = \langle \text{Tr} M^l \rangle \langle \text{Tr} M^m \rangle + \mathcal{O}(1/N^2). \tag{2.6}$$

Then the loop equation reduces to

$$\sum_{j=1}^{d} g_j \, \mathcal{W}_{k+j} = \sum_{l=0}^{k-1} \mathcal{W}_l \, \mathcal{W}_{k-l+1}. \tag{2.7}$$

The simplest way to solve (2.7) is to introduce the generating function of moments - the resolvent - as a formal power series in terms of z^{-1}:

$$G(z) = \sum_{k=0}^{\infty} z^{-k-1} \mathcal{W}_k. \tag{2.8}$$

---

[6]We believe that our final conclusion can be generalized to non-polynomial potentials, but there may be some subtleties.

[7]For the "unstable" potentials, which do not satisfy one of these conditions, the matrix integral might still exist with appropriate deformation of the integration contour. The large N solutions can exist even independently of the contour deformation since they correspond to local minima of the effective potential for the eigenvalues.

[8]Here for the conciseness, we introduce the normalized trace $\text{Tr} = \frac{1}{N}\text{tr}$, so that $\text{Tr} I = 1$

We have not yet assumed anything about the convergence of the series. Multiplying (2.7) by z^{-k} and summing from $k = 1$ to ∞ we represent the loop equation in a compact form as a quadratic equation for the resolvent.

$$G(z)^2 + P(z) = V'(z)G(z). \tag{2.9}$$

The function $P(z)$ comes from carefully collecting in the summation the terms with small k's . It can be written compactly as:

$$P(z) = \langle \text{tr} \frac{V'(z) - V'(M)}{z - M} \rangle. \tag{2.10}$$

This is a polynomial of z and a linear function of $\mathcal{W}_k, (k = 1, ..., d-1)$. For example, if $V'(z) = z + gz^3$, then we have $P(z) = 1 + gz^2 + g\mathcal{W}_2 + gz\mathcal{W}_1$. We can solve (2.9), picking the relevant branch of the root which reproduces the leading z^{-1} behavior of the resolvent $G(z) = \frac{1}{z} + \mathcal{O}(\frac{1}{z^2})$ at infinity:

$$G(z) = \frac{1}{2}(V'(z) - \sqrt{V'(z)^2 - 4P(z)}). \tag{2.11}$$

This result will play an important role in our work, so we make several comments on it:

1. By (2.11), the resolvent is understood as a genuine analytic function, at least in the neighborhood of infinity point. So the formal series defined in (2.8) has a finite radius of convergence. As a consequence, there must be an exponential bound for the moments[9]:

$$\mathcal{W}_n \leq C_0 R(g_k, \mathcal{W}_1, ... \mathcal{W}_{d-1})^n. \tag{2.12}$$

2. It is clear from this formula, that all the moments are determined by several low-order moments in $P(z)$ and the couplings:

$$\mathcal{W}_n = \mathcal{W}_n(g_k, \mathcal{W}_1, ..., \mathcal{W}_{d-1}). \tag{2.13}$$

   This is what the loop equation tells us. But the loop equation doesn't tells us how to fix the low-order moments involved in $P(z)$. Those can be fixed only by additional assumptions on the solution, such as for example the single support solution for the eigenvalues (single cut on the physical sheet of $G(z)$). We will see how to classify the solutions which are picked up by the bootstrap method.

To have more intuitive ideas of possible large N solutions it is useful to reduce the matrix integration (2.1) to the integration over the eigenvalues of the Hermitian matrix. Namely, if we represent it as $M = \Omega^\dagger X \Omega$ where $X = \text{diag}(x_1, x_2, \ldots, x_N)$ is the diagonal matrix of eigenvalues and Ω is the diagonalizing unitary matrix, the matrix integral reduces to only N integrations over the eigenvalues [14]:

$$Z_N = \int \prod_{j=1}^{N} \left(dx_j \, e^{-NV(x_j)} \right) \Delta^2(x_1, \ldots, z_N) \tag{2.14}$$

---

[9] Strictly speaking the radius of convergence is the inverse of the module of largest root of the polynomial under the square root in (2.11), unless two of such roots merge. Here it is enough for us that it is bounded exponentially.

where the square of the Vandermonde determinant $\Delta(x_1, \ldots, z_N) = \prod_{i>j}(x_i - x_j)$ represents the Jacobian of the change of integration variables (Dyson measure). Here the integrand is of the order $e^{N^2(\cdots)}$ whereas the number of variables is reduced to N. This allows for the application of the saddle point approximation, giving the BIPZ saddle point equations (SPE) [14]

$$V'(x_j) = \sum_{k(\neq j)} \frac{2}{x_j - x_k}, \qquad j = 1, 2, \ldots N. \tag{2.15}$$

It looks as the condition of electrostatic equilibrium of two-dimensional point-like electric charges (of the same sign) with coordinates x_j on a line, locked in the potential $V(x)$ (see the Fig 1.)
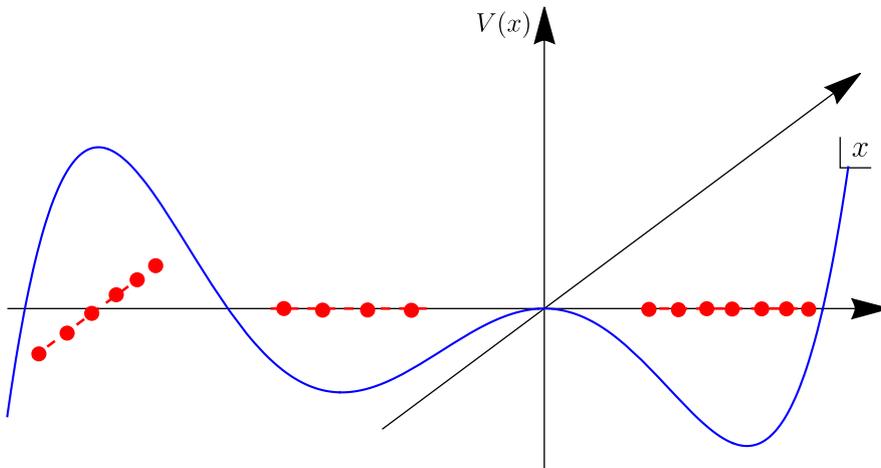
Figure 1: Coulomb gas interpretation for the eigenvalue configurations and a typical cut configuration. For a general solution of the SDP (2.15), we can have a complex cut at the maximum of the potential.

The possible physical solutions correspond to filling n minima of such a potential with fractions $N_1, N_2, \ldots, N_n$ of these charges, such that $\sum_{l=1}^{n} N_k = N$. The eigenvalues then form a continuous distribution with n finite supports along the real axis.

The SPE describes all extrema of the effective potential

$$V_{\text{eff}} = N \sum_k V(x_k) + \log \Delta^2(x_1, \ldots, z_N), \tag{2.16}$$

not only the minima but also the maxima. For the solutions with the filling of some maxima of the potential the linear supports of distributions around the maxima should inevitably turn into the complex plane, with the complex conjugate endpoints, as shown in Fig 1. We will call such solutions "unphysical". The values of fractions $\nu_j = N_j/N$, $j = 1, 2, \ldots, d$ are in one-to-one correspondence with the values of first $d - 1$ moments $\mathcal{W}_1, \ldots \mathcal{W}_{d-1}$ and they completely fix the algebraic curve of the solution [8, 9]. The solutions where we fill only the minima of the effective potential will be called "physical". The supports for such

solutions will be located only on the real axis, with positive weight for the distribution of the eigenvalues.

In the large N limit, the distribution of eigenvalues converges to a continuous function $\rho(x)$ and the corresponding SPE actually becomes the quadratic equation for resolvent (2.9). In this limit, the resolvent function, the eigenvalue distribution and the series of moments are closely related.

The moments can be computed via the resolvent (2.8) by a simple contour integration formula:

$$\mathcal{W}_n = \frac{1}{2\pi i} \oint_\Gamma z^n G(z) \mathrm{d}z = -\frac{1}{4\pi i} \oint_\Gamma z^n C(z) \mathrm{d}z \tag{2.17}$$

where the contour Γ must encircle all branch points of $G(z)$ (see [8, 9] for the details). We introduced here the "cut-function" – the square root of the discriminant – by the formula

$$C(x) = \sqrt{V'(x)^2 - 4P(x)} = \sqrt{D(x)} = g_{d+1} \sqrt{\prod_{k=1}^d (x - a_k)(x - b_k)}. \tag{2.18}$$

The roots $\{a_k, b_k\}$ of the discriminant become the branch points of the cut-function. Their number is always even. For real couplings in the potential the branch points lay only on the real axis or come in complex conjugate pairs. Note that it is easy to relate the eigenvalue fractions to these branch points:

$$\nu_j = \frac{1}{2\pi i} \oint_{\Gamma_j} G(z) \mathrm{d}z = -\frac{1}{4\pi i} \oint_{\Gamma_j} C(z) \mathrm{d}z \tag{2.19}$$

where the contour Γ_j encircles anticlockwise only the branch points $\{a_k, b_k\}$, and ν_j can be in principal of either sign.

The eigenvalue density is expressed as the discontinuity of the cut function $C(x)$:

$$\rho(x) = \frac{1}{4\pi i}(C(x + i0) - C(x - i0)) = \frac{1}{2\pi}\Im C(x + i0) \tag{2.20}$$

and the moments can be expressed by the eigenvalue density:

$$\mathcal{W}_n = \int_{-\infty}^{\infty} x^n \rho(x) \mathrm{d}x. \tag{2.21}$$

2.2 Bootstrap method for the large N one matrix model

As we stated above, the loop equation (2.7),(2.9) has in general a continuum of solutions of the form (2.11) labeled by a finite number of parameters – the lowest moments $\mathcal{W}_1, ... \mathcal{W}_{d-1}$ which can take a priori arbitrary values. But not all of these solutions are "physical", i.e. rendering all moments $\mathcal{W}_k$, $k \in \mathbb{Z}_+$ real and compatible with the finite N Hermitian matrix ensemble. For example, the physical even moments should be positive, but this condition is not the only one.

A more general physical condition on a solution is the positivity of inner product for the matrix integral. This condition states that, for any operator of the form $\mathcal{O} =$

$\sum_{i=0}^{n-1} \alpha_i M^i$ s.t. $\boldsymbol{\alpha} \in \mathbb{R}^n$, and for any $n \in \mathbb{Z}_+$, we have the positive semi-definite quadratic form[10]:

$$\langle \mathrm{Tr}\mathcal{O}^\dagger \mathcal{O} \rangle = \boldsymbol{\alpha}^{\mathrm{T}} \mathbb{W} \boldsymbol{\alpha} \geq 0 \quad \forall \boldsymbol{\alpha} \in \mathbb{R}^n. \tag{2.22}$$

Here we introduced the matrix $\mathbb{W}_{ij} = \mathcal{W}_{i+j-2}$ which will be called below for convenience the correlation matrix. The above condition is equivalent to the positive definiteness of correlation matrix[11]:

$$\mathbb{W} \succeq 0. \tag{2.23}$$

The condition (2.22) is obvious for a finite N matrix model with converging integral (2.1), i.e. when $d+1$ is even and $g_{d+1} > 0$ in the potential (2.2), since the moments are just given by the integration of positive definite functions with a positive measure. In addition, at finite N there exists only one solution for the moments [12]. But it is far from trivial in large N limit, where we have to understand what solutions from the continuum are really physical.
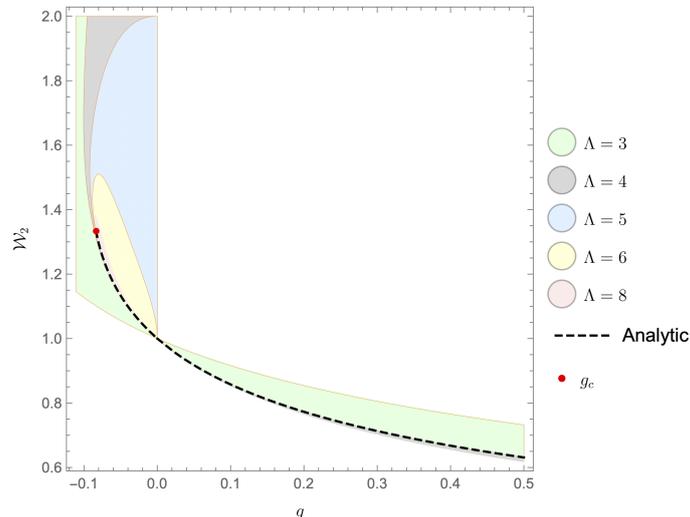
Figure 2: The allowed region for quartic model $V(z) = \frac{1}{2}z^2 + \frac{g}{4}z^4$ for different cutoff Λ, compared with the analytic solution. Here we assuming $\mathcal{W}_1 = 0$, we also note that for $g > 0$, we didn't plot $\Lambda \geq 5$ since they are almost indistinguishable from the analytic solution on the figure.

---

[10]Here we assume that all the expectation values we study are real. This is actually a non-trivial result from the $M \to M^{\mathrm{T}}$ symmetry of the potential. Since this symmetry is always present for all the models considered in this article, we will implicitly assume this to be always true.

[11]Here we slightly abused the notations: $\mathbb{W}$ sometimes means the matrix with finite size, involving only the moment up to a certain order Λ ("cutoff"), and sometimes it means the infinite dimensional matrix. But the positive semi-definiteness is always well defined as a positivity of the corresponding quadratic form.

[12]To define the matrix integral for unstable potentials, when $d+1$ odd or/and $g_{d+1} < 0$ one usually deforms appropriately the integration contours. Then the questions of positivity become less obvious for finite N. But we will see on the example of quartic potential that at infinite N we can still have positivity for certain solutions, even for such, globally unstable, potentials.

To do numerical bootstrap, we set a finite cutoff Λ, i.e. the highest moment in the correlation matrix $\mathbb{W}$ and loop equations is $\mathcal{W}_{2\Lambda}$ and the size of the correlation matrix is $(\Lambda + 1) \times (\Lambda + 1)$. We can use the loop equations to express the higher moments through a certain number of the lower moments and substitute them into the correlation matrix as functions of lower moments. Then the positivity of the correlation matrix provides us with algebraic inequality on these lower moments. In general, we expect to get the inequalities for each of the lower moments both from above and from below, for example:

$$\mathcal{W}_{2\Lambda}^{\min} \leq \mathcal{W}_2 \leq \mathcal{W}_{2\Lambda}^{\max} \tag{2.24}$$

at a cutoff Λ. In practice, the allowed region $[\mathcal{W}_{2\Lambda}^{\min}, \mathcal{W}_{2\Lambda}^{\max}]$ shrinks fast as we increase Λ, giving us tight bounds on $\mathcal{W}_2$.

We exemplify this approach on the case of quartic potential $V(z) = \frac{1}{2}z^2 + \frac{g}{4}z^4$. We plot in Fig 2 the region for the allowed values of function $\mathcal{W}_2(g)$ under the assumption of $M \Leftrightarrow -M$ symmetry of the solution, i.e. $\mathcal{W}_{2l+1} = 0$. Under this assumption, all the higher moments are polynomials in terms of $\mathcal{W}_2$ and g. The positivity of the correlation matrix reduces to a list of algebraic inequalities on $\mathcal{W}_2$.[13]

It is a bit surprising that the bootstrap scheme described above for Hermitian one-matrix model is generally analytically solvable, considering that it is usually non-trivial to solve an infinite series of algebraic inequalities. In the next section we will propose a necessary and sufficient condition for the positivity constraint (2.23) by virtue of a result of solution of Hamburger moment problem. By this condition we can not only generally solve the bootstrap problem analytically but also justify why the numerical bootstrap process excludes the unphysical solutions of SPE described in Section 2.1.

3   Hamburger moment problem and positivity of resolvent

As it should be clear from the previous section, the bootstrap method for one-matrix model has two main ingredients: 1. The Schwinger-Dyson loop equations for the moments of the random matrix variables; 2. The positive definiteness of the correlation matrix of these moments. We will rigorously prove that the second ingredient, in virtue of the Hamburger moment problem [41], picks up in the planar limit the solutions of loop equations only with real-positive supports of the matrix eigenvalue distribution. We will employ this condition to analytically solve the bootstrap condition.

3.1   Hamburger problem versus the positivity condition on resolvent

The loop equation (2.7) renders all possible large N, saddle point solutions of the Hermitian one matrix model. Some of them "look" physical, i.e. corresponding to the stable equilibrium in the Coulomb gas picture for the eigenvalues locked in the effective potential (2.16). For the other, the stable solution corresponds to "unphysical" picture when the supports of

---

[13]To depict the allowed region, maybe the simplest way is the Mathematica **RegionPlot** function. Although not really numerically efficient, it is already good enough for the simplest quartic one-matrix model.

eigenvalue distribution become complex. What are the solutions captured by our bootstrap procedure?

As we just reviewed, numerical bootstrap of one matrix model consists of two ingredients: loop equation and positivity of correlation matrix. It sets a cutoff on both constraints and gets a rigorous bound on the physical quantities we are interested in. Analytically all the information contained in the loop equations is encoded in the quadratic equation of resolvent (2.9), which has a simple solution (2.11). It describes the hyper-elliptic algebraic curve parameterized by complex variable x. It is natural to ask the question: can the positivity of correlation matrix also be expressed as a simple condition on the resolvent? The answer is, luckily and a bit surprisingly, yes.

For convenience, we make the following definition: a resolvent satisfies the positivity condition if the corresponding eigenvalue density (2.20) is supported on the real axis and is positive on its support. Our main conclusion of this section will be:

$$Positivity\ of\ correlation\ matrix \Leftrightarrow Positivity\ of\ Resolvent \tag{3.1}$$

We prove the necessity first. The proof is based on a well-known mathematical conclusion that will play an important role in our demonstration – the result of the solution of the Hamburger moment problem [41]:

For a given series of real numbers $\{m_n\}_{n=0}^{\infty}$, there exists a positive Borel measure μ such that:

$$m_n = \int x^n \mathrm{d}\mu \tag{3.2}$$

if and only if the matrix $H_{ij} = m_{i+j-2}$ is positive semi-definite. Moreover, if there exist the constants C and D, such that $|m_n| \leq CD^n n!$, the measure is unique.

Applying the result of Hamburger momentum problem (3.2), we have for each moment $\mathcal{W}_n = \int_{\mathbb{R}} x^n \mathrm{d}\mu(x)$. We notice from the exponential bound condition (2.12) that μ must be supported in a finite region $[-R, R]$, since otherwise, if we have $\epsilon > 0$, such that $\mu\big((-\infty, -(R + \epsilon)) \bigcup (R + \epsilon, \infty)\big) = \mu_0 > 0$, then

$$\mathcal{W}_{2n} = \int_{\mathbb{R}} x^{2n} \mathrm{d}\mu(x) > (R + \epsilon)^{2n} \mu_0, \tag{3.3}$$

which contradicts the exponential bound (2.12).

Consequently for $|z| > R$:

$$G(z) = \sum_{k=0}^{\infty} z^{-k-1} \mathcal{W}_k = \sum_{k=0}^{\infty} z^{-k-1} \int_{[-R,R]} x^k \mathrm{d}\mu(x) = \int_{[-R,R]} \frac{\mathrm{d}\mu(x)}{z - x} . \tag{3.4}$$

The exchange of infinite sum and integration is justified by Fubini's theorem. Due to this equation, $G(z)$ is analytic in the region outside of the disk $|z| > R$. The last equality in (3.4) enables us to analytically continue $G(z)$ to the whole region $\mathbb{C}\backslash[-R, R]$. So the function $G(z)$ must be analytical away from the real line, which eliminates the possibility of cuts between complex branch points. Comparing with (2.11) and (2.20), we come to the conclusion that all supports of $\rho(x)$ function must be located on the real line. For the

positivity of eigenvalue density, we note that we can extract by contour deformation the coefficient of the series in (2.8):

$$\mathcal{W}_n = \frac{1}{2\pi i} \oint z^n G(z) \mathrm{d}z = \int_{[-R,R]} x^n \rho(x) \mathrm{d}x. \tag{3.5}$$

By the uniqueness of solution of the Hamburger momentum problem, we must have $\rho(x)\mathrm{d}x = \mathrm{d}\mu$ i.e. they are equal in terms of positive measure.[14] So we have $\rho(x)$ real supported and positive. This concludes our proof of necessity for (3.1).

The proof of sufficiency is straightforward. It is already true because the sufficiency is a part of the result of the solution of Hamburger moment problem. For a more direct argument, suppose we have a resolvent that satisfies the positivity condition, i.e. (2.21) with $\rho(x) > 0$. We notice that the matrix $(\boldsymbol{X})_{ij} = x^{i+j-2}$ is trivially positive semi-definite for real x, so that if we integrate the matrix $\boldsymbol{X}$ w.r.t. the positive measure $\rho(x)\mathrm{d}x$, it stays positive semi-definite as well. The result of the integration is actually our correlation matrix $\mathbb{W}$. This concludes the proof of sufficiency and hence of the equivalence (3.1).

It is easy to demonstrate by the direct computation that in the presence of complex branch points in $G(x)$ the corresponding correlation matrix is *not* positive definite. A simple example is the resolvent for the matrix model with the unstable potential $V(M) = -\frac{1}{2}\mathrm{Tr}\, M^2$, which is $G(x) = \sqrt{x^2 + 2} - x = \frac{1}{x} - \frac{1}{2x^3} + O\left(\left(\frac{1}{x}\right)^4\right)$. We see that $\langle \mathrm{Tr}M^2 \rangle = -\frac{1}{2}$ so that the correlation matrix is not positive definite.

This suggests the validity of the numerical bootstrap approach at least in the case of the one-matrix model: by imposing the positive semi-definiteness condition on the solutions of loop equations, at least for a finite cutoff Λ, we exclude the "unphysical" large N solutions with the eigenvalue distributions having complex or negative supports, i.e. violating the hermiticity of the matrix measure.

The result of the present section actually enables us to analytically solve the bootstrap constraints, since the infinite series of inequalities from the positivity of the correlation matrix have been proven to be equivalent to the positivity property of resolvent. As an example, in the next subsection we will present the analytic result of solving the bootstrap problem of quartic one-matrix model.

The application of numerical bootstrap to the multi-matrix models, such as the one studied in Section 5, has not as strong theoretical basis as the one presented in this section for the one-matrix model. However the arguments presented here give a good intuition why the numerical bootstrap can work even in the multi-matrix model case. In the following sections we will demonstrate its viability empirically, by showing its numerical efficiency for a specific, "unsolvable" matrix model.

3.2 Classification of physical solution of quartic one-matrix model

In Fig 2, we saw that as we increase Λ the allowed region converges to the analytic solution. One may ask whether the allowed region will ultimately exclude all other solutions as Λ

---

[14]We note that the uniqueness is not strictly necessary here. To see this, the reader can combine Stone-Weierstrass theorem and the fact that compactly supported continuous function is dense in L_p, $1 \leq p < \infty$. Then if $\rho(x)\mathrm{d}x$ is not positive almost everywhere then the positivity of correlation matrix is violated.

increases, or it will stabilize to a very tiny island which will not shrink further. The results of the current section will support the first of these options.

In this section, we will apply the positivity of resolvent to the one-matrix model with quartic potential

$$V(x) = \frac{1}{2}\mu x^2 + \frac{1}{4}g x^4 \tag{3.6}$$

in order to fully classify all physical solutions. This is equivalent to solving the positivity condition of one-matrix bootstrap analytically. Since in the previous subsection we have already formulated this problem as a precise mathematical theorem, we will not present the formal mathematical derivation here. For the details the reader can refer to the Appendix B.

For the bootstrap problem we are trying to solve, we will not assume the $\mathbb{Z}_2$ symmetry of the solutions. This symmetry would mean $\mathcal{W}_{2k+1} = 0$. We will see that there exist solutions that break this symmetry. In fact, for solutions we find numerically the breakdown or preservation of $\mathbb{Z}_2$ symmetry will be established dynamically and not necessarily imposed as an input. Alternatively, if we assume $\mathbb{Z}_2$ symmetry from the beginning, the numerical efficiency for such solutions considerably increases.

For the specific potential (3.6) the positivity condition for the resolvent

$$\begin{aligned}
G(x) &= \frac{1}{2}(V'(x) - \sqrt{V'(x)^2 - 4P(x)}) \\
&= \frac{1}{2}\left(-\sqrt{-4g(\mathcal{W}_2 + x(\mathcal{W}_1 + x)) + (gx^3 + \mu x)^2 - 4} + gx^3 + \mu x\right)
\end{aligned} \tag{3.7}$$

translates into the condition that it has a only real positive eigenvalue distribution. This condition can be solve rigorously, namely:

1. $\mu = 1$ and $g \geq -\frac{1}{12}$: $\mathcal{W}_1 = 0$, $\mathcal{W}_2 = \frac{(12g+1)^{3/2}-18g-1}{54g^2}$.

2. $\mu = 1$ and $g < -\frac{1}{12}$, there is no possible solution.

3. $\mu = -1$ and $g \leq 0$, there is no possible solution.

4. $\mu = -1$ and $g \geq \frac{1}{4}$: $\mathcal{W}_1 = 0$, $\mathcal{W}_2 = \frac{(12g+1)^{3/2}+18g+1}{54g^2}$.

5. $\mu = -1$ and $0 < g < \frac{1}{4}$: This situation is a bit involved. The bootstrap solution is a curve segment parametrized by $\mathcal{W}_1$. Explicitly, the solution is a branch of the algebraic equation:

$$\begin{aligned}
0 =\ & 11664g^6 \mathcal{W}_2^5 + \left(-27216g^5 - 864g^4\right)\mathcal{W}_2^4 + \mathcal{W}_2^3\left(-16200g^5\mathcal{W}_1^2 - 13824g^5 + 19872g^4 + 1440g^3 + 16g^2\right) + \\
& \mathcal{W}_2^2\left(\left(43200g^5 + 33480g^4 + 888g^3\right)\mathcal{W}_1^2 + 23040g^4 - 3232g^3 - 544g^2 - 16g\right) + \\
& \mathcal{W}_2\left(\left(4125g^4 - 22500g^5\right)\mathcal{W}_1^4 + \left(-65280g^4 - 24568g^3 - 1480g^2 - 16g\right)\mathcal{W}_1^2 + 4096g^4 - 8704g^3 - 1072g^2 - 32g\right) \\
& + 3125g^5\mathcal{W}_1^6 + \left(18500g^4 - 3925g^3 - 16g^2\right)\mathcal{W}_1^4 + \\
& \left(-1024g^4 + 22848g^3 + 7096g^2 + 608g + 16\right)\mathcal{W}_1^2 - 4096g^3 - 512g^2 - 16g.
\end{aligned} \tag{3.8}$$

The physical branch of solution is selected by the one passing through $\mathcal{W}_1 = 0$, $\mathcal{W}_2 = \frac{1}{g}$,[15] with $-\mathcal{W}_{1c} \leq \mathcal{W}_1 \leq \mathcal{W}_{1c}$.

---

[15] Actually for $\mu = -1$ and $0 < g \leq \frac{1}{4}$, the $\mathbb{Z}_2$ symmetry preserving solution is just $\mathcal{W}_1 = 0$, $\mathcal{W}_2 = \frac{1}{g}$. So the first discontinuity of $\mathcal{W}_2(g)$ at $g = 1/4$ happens for second derivative.

For $0 < g \leq \frac{1}{15}$,

$$\mathcal{W}_{1c} = \frac{2\sqrt{4500g^2 + 75g - 2(1 - 15g)^{3/2}(60g + 1) + 2}}{75\sqrt{5}g^{3/2}},$$ (3.9)

and for $\frac{1}{15} < g < \frac{1}{4}$,

$$\mathcal{W}_{1c} = \frac{2\sqrt{12000g^2 + 1200g - \sqrt{3}(20g + 7)^{3/2}(60g + 1) + 102}}{75\sqrt{5}g^{3/2}}.$$ (3.10)

This reproduces the exact solution of quartic one-matrix model. In Fig 2 we have already compared the exact solution and the numerical bootstrap result for $\mu = 1$. A typical comparison for $\mu = -1$ case is Fig 3.

In Fig 3 we take a representative from each phase and compare it with the above analytic solutions. We see that the numerical bootstrap results converge quickly to the analytic result. A distinguishable feature of these figures is that the allowed region is not guaranteed to be convex. This is very different from the convex optimization problems which we encountered in CFT bootstrap and S-matrix bootstrap. Generally, the large-scale non-convex problem is hard and usually unsolvable. We will discuss in the next section how to overcome this difficulty.

3.3   Comments

Here we present several comments on the results of this section:

1. There may exist certain doubts on particular choices of the positivity condition of the correlation matrix in numerical bootstrap. In the work [28, 30], the authors showed that in some cases one only needs the positivity of even moments $\mathcal{W}_{2k} \geq 0$ to make bootstrap converging to the analytically known solution. But in general one should be careful about the choices of the positivity condition. For example, consider the model with $V(x) = -\frac{1}{2}x^2 + \frac{1}{4}x^4$. Under the assumption of the $\mathbb{Z}_2$ symmetry, the loop equations of this model read:

$$\mathcal{W}_{2k} = \mathcal{W}_{2k-2} + \sum_{l=0}^{k-2} \mathcal{W}_{2l}\mathcal{W}_{2k-4-2l} \quad k = 2, 3, 4, ...$$ (3.11)

We see that the positivity condition on even moments only provides us with the constraint $\mathcal{W}_2 \geq 0$, evident by induction in loop equations. In this situation we can bootstrap the physical solution only with the positivity condition on the full correlation matrix. This fact explains to some extent why the convergence in Fig 3 is not as fast as for the model with positive quadratic coefficient.

2. For the one-matrix integral with integration over the unitary matrix instead of the Hermitian matrix, we can establish and justify a similar bootstrap method. This enables us with the analytic solution of such bootstrap problems. The main difference in this case comparing to the Hermitian integral is that the correlation matrix is of
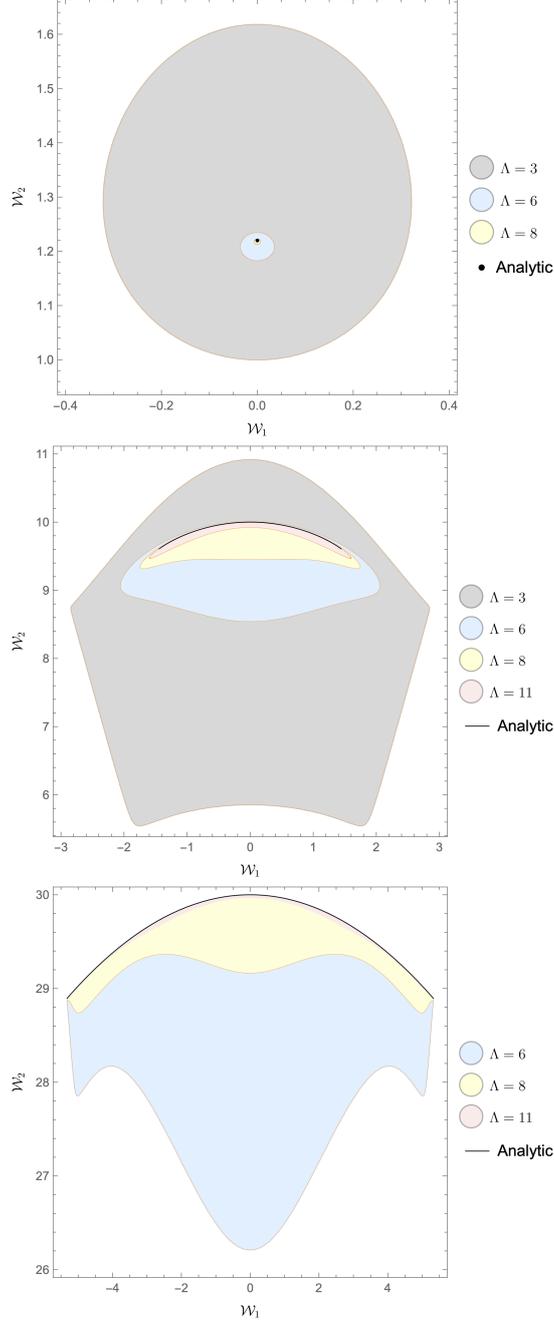
Figure 3: The comparison of numerical bootstrap with our analytic bootstrap results (the black point or the black curve on the figures) in Section 3.2 with $\mu = -1$ in potential (3.6). They are representatives from different phases of the model, with $g = 1, \frac{1}{10}, \frac{1}{30}$ (for the figures from above to below, respectively). We notice even visually that for $g < \frac{1}{4}$ i.e. when the symmetry breaks, the exact solution is a non-convex set.

the form $\mathbb{W}_{ij} = \mathcal{W}_{i-j}$. It is called the Toeplitz matrix in linear algebra[16]. For this

---

[16]For the Hermitian integral the correlation matrix is of the form of the Hankel matrix.

correlation matrix, we have the following result of solution, this time for trigonometric moment problem:

For a given series of real numbers $\{m_n\}_{n=-\infty}^{\infty}$ such that $m_{-k} = m_k^*$, there exists a positive Borel measure μ on $[0, 2\pi]$ such that:

$$m_n = \frac{1}{2\pi} \int_0^{2\pi} \exp(-int) \mathrm{d}\mu(t) \tag{3.12}$$

if and only if the matrix $T_{ij} = m_{i-j}$ is positive semi-definite.

Applying this result to our unitary matrix integral, we come to the conclusion that the positivity of correlation matrix for large N unitary matrix integral is equivalent to the positivity of the eigenvalue density which is supported on the unit circle in the complex plain.

4   Relaxation bootstrap method

Now we turn to the discussion of the bootstrap method for multi-matrix models. We will see that a naive generalization of the previous one-matrix model bootstrap will lead to a Non-linear SDP [17]. But it is widely known that a general large-scale Non-linear SDP cannot be solved efficiently. In this section we will propose a systematic numerical bootstrap procedure to solve the large N multi-matrix models via SDP.

SDP, unlike the Nonlinear-SDP which is directly applicable in the case of large N matrix model bootstrap [28, 30], has a long history in academic research as well as in applied sciences. The standard primal form of SDP is[18]:

$$
\begin{aligned}
\text{minimize} \quad & \sum_{i=1}^{m} c_i x_i \quad \text{w.r.t. } \{x_1, x_2, \ldots, x_m\} \in \mathbb{R}, \\
\text{subject to} \quad & \sum_{i=1}^{m} \boldsymbol{F}_i x_i - \boldsymbol{F}_0 \succeq 0, \qquad \boldsymbol{F}_i \in \mathcal{S}^n.
\end{aligned}
\tag{4.1}
$$

Here $\mathcal{S}^n$ denotes the space of $n \times n$ real symmetric matrices. As long as we can transform our bootstrap problem to the form (4.1), we can get rigorous bounds on the physical quantities of interest – linear functions of $\{x_1, x_2, \ldots, x_m\}$ – by efficiently solving the SDP problem (4.1).

So the problem reduces to the question how to efficiently transform our matrix integral problem into the constraints of the form (4.1). Then the original physical problem is transformed into a purely numerical SDP problem.

In this section we will describe our relaxation bootstrap method on the example of single trace moments in a large N two-matrix model with the partition function[19]:

$$Z = \lim_{N \to \infty} \int d^{N^2} A \, d^{N^2} B \, \mathrm{e}^{-N \mathrm{tr} V(A,B)} \tag{4.2}$$

---

[17]SDP means semi-definite programming

[18]There exists also the dual form of these problems, which will be discussed in Appendix C. We also note that in some literature different conventions for dual and primal for SDP are used.

[19]The generalization to multi-matrix models with more matrices is straightforward.

where $V(A, B)$ is assumed to be a so far general polynomial in A and B, to make the loop equations more tractable. In the next section we will apply it to a model with a concrete potential, generally unsolvable by the known analytic methods. We will see that our method has four types of constraints: loop equations, global symmetries, positivity of correlation matrix and positivity of relaxation matrix (which will be explained later).

4.1 Physical constraints

To make this section as self-contained as possible, we briefly review here the terminology already introduced in the previous sections and show how the constraints of the type (4.1) are specified in the two-matrix model.

The positivity of correlation matrix is still at the heart of our method. Since we are doing numerical analysis, we set the cutoff 2Λ to the length of operators that we are considering, i.e. to the length of "words" built from two "letters" – the matrices A and B: $\mathcal{O} = ABBAAAB\ldots$. For any word $\mathcal{O}$ of the length$\leq \Lambda$, we assume:

$$\langle \text{Tr}\mathcal{O}^\dagger \mathcal{O}\rangle \geq 0. \tag{4.3}$$

The set of words with length$\leq \Lambda$ is a vector space spanned by all the words constructed from two letters with the length cutoff Λ. This is a set of $L = 2^{\Lambda+1} - 1$ elements which we denote as $\mathcal{O}_i$, where i runs from 1 to $L = 2^{\Lambda+1} - 1$. For example, when $\Lambda = 2$ the basis of this vector space reads:

$$I, \ A, \ B, \ A^2, \ AB, \ BA, \ B^2. \tag{4.4}$$

We can expand the equation (4.3) w.r.t. this base:

$$\langle \text{Tr}(\sum_{i=1}^{L} \alpha_i \mathcal{O}_i)^\dagger (\sum_{i=1}^{L} \alpha_i \mathcal{O}_i)\rangle = \boldsymbol{\alpha}^{\text{T}} \mathcal{M}_L \boldsymbol{\alpha} \geq 0. \tag{4.5}$$

Let us introduce the correlation matrix $\mathcal{M}_{Lij} = \langle \text{Tr}\mathcal{O}_i^\dagger \mathcal{O}_j\rangle$ which consists of expectation values of operators with the lengths up to 2Λ. Since (4.3) is true for all operators, the condition (4.5) holds for all $\boldsymbol{\alpha} \in \mathbb{R}^L$, i.e. the semi-definite positivity of correlation matrix is ensured:

$$\mathcal{M}_L \succeq 0. \tag{4.6}$$

This correlation matrix condition can be directly applied to the two-matrix model. We see that the main difference with the one-matrix model is that the dimension of correlation matrix grows exponentially with Λ.

Another important ingredient for our bootstrap method is the loop equations. For the two-matrix model it can be schematically represented as:

$$\int d^{N^2}A\, d^{N^2}B \ \text{tr}(\partial_M(\text{Word} \times e^{-N\text{tr}\,V(A,B)})) = 0, \qquad M = \{A, B\} \tag{4.7}$$

where "Word" means the matrix word built by arbitrary finite product of matrices A and B.[20] The differentiation ∂_M can be either w.r.t. the matrix A or w.r.t. the matrix B.

---

[20]Note that "word" is not yet traced, so that generically it is not cyclically symmetric: a cyclic transformation gives in general a new word.

The loop equations for large N multi-matrix model in general close on *all* words.[21] Schematically, they have the following quadratic form:

$$\langle \mathrm{Tr}\,(\mathrm{Word}_l \times \partial_M V(A,B))\rangle = \sum_{l_1=1}^{l} \langle \mathrm{Tr}\,\mathrm{Word}_{l_1-1}^{(M)}\rangle \cdot \langle \mathrm{Tr}\,\mathrm{Word}_{l-l_1}^{(M)}\rangle \tag{4.8}$$

which is a direct generalization of (2.7) of the one-matrix model. Here Word_{l_1-1} and Word_{l-l_1} are the words obtained by cutting the word Word_l in two words whenever one has the matrix M on the l_1-th place in Word_l. The matrix factor $\partial_M V(A,B)$ in the l.h.s. comes from the derivative of the exponential factor in (4.7), which generically renders a sum over single trace operators with lengths from l_1 to $l_1 + d$ (the degree of polynomial $V(A,B)$ is assumed to be $d+1$). So we expect that a loop equation of length l_1 involves quadratic relations of operators with lengths up to $l_1 + d$. In the next section we will precise all these steps on a particular example of the two-matrix model.

The set of all loop equations can be efficiently generated by applying the derivatives in $M = \{A, B\}$ to any word of the length less than a certain cutoff[22]. However, the loop equations obtained in this way are not all independent, which means that there may exist linear dependence and/or algebraic dependence among them. It turns out that these redundancies are numerically crucial when applying the SDP solver to the constraints of our system, but they are not important at this stage of explanation. We will discuss these technicalities in Appendix D.

If the model has some discrete symmetries, such as $M \to -M$ or $A \leftrightarrow B$, it is not necessary to assume them from the beginning in our bootstrap scheme, but factoring it out will significantly increase our numerical efficiency if we are only interested in the symmetry preserving solution. Generally, the symmetry assumptions not only simplify the loop equation by reducing the number of operators[23] but in certain cases they make the correlation matrix block diagonal, thus greatly simplifying our problem. We will encounter this situation in the next section for a concrete model.

At last, we identify all the operators related by cyclicity of trace and the reversion of the word. These transformations also reduce considerably the number of unknowns in our scheme.

In summary, for the two-matrix integral (4.2), assuming the global symmetries or not, we set up all the physical constraints. A natural question is what is the solution of these constraints. But this is not a good question since generally, apart from some solvable models where the loop equations close on a very limited subclass of operators (like in a two-matrix model [42, 43] or some n-matrix models [6, 19, 20]), the number of operators grows faster than the number of constraints, which means that the solution is a region in an extremely high dimensional space. A constructive question at this stage is: given a cutoff to the length $\leq 2\Lambda$, what is the minimal or maximal possible value of a physical quantity? This

---

[21]Here we mean that there is generally no infinite subset of loop equations and operators closed among themselves. This fact will be explored further in Section F.

[22]We will discuss the detail of the choice of the cutoff in the Appendix D.

[23]For example, if the potential has $\mathbb{Z}_2$ symmetry $A \leftrightarrow B$, we could identify all the operators identical by $A \leftrightarrow B$ transformation.

amounts to asking what is the allowed interval when the region allowed by the constraints is projected on the linear subspace corresponding to the specific physical quantity.

Rephrasing it in the language of optimization theory, we deal with the problem of the form:

$$\begin{aligned} \text{minimize} \quad & c^{\mathrm{T}}x \\ \text{subject to} \quad & x^{\mathrm{T}}\mathcal{A}_i x + b_i^{\mathrm{T}} x + a_i = 0 \quad (i\text{'th loop equation}), \\ \text{and} \quad & M_0 + \sum_{j=1}^{L} M_j x_j \succeq 0 \end{aligned} \tag{4.9}$$

where c is a vector defining the dynamical quantity we want to optimize and x is the column vector of all our operator expectations $x_i = \langle \mathrm{Tr}\mathcal{O}_i \rangle$, up to the length 2Λ. The quadratic loop equation (in the middle) is written in the vector form, where $\mathcal{A}_i$ is the quadratic form encountered in the ith equation; linear and constant terms are represented accordingly. The matrix inequality is the expansion of the correlation matrix in terms of the operator expectations. This is certainly not equivalent to the standard SDP which we introduced by (4.1) since the quadratic equations represent non-convex conditions. One of the conventional methods to deal with it is relaxation.

4.2   Relaxation matrix

The constraints discussed in the last section define a problem which is called Non-Linear SDP in optimization theory. There are indeed some solvers specialized for it but, from our limited trials, they are not mature enough to solve large-scale problems such as the ones we encountered in matrix bootstrap. To improve the situation, we propose to modify the problem (4.9) by relaxing the non-convex conditions involving the non-linear loop equations, into convex ones. Our intuition here is that we don't really need all of the loop equation constraints for our bootstrap method to converge as Λ increases.

To see how our method works, let us begin with a simple example which will provide us with a heuristic argument. Suppose we have only three quadratic "loop equations":

$$\begin{cases} x^2 = T_1 \\ y^2 = T_2 \\ xy = T_3 \end{cases} \tag{4.10}$$

Here $T_i = \sum_j q_i^j w_j$, $(i = 1,2,3)$ denote linear combinations of some other variables $w_1, w_2, \dots$. These equations are of course non-convex. But we can relax them to make them convex by replacing $x^2 = T_1$ with $x^2 \leq T_1$ or, in the positive semi-definite matrix form,

$$\begin{pmatrix} 1 & x \\ x & T_1 \end{pmatrix} \succeq 0 \,. \tag{4.11}$$

We can do the same thing with the second equation $y^2 = T_2$, to relax it to a convex condition. But the same operation cannot be reproduced for equation $xy = T_3$, since

neither $xy \leq T_3$ nor $xy \geq T_3$ is convex [24]. It is tempting to consider the positive semi-definite combinations:

$$(x + \alpha y)^2 \leq T_1 + \alpha^2 T_2 + 2\alpha T_3, \; \forall \alpha \in \mathbb{R}. \tag{4.12}$$

It is not very elegant to implement (4.12) by introducing extra parameters like α, although numerically this is viable. Can we write instead of (4.12) a condition that does not contains explicitly α? In fact yes. Since $T_1 \geq x^2 \vee T_2 \geq y^2$, we only need the discriminant of (4.12) w.r.t. α to be non-positive, to exclude the existence of real solution for α when (4.12) becomes an equality. That means

$$\left(T_1 T_2 - T_1 y^2 - T_2 x^2 - T_3^2 + 2T_3 xy\right) \geq 0 \tag{4.13}$$

is equivalent to (4.12) for all $\alpha \in \mathbb{R}$. In its turn, it is equivalent to:

$$\mathrm{Det} \begin{pmatrix} 1 & x & y \\ x & T_1 & T_3 \\ y & T_3 & T_2 \end{pmatrix} \geq 0. \tag{4.14}$$

Combining (4.11) and (4.14) we come to the conclusion that:

$$\begin{pmatrix} 1 & x & y \\ x & T_1 & T_3 \\ y & T_3 & T_2 \end{pmatrix} \succeq 0. \tag{4.15}$$

This is mathematically more elegant and numerically more efficient.

To apply this relaxation method to the case of our loop equations is a simple generalization of what we just proposed. We make in the loop equation the substitution $\langle \mathrm{Tr} \mathcal{O}_i \rangle \langle \mathrm{Tr} \mathcal{O}_j \rangle = X_{ij}$, or in matrix notations:

$$X = xx^{\mathrm{T}} \tag{4.16}$$

where again x is the column vector whose components are $\langle \mathrm{Tr} \mathcal{O}_i \rangle$. Formally, this changes the loop equations in (4.9) to a linear form:

$$\mathrm{Tr} X \mathcal{A}_i + b_i^{\mathrm{T}} x + a_i = 0. \tag{4.17}$$

To apply the relaxation method sketched above, we relax (4.16) by imposing the inequality:

$$(\alpha^{\mathrm{T}} x)^2 \leq \alpha^{\mathrm{T}} X \alpha, \quad \forall \alpha \in \mathbb{R}^L \tag{4.18}$$

which is equivalent to:

$$X \succeq xx^{\mathrm{T}}. \tag{4.19}$$

By Schur's complement, this can be re-arranged into a more compact form:

$$\mathcal{R} = \begin{pmatrix} 1 & x^{\mathrm{T}} \\ x & X \end{pmatrix} \succeq 0. \tag{4.20}$$

---

[24]Because the bilinear form xy is not positive semi-definite.

Here we introduced the relaxation matrix by $\mathcal{R}_{ij} = X_{ij}$ and $\mathcal{R}_{0i} = \mathcal{R}_{i0} = \langle \mathrm{Tr}\mathcal{O}_i \rangle = x_i$. This step concludes our translation of the nonlinear bootstrap problem into an SDP. This SDP takes now a numerically much more tractable, convex form:

$$
\begin{aligned}
\text{minimize} \quad & c^{\mathrm{T}}x \\
\text{such that} \quad & \mathrm{Tr}X\mathcal{A}_i + b_i^{\mathrm{T}}x + a_i = 0 \,, \\
\text{and} \quad & M_0 + \sum_{j=1}^{L} M_j x_j \succeq 0 \,, \\
\text{and} \quad & \begin{pmatrix} 1 & x^{\mathrm{T}} \\ x & X \end{pmatrix} \succeq 0 \,.
\end{aligned}
\tag{4.21}
$$

It has now two types of variables to bootstrap: a column vector variable x and a symmetric matrix variable X.

Several comments are in order:

- One of the primary questions to the method is: does the relaxed SDP generate the same bounds as the previous Non-linear SDP problem? Generally, the answer is "no". It is obvious that when the optimal solution of the relaxed problem satisfies the constraint of the original problem the relaxed problem will generate the same bound as the original one. From our experience, this is not the case for any finite Λ. [25] But as we increase the cutoff Λ, the mismatches for the quadratic conditions are tending to zero. So we are tempted to believe that for infinite Λ, the relaxed problem and the original problem give the same result for most of the questions we are interested in. This indicates that the non-linear constraints in the loop equations are somehow contained in the positivity conditions for correlation matrix and relaxation matrix.

- One can regard our relaxation scheme as a numerical compromise: doing relaxation we replace the nonlinear equalities by linear inequalities but we can thus explore the correlation matrices of a much higher order since we can significantly increase the length cutoff Λ. This enable us to embrace more information from correlation matrix. Our numerical results in the next section will show that this is a worthy trade-off.

- There is another point of view on our relaxation formulation (4.21). The problem (4.21) is actually the dual of the dual of the problem of (4.9). Although this fact is in principle simple to show its proof is quite lengthy, so we put it into the Appendix C. In that appendix, we also briefly review the definition and basic facts about the dual formulation. As it is known, the dual problem of any general optimization problem is always convex [44], so the double dual is guaranteed to be convex. In some sense, this point of view is more general and universal.

---

[25]More precisely, if the relaxation is saturated for the optimal solution, we expect that the relaxation matrix will only have one non-zero eigenvalue. But practically, we always observe multiple non-zero eigenvalues for the relaxation matrix.

- We believe that the key condition for the relaxation method to work well is that, under our bootstrap assumption, there is a unique exact solution.[26] Then since a single point (corresponding to the $\Lambda = \infty$ solution of bootstrap) is convex, our relaxation procedure leading to convex constraints will not make the results too different even for a finite but sufficiently large Λ. However, we observed in Section 3.2 that the set of exact solutions may become non-convex in the presence of a symmetry breaking. In such situation, we need further assumptions to make the exact solution unique. We will further discuss these aspects in the next section when bootstrapping the symmetry breaking solutions.

5 Bootstrap for "unsolvable" two-matrix model with $\mathrm{Tr}[A,B]^2$ interaction

In this section, we implement the relaxation bootstrap method described in the previous section to the case of generically unsolvable large N two-matrix model:

$$Z = \lim_{N \to \infty} \int d^{N^2}A \, d^{N^2}B \, e^{-N\mathrm{tr}\left(-h[A,B]^2/2 + A^2/2 + gA^4/4 + B^2/2 + gB^4/4\right)} \tag{5.1}$$

where the integration goes over Hermitian matrices A and B. This model is unsolvable analytically for generic parameters h and g, at least with the known methods, such as reduction to eigenvalues or the character expansion. It is still analytically solvable for some particular values: for $g = 0$ it can be reduced to a specific one-matrix model and solved via saddle point method or via the reduction to a KP equation [34, 45]; for $h = 0$ it reduces to two decoupled one-matrix models; for $h = \infty$ we have $[A, B] = 0$ and it reduces again explicitly to another eigenvalue problem. These particular solvable cases are useful to test the power of our numerical method.

The present section is organized as follows: The bootstrap results for the model (5.1) with particular choice of parameters $g = 1$, $h = 1$ (which represent a generic analytically "unsolvable" example) are shown in Section 5.1. Then in Section 5.2 we compare the bootstrap result for the analytically solvable cases $h = 0$ or $g = 0$ with the corresponding analytic solution, to test our method. In Section 5.3, we explore the phase diagram of the this model and make several comments about the convergence rate in different regions. At last, in Section 5.4, we investigate the symmetry breaking in the model by our relaxation bootstrap method.

5.1 Bootstrap solution for a generic choice of g, h

In this subsection, we present the results of the bootstrap for the model (5.1) where we specify, for definiteness, the parameters: $g = 1, h = 1$. We stress that this choice has nothing specific for the properties of the model and it is made mostly for the demonstrative reasons, as an example of generic values of parameters. The method appears to be very efficient almost everywhere in the physical domain of parameters g, h, except when we approach the critical lines where it is less efficient. We will discuss in the next subsection the phase structure of the model in the $g - h$ plane.

---

[26]Here exact solution means bootstrap solution with infinite cutoff.

The symmetry of this model can be described by the Dihedral Group D_4[27], with generator:

$$\begin{cases} A \to -A \\ B \to -B \\ A \leftrightarrow B \end{cases} \tag{5.2}$$

We saw already on the example of the one matrix model that in the large N limit there could be a multitude of saddle point solutions, many of them breaking this kind of symmetries. We begin with the study of D_4 symmetric large N solutions. Later we will discuss the solutions with broken symmetries as well.

In the fully D_4 symmetric solutions, only the operators with even number of A and even number of B can be non-vanishing, and we should identify the operators under the exchange $A \leftrightarrow B$. Obviously this assumption of D_4 symmetry of solution is in principle not necessary for our bootstrap method to work. However, assuming this symmetry we gain a lot in the efficiency since we are left with approximately $1/8$ of operators comparing to a general non-symmetric setup. It also happens that the symmetry assumption simplifies the correlation matrix by much. Namely, when constructing the correlation matrix, only the words with the same $\mathbb{Z}_2$ parity in both A and B can appear in the inner product for a non-vanishing correlator. So our correlation matrix break into 4 block-diagonal matrices, corresponding to $\mathbb{Z}_2$ parities in A and B: even-even, even-odd, odd-even, odd-odd. By $A \leftrightarrow B$ symmetry, the even-odd and odd-even blocks are actually the same. So the original correlation matrix can be reduced to three block diagonal matrices: even-even, even-odd, and odd-even.

Here we bootstrap the allowed region for the first two non-vanishing operators $t_2 = \langle \mathrm{Tr} A^2 \rangle$, $t_4 = \langle \mathrm{Tr} A^4 \rangle$[28]. According to (4.21), this corresponds to setting the objective function of the optimization problem as:

$$\text{Minimize: } t_2 \cos\theta + t_4 \sin\theta \tag{5.3}$$

Scanning it in the interval $0 \le \theta < 2\pi$ we can fix the allowed region for these two operators. Using the general method described in the last section we can use the SDP solvers to solve these problem. The readers interested in the details of the implementation can refer to the Appendix D, where we gather all the technical detail of numerical implementations. We also demonstrated in Appendix E our numerical procedure explicitly, step by step, on the example of the system with $\Lambda = 4$ cutoff.

Let us demonstrate our results for various values of the length cutoff Λ. We summarized the allowed regions for the first two correlators $t_2 = \langle \mathrm{Tr} A^2 \rangle$ and $t_4 = \langle \mathrm{Tr} A^4 \rangle$ in Fig 4. The regions for $\Lambda = 10$ and $\Lambda = 11$ are too small to be plotted on the figure, so we give here

---

[27]Actually we implicitly assume the $A \to A^{\mathrm{T}}$, $B \to B^{\mathrm{T}}$ which basically means that all the moments are real. We will assume throughout this paper that this symmetry cannot be broken. At least intuitively, this is unlikely to happen in our model 5.1.

[28]Here we give up the $\mathcal{W}_k$ notation for the moments we used in one-matrix model since for two-matrix model the moments cannot be characterize by a single positive number.
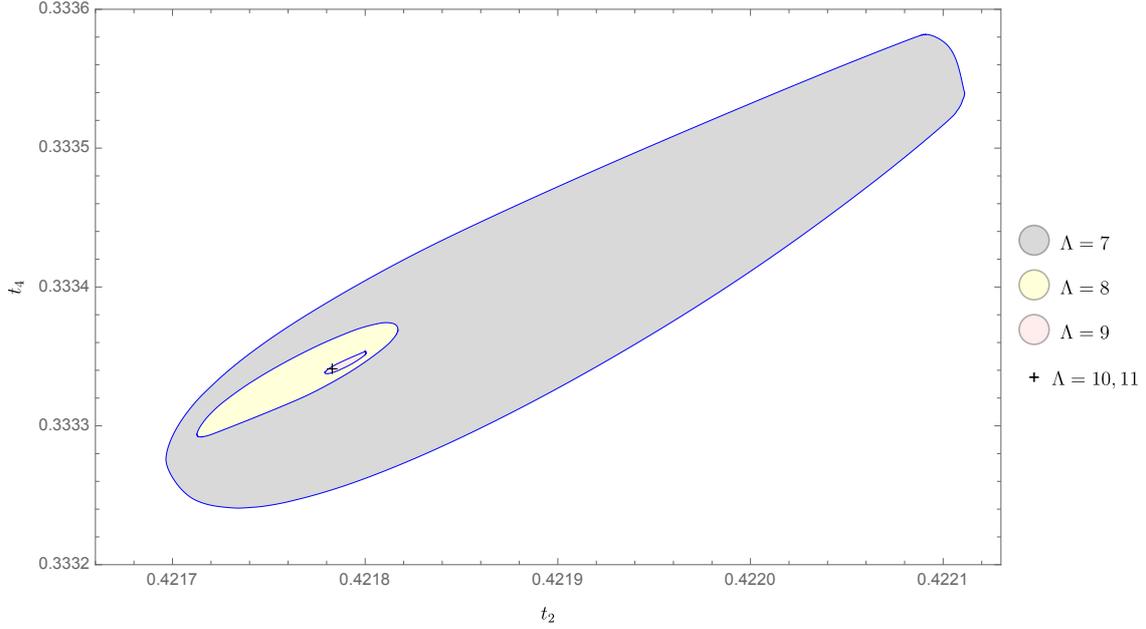
Figure 4: The allowed region of $t_2 - t_4$ of model (5.1) with parameter $g = 1, h = 1$ for the cutoff $\Lambda = 7, 8, 9, 10, 11$. We recall the definition of Λ: the longest operators in the correlation matrix and in the loop equations have the length 2Λ.

the upper and lower bound of t_2 and t_4. For $\Lambda = 10$:

$$
\begin{cases}
0.421780275 \leq t_2 \leq 0.421785491 \\
0.333339083 \leq t_4 \leq 0.333343006
\end{cases}
\tag{5.4}
$$

and for $\Lambda = 11$:

$$
\begin{cases}
0.421783612 \leq t_2 \leq 0.421784687 \\
0.333341358 \leq t_4 \leq 0.333342131
\end{cases}
\tag{5.5}
$$

We see here that for $\Lambda = 11$ we already have a six digits precision at $g = h = 1$. The $\Lambda = 11$ calculation is the largest problem in this work, it is done with SDPA-dd, a solver in SDPA family with the double-double float type. The input to SDPA has 95 variables, with the correlation matrix size: even-even 683, odd-odd 682, even-odd 1365, and with relaxation matrix size 8. We note that this is still within the capability of a single laptop, it only takes $150000s$ CPU time for a single maximization cycle. We also stress that these inequalities, unlike the Monte Carlo methods, are exact: increasing the cutoff Λ we can only improve the margins.

5.2 Demonstration for analytically solvable cases

It is instructive to apply our numerical method to the analytically solvable cases $g = 0$ or $h = 0$, which is a good check for our approach, convincing us that it works well indeed even for the generic parameters, where we have no analytic data to compare with. In this

part we will firstly review the analytic solution for both cases and then compare it with the numerical results of our relaxation bootstrap method.

As we mentioned, for $h = 0$ this model reduces to two decoupled one-matrix models – the case which we already discussed and studied analytically in Section 3.2. Integrating out one of the decoupled matrices, we expect the operator containing only one matrix to have exactly the same expectation value as for the result in Section 3.2:

$$g_c = -\frac{1}{12}, \quad t_2 = \frac{(12g + 1)^{3/2} - 18g - 1}{54g^2}. \tag{5.6}$$

For $g = 0$, this model is already solved analytically in [34, 45]. Here we simply present the analytic solution derived there in our notations and normalization. To have a compact form, we introduce the short-hand notations $E = E(m)$, $K = K(m)$, $\vartheta = E/K$, where K and E are the complete elliptic integrals of first and second kind:

$$K(m) = \int_0^{\pi/2} \frac{\mathrm{d}\theta}{\sqrt{1 - m^2 \sin^2(\theta)}}, \quad E(m) = \int_0^{\pi/2} \sqrt{1 - m^2 \sin^2(\theta)}\mathrm{d}\theta. \tag{5.7}$$

We introduce the new parameter m related with h by:

$$h(m) = \frac{K\left((m - 1) - 2(m - 2)\vartheta - 3\vartheta^2\right)}{6\pi^4}, \tag{5.8}$$

and we can express t_2 as:

$$h(m)t_2(m) = \frac{1}{12} - \frac{K^2\left(-(m - 2)(m - 1) + 10(m - 2)\vartheta^2 + 2((m - 6)m + 6)\vartheta + 10\vartheta^3\right)}{5\pi^2\left(-(m - 1) + 2(m - 2)\vartheta + 3\vartheta^2\right)}. \tag{5.9}$$

This formula is valid when $h > 0$. For $h < 0$, we need to analytically continue the solution to the other sheet of Riemann surface of the variable m. For that we introduce the analytic continuation of the elliptical integral $K(m)$ and $E(m)$:

$$K_a = K_a(m) = \frac{K\left(\frac{1}{m}\right) + iK\left(1 - \frac{1}{m}\right)}{\sqrt{m}},$$

$$E_a = E_a(m) = \frac{-(m - 1)K\left(\frac{1}{m}\right) + iK\left(\frac{m-1}{m}\right) + mE\left(\frac{1}{m}\right) - imE\left(\frac{m-1}{m}\right)}{\sqrt{m}}, \tag{5.10}$$

$$\vartheta_a = E_a/K_a.$$

To make (5.8) and (5.9) valid for $h < 0$, we simply replace all the K, E, ϑ by K_a, E_a, ϑ_a.

The critical point of the smallest possible h_c for $h < 0$ can be defined as the solution of the equation[29]:

$$\frac{dh(m)}{dm} = 0 \tag{5.11}$$

which can be numerically solved as:

$$h_c \approx -0.04965775; \ t_{2c} \approx 1.18960475. \tag{5.12}$$
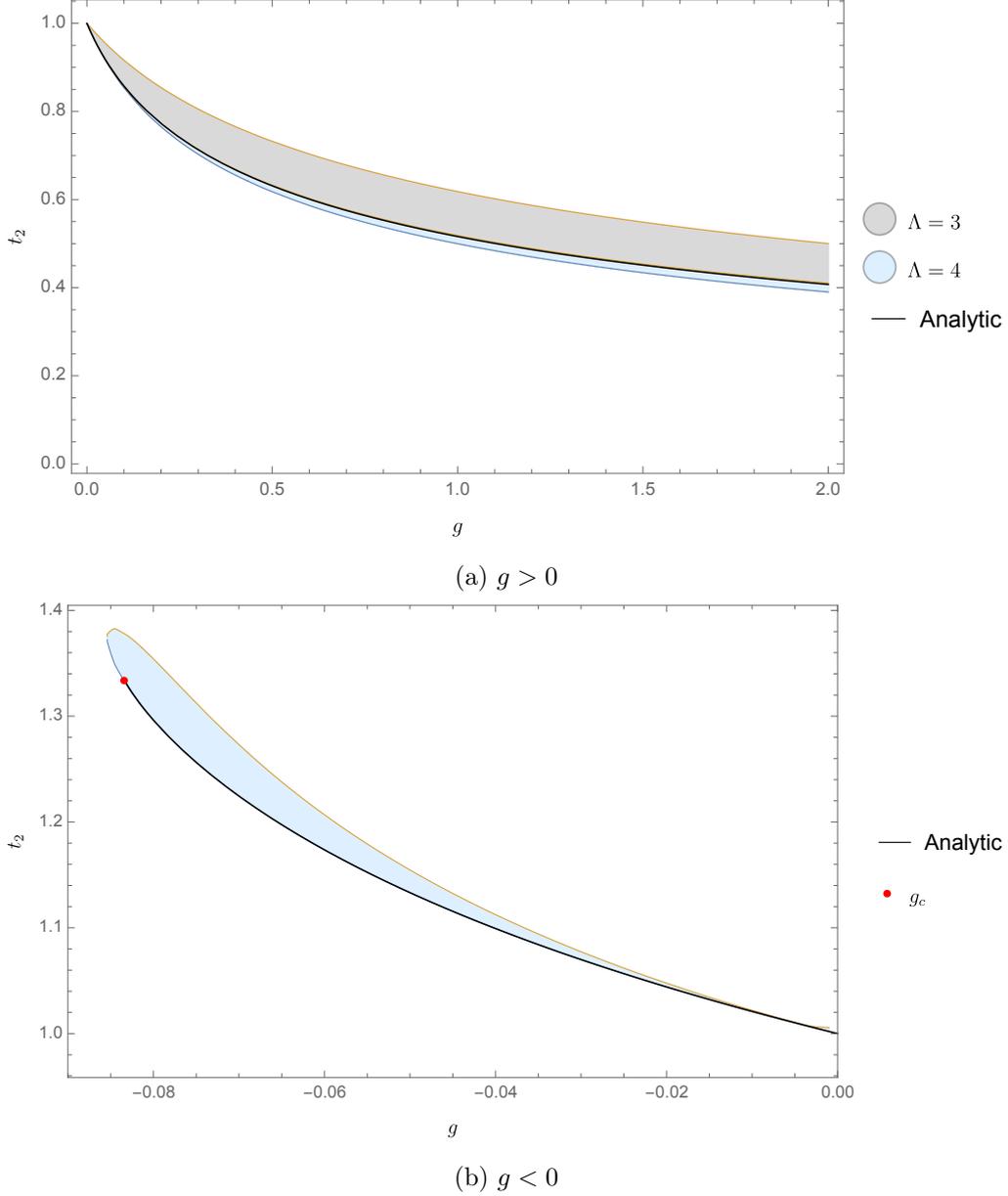
(a) $g > 0$

(b) $g < 0$

Figure 5: Comparison with the exact analytic solution of model (5.1) with $h = 0$, i.e. two decoupled quartic one-matrix model. The lower plot is for $\Lambda = 8$.

The comparison of our numerical results with analytic result is presented on Fig 5 and Fig 6. Indeed, we see that our numerical results nicely agree with the analytic formula (5.6) and (5.9). An apparent feature of these plots is that when $g < 0$ or $h < 0$, the allowed region is much larger than the one for the positive coupling case, thus giving less of precision. In general we have the worst convergence in the neighborhood of critical value. We will discuss this feature in more details in the next subsection.

---

[29]We thank Nikolay Gromov for sharing with us his computation of h_c.
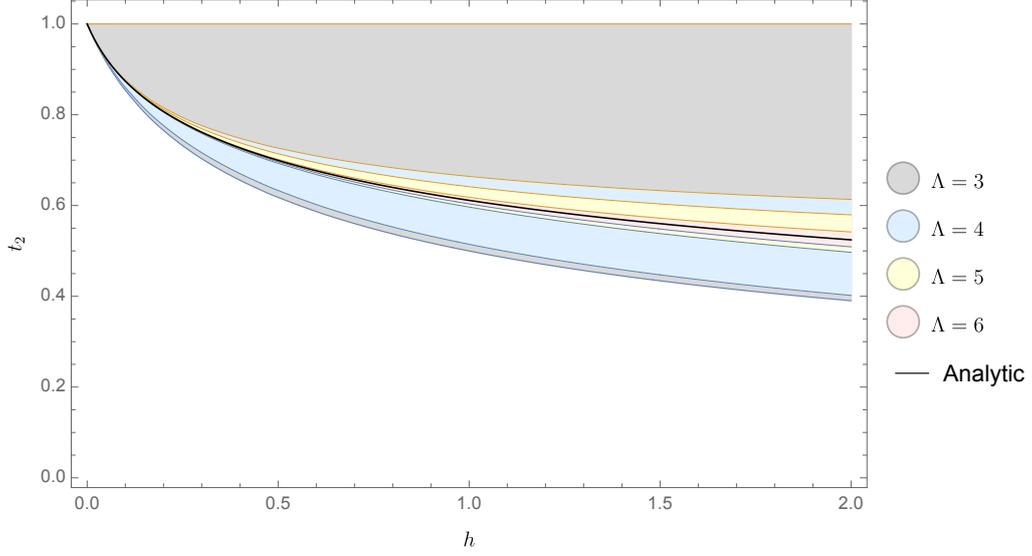
(a) $h > 0$
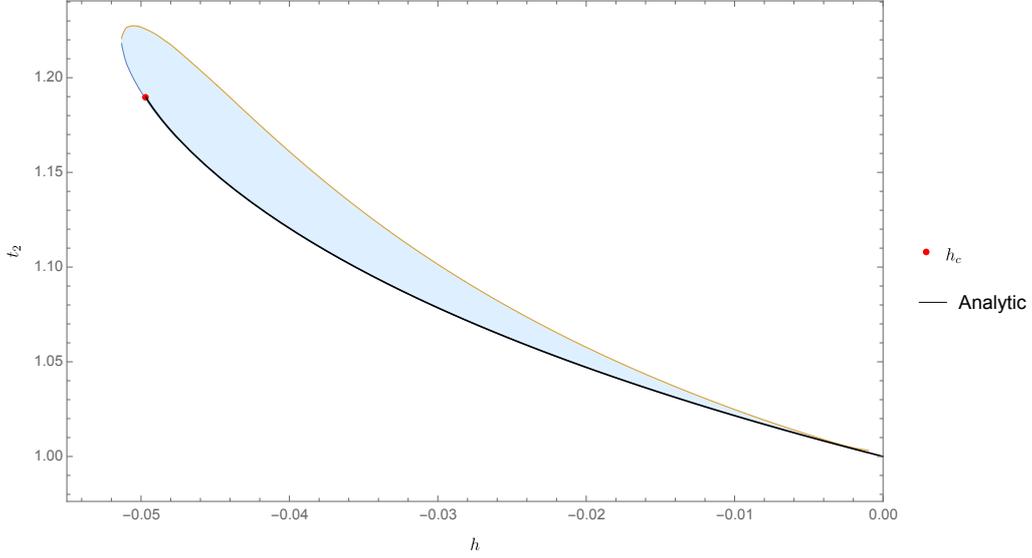
(b) $h < 0$

Figure 6: Comparison of the numerical bootstrap results with the exact analytic solution of the model (5.1) with $g = 0$. The lower plot is for $\Lambda = 8$.

There is another fact which is not obvious from the Fig 5. If we compare this figure with Fig 2 in Section 2 we will find that for same values of Λ, the non-relaxed one-matrix bootstrap bound for t_2 (denoted by $\mathcal{W}_2$ in that section) and our relaxation bootstrap bound for $h = 0$ case of the 2-matrix model actually coincides within the error bar. This is a very striking feature of our relaxation method since we relaxed all the quadratic equalities to inequalities but we compensated this with many more mixed operators of two decoupled matrices. So the correlation matrix is much larger in the relaxed case and the final results

are basically the same. We will see this feature of relaxation again when we discuss later the bootstrapping of the symmetry breaking solutions. We don't have a very clear explanation for these phenomena in general.

5.3   Phase Diagram and convergence rate

In this part, we will discuss the phase diagram of the matrix model (5.1) and the corresponding convergence rate in different regions of the diagram.

In general, for finite N matrix integral the potential $V(A, B)$ must be bounded from below to define a sensible integral over Hermitian matrices. But this is not necessary for a large N theory, where we only need deep enough local minima to have a stable saddle point solution. Even for the unstable potentials, the tunnelling effects between the local minima, or to the infinity are suppressed exponentially. We saw this in Section 5.2, where the bootstrap procedure allowed the existence of solutions with negative values of g and h. This provides us with a possibility to study the boundaries of possible g and h values (we will call the region of possible g and h values the feasible region in the following) even when the corresponding potential is not bounded from below.

Before going deeper into the technicalities of bootstrapping the boundaries of the feasible region, we can get a rough estimate of them by deriving the parameter region of g and h which leads to the matrix potential bounded from below. It is obvious that the domain $(h \geq 0, g \geq 0)$ is one part of the region we are looking for. Another, less obvious part is $(h < 0, g \geq -4h)$, as in this case we should have:

$$
\begin{aligned}
\mathrm{tr}V(A, B) &= \mathrm{tr}\left(-h[A, B]^2/2 + A^2/2 - h(A^4 + B^4) + B^2/2 + (g + 4h)(A^4/4 + B^4/4)\right) \\
&= \mathrm{tr}\left(-h((AB + BA)^2/2 + (A^2 - B^2)^2) + A^2/2 + B^2/2 + (g + 4h)(A^4/4 + B^4/4)\right) \quad (5.13) \\
&\geq 0\,.
\end{aligned}
$$

The union of these two domains represents the maximal region where the matrix potential is bounded from below, since for $(h \geq 0, g < 0)$ and $(h < 0, g < -4h)$ we can always find A, B configurations where the potential is not bounded from below. For $(h \geq 0, g < 0)$, one of these configurations is taking $B = 0$ and $A \to \infty$. For $(h < 0, g < -4h)$, we simply put A and B to be some constants α times generalized Pauli matrices of dimension N $\alpha\sigma_1$ and $\alpha\sigma_2$, where α is a large real number. Then we have:

$$
\mathrm{tr}V(\alpha\sigma_1, \alpha\sigma_2) = N(\alpha^2 + (g + 4h)\alpha^4)\,. \tag{5.14}
$$

This must be unbounded from below when $(h < 0, g < -4h)$.

In conclusion, the region of potential bounded from below is $(g \geq 0 \bigcap g \geq -4h)$. In addition, the domain $(g \geq 0 \bigcap g \geq -4h)$ is guaranteed to lie within the feasible region. But due to the large N effects, we expect the feasible region to be a little bigger than that. Specifically, for analytically solvable cases, when $h = 0$ we have $g \geq -\frac{1}{12}$ and when $g = 0$ we have $h \gtrsim -0.04965775$. These facts give us an additional information about the location of the boundary of the feasible region.

To numerically bootstrap the boundary of the feasible region, we can obtain the critical boundary between the allowed and forbidden parameter regions by bisection. Namely, for

a given Λ we fix h and take two values of g, as g_1 and g_2. Here g_1 is a point that is guaranteed to be forbidden for a given h, and g_2 is a point that is guaranteed to be allowed. Then we test the geometric average value $g_m = \frac{g_1 g_2}{g_1 + g_2}$. If g_m is allowed, then we make the substitution $g_2 = g_m$, otherwise we take $g_1 = g_m$. In this way we can recursively approach the maximal forbidden value of g at fixed h. Then we scan over the values of h and get the plot shown in Fig 7.
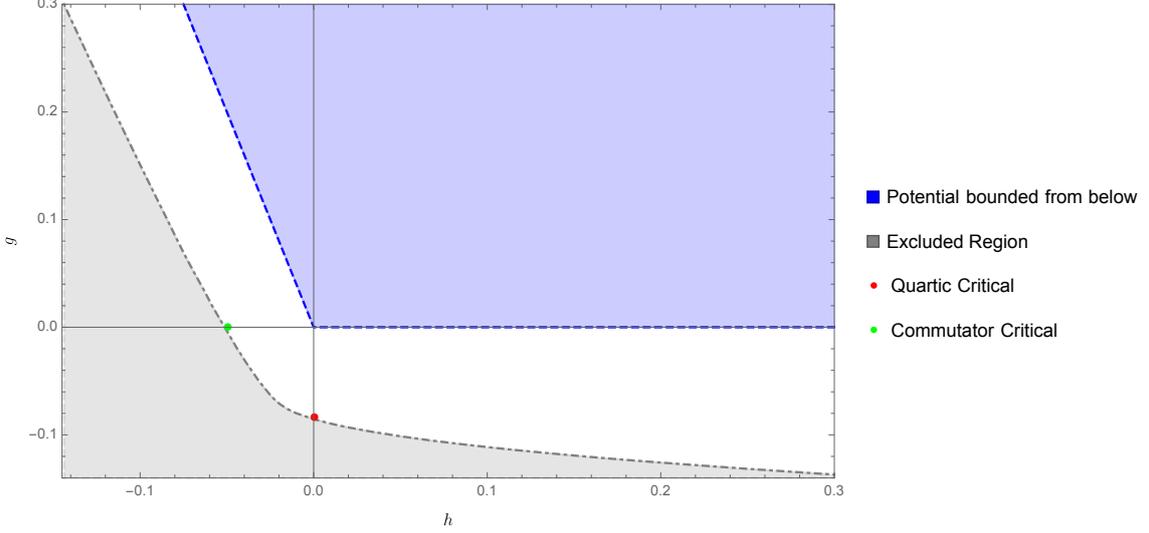

Figure 7: The numerical phase diagram of the model (5.1). The gray region is strictly excluded by our relaxation bootstrap method at $\Lambda = 8$. In the blue region the matrix potential is bounded from below and its boundary is located above the straight lines $g = 0$ and $h = -\frac{1}{4}g$. The red and green dots are the critical valus for $h = 0$ and $g = 0$.

Some explanations for the plot Fig 7 are in order. The gray region is rigorously forbidden as the result of bootstrap at $\Lambda = 8$. On the contrary, the white region is not guaranteed to be allowed for any physical large N solution. As we increase Λ, the gray region will expand a little. But we have several hints about the position of the exact boundary line:

- We notice the red and green dots on the plot, which are the critical points of the analytic solutions. They are located on the exact boundary of feasible region, i.e. no matter how large is Λ, the gray curve cannot go beyond these two points. From this fact we convince ourselves that our numerical curve in Fig 7 is already very accurate, since the red dot and the green dot are very close to the gray curve.

- The blue region is the region where the potential is strictly bounded from below. It is enclosed by the lines $g = -4h$ and $g = 0$. Its boundary can be considered as the exact solution in the "classical" limit $\hbar \to 0$ for this matrix integral, where $1/\hbar$ is the coefficient put in front of the potential. In this case we scale the couplings as $h \to 1/\hbar$, $g \to 1/\hbar$. The boundary of the gray will coincide for $\hbar \to 0$ with the boundary of the blue area on Fig 7. Then inside the blue area we have a well-defined

theory even for finite N. At large N and finite h, g there is a gap between blue region and gray region, as is visible on the Fig 7.

5.3.1 Rate of convergence

As the reader may have noticed already in Section 5.2, when $g < 0$ or $h < 0$ the convergence is very bad compared to the case $g > 0$ and $h > 0$. From our experience, this is a generic situation when we are outside of the blue region in Fig 7, which is defined by the region of parameters yielding a potential bounded from below. For example, Fig 8 depicts the allowed region for t_2 when we fix $g = 1$ and scan over h in the neighborhood of $h = -1/4$. It is clear from this figure that for $h < -1/4$ there is drop in the rate of convergence. Actually, from numerical data, the difference of the upper bound and the lower bound varies between the orders of magnitude from 10^{-4} to around 10^{-2} when h varies from $h = -0.25$ to $h = -0.26$.

Nonetheless we can get a rather accurate estimate of physical quantities in the region discussed in the last paragraph. We note that in Fig 5 and Fig 6, the analytic solution is very close to the lower bound, comparing to the upper bound[30]. Actually, as we increase Λ, the lower bound stabilizes already at rather small Λ. Empirically this is a typical behavior in the unbounded region. Under the assumption that there is a unique solution satisfying the constraint for arbitrarily large Λ, we expect that the optimization results for the maximum and the minimum of t_2 will ultimately converge with increasing Λ to the same value. This has been proven for some parameters of the one-matrix model in Section 3.2, and we have strong numerical evidence to believe it will hold for our model (5.1) as well. So we can simply bootstrap the physical quantities by the minimization of t_2 in this region (in the following, we will call this procedure the minimization scheme as opposed to the maximization scheme). Comparing it to the analytically solvable particular cases we learned that this method can yield especially accurate estimate of physical quantities. However, we lost the rigorous margin in the region with good convergence (blue region in Fig 7). [31]

There exists a region in the phase diagram Fig 7 where the bootstrap is valid only for very high cutoff Λ: it is $g < 0$, $|g| \ll h$. The Fig 9 shows the allowed region when we fix $h = 1$ and vary g. For the lower bound of pink region $\Lambda = 9$, there are some numerical instabilities for $-0.09 < g < 0$. From careful inspection of our data at various values of Λ it seems that the lower bound at $\Lambda = 9$ should stabilize in this region at the value $t_2 \simeq 0.5$ if no numerical instabilities happened in our SDP solver. We notice a few very distinguishable features of this plot:

1. For a fixed Λ, there is a region where t_2 is slightly larger than 0.5 and not bounded from above. In other words, the dual SPD problem for the upper bound is infeasible. In this bad region of parameter space, the bootstrap with such Λ essentially tells us nothing about the right physical values. Luckily, the "bad" region is shrinking when we increase Λ, and hopefully it will disappear when we have a high enough cutoff.

---

[30]We believe that the upper bound and the lower bound converge to the same value, but it seems they have rather different convergence behaviors.

[31]This situation is similar to that of the early days of conformal bootstrap when people used the kink of a plot to estimate the dimension of operators in the 3d Ising model, c.f. [46]
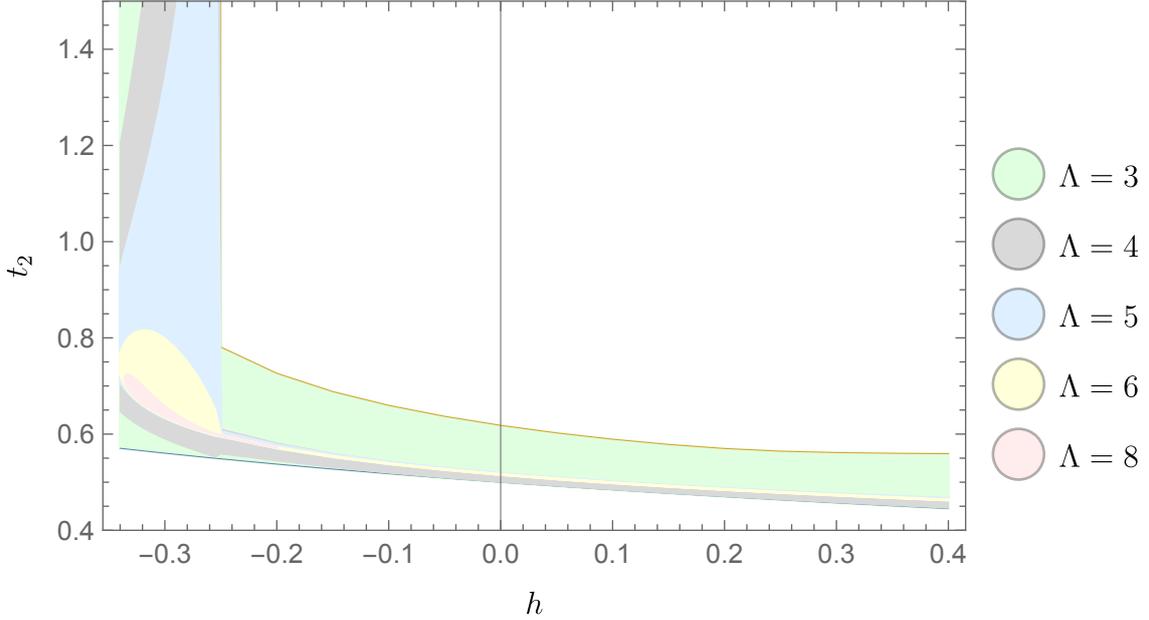
Figure 8: The allowed region for t_2 when we fix $g = 1$ and vary h. In the region where the potential is bounded from below i.e. $h \geq -\frac{1}{4}$, we have a decent convergence whereas for $h < -\frac{1}{4}$ the convergence gets much slower.

2. As already stated in the last paragraph, when we are not in the "bad region", the minimization scheme converges much faster than the maximization scheme. So for a reasonable estimate of the operator expectation we should privilege the minimization scheme.

3. We also notice that for the region $g > 0$, $h > 0$, the convergence is excellent as expected, but there is a huge drop in the rate of convergence in the neighborhood of $h = 0$.

5.4 Bootstrapping the symmetry breaking solution

In the previous parts of this section, we always assumed the global symmetry, or in other words, we bootstrapped the symmetry preserving solutions. Here in the following, we will make the first attempt to study the symmetry breaking solutions with our relaxation bootstrap method. Consequently, in this subsection we will not make assumptions on a specific global symmetry of operator expectations. For example, we will assume that it is possible to have:

$$t_1 = \langle \mathrm{Tr} A \rangle = \langle \mathrm{Tr} B \rangle \neq 0 \tag{5.15}$$

and any other nonzero expectations containing odd number of letter A or B, unlike the solutions with such $A \rightarrow -A$, $B \rightarrow -B$ symmetry.

To understand the general features of symmetry breaking solutions, Fig 3 in Section 3.2 is a good source for our intuition. We see on that figure that the exact solution is not unique
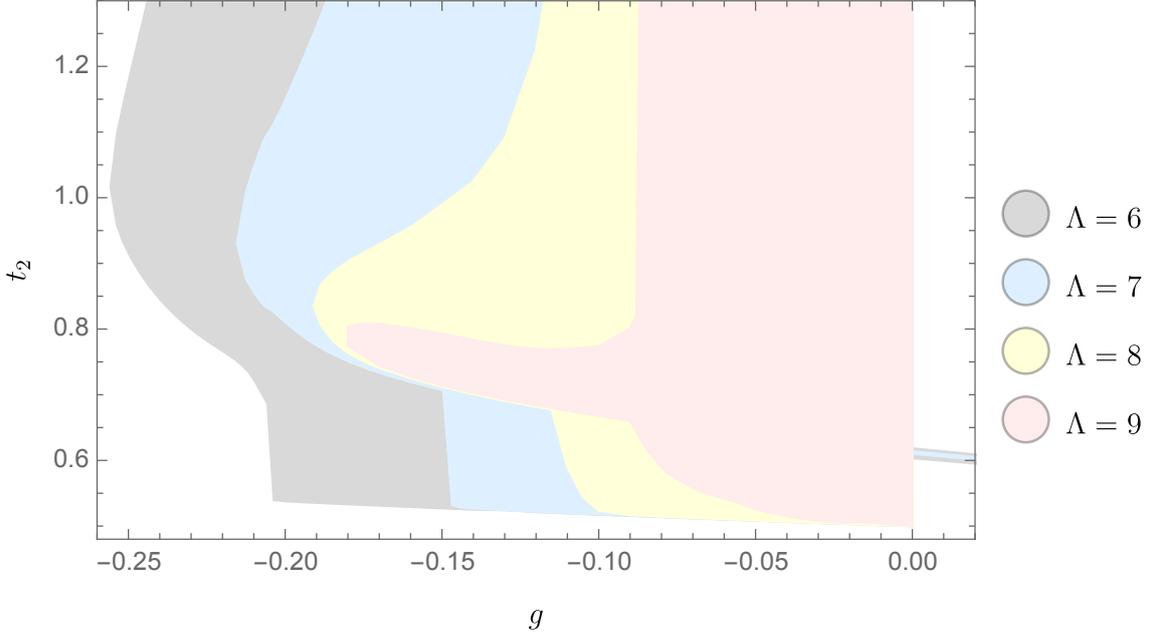
49

Figure 9: The allowed region for the fixed $h = 1$ and varying g. For the lower bound of the pink region $\Lambda = 9$, there are some numerical instabilities at $-0.09 < g < 0$. From careful inspection of our data at various values of Λ it seems that the lower bound at $\Lambda = 9$ should stabilize in this region at the value $t_2 \simeq 0.5$ if no numerical instabilities happened in our SDP solver.

anymore but there is rather a continuous family of solutions parametrized by t_1. This is a non-convex set of exact solutions, so we don't expect that our relaxation bootstrap method, as applied in the case of Fig 4, will converge to such a non-convex set as Λ increases. Namely, if we impose the relaxation bootstrap constraint without the assumption of $A \to -A$, $B \to -B$ symmetry, then minimize the value of

$$t_1 \cos\theta + t_2 \sin\theta \tag{5.16}$$

and then scan over θ in $[0, 2\pi)$, we expect to get a convex set instead of the non-convex one, due to the convex nature of the relaxation method.

So to bootstrap the symmetry breaking solutions, new techniques are needed to tackle the non-convexity. We will describe the general method for bootstrapping solutions and then we apply it to the study of our model (5.1).

5.4.1 Schemes for symmetry breaking bootstrap

The main problems in the study of symmetry breaking solutions in the multi-matrix model of the type considered here are:

1. How to identify the range of parameters for which the model has a possible symmetry breaking solution?

50

2. How to numerically bootstrap the symmetry breaking solution?

The answer to the first problem is quiet straightforward. We can establish the relaxed constraint without the symmetry assumption, and bootstrap a dynamical quantity which signals the symmetry breaking. For example, for the $A \to -A$, $B \to -B$ symmetry breaking solution we take the objective function ($c^{\mathrm{T}}x$ in (4.21)) as:

$$t_1 = \langle \mathrm{Tr}A \rangle \tag{5.17}$$

and for the $A \leftrightarrow B$ symmetry breaking we take the objective function as[32]:

$$\langle \mathrm{Tr}A^2 \rangle - \langle \mathrm{Tr}B^2 \rangle. \tag{5.18}$$

If the bound of the symmetry breaking expectation is significantly larger than the error bar at the current Λ for a given value of parameters, we believe that this is a strong signal of existence of a symmetry breaking solution.

For the second problem, we propose to transform the non-convex set of exact solutions to a convex one, which means that for the case of Fig 3 we fix t_1 by $t_1 = t_1^{(0)}$ in our bootstrap procedure. For this particular value of t_1 we should have at infinite cutoff Λ a unique exact solution for t_2 and for other higher moments, which is definitely a convex set. Therefore our relaxation bootstrap method with a finite cutoff Λ will yield a rigorous upper bound and lower bound for t_2. Next we scan over $t_1^{(0)}$ until such values that the problem becomes infeasible. In this way we get the allowed region in t_1, t_2 plane.

The above method is easily generalizable to the problem of bootstrapping solutions with the other symmetry breaking patterns. Namely, we establish the bootstrap scheme by fixing the dynamical quantity signaling the symmetry breaking, and then we bootstrap the quantities we are interested in. At this step, we expect that after fixing such dynamical quantity, the exact solution of the bootstrap problem is unique. At the next step, we scan over all possible values of the quantity which was fixed in the previous step. In this way we can bootstrap a non-convex set of solutions.

There is another possibile solution for the first problem, i.e. to locate the symmetry breaking region. We can assign to the dynamical quantity signaling the symmetry breaking a specific value and then use the method similar to that of Section 5.3, i.e. using a bisection to approach the maximal possible value of expectation signaling the symmetry breaking. In principle this bisection method could have given us a tighter bound than our initially proposed method. However, from our test, the two methods yield basically the same numerical result, so we will not bother to use the bisection method in what follows.

5.4.2 Numerical results for symmetry breaking solution

Here we apply the method proposed above to the model (5.1). Our results in this part concern the breaking of the following symmetries:

$$A \to -A, \ B \to -B \tag{5.19}$$

---

[32]Here in these two situations the dynamical quantity signaling the symmetry breaking is respectively $\langle \mathrm{Tr}A \rangle$ and $\langle \mathrm{Tr}A^2 \rangle - \langle \mathrm{Tr}B^2 \rangle$.

and

$$A \leftrightarrow B. \tag{5.20}$$

In the bootstrap setup, we don't impose the global symmetry assumptions for the corresponding symmetries, i.e. that the non-singlet operator expectations of the $\mathbb{Z}_2$ symmetry vanish. Then we pick up the dynamical quantities signaling the symmetry breaking as:

$$\langle \mathrm{Tr} A \rangle \tag{5.21}$$

and

$$\langle \mathrm{Tr} A^2 \rangle - \langle \mathrm{Tr} B^2 \rangle, \tag{5.22}$$

respectively and set them as the objective functions in the corresponding bootstrap problem.

As the result, in the feasible region of Fig 7 we didn't find any evidence of the existence of a symmetry breaking solution for the model (5.1). We tried several points in different regions of Fig 7. The results show that the maximized values are always lying within the error bar (typically 10^{-3} and 10^{-4}, depending on the cutoff Λ and the parameters g and h). In particular, for $\Lambda = 8$ and some generic values of g and h, we have:

$$-10^{-4} \lesssim \langle \mathrm{Tr} A \rangle, \langle \mathrm{Tr} A^2 \rangle - \langle \mathrm{Tr} B^2 \rangle \lesssim 10^{-4}. \tag{5.23}$$

We believe this to be a strong evidence that the two symmetries we investigated are not spontaneously broken for all the regions in Fig 7.

Some other interesting facts:

1. For $g = 0$, i.e. when the quartic coefficient vanishes, the preservation of symmetry is automatic from the loop equation. This fact provides us with the intuition that the commutator square interaction is to some extent not a symmetry-breaking interaction. Regarding that at $h = 0$ the model is not in symmetry breaking phase, since it reduces to two decoupled one-matrix models, intuitively it points on the absence of symmetry breaking phase the for model (5.1) (with positive coefficients in front of quadratic terms).

2. For the region $h > 0$ and g slightly smaller than zero, we have a very large upper bound for the exposed quantities, sometimes of order 10, which might signal the symmetry breaking. But we note that the bootstrap convergence is really bad in this region where some bootstrap results for symmetry preserving solution are presented on Fig 9, and the error bar here is almost infinitely big. So we believe this cannot be a reliable evidence that there a symmetry breaking takes place in this region.

As we don't find evidence for the existence of symmetry breaking solutions for the model (5.1), we consider the same model but with negative coefficients in front of quadratic terms:

$$Z = \lim_{N \to \infty} \int d^{N^2} A \, d^{N^2} B \, \mathrm{e}^{-N \mathrm{tr}\left(-h[A,B]^2/2 - A^2/2 + gA^4/4 - B^2/2 + gB^4/4\right)}. \tag{5.24}$$

We know from the Section 3.2 that for $h = 0$ where we have just two decoupled one-matrix models, we have a symmetry breaking phase for $g < 1/4$. At such values of g we can test our method for bootstrapping the symmetry breaking solutions.
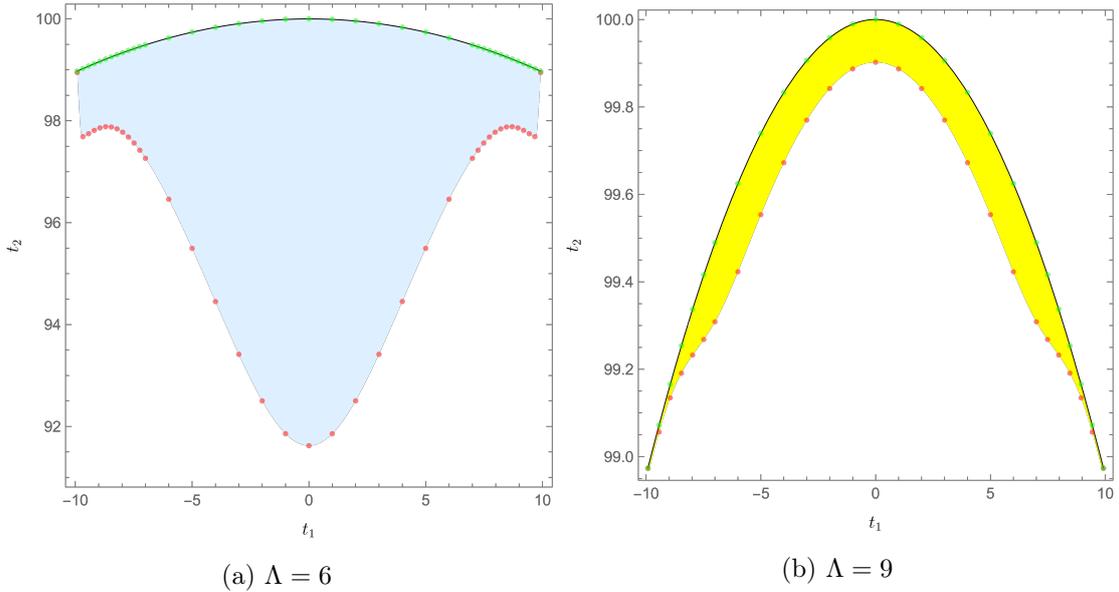
(a) $\Lambda = 6$

(b) $\Lambda = 9$

Figure 10: The allowed $t_1 - t_2$ region for $\Lambda = 6$ and $\Lambda = 9$. The corresponding parameters in the model (5.24) are $g = \frac{1}{100}$, $h = 0$. The shaded region is the result of one-matrix bootstrap. The black line is the exact analytic solution described in Section 3.2. The green and red dots are the upper bounds and lower bounds of our relaxation method from scanning over t_1.

In Fig 10 we compare the results of our relaxation method described above with the exact results and the one-matrix bootstrap plot at the same cutoff and the parameters $g = \frac{1}{100}$, $h = 0$. We see that our method is indeed able to bootstrap the symmetry breaking solution, even though it is non-convex. It is especially striking that not only our relaxation method converges to the highly non-convex exact solution, but it even coincides with the one-matrix bootstrap at each cutoff Λ within the error bars. It seems that, in spite of some loss of information when applying the relaxation method, we recover this information by considering the positivity condition of the mixed operators containing both matrices, such as $\langle \mathrm{Tr} ABAB \rangle$. We don't have yet a good explanation why these two approaches give equal or very close results. We also note that in this case the maximization scheme converges faster than the minimization scheme. Namely, the upper bound (green dots) in the plot is much closer to the exact solution than the lower bound (red dots). This suggests that if we are looking for a good approximation for the exact solution, we should use the upper bound solution as the best approximation.

For generic values of h and g for the model (5.24), the convergence is slower than in the analytically solvable particular case. It would be good to understand whether such a situation for solvable versus unsolvable models is typical. In Fig 11 we plot the bootstrap result for $g = \frac{1}{30}$, $h = \frac{1}{15}$. Obviously, it is still a symmetry breaking solution. We expect that taking the upper bound we can get a very accurate estimation of the physical quantities. We didn't try to further increase the value of Λ, being already satisfied to see that the proposed method works for rather generic values of parameters.
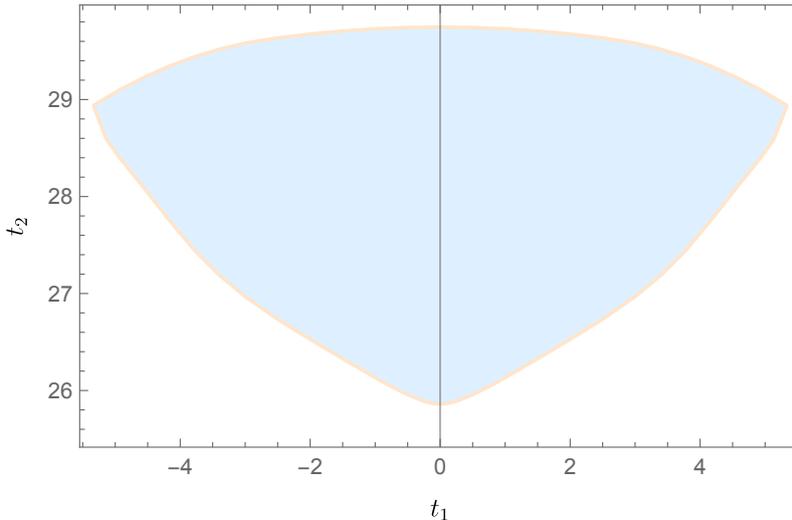
Figure 11: The allowed region for $g = \frac{1}{30}$ and $h = \frac{1}{15}$. These numerical results are obtained for $\Lambda = 8$.

6 Conclusion and discussion

In this work, we develop further the matrix bootstrap method pioneered in the papers [28, 30] and propose a crucial improvement – the relaxation procedure – applicable to a large class of multi-matrix problems and allowing to bootstrap them with a much higher precision. The relaxation transforms a Non-linear SDP, with the non-linearity due to the structure of loop equations, to the usual, linear SDP. We demonstrate the efficiency of our approach on the analytically unsolvable two-matrix model and establish its phase structure with rather high precision. The method appears to work well even for the discrete symmetry breaking large N solutions.

Actually, the efficiency of the matrix bootstrap, based on the positivity of the correlation matrix, remains an enigma. Nevertheless we managed to theoretically study this question in the one-matrix model and to establish precisely the class of physical solution singled out by such bootstrap.

As it was noticed in [28, 30, 47] the numerical bootstrap for large N multi-matrix models presents a higher degree of difficulty than the bootstrap of the large N one-matrix model. The bootstrap study of multi-matrix models was restricted to low orders in the length cut-off for the moments (or "words" forming them) and consequently it provided us with a limited precision. The main reason for this inefficiency is the non-convex formulation of the problem. Our main task in this work was to overcome these drawbacks of the matrix bootstrap.

Compared to the cited above papers we achieved a better understanding and efficiency of the matrix bootstrap in the following aspects:

- In the case of the large N Hermitian one-matrix model, we managed to prove that the bootstrap constraints pick up precisely the exact "physical" solutions, with positive

54

measure for the distribution of the eigenvalues (the corresponding resolvent has only the cuts on the real axis). In other words, we established the exact analytic solutions of the bootstrap conditions for the one-matrix model, thus justifying the numerical bootstrap techniques. We don't have yet the generalization of such analytic argument for the multi-matrix models, which is an interesting question to address.

- Then for the multi-matrix models, we developed the relaxation bootstrap method to overcome the crucial obstacle of non-convexity of the original problem. We demonstrated that this relaxation method was a systematic approach, capable to provide the numerically viable procedure for the large N multi-matrix models. We tested this method on a model that is genuinely analytically unsolvable (unlike Lin's 2-matrix model with cubic interactions in [28]). For particular parameters, when the analytic solution is known, our numerics reproduces extremely well the analytic results. For generic values of these parameters, we bootstrap the physical values with a remarkable precision (6 digits).

- This method is also able to detect critical behaviors, though the precision gets less impressive in the vicinity of critical lines.

- Remarkably, our bootstrap method is also applicable for bootstrapping the symmetry-breaking solutions and transform the non-convex problem to a convex one.

Here we make several comments on the bootstrap method proposed here and sketch out some further directions:

- All the numerical results in this study can be, in principle, reproduced on a single decent laptop in a decent time laps. So it looks very promising to implement it on a big cluster with parallelization. The main technical difficulty of the method is that we used the precision bigger than the machine precision (double-double or quad-double) in our current work. We believe that this is mainly due to the fact that our problem is badly-scaled as an SDP: the involved variables can have very different orders of magnitude. It would be good to find a systematic approach to scale appropriately the variables for very large-scale problems.

- The positivity of the correlation matrix in the matrix bootstrap method must be satisfied for any multi-matrix integrals with a reasonably converging positive measure. It follows from the fact that the integral of a positive function against a positive measure is positive. Contrary to the conformal bootstrap and S-matrix bootstrap where unitarity is one of the most important conditions, we don't know whether the unitarity or reflection positivity can be imposed in the bootstrap method for the matrix models. We also hope that our method can be generalized for bootstrapping non-unitary quantum field theories.

- We expect that the correlation matrix contains a lot of redundancies, i.e. very few of its minors may contain 99% of the information of the whole correlation matrix. This is reminiscent of a similar feature of the conformal bootstrap: we don't impose

the positivity condition on all spin channels, rather a very limited number of spin channels are good enough to make the algorithm to converge [26]. At the moment we don't have any scheme to isolate the minors of the correlation matrix that are more important than the other, which would be very beneficial when considering large-scale problems.

- It would be interesting to apply our methods to the Matrix Quantum Mechanics, in the spirit of the work [29], including for the non-singlet states there. Another interesting two-matrix model to study by bootstrap would be the generalization of (1.6) by taking the q-deformed version of interaction: $\mathrm{tr}[A, B]_q^2 = \mathrm{tr}(qAB - q^{-1}BA)^2$. This model interpolates between the solvable cases with $\mathrm{tr}(A^2B^2)$ or $\mathrm{tr}(BABA)$ interactions [35].

- An obvious, and one of the most ambitious possible applications of our relaxation bootstrap methods is the lattice Yang-Mills theory. We have thus good chances to significantly improve on this way the very preliminary results of [30]. A method alternative to the wide-spread Monte-Carlo simulations, even at large N [48], would be extremely welcome for the study and a deeper understanding of QCD. Obvious advantages of the bootstrap method based on Migdal-Makeenko loop equations [31] w.r.t. Monte-Carlo are: i) Exact inequalities on loop averages, no statistical error; ii) absence of finite boundary conditions (the lattice is infinite); iii) One gets some information on all loops at once up to a given length, although with better precision for short loops. That gives access to more of the physical quantities. The obvious drawback is the limited length of Wilson loops. We hope to establish by the future numerical work whether this drawback is crucial indeed.

Appendices

A Analytic solvability of two-matrix model with cubic interactions and arbitrary potentials

The Hermitian 2-matrix model with the general cubic interactions between two matrices and general potentials in the action

$$S = \mathrm{tr}\left(h(AB^2 + BA^2) + W(A) + \tilde{W}(B) \right), \tag{A.1}$$

has been studied in [28] by numerical bootstrap method, as an example of bootstrap approach to an analytically "unsolvable" matrix integral. Here we show that this matrix model is in fact analytically solvable for generic potentials W and $\tilde{W}$, in the sense that the matrix integral can be explicitly reduced to $\sim N$ amount of variables, instead of the original $\sim N^2$ matrix variables, which in principal allows the application of the saddle point method at large N. Our derivation will be schematic and we will repeatedly neglect the non-dynamical factors before the integral of partition function. It is unclear whether this integrability influences the efficiency of Lin's bootstrap method but this is our motivation to choose a different, truly "unsolvable" 2-matrix integral, with the interaction $\mathrm{tr}[A, B]^2$, as the main example of application of bootstrap in this paper.

Since $\mathrm{tr}(A+B)^3 = \mathrm{tr}(A^3 + 3A^2B + 3AB^2 + B^3)$ we can always rewrite it as

$$S = \mathrm{tr}\left((A+B)^3/3 - V(A) - \tilde{V}(B)\right) \tag{A.2}$$

where $V(A) = A^3/3 - W(A)$ and $\tilde{V}(B) = B^3/3 - \tilde{W}(B)$ and we have set wit1out loss of generality $h = 1$.

We can always reduce it to Itzykson-Zuber-Charish-Chandra (IZC) integral by an extra matrix integration, following the trick similar to proposed in [6] in the context of solution of the Potts model on dynamical planar Feynman graphs. Namely, represent the first term in (A.2) in terms of an extra hermitian matrix integral over X [33]

$$e^{\mathrm{tr}\,C^3/3} = \int d^{N^2} X \, e^{\mathrm{tr}(iXC + F(X))}, \qquad C = A + B \tag{A.3}$$

where the function $F(X)$ is defined as the inverse matrix Fourier transform:

$$e^{\mathrm{tr}F(X)} = \int d^{N^2} C \, e^{\mathrm{tr}(-iXC + C^3/3)} = \int \prod_j dc_j \, e^{c_j^3/3} \, \Delta^2(c) \frac{\det_{j,k} e^{-ix_j c_k}}{\Delta(c)\Delta(x)}, \tag{A.4}$$

i.e. it represents the matrix Airy function. In the last equality we applied the IZC integral. Then we rotate the contour of X integration, change variable $C \to -C$ and write the partition function of cubic 2MM model in the form

$$Z = \int d^{N^2} X \int d^{N^2} C \, e^{\mathrm{tr}(XC - C^3/3)} \int d^{N^2} A \, e^{\mathrm{tr}[XA - V(A)]} \int d^{N^2} B \, e^{\mathrm{tr}[XB - \tilde{V}(B)]}. \tag{A.5}$$

We can compute the function $F(X)$ in terms of the eigenvalues of $X = \Omega^\dagger x \Omega$ where $x = \mathrm{diag}\{x_0, x_1, \ldots, x_{N-1}\}$. We compute the angular integral in (A.4) via IZC integrals:

$$e^{\mathrm{tr}F(X)} = \Delta^{-1}(x) \int \prod_j dc_j \, e^{x_j c_j - c_j^3/3} \, \Delta(c) = \frac{W[-\mathrm{Ai}(x_0), \cdots - \mathrm{Ai}(x_{N-1})]}{\Delta(x)} \tag{A.6}$$

where in the denominator we have the $N \times N$ "Wronskian" of Airy-type functions:

$$\mathrm{Ai}(x) = \int_{\mathcal{C}} dc \, e^{-xc + \frac{1}{3}c^3}, \tag{A.7}$$

and:

$$W[f_0(x_0), \ldots f_{N-1}(x_{N-1})] = \sum_{\sigma \in S_n} \mathrm{sgn}(\sigma) \prod_{i=0}^{N-1} \partial_{x_i}^{\sigma(i)} f_i(x_i). \tag{A.8}$$

Here the complex contour $\mathcal{C}$ is usually chosen so that it goes from infinity with the slope $-\pi/3$ and ends up at infinity with the slope $\pi/3$. However, when we study the limit $N \to \infty$ the saddle point configuration of the eigenvalues will adjust itself to the relevant distribution on the real axis given by a solution of the integral saddle point equation. Similarly, the bootstrap numerical procedure should single out such solutions.

---

[33]We drop here and further all inessential overall factors

Then we treat similarly the other two integrals in (A.5) and represent them also in terms of Wronskians of

$$f(x) = \int da \, e^{xa-V(a)}, \qquad \tilde{f}(x) = \int db \, e^{xb-\tilde{V}(b)}. \tag{A.9}$$

In this way, we managed to re-wrtite the cubic 2MM entirely in terms of eigenvalue integral:

$$Z = \int \prod_j dx_j \, \frac{W[-\text{Ai}(x_0), \dots] \, W[f(x_0), \dots] \, W[\tilde{f}(x_0), \dots]}{\Delta(x)}. \tag{A.10}$$

Hence we reduced the cubic two-matrix integral (A.2) to an explicit integral over N eigenvalues of an auxiliary matrix X. We treat such a matrix model as "solvable" though the further details of the explicit solution can be rather involved. Instead of studying the saddle point in terms of wronskians it is better to apply the method (inspired by [49]) which was proposed by V.Kazakov and I.Kostov for solution of Potts model on random planar graphs [50]; it is well presented in [20]. We will not pursue here this route and we leave it for the future work.

B Solving the positivity condition of the resolvent

We saw in Section 3.1 that the positivity of correlation matrix is equivalent to the positivity of the resolvent. As it was noticed there, this equivalence enables us to analytically solve the bootstrap condition. Here we propose a general method to solve the lower moments from the positivity condition of resolvent. This finishes our analytic solution of the bootstrap problem corresponding to the Hermitian one-matrix model. As a specific example, we also apply this method to one-matrix model with quartic potential, for which the results were summarized in Sec. 3.2.

B.1 Cuts and zeros

Finding the lower moments from the positivity of the resolvent is a well-posed problem in complex analysis, and abundant mathematical tools can be employed to solve it. Here we study the configuration of cuts and zeros of the cut function defined in the main text (2.18). Due to the polynomiality of the discriminant $D(x) = C(x)^2$ we can give the full classification of all possible configurations of cuts and zeros of the cut function $C(x)$ on the real line. It turns out that the properties of these configurations provide not only necessary but also sufficient condition for the positivity of the resolvent. Generally, if we know a configuration of the cuts and zeros, we are able to fix a few lowest moments which we want to find the solution. This is how we solve the positivity condition of the resolvent. In the following we will be considering a Hermitian one-matrix model with general polynomial potential $V(x)$.

First let us pick a single cut of $C(x)$ on the real axis, namely $[a_i, b_i]$, as shown in Fig 12. The positivity condition of the resolvent implies that for $x \in [a_i, b_i]$ we have $\text{Im} C(x + i0) \propto \rho(x) \geq 0$. From the definition of the cut function, we must have $C(x) > 0$ in the right neighborhood of b_i, and $C(x) < 0$ in the left neighborhood of a_i. A direct

Figure 12: The left plot shows the sign of $C(x)$ in the neighborhood of a positive cut. The right plot shows there must be at least one zero, or generally odd number of zeros, between two cuts to fix the sign.

consequence is that we must have at least one zero, or generally odd number of zeros, between two positive cuts to fix the sign. This is also illustrated in Fig 12.

There is yet another constraint on the zeros. We notice that $V'(x)$ and $C(x)$ get unbounded at infinity, but $G(z) \underset{z \to \infty}{\to} \frac{1}{z}$, i.e. it is analytic there. As a result, asymptotic behavior of $C(x)$ must match the asymptotics of $V'(x)$. For example, if $\lim_{x \to \infty} V'(x) < 0$, we must add another zero to the right of all the cuts to fix the sign of $C(x)$, preserving both positivity of the resolvent and the asymptotic behavior.

For the zeros of $D(x)$ which are not located on the real axis, there exist roots with even multiplicities since there shouldn't exist complex cuts for $C(x)$. We also note that since $D(x)$ is a polynomial with real coefficients, all its complex roots must come in pairs.

The above analysis gives the way to count the possible number of cuts. Here we list the maximum number of cuts m when the degree of the potential is $d+1$, under the asymptotic behavior $(\pm, \pm)$[34]:

- $(-, +)$: $2m + 2(m - 1) \leq 2d \Rightarrow m \leq (d + 1)/2$,

- $(+, -)$: $4 + 2m + 2(m - 1) \leq 2d \Rightarrow m \leq (d - 1)/2$,

- $(+, +)$ and $(-, -)$: $2 + 2m + 2(m - 1) \leq 2d \Rightarrow m \leq d/2$.

B.2 A working example

In this part, we will use these cuts and zeros considerations solve the bootstrap condition of the model with potential:

$$V(x) = \frac{1}{2}x^2 + \frac{1}{4}gx^4, \quad g < 0. \tag{B.1}$$

This potential has a $(+, -)$ asymptotic, so in the minimal case, we must have a positive cut in the middle, and two zeros, one placed on the right and another one on the left of the cut, to fix the asymptotics. Since the polynomial $D(x) = V'(x)^2 - 4P(x)$ is of 6th degree, we have already reached the maximum number of zeros. The conclusion is that the cut configuration in Fig 13 is the only possibility for such asymptotic behavior.

To see when this cut configuration is possible, we note that:

$$D(x) = V'(x)^2 - 4P(x) = \left(gx^3 - x\right)^2 - 4gx^2 + 4g - 4g\left(\mathcal{W}_1 x + \mathcal{W}_2\right) = D_1(x) - D_2(x). \tag{B.2}$$

---

[34]For example, $(-, +)$ means $\lim_{x \to -\infty} V'(x) < 0$ and $\lim_{x \to \infty} V'(x) > 0$
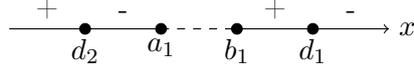
Figure 13: The only possible cut configuration for asymptotic $(+, -)$

Here we split the discriminant into the part depending on $\mathcal{W}_1$ and $\mathcal{W}_2$:

$$D_1(x) = \left(gx^3 - x\right)^2 - 4gx^2 + 4g \tag{B.3}$$

and the part depending only on g:

$$D_2(x) = 4g\left(\mathcal{W}_1 x + \mathcal{W}_2\right). \tag{B.4}$$

$D_2(x)$ is a straight line with negative intercept. As depicted in Fig 14, it is possible that a straight line crosses $D_1(x)$ with sufficient number of intersections, but only for $g \geq g_c = -\frac{1}{12}$. For $g < g_c$ the qualitative shape of the graph of $D_1(x)$ disqualifies the only possible cut configuration Fig 13, excluding the existence of any bootstrap solution.
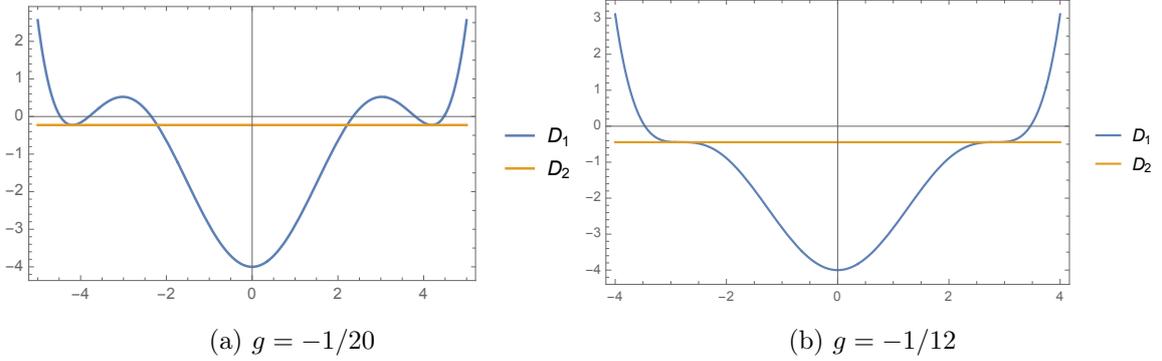

(a) $g = -1/20$ (b) $g = -1/12$

Figure 14: The only possible cut configuration for $\mu = 1$ and $g < 0$. The critical case is $g = -\frac{1}{12}$, below that, there is no more bootstrap solution.

From the Fig 14, it is obvious that $\mathcal{W}_1 = 0$. Otherwise we won't have a resolvent satisfying the positivity condition. We can find $\mathcal{W}_2$ from the vanishing of the discriminant of the polynomial $D(x)$, namely:

$$\mathcal{W}_2 = \frac{(12g + 1)^{3/2} - 18g - 1}{54g^2} \tag{B.5}$$

which corresponds to the standard one-cut IBPZ solution [14].

To make our intuitive arguments above more systematic, and applicable to higher degree potentials, let us list the conditions by which the positivity of the resolvent translates into the properties of the polynomial $D(x)$:

1. $D(x)$ has 6 real roots counting multiplicity, two of them are double roots. Two of them are single roots.

2. The simple roots of $D(x)$ lie in between the double roots on the real line.
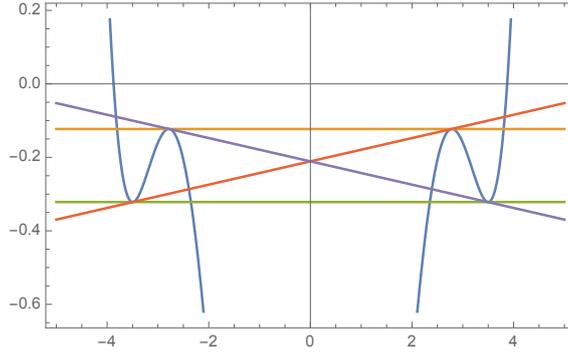
60

Figure 15: 4 solutions under the condition 1 when $g = -1/15$. The blue line is the function $D_1(x)$ which is independent of moments $\mathcal{W}_1$, $\mathcal{W}_2$, whereas other color straight lines are different solution of $D_2(x)$. We see only the green line has the correct configuration of zeros depicted in Fig 14.

The property 1 boils down to the condition that the degree of the greatest common divisor of $(D(x), D'(x))$ is 2. We apply the Euclidean algorithm to $D(x)$ and $D'(x)$ to rewrite them in the form:

$$\begin{cases} D = q_1 D' + r_1 \\ D' = q_2 r_1 + r_2 \\ r_1 = q_3 r_2 + r_3 \\ r_2 = q_4 r_3 + r_4 \end{cases} \tag{B.6}$$

The remainder r_4 is a polynomial of degree 1 in x and we set all its coefficients to zero. In this way we get 2 algebraic equations which, in principle, fix $\mathcal{W}_1$ and $\mathcal{W}_2$ in terms of g. For the reality of the roots, we note that this means the discriminant of $(D(x), D'(x)) = r_3$ and the discriminant of $D(x)/r_3^2$ is non-negative. These are already a lot of conditions. Luckily the mathematica **Reduce** function can treat these conditions efficiently, leaving us with four solutions. The four solutions correspond to different orders of single zeros and double zeros. We show the corresponding solutions in Fig 15. We can take advantage of the condition 2 to select the only physical solution for this case:

$$\begin{cases} -\frac{1}{12} \le g < 0 : \mathcal{W}_1 = 0, \mathcal{W}_2 = \frac{(12g+1)^{3/2} - 18g - 1}{54g^2}. \\ g < -\frac{1}{12} : \text{No bootstrap solution.} \end{cases} \tag{B.7}$$

C   Dual formulation and relaxation

In this appendix, we review some basic facts about dual formulation in optimization theory and clarify the relationship between our relaxation method introduced in Section 4 and the dual formulation. For the readers interested in more details about the optimization theory, the book [44] is a good starting point.

C.1 Dual problem of general optimization problem

Consider a general optimization problem of the form:

$$
\begin{aligned}
\min \quad & c(x) \\
\text{subject to} \quad & f_i(x) \leq 0, \quad i = 1, ..., m \\
& h_j(x) = 0, \quad j = 1, ..., p \\
& x \in \mathbb{R}^n.
\end{aligned}
\tag{C.1}
$$

For convenience, we denote the optimal value for (C.1) by $p^\star$. Whenever $c(x)$, $f_i(x)$ are convex functions and $h_j(x)$ are linear functions the problem (C.1) is defined to be convex, otherwise it is non-convex. [35]

For a general problem of the form (C.1), convex or not, we can construct its dual problem starting with the Lagrangian defined by:

$$
\mathcal{L}(x, u, v) = c(x) + \sum_{i=0}^{m} u_i f_i(x) + \sum_{j=0}^{p} v_j h_j(x), \quad u_i \geq 0
\tag{C.2}
$$

and minimize over x[36]:

$$
g(u, v) = \min_{x \in \mathbb{R}^n} \mathcal{L}(x, u, v).
\tag{C.3}
$$

It is a simple exercise to show that $g(u, v)$ is concave, since it is a minimization over a family of linear functions in u, v. For all u, v under the constraints $u_i \geq 0$, we have:

$$
g(u, v) \leq \max g(u, v) \leq p^\star.
\tag{C.4}
$$

This indicates us the formulation of the dual problem:

$$
\begin{aligned}
\max \quad & g(u, v) \\
\text{s.t.} \quad & u_i \geq 0 \quad i = 1, ..., m.
\end{aligned}
\tag{C.5}
$$

We denote the optimal solution of this problem to be $d^\star$. This optimization problem is guaranteed to be convex, since it is maximizing a concave function $g(u, v)$. In this sense the dual problem (C.5) is simpler when the primal problem is non-convex. Of course we always have:

$$
d^\star \leq p^\star
\tag{C.6}
$$

due to (C.4). The inequality (C.6) is conventionally called weak duality. It would be actually nice to have the equality, i.e. when *strong duality* holds. For that case we have the well-known Slater's condition:

The strong duality holds if the primal problem is convex and it has a strictly feasible solution.

By definition, a solution x^* is strictly feasible when:

$$
\begin{aligned}
f_i(x^*) &< 0 \quad i = 1, ..., m \\
h_j(x^*) &= 0, \quad j = 1, ..., p.
\end{aligned}
\tag{C.7}
$$

In general, we don't have strong duality for non-convex problem.

---

[35] It turns out that usually we can only solve the convex optimization problem efficiently, and non-convex problems are generally NP-hard.

[36] We stress here that the minimization is the unconstrainted minimization, i.e. $x \in \mathbb{R}^n$

C.2   Relaxation problem and dual problem.

In this section, for completeness we present a proof that the relaxation problem introduced in (4.21) is the dual of the dual problem of the original problem (4.9). The proof is actually trivial but lengthy, so the reader could treat it as an implementation example of the dual formulation introduced in the last section.

First we transform the original problem (4.9) to the following form:

$$\begin{aligned} \min \quad & c^{\mathrm{T}} x \\ \text{s.t.} \quad & \mathrm{tr} X A_i + b_i^{\mathrm{T}} x + a_i = 0, \\ & M_0 + \sum_{j=1}^{L} M_j x_j \succeq 0, \\ & X = x x^{\mathrm{T}}. \end{aligned} \tag{C.8}$$

To take the dual problem of it, we write down its Lagrangian:

$$\mathcal{L}(x, X, \lambda, Y, Z) = c^{\mathrm{T}} x + \sum_i \lambda_i (\mathrm{tr} X A_i + b_i^{\mathrm{T}} x + a_i) - \mathrm{tr}(Y(M_0 + \sum_{j=1}^{L} M_j x_j)) + \mathrm{tr}(Z(x x^{\mathrm{T}} - X)). \tag{C.9}$$

The matrices Y and Z introduced here are real symmetric matrix variables, satisfying $Y \succeq 0$ due to the inequality condition in (C.8). To minimize the Lagrangian, we collect all the terms involving primal variables x and X:

$$\mathcal{L}(x, X, \lambda, Y, Z) = \mathrm{tr}((\sum_i \lambda_i A_i - Z) X) + x^{\mathrm{T}} Z x + (c + d + \sum_i \lambda_i b_i)^{\mathrm{T}} x + \sum_i \lambda_i a_i - \mathrm{tr}(Y M_0) \tag{C.10}$$

where we introduced the vector variable $d_k = -\mathrm{Tr}(Y M_k)$ to make the formula more compact. We get $g(\lambda, Y, Z)$ by taking the minimization over x, X:

$$\begin{aligned} g(\lambda, Y, Z) &= \sum_i \lambda_i a_i - \mathrm{tr}(Y M_0) - \frac{1}{4}(c + d + \sum_i \lambda_i b_i)^{\mathrm{T}} Z^{\dagger}(c + d + \sum_i \lambda_i b_i), \\ \text{if} \quad & \sum_i \lambda_i A_i - Z = 0, \quad Z \succeq 0, \quad (I - Z Z^{\dagger})(c + d + \sum_i \lambda_i b_i) = 0. \end{aligned} \tag{C.11}$$

The reader can verify that if the conditions in the second line of (C.11) are not saturated, the minimal value $g(\lambda, Y, Z)$ is $-\infty$, which is irrelevant since we are only interested in its the maximal. Note that $Z^{\dagger}$ here denotes the pseudo-inverse of the matrix Z:

$$Z^{\dagger} = \lim_{\epsilon \to 0^+} (Z^{\mathrm{T}} Z + \epsilon I)^{-1} Z^{\mathrm{T}}. \tag{C.12}$$

Introducing an auxiliary variable γ by Schur complement, we can formulate the dual problem in a more compact form:

$$\begin{aligned} \max \quad & \gamma \\ \text{s.t.} \quad & \sum_i \lambda_i A_i - Z = 0, \quad Y \succeq 0, \\ & \begin{pmatrix} \sum_i \lambda_i a_i - \mathrm{tr}(Y M_0) - \gamma & (c + d + \sum_i \lambda_i b_i)^{\mathrm{T}}/2 \\ (c + d + \sum_i \lambda_i b_i)/2 & Z \end{pmatrix} \succeq 0. \end{aligned} \tag{C.13}$$

63

To do the second dualization, we introduce again the Lagrangian:

$$\mathcal{L}_2(x, X, \delta, W, S, \gamma, \lambda, Y, Z) = -\gamma - \mathrm{tr}(SY) + \mathrm{tr}(W(\sum_i \lambda_i A_i - Z))$$

$$- \mathrm{tr}\left(\begin{pmatrix} \delta & x^{\mathrm{T}} \\ x & X \end{pmatrix} \begin{pmatrix} \sum_i \lambda_i a_i - \mathrm{tr}(Y M_0) - \gamma & (c + d + \sum_i \lambda_i b_i)^{\mathrm{T}}/2 \\ (c + d + \sum_i \lambda_i b_i)/2 & Z \end{pmatrix}\right) \tag{C.14}$$

Here we slightly abuse the notation by introducing a dual variable contains x and X, which satisfies:

$$\begin{pmatrix} \delta & x^{\mathrm{T}} \\ x & X \end{pmatrix} \succeq 0. \tag{C.15}$$

We also note that $S \succeq 0$. The dual problem becomes apparent when we collect the coefficients of γ, Y, Z, γ:

$$\mathcal{L}_2(x, X, \delta, W, S, \gamma, \lambda, Y, Z) = (\delta - 1)\gamma + \mathrm{tr}((M_0 \delta - S + \sum_k M_k x_k)Y) - \mathrm{tr}((W + X)Z)$$

$$+ \sum_i \lambda_i(\mathrm{tr}(W A_i) - a_i \delta - b_i^{\mathrm{T}} x) - c^{\mathrm{T}} x. \tag{C.16}$$

Again, all the coefficients of the linear terms must vanish, otherwise the minimal value of $\mathcal{L}_2$ will be $-\infty$ when we take the minimization. So this time we can write down the dual problem as:

$$\begin{aligned} \min \quad & c^{\mathrm{T}} x, \\ \text{subject to} \quad & M_0 + \sum_k M_k x_k \succeq 0 \\ & \mathrm{tr}(X A_i) + b_i^{\mathrm{T}} x + a_i = 0, \\ & \begin{pmatrix} 1 & x^{\mathrm{T}} \\ x & X \end{pmatrix} \succeq 0 \end{aligned} \tag{C.17}$$

which is exactly our original problem with relaxation.

D   Implementation in SDPA

Here we gather the details on the implementation of our methods which are not covered in Section 5. We stress that although we are quite satisfied by the current efficiency of the method, we cannot guarantee that the choices we made are the best possible. In Appendix E, we will demonstrate explicitly the importance of all these details on a simple example.

D.1   Choice of SDP solvers

The SDP solver for all of the numerical results in Section 5 is SDPA[51]. In the search for a better performance, we tried a lot of other solvers, including PENLAB, SDPB, SDPA, MOSEK, SDPT3 and SeDuMi. In the early stage of this work, we were mainly working with SDPB[52]. Our experience shows that SDPB gives the most stable convergence in all

situations, even when we set the SPDB precision to 64. All other solvers sometimes fail to converge. The disadvantage of SDPB is that it is much slower and uses much more memory compared to all other solvers. This is due to the fact that SDPB is an arbitrary precision solver relying on GMP, which potentially slows the program by more than 1000 times. Due to this reason, when we try to deal with large-scale problems, we switch to SDPA which, according to our limited tests, converges better than all other SDP solvers on large-scale problems.

D.2   Generation of the loop equations

For loop equations of a given length l, the set of all loop equations could be generated by exhaustive method[37]. This is conceptually simple and numerically easy to implement. In fact, a slight optimization of Lin's code in [28] is efficient enough to generate loop equations up to $\Lambda = 11$ in our work. The tricky part here is to determine what is the sufficient length cutoff of loop equations for our numerics.

Let's take the model (5.1) as an example again. Suppose we are considering a cutoff Λ, which means that the longest operator in the correlation matrix is 2Λ. We recall that in loop equation of length l in this model, we have the operator expectations of lengths $l - 1, l + 1, l + 3$[38]. We can consider only the loop equations up to the length $l = 2\Lambda - 3$, since they contain only the operators we are interested in. But higher length loop equations could also generate non-trivial relations on the operator expectations of lengths within the cutoff. Namely, as loop equations of higher length contain lower operators that we are interested in, we could eliminate higher operators and get new, generally linear independent loop equations containing only operators up to the length $l = 2\Lambda$. However, empirically for the model (5.1) this doesn't happen: the procedure described above does not produce any new independent loop equations, in addition to the standard ones, constraining the operators of lengths $l \leq 2\Lambda - 3$. One exception is the case $h = 0$ and $g = 0$, i.e. when the model is solvable. Then we need to consider the loop equations up to the lengths $l = 2\Lambda + 1$ and $l = 2\Lambda - 1$ to generate all the equations between operators we are interested in. We don't have any proof why this is true. But this is not hard to understand intuitively. For example, when $g = 0$ and we consider the loop equations only up to $l = 2\Lambda - 3$, so we have a smaller number of length 2Λ operators comparing to the case $g \neq 0$ in the loop equations. But we also note that even for $h = 0$ or $g = 0$, when we consider only the loop equation up to length $l = 2\Lambda - 3$ in our bootstrap assumptions, we still get a bound very close to the one using the higher length loop equations as well. This example supports our general intuition that higher loop equations are expected to have a relatively limited influence on small length operators.

In conclusion, for the model (5.1) with cutoff 2Λ, it is enough to take into account the loop equations up to the length $l = 2\Lambda - 3$.

---

[37]Here exhaustive method means that we generate all the loop equations by taking matrix derivatives on all possible positions of all possible words in Schwinger-Dyson equations.

[38]Here we define the length of quadratic terms in loop equations as the sum of the lengths of their factors.

D.3 Solving the loop equations

Unlike other solvers, the input form of SDPA is rather demanding. It only admits an input problem strictly of the (4.1) form. As a consequence, we need to solve the loop equation and substitute the solution into the correlation matrix and relaxation matrix. More precisely, by solving the loop equations we mean that there is a reduced set of operator expectations, such that all other operator expectations and all the quadratic terms $\mathcal{R}_{ij}$ can be solved by loop equations as linear combinations of them. For later convenience, we denote the vector of this reduced set by x_{red}.

A bad news is that the loop equations generated by exhaustive method are not linearly independent, so solving it with floating point numbers will cause some numerical instabilities. One way out of this difficulty is to remove the linear redundancies in loop equations. Another way is to use exact numbers in Mathematica. The first is hard since we found that for some specific values of h and g, there will be coincident degeneracies. So we doubt we could have a systematic way to select the linear independent loop equations. Actually we are using the second way, i.e. only using the exact number computation when generating and solving loop equations. The exact number arithmetics consumes a lot of memory and makes the solving procedure much slower, but up to the most involved case $\Lambda = 11$ in this article, we still have enough of memory(around 200 Gigabytes) and the solving functions are efficient enough.

D.4 Relaxation matrix

There are some technical details concerning generating the relaxation matrix constraints. First we note that if we are considering loop equations up to $l = 2\Lambda - 3$, they contain quadratic terms only up to length $2\Lambda - 4$. The operators in the bottom right corner of the relaxation matrix $\mathcal{R}$ are neither constrained at all, nor contained in the objective function (cf (4.20)). So they are actually irrelevant. Formally these can be shown by Schur complement[39]:

$$\mathcal{R} = \begin{pmatrix} X_1 & B_1 \\ B_1^{\mathrm{T}} & X_2 \end{pmatrix} \succ 0 \Leftrightarrow X_1 \succ 0 \wedge X_2 - B_1^{\mathrm{T}} X_1^{-1} B_1 \succ 0. \tag{D.1}$$

Here X_1 is the sub-matrix contain the product of $\langle \mathrm{Tr}\mathcal{O}_i \rangle \langle \mathrm{Tr}\mathcal{O}_j \rangle$, where the length of $\mathcal{O}_i$ plus $\mathcal{O}_j$ is less or equal than $\Lambda - 2$. Since X_2 is not constrained at all, the second inequality can always be satisfied. In this way, the positivity condition of $\mathcal{R}$ is equivalent to the positivity of the X_1.

The matrix X_1 needs to be further reduced. Since we know that the operator expectations are linearly dependent on the loop equations, it is not surprising that the quadratic terms are linearly dependent. We must reduce this linear dependency, otherwise it will induce numerical instabilities for SDPA. To solve this potential problem, we consider the minor $X_{1\text{red}}$ in the form:

$$X_{1\text{red}} = x_{1\text{red}} x_{1\text{red}}^{\mathrm{T}}. \tag{D.2}$$

---

[39]Numerically there is no difference between strict inequalities and non-strict ones.

The vector $x_{1\mathrm{re}}$ consists of operator expectations $\langle \mathrm{Tr}\mathcal{O}_i \rangle$, such that not only the lengths of $\mathcal{O}_i$ are equal or less than $\Lambda - 2$ but also they are in the set x_{red} derived by solving the loop equations. Then we impose the positivity condition on the reduced relaxation matrix:

$$\mathcal{R}_{1\mathrm{red}} = \begin{pmatrix} 1 & x_{1\mathrm{red}}^{\mathrm{T}} \\ x_{1\mathrm{red}} & X_{1\mathrm{red}} \end{pmatrix} \succeq 0 \,. \tag{D.3}$$

D.5 Feasibility

In Section 5.3, in the bisection process we need to test whether the SDP is feasible. However, SDPA doesn't have a built-in option to test the feasibility of a SDP. To deal with this difficulty, we introduce a slack variable μ in addition to the original variables in the SDP, to transform the original problem (4.21) into the form:

$$
\begin{aligned}
\min \quad & \mu \\
\text{subject to} \quad & M_0 + \sum_k M_k x_k + \mu I_1 \succeq 0, \\
\text{and} \quad & \mathrm{tr}(X A_i) + b_i^{\mathrm{T}} x + a_i = 0, \\
\text{and} \quad & \begin{pmatrix} 1 & x^{\mathrm{T}} \\ x & X \end{pmatrix} + \mu I_2 \succeq 0.
\end{aligned}
\tag{D.4}
$$

Here I_1 and I_2 are the identity matrices of the appropriate size. If the optimal value is negative, then the original problem (4.21) is feasible, otherwise it is infeasible.

D.6 Normalization

When we are dealing with a large-scale SDP, a common problem is that our input data is badly-scaled. We usually need to adjust our normalization to make all the numbers in the optimization problem to be of similar order of magnitude. In our problem, we make the substitution:

$$\mathcal{O}_l' = g_s^{l/2} \mathcal{O}_l \tag{D.5}$$

and then we bootstrap the primed operator instead of the original one. Here l is the length of the operator. When g and h are not vanishing we put $g_s = \min\{|g|, 2|h|\}$. When it is vanishing, we take g_s to be the absolute value of the non-vanishing coupling.

This naive choice to scale is not guaranteed to be the best for the problem, though it appears to lead to decent results for our range of cutoffs. It may be more advantageous to scale this problem according to the asymptotic behavior of large length operator expectations, which would be interesting to study analytically.

D.7 Precision of the solver

Finally, we want to make some comments on the numerical precision. Most of the SDP solvers including SDPA are machine precision solvers. Numerical instabilities may happen when we are too ambitious about the precision of the results or the input data is badly scaled. In this situation, one could try arbitrary precision solvers like SDPB and SDPA-GMP, or other solvers in SDPA family called SDPA-DD and SDPA-QD, which is actually

our recommendation. SDPA-DD and SDPA-QD is based on double-double and quad-double data type in QD library. From our tests, 32 digits or 64 digits are always enough for our purpose, and they are still efficient enough to solve the problem.

E $\quad \Lambda = 4$ example

In this appendix, we demonstrate the numerical implementation of SDPA introduced in the Appendix D on the simplest non-linear case $\Lambda = 4$ of the model (5.1), under the assumption of $\mathbb{Z}_2^3$ symmetry.

E.1 Operators and Loop equations

Before generating the loop equations, one of the preparatory work is to generate all the nonequivalent operators and possible quadratic terms up to the cutoff $\Lambda = 4$. As already discussed in Section 5, we have only very few operators that are non-equivalent up to identifications due to the symmetries of the problem and of the class of solutions considered here[40]. There are 20 operators with the length smaller or equal to 8:

$$\mathrm{Tr}A^2,\ \mathrm{Tr}A^4,\ \mathrm{Tr}A^2B^2,\ \mathrm{Tr}ABAB,\ \mathrm{Tr}A^6,\ \mathrm{Tr}A^4B^2,\ \mathrm{Tr}A^3BAB,\ \mathrm{Tr}A^2BA^2B,\ \mathrm{Tr}A^8,$$
$$\mathrm{Tr}A^6B^2,\ \mathrm{Tr}A^5BAB,\ \mathrm{Tr}A^4BA^2B,\ \mathrm{Tr}A^4B^4,\ \mathrm{Tr}A^3BA^3B,\ \mathrm{Tr}A^3BAB^3,\ \mathrm{Tr}A^3B^2AB^2,$$
$$\mathrm{Tr}A^2BABAB^2,\ \mathrm{Tr}A^2BAB^2AB,\ \mathrm{Tr}A^2B^2A^2B^2,\ \mathrm{Tr}ABABABAB\,.$$
$$\text{(E.1)}$$

All other operators are identical to those in this list or they vanish under the $\mathbb{Z}_2^3$ symmetry assumption. There is only one quadratic term left under this assumption. For conciseness, we denote it by β in this appendix:

$$\beta = (\mathrm{Tr}A^2)^2 = (\mathrm{Tr}B^2)^2 = \mathrm{Tr}A^2\mathrm{Tr}B^2. \tag{E.2}$$

To generate the loop equations, we simply apply the exhaustive method and then delete the duplicates. For general couplings h and g, we have 14 loop equations left:

$$1 = \mathrm{Tr}A^2 + g\mathrm{Tr}A^4 - h(-2\mathrm{Tr}A^2B^2 + 2\mathrm{Tr}ABAB)$$
$$0 = -2\mathrm{Tr}A^2 + \mathrm{Tr}A^4 - h(2\mathrm{Tr}A^3BAB - 2\mathrm{Tr}A^4B^2) + g\mathrm{Tr}A^6$$
$$0 = -\mathrm{Tr}A^2 + \mathrm{Tr}A^2B^2 - h(-\mathrm{Tr}A^2BA^2B + 2\mathrm{Tr}A^3BAB - \mathrm{Tr}A^4B^2) + g\mathrm{Tr}A^4B^2$$
$$0 = -h(2\mathrm{Tr}A^2BA^2B - 2\mathrm{Tr}A^3BAB) + g\mathrm{Tr}A^3BAB + \mathrm{Tr}ABAB$$
$$\beta = -2\mathrm{Tr}A^4 + \mathrm{Tr}A^6 - h(2\mathrm{Tr}A^5BAB - 2\mathrm{Tr}A^6B^2) + g\mathrm{Tr}A^8$$
$$\beta = -\mathrm{Tr}A^2B^2 + \mathrm{Tr}A^4B^2 - h(-\mathrm{Tr}A^3B^2AB^2 + 2\mathrm{Tr}A^3BAB^3 - \mathrm{Tr}A^4B^4) + g\mathrm{Tr}A^6B^2$$
$$0 = -2\mathrm{Tr}A^2B^2 - h(-\mathrm{Tr}A^2B^2A^2B^2 + 2\mathrm{Tr}A^2BABAB^2 - \mathrm{Tr}A^3B^2AB^2) + \mathrm{Tr}A^4B^2 + g\mathrm{Tr}A^6B^2$$
$$0 = -\mathrm{Tr}A^4 + \mathrm{Tr}A^4B^2 + g\mathrm{Tr}A^4B^4 - h(-\mathrm{Tr}A^4BA^2B + 2\mathrm{Tr}A^5BAB - \mathrm{Tr}A^6B^2)$$
$$0 = \mathrm{Tr}A^3BAB - h(2\mathrm{Tr}A^2BAB^2AB - \mathrm{Tr}A^2BABAB^2 - \mathrm{Tr}A^3BAB^3) + g\mathrm{Tr}A^5BAB - \mathrm{Tr}ABAB$$
$$0 = \mathrm{Tr}A^3BAB + g\mathrm{Tr}A^5BAB - 2\mathrm{Tr}ABAB - h(-2\mathrm{Tr}A^2BABAB^2 + 2\mathrm{Tr}ABABABAB)$$
$$0 = \mathrm{Tr}A^3BAB + g\mathrm{Tr}A^3BAB^3 - h(-\mathrm{Tr}A^3BA^3B + 2\mathrm{Tr}A^4BA^2B - \mathrm{Tr}A^5BAB)$$
$$0 = g\mathrm{Tr}A^3BA^3B + \mathrm{Tr}A^3BAB - h(2\mathrm{Tr}A^3B^2AB^2 - 2\mathrm{Tr}A^3BAB^3)$$
$$0 = -\mathrm{Tr}A^2B^2 + \mathrm{Tr}A^2BA^2B - h(-\mathrm{Tr}A^2BAB^2AB + 2\mathrm{Tr}A^2BABAB^2 - \mathrm{Tr}A^3B^2AB^2) + g\mathrm{Tr}A^4BA^2B$$
$$\beta = \mathrm{Tr}A^2BA^2B + g\mathrm{Tr}A^3B^2AB^2 - h(2\mathrm{Tr}A^3BA^3B - 2\mathrm{Tr}A^4BA^2B).$$
$$\text{(E.3)}$$

---

[40]We slightly abuse the notations in this appendix: all single trace operators in this section actually mean their expectation values. For example $\mathrm{Tr}A^2$ is actually $\langle \mathrm{Tr}A^2 \rangle$

This is a system of 14 linear equations for 21 variables. For generic values of h and g, like the one we often chose in this paper $h = g = 1$, they are all linearly independent. So we can express 14 variables including β through seven variables of shortest lengths. These seven variables form the subset x_{red} introduced in Appendix D.4. For $h = g = 1$, we can take it as:

$$x_{\text{red}} = (\text{Tr}A^2, \ \text{Tr}A^4, \ \text{Tr}A^2B^2, \ \text{Tr}A^6, \ \text{Tr}A^8, \ \text{Tr}A^6B^2, \ \text{Tr}A^5BAB)^{\text{T}}. \tag{E.4}$$

The other operators, including β, can be expressed as linear combinations of these variables:

$$
\begin{aligned}
\text{Tr}ABAB &= \tfrac{1}{2}\text{Tr}A^2 + \tfrac{1}{2}\text{Tr}A^4 + \text{Tr}A^2B^2 - \tfrac{1}{2} \\
\text{Tr}A^4B^2 &= \tfrac{1}{6}\text{Tr}A^2 - \text{Tr}A^2B^2 + \tfrac{1}{6}\text{Tr}A^6 + \tfrac{1}{6} \\
\text{Tr}A^3BAB &= -\tfrac{5}{6}\text{Tr}A^2 + \tfrac{1}{2}\text{Tr}A^4 - \text{Tr}A^2B^2 + \tfrac{2}{3}\text{Tr}A^6 + \tfrac{1}{6} \\
\text{Tr}A^2BA^2B &= -\text{Tr}A^2 + \text{Tr}A^4 - \text{Tr}A^2B^2 + \text{Tr}A^6 \\
\text{Tr}A^4BA^2B &= -\tfrac{8}{3}\text{Tr}A^2 + 9\text{Tr}A^4 - \tfrac{14}{3}\text{Tr}A^2B^2 - \tfrac{1}{3}\text{Tr}A^6 - \tfrac{8}{3}\text{Tr}A^8 - \tfrac{16}{3}\text{Tr}A^6B^2 + \tfrac{28}{3}\text{Tr}A^5BAB + \tfrac{1}{3} \\
\text{Tr}A^4B^4 &= \tfrac{5}{2}\text{Tr}A^2 - 8\text{Tr}A^4 + \tfrac{17}{3}\text{Tr}A^2B^2 + \tfrac{1}{6}\text{Tr}A^6 + \tfrac{8}{3}\text{Tr}A^8 + \tfrac{13}{3}\text{Tr}A^6B^2 - \tfrac{22}{3}\text{Tr}A^5BAB - \tfrac{1}{2} \\
\text{Tr}A^3BA^3B &= -\tfrac{9}{2}\text{Tr}A^2 + \tfrac{31}{2}\text{Tr}A^4 - \tfrac{23}{3}\text{Tr}A^2B^2 - \tfrac{2}{3}\text{Tr}A^6 - \tfrac{14}{3}\text{Tr}A^8 - \tfrac{28}{3}\text{Tr}A^6B^2 + \tfrac{46}{3}\text{Tr}A^5BAB + \tfrac{1}{2} \\
\text{Tr}A^3BAB^3 &= 2\text{Tr}A^4 - \tfrac{2}{3}\text{Tr}A^2B^2 - \tfrac{2}{3}\text{Tr}A^6 - \tfrac{2}{3}\text{Tr}A^8 - \tfrac{4}{3}\text{Tr}A^6B^2 + \tfrac{7}{3}\text{Tr}A^5BAB \\
\text{Tr}A^3B^2AB^2 &= -\tfrac{8}{3}\text{Tr}A^2 + 10\text{Tr}A^4 - 5\text{Tr}A^2B^2 - \tfrac{2}{3}\text{Tr}A^6 - 3\text{Tr}A^8 - 6\text{Tr}A^6B^2 + 10\text{Tr}A^5BAB + \tfrac{1}{3} \\
\text{Tr}A^2BABAB^2 &= -\tfrac{14}{3}\text{Tr}A^2 + 14\text{Tr}A^4 - \tfrac{26}{3}\text{Tr}A^2B^2 - 4\text{Tr}A^8 - 8\text{Tr}A^6B^2 + 14\text{Tr}A^5BAB + \tfrac{2}{3} \\
\text{Tr}A^2BAB^2AB &= -3\text{Tr}A^2 + 8\text{Tr}A^4 - \tfrac{17}{3}\text{Tr}A^2B^2 - \tfrac{7}{3}\text{Tr}A^8 - \tfrac{14}{3}\text{Tr}A^6B^2 + \tfrac{26}{3}\text{Tr}A^5BAB + \tfrac{2}{3} \\
\text{Tr}A^2B^2A^2B^2 &= -\tfrac{41}{6}\text{Tr}A^2 + 18\text{Tr}A^4 - \tfrac{28}{3}\text{Tr}A^2B^2 + \tfrac{1}{2}\text{Tr}A^6 - 5\text{Tr}A^8 - 11\text{Tr}A^6B^2 + 18\text{Tr}A^5BAB + \tfrac{5}{6} \\
\text{Tr}ABABABAB &= -\tfrac{67}{12}\text{Tr}A^2 + \tfrac{55}{4}\text{Tr}A^4 - \tfrac{61}{6}\text{Tr}A^2B^2 + \tfrac{1}{3}\text{Tr}A^6 - 4\text{Tr}A^8 - 8\text{Tr}A^6B^2 + \tfrac{29}{2}\text{Tr}A^5BAB + \tfrac{5}{4} \\
\beta &= -2\text{Tr}A^4 + \text{Tr}A^6 + \text{Tr}A^8 + 2\text{Tr}A^6B^2 - 2\text{Tr}A^5BAB.
\end{aligned} \tag{E.5}
$$

E.2 Correlation matrix and relaxation matrix

As we discussed in Section 5, under the $\mathbb{Z}_2^3$ symmetry our correlation matrix decouples into a block-diagonal matrix with three blocks. They are, respectively, the inner product[41] matrix of even-even words:

$$I, AA, BB, AAAA, AABB, ABAB, ABBA, BAAB, BABA, BBAA, BBBB \tag{E.6}$$

odd-odd words:

$$AB, BA, AAAB, AABA, ABAA, ABBB, BAAA, BABB, BBAB, BBBA \tag{E.7}$$

and even-odd words:

$$B, AAB, ABA, BAA, BBB\,. \tag{E.8}$$

For example, the block for the even-odd words reads:

$$
\begin{pmatrix}
\text{Tr}A^2 & \text{Tr}A^4 & \text{Tr}A^2B^2 & \text{Tr}ABAB & \text{Tr}A^2B^2 \\
\text{Tr}A^4 & \text{Tr}A^6 & \text{Tr}A^4B^2 & \text{Tr}A^3BAB & \text{Tr}A^4B^2 \\
\text{Tr}A^2B^2 & \text{Tr}A^4B^2 & \text{Tr}A^4B^2 & \text{Tr}A^3BAB & \text{Tr}A^2BA^2B \\
\text{Tr}ABAB & \text{Tr}A^3BAB & \text{Tr}A^3BAB & \text{Tr}A^2BA^2B & \text{Tr}A^3BAB \\
\text{Tr}A^2B^2 & \text{Tr}A^4B^2 & \text{Tr}A^2BA^2B & \text{Tr}A^3BAB & \text{Tr}A^4B^2
\end{pmatrix} \tag{E.9}
$$

---

[41] Here inner product of $\mathcal{O}_1$ and $\mathcal{O}_2$ is defined to be $\langle \text{Tr}\mathcal{O}_1^\dagger \mathcal{O}_2 \rangle$.

It is easy to construct the relaxation matrix for this example using the explanations of Appendix D.4. It is:

$$\begin{pmatrix} 1 & \mathrm{Tr}A^2 \\ \mathrm{Tr}A^2 & \beta \end{pmatrix} \succeq 0. \tag{E.10}$$

We note that in our current setting the vector $x_{1\mathrm{red}}$ is a single component vector with the component $\mathrm{Tr}A^2$.

To turn the original problem into the form (4.1), we substitute the "solution" of the loop equations (E.5) into the correlation matrix and the relaxation matrix. As for the objective function, we choose it to minimize $\mathrm{Tr}A^2$ and $-\mathrm{Tr}A^2$ to find the minimal and the maximal value of $\mathrm{Tr}A^2$, respectively. In this way, we can get the allowed region of $\mathrm{Tr}A^2$. At the next step we generate the input file for SDPA and solve it. With the appropriate setup, the entire time consumed for generating the input and solving it should last less than 0.1s CPU time. The result for $\Lambda = 4$ bootstrap is then:

$$0.393566 \leq \mathrm{Tr}A^2 \leq 0.431148. \tag{E.11}$$

F   Structure of loop equations and solvable 2-matrix model

Generalizing the results derived in Section 3.1 to multi-matrix model is far from straightforward. In one-matrix model, all the information contained in the loop equations and the positivity conditions can be encoded compactly into the resolvent function. On the contrary, for the multi-matrix model, as the loop equations and the correlation matrix both get much more involved, we don't expect to have such an analytic function enclosing the information of all the moments. Due to this complication, the bootstrap problem for a general multi-matrix model is generally not exactly solvable. In this appendix, we will discuss the nature of these complications in the structure of the loop equations and remind, from this point of view, an old result for the simplest 2-mattrix model with $\mathrm{tr}(AB)$ interaction when the loop equations greatly simplify [43, 53].

F.1   Base moments

As demonstrated in Section 2 by the loop equations, all higher moments of one-matrix model are fully determined by a fixed number of lower moments (which we will call the *base moments*). But this is not generally true in multi-matrix model: namely, the number of such base moments generally grows with the increase of the cutoff Λ. Let us take the model d (5.1) as an example. The following results can be observed from our numerical investigation [42]:

1. In the simplest case $h = 0$ when the model effectively factorizes into two decoupled one-matrix models, all the moments can be expressed by a polynomial of $t_2 = \langle \mathrm{Tr}A^2 \rangle$ and g. The number of base moments is 1 here.[43]

---

[42]at some finite but high cutoffs, but we strongly believe that it holds also for arbitrarily high cutoff.

[43]We assumed the global symmetry.

2. For $g = 0$ which is also solvable, all the moments are fixed by $t_{2k} = \langle \mathrm{Tr} A^{2k} \rangle$, $k = 1, 2, \dots$. This is very different from the one-matrix model since here we have to specify the value of infinite number of moments to determine the value of the remaining moments. If we set a finite cutoff 2Λ to the length of the moments, we have a set of truncated set of base moments of the size Λ.

3. For the general parameters ($g \neq 0$, $h \neq 0$), there are much more base moments than the case $g = 0$.

The intuition here is that, for a given multi-matrix model, the number of the base moments is negatively related with the solvability of the multi-matrix model. For a given cutoff, the number of the base moments are relatively easy to calculate. So one of the possible application of this intuitive observation is that one can use the number of the base moments for a finite but high cutoff to predict the solvability of the model.

F.2 Closed subset of loop equations

Sometimes, the loop equations can be closed on a proper, much reduced subset of all moments. This usually leads to a great simplification of the system of loop equations and potentially makes the bootstrap problem for the multi-matrix model exactly solvable. we demonstrate this on the simplest solvable 2-matrix model, with a long history of stydy and applications [15–17] and used in [28] to demonstrate the matrix bootstrap:

$$Z = \lim_{N \to \infty} \int d^{N^2}A \, d^{N^2}B \, \mathrm{e}^{-N\mathrm{tr}(-AB + V(A) + V(B))}, \qquad V(x) = g_2 x^2/2 + g_3 x^3/3. \quad \text{(F.1)}$$

We notice that the following subset of loop equations:

$$-g_3 t_{n+1} = g_2 t_n - t_{n-1,1} - \sum_{j=0}^{n-2} t_j t_{n-2-j},$$

$$-g_3 t_{n+1,1} = g_2 t_{n,1} - t_{n-1,2} - \sum_{j=0}^{n-2} t_j t_{n-2-j,1}, \quad \text{(F.2)}$$

$$-g_3 t_{n-1,2} = g_2 t_{n-1,1} - t_n,$$

are closed among the operators t_n, $t_{n,1}$, $t_{n,2}$, here:

$$t_n = \langle \mathrm{Tr} A^n \rangle, \, t_{n,m} = \langle \mathrm{Tr} A^n B^m \rangle. \quad \text{(F.3)}$$

Summing over the equations by the way in Section 2.1, we can get the *Master loop equation* for model (F.1) [53]:

$$(Y(z) - V'(z))(z - V'(Y(z))) + P(Y(z), z) = 0, \quad \text{(F.4)}$$

where

$$P(x, y) = -\langle \mathrm{Tr} \frac{V'(x) - V'(A)}{x - A} \frac{V'(y) - V'(B)}{y - B} \rangle + 1,$$

$$G(z) = \langle \mathrm{Tr} \frac{1}{z - A} \rangle = \sum_{i=0}^{\infty} z^{-i-1} t_i, \quad \text{(F.5)}$$

$$Y(z) = V'(z) - G(z).$$

Since this is a closed subset of loop equations, we assume that the sub-correlation matrix defined by $T_{i,j} = t_{i+j-2}$ is positive semi-definite, which is the positivity condition for the minor of the whole correlation matrix consisting of the elements t_n. This brings us back to the one-matrix type bootstrap problem considered in Section 3.2. Here the positivity condition is equivalent to that the eigenvalue distribution corresponding to $G(z)$ is real and positive, or $Y(z)$ has a negative cut. In principle, this problem is analytically solvable, the complication compared with one-matrix model is that we have a cubic equation instead of a quadratic one (or an equation of nth degree for the potentials of order n). The solution of these loop equations has been found in [54] in terms of an algebraic curve depending on the base moments [55].

Acknowledgments

References

[1] G. 't Hooft, *A Planar Diagram Theory for Strong Interactions*, *Nucl. Phys. B* **72** (1974) 461.

[2] A.A. Migdal, *Loop Equations and 1/N Expansion*, *Phys. Rept.* **102** (1983) 199.

[3] F. David, *Planar Diagrams, Two-Dimensional Lattice Gravity and Surface Models*, *Nucl. Phys. B* **257** (1985) 45.

[4] V.A. Kazakov, A.A. Migdal and I.K. Kostov, *Critical Properties of Randomly Triangulated Planar Random Surfaces*, *Phys. Lett. B* **157** (1985) 295.

[5] V.A. Kazakov, *Bilocal Regularization of Models of Random Surfaces*, *Phys. Lett. B* **150** (1985) 282.

[6] V.A. Kazakov, *EXACTLY SOLVABLE POTTS MODELS, BOND AND TREE LIKE PERCOLATION ON DYNAMICAL (RANDOM) PLANAR*, in *International Symposium on Field Theory of the Lattice*, 12, 1987.

[7] O. Bohigas, M.J. Giannoni and C. Schmit, *Characterization of chaotic quantum spectra and universality of level fluctuation laws*, *Phys. Rev. Lett.* **52** (1984) 1.

[8] R. Dijkgraaf and C. Vafa, *Matrix models, topological strings, and supersymmetric gauge theories*, *Nucl. Phys. B* **644** (2002) 3 [`hep-th/0206255`].

[9] R. Dijkgraaf, S. Gukov, V.A. Kazakov and C. Vafa, *Perturbative analysis of gauged matrix models*, *Phys. Rev. D* **68** (2003) 045007 [`hep-th/0210238`].

[10] B. Eynard and N. Orantin, *Invariants of algebraic curves and topological expansion*, *Commun. Num. Theor. Phys.* **1** (2007) 347 [`math-ph/0702045`].

[11] M. Kontsevich, *Intersection theory on the moduli space of curves and the matrix Airy function*, *Commun. Math. Phys.* **147** (1992) 1.

[12] H.L. Montgomery, *The pair correlation of zeros of the zeta function*, in *Proc. Symp. Pure Math*, vol. 24, pp. 181–193, 1973.

[13] T. Eguchi and H. Kawai, *Reduction of Dynamical Degrees of Freedom in the Large N Gauge Theory*, *Phys. Rev. Lett.* **48** (1982) 1063.

[14] E. Brezin, C. Itzykson, G. Parisi and J.B. Zuber, *Planar Diagrams*, *Commun. Math. Phys.* **59** (1978) 35.

[15] C. Itzykson and J.B. Zuber, *The Planar Approximation. 2.*, *J. Math. Phys.* **21** (1980) 411.

[16] M.L. Mehta, *A Method of Integration Over Matrix Variables*, *Commun. Math. Phys.* **79** (1981) 327.

[17] V.A. Kazakov, *Exact Solution of the Ising Model on a Random Two-dimensional Lattice*, *JETP Lett.* **44** (1986) 133.

[18] D.V. Boulatov and V.A. Kazakov, *The Ising Model on Random Planar Lattice: The Structure of Phase Transition and the Exact Critical Exponents*, *Phys. Lett. B* **186** (1987) 379.

[19] I.K. Kostov, *O(n) Vector Model on a Planar Random Lattice: Spectrum of Anomalous Dimensions*, *Mod. Phys. Lett. A* **4** (1989) 217.

[20] J.-M. Daul, *Q states Potts model on a random planar lattice*, `hep-th/9502014`.

[21] V.A. Kazakov and A.A. Migdal, *Recent Progress in the Theory of Noncritical Strings*, *Nucl. Phys. B* **311** (1988) 171.

[22] V.A. Kazakov, *Solvable matrix models*, 2, 2000 [`hep-th/0003064`].

[23] A. Jevicki, O. Karim, J.P. Rodrigues and H. Levine, *Loop Space Hamiltonians and Numerical Methods for Large N Gauge Theories*, *Nucl. Phys. B* **213** (1983) 169.

[24] A. Jevicki, O. Karim, J.P. Rodrigues and H. Levine, *Loop Space Hamiltonians and Numerical Methods for Large N Gauge Theories. 2.*, *Nucl. Phys. B* **230** (1984) 299.

[25] J.P. Rodrigues, *Numerical Solution of Lattice Schwinger-dyson Equations in the Large N Limit*, *Nucl. Phys. B* **260** (1985) 350.

[26] R. Rattazzi, V.S. Rychkov, E. Tonni and A. Vichi, *Bounding scalar operator dimensions in 4D CFT*, *JHEP* **12** (2008) 031 [`0807.0004`].

[27] D. Simmons-Duffin, *The lightcone bootstrap and the spectrum of the 3d Ising CFT*, *Journal of High Energy Physics* **2017** (2017) 86 [`1612.08471`].

[28] H.W. Lin, *Bootstraps to strings: solving random matrix models with positivite*, *Journal of High Energy Physics* **2020** (2020) 90 [`2002.08387`].

[29] X. Han, S.A. Hartnoll and J. Kruthoff, *Bootstrapping Matrix Quantum Mechanics*, *Phys. Rev. Lett.* **125** (2020) 041601 [`2004.10212`].

[30] P.D. Anderson and M. Kruczenski, *Loop equations and bootstrap methods in the lattice*, *Nuclear Physics B* **921** (2017) 702 [`1612.08140`].

[31] Y.M. Makeenko and A.A. Migdal, *Exact Equation for the Loop Average in Multicolor QCD*, *Phys. Lett. B* **88** (1979) 135.

[32] M.F. Paulos, J. Penedones, J. Toledo, B.C. van Rees and P. Vieira, *The S-matrix bootstrap II: two dimensional amplitudes*, *Journal of High Energy Physics* **2017** (2017) 143 [`1607.06110`].

[33] D. Mazáč and M.F. Paulos, *The analytic functional bootstrap. Part I: 1D CFTs and 2D S-matrices*, *Journal of High Energy Physics* **2019** (2019) 162 [`1803.10233`].

[34] V.A. Kazakov, I.K. Kostov and N. Nekrasov, *D-particles, matrix integrals and KP hierarchy*, *Nuclear Physics B* **557** (1999) 413 [`hep-th/9810035`].

[35] V.A. Kazakov and P. Zinn-Justin, *Two matrix model with ABAB interaction*, *Nucl. Phys. B* **546** (1999) 647 [`hep-th/9808043`].

[36] I.K. Kostov, *Exact solution of the six vertex model on a random lattice*, *Nucl. Phys. B* **575** (2000) 513 [`hep-th/9911023`].

[37] P. Zinn-Justin, *The Six vertex model on random lattices*, *Europhys. Lett.* **50** (2000) 15 [`cond-mat/9909250`].

[38] R.G. Jha, *Introduction to Monte Carlo for Matrix Models*, `2111.02410`.

[39] B. Eynard, *Topological expansion for the 1-Hermitian matrix model correlation functions*, *JHEP* **11** (2004) 031 [`hep-th/0407261`].

[40] P. Di Francesco, P.H. Ginsparg and J. Zinn-Justin, *2-D Gravity and random matrices*, *Phys. Rept.* **254** (1995) 1 [`hep-th/9306153`].

[41] M. Reed and B. Simon, *II: Fourier Analysis, Self-Adjointness*, vol. 2, Elsevier (1975).

[42] V.A. Kazakov, *The Appearance of Matter Fields from Quantum Fluctuations of 2D Gravity*, *Mod. Phys. Lett. A* **4** (1989) 2125.

[43] M. Staudacher, *Combinatorial solution of the two matrix model*, *Phys. Lett. B* **305** (1993) 332 [`hep-th/9301038`].

[44] S. Boyd and L. Vandenberghe, *Convex Optimization*, Cambridge University Press (2004), 10.1017/CBO9780511804441.

[45] J.R. Hoppe, *Quantum Theory of a Massless Relativistic Surface and a Two-Dimensional Bound State Problem.*, Ph.D. thesis, MASSACHUSETTS INSTITUTE OF TECHNOLOGY., Jan., 1982.

[46] S. El-Showk, M.F. Paulos, D. Poland, S. Rychkov, D. Simmons-Duffin and A. Vichi, *Solving the 3D Ising Model with the Conformal Bootstrap*, *Phys. Rev. D* **86** (2012) 025022 [`1203.6064`].

[47] Y. Shimamune, *On the phase structure of large N matrix models and gauge models*, *Physics Letters B* **108** (1982) 407.

[48] M. Teper, *Large N*, *PoS* **LATTICE2008** (2008) 022 [`0812.0085`].

[49] E. Brezin and D.J. Gross, *The External Field Problem in the Large N Limit of QCD*, *Phys. Lett. B* **97** (1980) 120.

[50] I.K. Kostov, *RANDOM SURFACES, SOLVABLE LATTICE MODELS AND DISCRETE QUANTUM GRAVITY IN TWO-DIMENSIONS*, in *XIX International Seminar on Theoretical Physics: Nonperturbative Aspects of the Standard Model (GIFT Seminar)*, 6, 1988.

[51] M. Yamashita, K. Fujisawa, M. Fukuda, K. Kobayashi, K. Nakata and M. Nakata, *Latest developments in the sdpa family for solving large-scale sdps*, in *International Series in Operations Research and Management Science*, International Series in Operations Research and Management Science, pp. 687–713, Springer New York LLC (2012), DOI.

[52] D. Simmons-Duffin, *A semidefinite program solver for the conformal bootstrap*, *Journal of High Energy Physics* **2015** (2015) 174 [`1502.02033`].

[53] B. Eynard, *Large N expansion of the 2 matrix model*, *JHEP* **01** (2003) 051 [`hep-th/0210047`].

[54] V.A. Kazakov and A. Marshakov, *Complex curve of the two matrix model and its tau function*, *J. Phys. A* **36** (2003) 3107 [`hep-th/0211236`].

[55] V.A. Kazakov and I.K. Kostov, *Instantons in noncritical strings from the two matrix model*, in *From Fields to Strings: Circumnavigating Theoretical Physics: A Conference in Tribute to Ian Kogan*, 3, 2004, DOI [`hep-th/0403152`].

Paper II

Bootstrap for Lattice Yang-Mills theory

Vladimir Kazakov *and* Zechuan Zheng*
Laboratoire de physique de l'École normale supérieure,
ENS, Université PSL, CNRS, Sorbonne Université,
Université Paris Cité, 24 rue Lhomond, F-75005 Paris, France and
Interdisciplinary Scientific Center Poncelet (CNRS UMI 2615)

We study the $SU(\infty)$ lattice Yang-Mills theory at the dimensions $D = 2, 3, 4$ via the numerical bootstrap method. It combines the LEs, with a cut-off $L_{\max}$ on the maximal length of loops, and positivity conditions on certain matrices of Wilson loop averages. Our algorithm is inspired by the pioneering paper of P.Anderson and M.Kruczenski but it is significantly more efficient, as it takes into account the symmetries of the lattice theory and uses the relaxation procedure in line with our previous work on matrix bootstrap. We thus obtain rigorous upper and lower bounds on the plaquette average at various couplings and dimensions. For $D = 4$, $L_{\max} = 16$ the lower bound data appear to be close to the Monte Carlo data in the strong coupling phase and the upper bound data in the weak coupling phase reproduce well the 3-loop perturbation theory. Our results suggest that this bootstrap approach can provide a tangible alternative to the, so far uncontested, Monte Carlo approach.

INTRODUCTION

The $SU(N_c)$ Yang-Mills (YM) lattice gauge theory (LGT) is a fundamental ingredient of modern particle physics. Its most illustrious applications are the Standard Model and, in particular, the Quantum Chromodynamics. Nowadays, most of the non-perturbative computations in Yang-Mills theory are done by Monte Carlo (MC) simulations for the lattice formulation of YM theory. Combined with the perturbation theory (PT) [1–5] and RG tools, MC methods have had a huge success, especially in the recent couple of decades, due to the development of supercomputers. It allowed us to compute with a reasonable precision certain masses of hadrons and the S-matrix elements in QCD, reproducing the experimental data [6, 7]. However, the absence of any systematic non-perturbative "analytic" alternative to MC is, practically and intellectually, somewhat uncomfortable. Moreover, the MC method has its inherent limitations: statistical errors, finite lattice size, high numerical cost of inclusion of dynamical quarks, difficulties in treating finite baryon density, and the real-time dynamics.

An interesting alternative for the study of the LGT is provided by Makeenko-Migdal loop equations (LE) [8, 9] for Wilson loop averages (WA). An early attempt at numerical study of LE in the large N_c, 't Hooft limit was proposed in [10–13], in the form of minimization of effective action in the loop space. A more recent brave attempt to bootstrap the LE, combining them with certain positivity conditions [14, 15] revived hopes of a more analytic approach. Slightly later, a similar bootstrap method was proposed in [16] for the multi-matrix models. In our work [17] we significantly improved matrix bootstrap by introducing a "relaxation" procedure and applied it to an "analytically unsolvable" large N 2-matrix model, with remarkable efficiency and precision, noticeably exceeding those of MC for the same model [18].
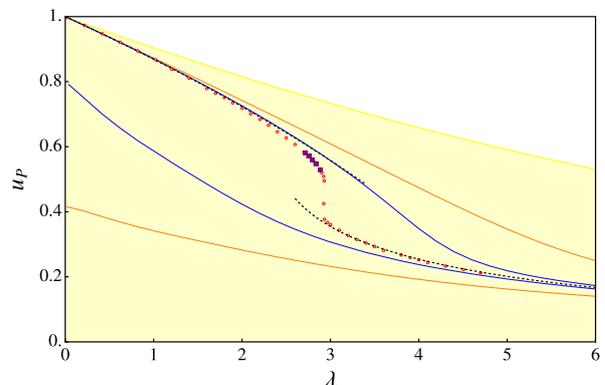

FIG. 1: Our bootstrap results for upper and lower bounds on plaquette average in $4D$ LGT (1): for $L_{\max} = 8$ (yellow domain) for $L_{\max} = 12$ (orange curves) and $L_{\max} = 16$ (blue curves). Red circles represent the MC data for $SU(10)$ LGT (with 5 purple squares for $SU(12)$). Dashed upper and lower lines represent the 3-loop PT (13) and strong coupling expansion (14), resp.

These developments have been considerably inspired by the success of the bootstrap approach to CFTs [19, 20] and S-matrices in massive QFTs [21–23].

Unlike MC where the result is given up to statistical error bars, the bootstrap methods provides rigorous inequalities giving upper and lower bounds on computed physical quantities. These bounds can only improve when increasing the number of bootstrapped variables and constraints on them.

Here we develop a powerful numerical bootstrap algorithm for solving the LEs [8, 9] in the lattice YM theory at $N_c \to \infty$ and demonstrate it on the computation of plaquette average $u_P = \frac{1}{N_c}\langle \operatorname{tr} U_P \rangle$. Its main ingredients are i) positivity of correlation matrix of WAs; ii) our
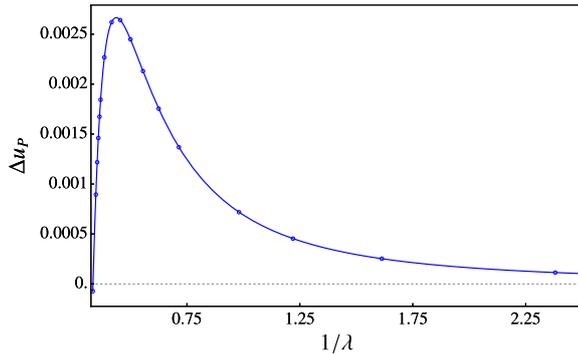
FIG. 2: The plot $\Delta u_P \equiv u_P^{\text{boot}} - u_P^{\text{PT}}$ which might capture the non-perturbative values of the gluon condensate $\langle \text{tr} \ (F_{\mu\nu} F^{\mu\nu}) \rangle$.

relaxation procedure of [17]; iii) positivity of reflection matrices due to lattice symmetries. iv) symmetry reduction of the positivity conditions. In the supplementary material we worked out a simple example for our general method together with some data points.

Our data (obtained on a single workstation), already for the modest length cutoff $L_{\max} = 16$, look quite encouraging: as seen on Fig.1, for $D = 4$, our lower(upper) bounds are quite close to the MC data [14, 15, 24, 25] in the strong(weak) coupling phase, at least far enough from the phase transition. The upper bound is remarkably close to the 3-loop PT.

On Fig.2 we plot the difference of the bootstrap upper bound and the 3-loop PT: $\Delta u_P \equiv u_P^{\text{boot}} - u_P^{\text{PT}}$ as function of $1/\lambda$. It might capture the non-perturbative effect for the gluon condensate $\langle \text{tr} \ (F_{\mu\nu} F^{\mu\nu}) \rangle$ – in principal a measurable observable [26–28]. The graph is very smooth and it is positive even slightly beyond the phase transition point $\lambda_c \simeq 2.9$. [29]

YANG-MILLS LOOP EQUATIONS AT LARGE N

We study the LGT with the Wilson action [30]:

$$S = -\frac{N_c}{\lambda} \sum_P \text{Re} \, \text{tr} \, U_P \tag{1}$$

where U_P is the product of four unitary link variables around the plaquette P and we sum over all plaquettes P, including both orientations. The main quantities of interest in 't Hooft limit $N_c \to \infty$ are the WAs:

$$W[C] = \langle \frac{\text{tr}}{N_c} \prod_{l \in C} U_l \rangle. \tag{2}$$

The matrix product goes over the link variables belonging to the lattice loop C. $W[C]$ are subject to LEs, i.e., the Schwinger-Dyson equations expressing measure invariance w.r.t. group shifts $U_l \to U_l(1 + i\epsilon)$. Schematically
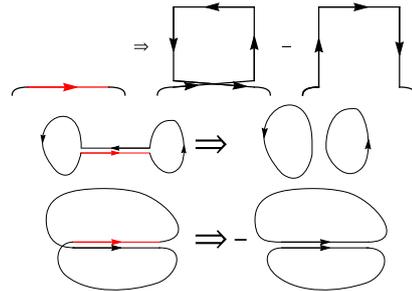

FIG. 3: Schematic representation of LEs: The first line shows the variation of a link of Wilson loop in the LHS of Eq.(3). The 2nd and 3rd lines show the splitting of the contour along the varied line into two sub-contours, for two different orientations of coinciding links in the RHS of Eq.(3).

LE reads:

$$\sum_{\nu \perp \mu} \left(W[C_{l_\mu} \cdot \overrightarrow{\delta C_{l_\mu}^\nu}] - W[C_{l_\mu} \cdot \overleftarrow{\delta C_{l_\mu}^\nu}] \right)$$
$$= \lambda \sum_{\substack{l' \in C \\ l' \sim l}} \epsilon_{ll'} W[C_{ll'}] \, W[C_{l'l}] \tag{3}$$

where the LHS represents the loop operator acting on the link l_μ by replacing it with the loop around plaquette $\overrightarrow{\delta C_{l_\mu}^\nu}$ or $\overleftarrow{\delta C_{l_\mu}^\nu}$ (depending on the orientation, as shown in the first line of Fig 3). The LHS sum goes around all $2(D-1)$ $\mu\nu$-plaquettes orthogonal to the direction μ. The RHS sum goes over all appearances of the the same lattice link l in the loop C. The RHS product corresponds to splitting of the contour $C \to C_{ll'} \cdot C_{l'l}$, as explained in the 2nd and 3rd lines of Fig.3. Finally, $\epsilon_{ll'} = \pm 1$ for links l and l' with opposite or colinear orientation, respectively. For more details on LEs, see [14, 31, 32].

Back-track loop equations

To get the full list of the LEs, we also consider the "back-track" LEs. They correspond to doing variations on the links at the end of "back-track" paths originating from the vertices of Wilson loop. These "back-tracks" are equivalent to inserting the identity, but their Schwinger-Dyson variation, can give independent LEs. Fig 4 shows an example of "back-track" LE:

The LEs close on single trace WAs (2) (due to the large N_c factorization of color traces), which means that
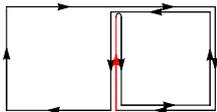
FIG. 4: An example of nonlinear "back-track" LE.

they behave as classical quantities on the loop space. At $L_{\max} = 16$, we have about $40,000$ LEs in $3D$ and about $100,000$ LEs in $4D$, and the back-track LEs constitute more than 80% of all these LEs. Around three-quarters of them are linearly independent and only a small minority are non-linear. Finding the solution to these equations is our primary task for any other progress in studying the physical quantities of planar QCD or its $1/N_c$ corrections. The problem is very complicated since it is formulated in extremely complex loop space. We will try to solve it using the bootstrap approach.

BOOTSTRAP ALGORITHM

Positivity Constraints

In general, our positivity conditions come from the positivity of possible inner products on the vector space or a subspace of the operators, i.e.

$$\langle \mathcal{O} | \mathcal{O} \rangle = \langle \mathcal{O}^\dagger \mathcal{O} \rangle = \alpha^{*\mathrm{T}} \mathcal{M} \alpha \geqslant 0 \Leftrightarrow \mathcal{M} \succeq 0. \quad (5)$$

where $\mathcal{O} = \sum \alpha_i \mathcal{O}_i$ is an operator with arbitrary coefficients α_i, and $\mathcal{O}_i$ are basis vectors of the operators.

One of possible adjoint operators $\mathcal{O}^\dagger$ comes from taking the Hermitian conjugation [14, 16, 17]. For a Wilson path, the Hermitian conjugation corresponds to reversing the path. By taking a linear combination of all Wilson paths $0 \to x$ (between the points 0 and x), with arbitrary coefficients, we can get non-trivial positivity conditions from their inner product. For example, we have only two paths $0 \to (1,1)$, at $L_{\max} = 2$

$$\mathrm{Path}_1 = \ulcorner \quad , \quad \mathrm{Path}_2 = \lrcorner \quad (6)$$

and the positivity condition reads:

$$\begin{array}{c} \phantom{\mathrm{Path}_1^\dagger} \quad \overset{\mathrm{Path}_1 \;\; \mathrm{Path}_2}{} \\ \begin{array}{c} \mathrm{Path}_1^\dagger \\ \mathrm{Path}_2^\dagger \end{array} \left(\begin{array}{cc} 1 & u_P \\ u_P & 1 \end{array} \right) \succeq 0. \end{array} \quad (7)$$

This gives $u_P^2 \leqslant 1$, obvious from unitarity. We call the positivity matrices arising from the Hermitian conjugation the correlation matrices.

Apart from Hermitian conjugation, we have additional reflection positivity conditions where adjoined operators $\mathcal{O}^\dagger$ come from reflection symmetries [33]. For LGT, there are three types of reflections w.r.t. different planes: site,
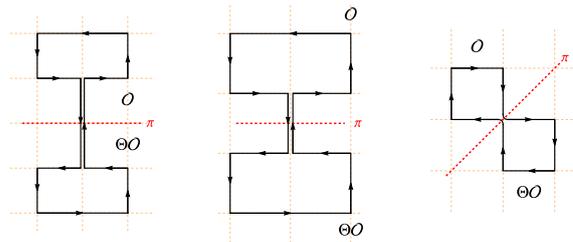

FIG. 5: Examples of three reflection symmetries on the lattice allowing new positivity conditions on WAs.

link and diagonal reflections [34, 35]. Fig 5 illustrates the corresponding adjoint paths for these reflections. The importance of 3 new reflection positivity conditions is illustrated on Fig 6 where we compare $L_{\max} = 12$ bootstrap results with and without reflection positivity.

For computations in this work, we consider the full positivity constraint $0 \to x$ for any possible x when $L_{\max} \leqslant 12$. But for $L_{\max} = 16$, we consider only the paths $0 \to 0$ for various positivity matrices since:

1. When constructing correlation matrices, all the positivity conditions on the open Wilson paths $0 \to x$ are already contained in $0 \to 0$ correlation matrix for higher lengths (due to back-trackings).

2. At $L_{\max} = 16$, we observe empirically that the $0 \to 0$ constraints are computationally the most efficient. One important reason for that is that the positive matrices corresponding to $0 \to 0$ are numerically more tractable w.r.t. symmetry reduction that we will discuss below.

Convex relaxation

In general, LEs are non-linear. Here we use the relaxation method to replace all the non-linear LE with linear ones where in the r.h.s. we replace the products of WAs with new variables Q_{ij}, subject to extra constraints [17]:

$$Q_{ij} = W_i W_j \overset{\text{replace}}{\Longrightarrow} \begin{pmatrix} 1 & W^{\mathrm{T}} \\ W & Q \end{pmatrix} \succeq 0. \quad (8)$$

Here $W = \{W_1, W_2, W_3, \dots\}$ denotes the column vector of all inequivalent WAs. Notice that the relaxation matrix has rank=1 precisely when $Q_{ij} = W_i W_j$.

The LEs combined with the convex relaxation and positivity conditions constitute the constraints of semi-definite programming (SDP). To get rigorous bounds on WAs, we can maximize or minimize u_P.

Dimension	Hermitian Conjugation	site&link reflection	diagonal reflection
2	$B_2 \times \mathbb{Z}_2$	$\mathbb{Z}_2 \times \mathbb{Z}_2$	$\mathbb{Z}_2 \times \mathbb{Z}_2$
3	$B_3 \times \mathbb{Z}_2$	$B_2 \times \mathbb{Z}_2$	$\mathbb{Z}_2^3$
4	$B_4 \times \mathbb{Z}_2$	$B_3 \times \mathbb{Z}_2$	$B_2 \times \mathbb{Z}_2^2$

TABLE I: Invariant groups of correlation and reflection matrices.

Reduction by Symmetry Group

In conformal and S-matrix bootstraps, the positivity conditions are well-known to be organized in different spin channels [19, 36] and different irreducible representations of global symmetry [37–40]. In parallel to that observation, we can greatly reduce the positivity matrices via the global lattice symmetries.

Formally, if we have an invariant group G preserving the inner product

$$\langle (g \circ \mathcal{O}_1) | (g \circ \mathcal{O}_2) \rangle = \langle \mathcal{O}_1 | \mathcal{O}_2 \rangle, \ \forall g \in G \qquad (9)$$

then the positivity condition on the matrix $\mathcal{M}$ defined in Eq 5 can be re-arranged into a block-diagonal form corresponding to the irreps of G.

This well-studied procedure is known under the name "Invariant Semidefinite Programming". Here we refer to a statement [41] directly related to our current problem: *If the vector space of the paths can be decomposed as a direct sum of irreducible representations* Rep_k *of the invariant group with multiplicity* m_k:

$$V = \bigoplus_{k=1}^{D} \text{Rep}_k^{\oplus m_k}, \qquad (10)$$

then the positivity condition of the inner-product matrix is equivalent to the collection of positivity conditions on the matrices corresponding to each Rep_k*, with matrix dimension* $m_k \times m_k$.

For the correlation matrix $0 \to 0$, the invariant group G is $B_d \times \mathbb{Z}_2$, where B_d is the Hyperoctahedral group in d spacetime dimensions. It acts on a Wilson path by corresponding rotations and reflections on the spacetime lattice. $\mathbb{Z}_2$ is the group action reversing the path.

For the reflection positivity matrices $0 \to 0$ the invariant groups are subgroups of $B_d \times \mathbb{Z}_2$, leaving the reflection plane invariant. These invariant subgroups are summarized in Table I.

Implementing this symmetry reduction is similar to projecting the physical state w.r.t spin and parity in conformal or S matrix bootstrap. Practically we do the following steps:

1. Find a specific realization of every irrep of the invariant group using GAP software [42].

2. Use the algorithm initiated in [43] to find an equivalent real representation (if the irrep by GAP is complex).

3. To decompose into such irreps, we use the projector to Rep_k [44] :

$$p_{\alpha\alpha,k} = \frac{\dim(\text{Rep}_k)}{\dim G} \sum_{g \in G} r_{\alpha\alpha}(g^{-1}) g \qquad (11)$$

Here $r_{\alpha\beta}$ is a matrix element of a real representation identified at the step 2, and $\alpha, \beta = 1, 2, \ldots, \dim(\text{Rep}_k)$. Taking $\alpha = 1$, $P_k = p_{11,k}$ gives us a projector to Rep_k.

Selection of multiplets of Wilson paths

The Wilson paths form different multiplets of the invariant group. Within each multiplet, the symmetry group permutes different Wilson paths. When constructing the positivity matrices, some multiplets are more important than others. We kept only the most important multiplets. More precisely, several WAs are not related to other WAs by the LEs, such as the 4×4 square Wilson loop at $L_{\max} = 16$. We believe that such WAs and the open Wilson paths out of which they are constructed are relatively unimportant.

As an example, take the correlation matrix for the paths $0 \to 0$ at $3D$ and $L_{\max} = 16$. It has a huge size 6505×6505. After the symmetry reduction and selection of the multiplets, the positivity of the correlation matrix reduces to postivity of 20 smaller matrices, each corresponding to its irrep, with sizes:

$$\begin{aligned} 38, 15, 25, 18, 62, 33, 68, 75, 56, 78, \\ 22, 18, 34, 15, 56, 33, 57, 76, 69, 73 \end{aligned} \qquad (12)$$

So the SDP gets greatly simplified.

DISCUSSION OF RESULTS

Here we present the results of computation of plaquette average $u_P(\lambda)$ for various bare couplings λ in LGT in $2D$, $3D$, and $4D$. On Fig 1 we compare our bootstrap data in $4D$ with MC for $SU(10)$ [15] and $SU(12)$ [24] LGT, assuming that, with our accuracy, $N_c = 10, 12$ are close enough to $N_c = \infty$. We also compare it with the known 3-loop $N_c = \infty$ PT result [46]:

$$u_P = 1 - \frac{\lambda}{8} - 0.005107\lambda^2 - 0.000794\lambda^3 + \mathcal{O}(\lambda^4) \quad (13)$$

as well as with the SC expansion valid in the SC phase, beyond the 1st order phase transition point $\lambda_c \simeq 2.9$ [47]:

$$u_P = \frac{1}{\lambda} + \frac{4}{\lambda^5} + \frac{60}{\lambda^9} + \frac{136}{\lambda^{11}} + \frac{1092}{\lambda^{13}} + \mathcal{O}(\lambda^{-15}). \quad (14)$$
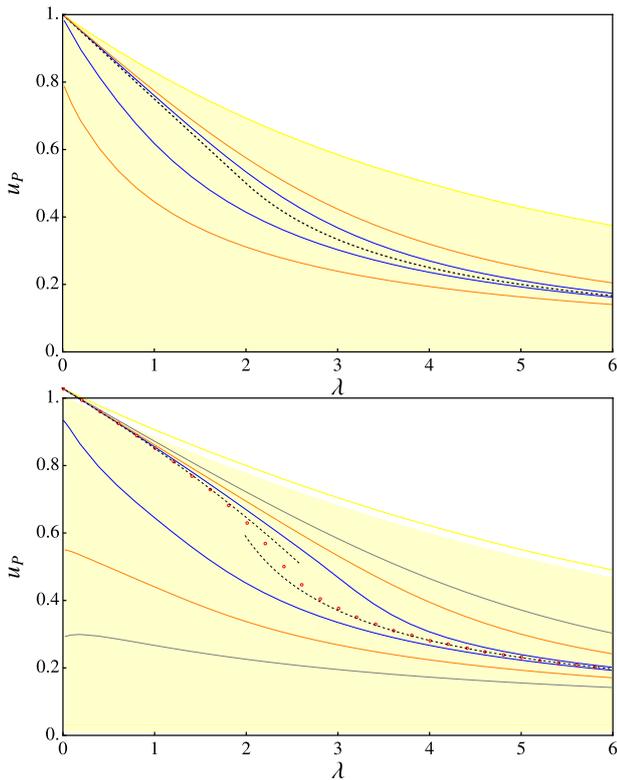
FIG. 6: u_P for $2D$ (upper) and $3D$ (lower) LGT: the upper and lower bounds from our bootstrap at $L_{\max} = 8$ (yellow region), $L_{\max} = 12$ (orange curves) and $L_{\max} = 16$ (blue curves). The $3D$ and $L_{\max} = 12$ result without reflection positivity (gray curve) is much less constraining. The line of red circles represents the MC data for $SU(10)$ LGT. The dashed black curve in $2D$ plot is the exact solution (15). The dashed black curve in $3D$ plot is the 3-loop PT result [45].

The bootstrap bounds on u_P given for $L_{\max} = 8, 12, 16$ on Fig. 1 are quickly improving with the increase of cutoff. The physically most interesting WC phase is much better described by the upper bound. Moreover, we see that the upper bound nicely reproduces the 3-loop PT (13) for a large range of coupling, even beyond the phase transition point where PT is, strictly speaking, not valid. However, comparing these results to MC data, we see that it is not yet so good at capturing the departure from the PT in the interval (2.4, 2.8) where the MC data of [24] (given by black squares on Fig.1) were used to compute the masses and the string tension. We expect a significant improvement for this range in our data if we reach $L_{\max} = 20$ or even 24. However, this will certainly demand much bigger computational resources.

Finally, we briefly discuss $2D$ and $3D$ cases. For $2D$ LGT the plaquette average can be computed exactly [48,

49] (as well as any loop average, see [50]):

$$u_P = \begin{cases} 1 - \frac{\lambda}{4}, & \text{for } \lambda \leqslant 2 \\ \frac{1}{\lambda}, & \text{for } \lambda \geqslant 2 \end{cases} \quad (15)$$

This example was important for both checking our algorithm and for observing how fast our bootstrap data approach the exact result when increasing $L_{\max}$. The results are presented on Fig. 6. For physically interesting and challenging case of $3D$ LGT, we compare on Fig. 6 our bootstrap bounds at $L_{\max} = 8, 12, 16$ with the MC data [15] as well as with the known 3-loop PT [45] and SC [47] results. We observe a reasonably fast approach of bootstrap bounds to the MC data when increasing $L_{\max}$, but they are not as close to PT as in $4D$ case.

We employ in LEs the WAs up to the maximal length $L_{\max}$, so it can be considered as our IR cutoff. The physical scale l_{ph} (set by inverse mass or square root of string tension) should, ideally, satisfy $1 \ll \frac{l_{ph}}{a_L} \ll L_{\max}$, where a_L is the lattice spacing. In this paper, we have, for the best of our data, $L_{\max} = 16$ which suggests that the window for the scale of measurable physical quantities in lattice units should be roughly $2 \lesssim \frac{l_{ph}}{a_L} \lesssim 6$ (compare it to Table 8 of [24] where the IR cutoff is set by the size of space-time torus, typically in the range 10 to 16, and the typical physical length is set by string tension $3 \lesssim \frac{l_{ph}}{a_L} \lesssim 6$).

We conclude that, even though the currently achieved values of $L_{\max}$ in our bootstrap approach may be not sufficient to match the precision and scope of the MC experiments, especially for the confinement sensitive physics (glueball masses, string tension, etc.), our results give good hopes on a considerable improvement when augmenting $L_{\max}$. Moreover, for sufficiently small couplings our upper bound data are already at least as good as MC.

PROSPECTS

The bootstrap procedure proposed here has a clear perspective for improving our results and advancing towards the computation of interesting observables. In particular, by choosing objective functions other than u_P, one can hope to get a better estimate for all involved physical quantities. For our current implementation at $L_{\max} = 16$, every data point takes $\backsim 20$ hours of CPU time for $4D$, and only half an hour for $3D$ [51]. First, we want to increase the cutoff to $L_{\max} = 20$ and even to $L_{\max} = 24$. This will certainly need supercomputer power. From our current results, we expect a quick narrowing of our bounds to the accuracy comparable to, or even better than MC (without its toll of statistical and systematic errors). Furthermore, since in the 't Hooft limit we don't have internal fermion loops, we can try to find the quark condensate and hadron masses by simply

summing up the WAs with the spinorial factors for the relevant one- and two-point functions. The $1/N_c$ corrections (which might be small enough even for the physical $N_c = 3$ case) seem to be not insurmountable tasks since they are subject to *linear* LEs [9], with coefficients given by the solution of LE (3). One of such problems is the computation of glueball masses from the connected correlator of two small Wilson loops. One can also try to bootstrap directly the $N_c = 3$ YM theory, where the absence of large factorization could be compensated by multiple functional relations between WAs, absent for $N_c = \infty$ case.

ACKNOWLEDGMENTS

---

* kazakov • lpt.ens.fr; zechuan.zheng.phy • gmail.com

[1] G. S. Bali, C. Bauer, and A. Pineda, Phys. Rev. D **89**, 054505 (2014), arXiv:1401.7999 [hep-ph].

[2] M. Lüscher, JHEP **04**, 142, arXiv:1412.5311 [hep-lat].

[3] M. Dalla Brida and M. Lüscher, Eur. Phys. J. C **77**, 308 (2017), arXiv:1703.04396 [hep-lat].

[4] L. Del Debbio, F. Di Renzo, and G. Filaci, EPJ Web Conf. **175**, 11023 (2018).

[5] M. G. Pérez, A. González-Arroyo, and M. Okawa, JHEP **10**, 150, arXiv:1708.00841 [hep-lat].

[6] C. Gattringer and C. B. Lang, *Quantum chromodynamics on the lattice*, Vol. 788 (Springer, Berlin, 2010).

[7] P. Weisz and P. Majumdar, Scholarpedia **7**, 8615 (2012), revision #137037.

[8] Y. M. Makeenko and A. A. Migdal, Phys. Lett. B **88**, 135 (1979), [Erratum: Phys.Lett.B 89, 437 (1980)].

[9] A. A. Migdal, Phys. Rept. **102**, 199 (1983).

[10] A. Jevicki, O. Karim, J. P. Rodrigues, and H. Levine, Nucl. Phys. B **213**, 169 (1983).

[11] A. Jevicki, O. Karim, J. P. Rodrigues, and H. Levine, Nucl. Phys. B **230**, 299 (1984).

[12] J. P. Rodrigues, Nucl. Phys. B **260**, 350 (1985).

[13] R. d. M. Koch, A. Jevicki, X. Liu, K. Mathaba, and J. a. P. Rodrigues, JHEP **01**, 168, arXiv:2108.08803 [hep-th].

[14] P. D. Anderson and M. Kruczenski, Nucl. Phys. B **921**, 702 (2017), arXiv:1612.08140 [hep-th].

[15] P. Anderson and M. Kruczenski, EPJ Web Conf. **175**, 11011 (2018).

[16] H. W. Lin, JHEP **06**, 090, arXiv:2002.08387 [hep-th].

[17] V. Kazakov and Z. Zheng, (2021), arXiv:2108.04830 [hep-th].

[18] R. G. Jha, (2021), arXiv:2111.02410 [hep-th].

[19] R. Rattazzi, V. S. Rychkov, E. Tonni, and A. Vichi, Journal of High Energy Physics **2008**, 031 (2008).

[20] D. Poland, S. Rychkov, and A. Vichi, Rev. Mod. Phys. **91**, 015002 (2019), arXiv:1805.04405 [hep-th].

[21] M. F. Paulos, J. Penedones, J. Toledo, B. C. van Rees, and P. Vieira, JHEP **11**, 133, arXiv:1607.06109 [hep-th].

[22] A. L. Guerrieri, J. Penedones, and P. Vieira, Phys. Rev. Lett. **122**, 241604 (2019), arXiv:1810.12849 [hep-th].

[23] J. Elias Miró and A. Guerrieri, JHEP **10**, 126, arXiv:2106.07957 [hep-th].

[24] A. Athenodorou and M. Teper, JHEP **12**, 082, arXiv:2106.00364 [hep-lat].

[25] A. Gonzalez-Arroyo and M. Okawa, JHEP **12**, 106, arXiv:1410.6405 [hep-lat].

[26] M. Campostrini, A. Di Giacomo, and Y. Gunduc, Phys. Lett. B **225**, 393 (1989).

[27] M. Campostrini and A. Di Giacomo, Phys. Lett. B **197**, 403 (1987).

[28] G. S. Bali, C. Bauer, and A. Pineda, Phys. Rev. Lett. **113**, 092001 (2014), arXiv:1403.6477 [hep-ph].

[29] We thank Maxim Chernodub for discussion and suggestions on this subject.

[30] K. G. Wilson, Phys. Rev. D **10**, 2445 (1974).

[31] S. R. Wadia, Phys. Rev. D **24**, 970 (1981).

[32] Y. Makeenko, *Methods of contemporary gauge theory*, Cambridge Monographs on Mathematical Physics (Cambridge University Press, 2005).

[33] Jiaxin Qiao and Zechuan Zheng, Work in progress.

[34] K. Osterwalder and E. Seiler, Annals of Physics **110**, 440 (1978).

[35] I. Montvay and G. Münster, *Quantum fields on a lattice* (Cambridge University Press, 1997).

[36] M. F. Paulos, J. Penedones, J. Toledo, B. C. van Rees, and P. Vieira, JHEP **12**, 040, arXiv:1708.06765 [hep-th].

[37] R. Rattazzi, S. Rychkov, and A. Vichi, J. Phys. A **44**, 035402 (2011), arXiv:1009.5985 [hep-th].

[38] Y. He, A. Irrgang, and M. Kruczenski, JHEP **11**, 093, arXiv:1805.02812 [hep-th].

[39] L. Córdova and P. Vieira, JHEP **12**, 063, arXiv:1805.11143 [hep-th].

[40] M. F. Paulos and Z. Zheng, JHEP **05**, 145, arXiv:1805.11429 [hep-th].

[41] C. Bachoc, D. C. Gijswijt, A. Schrijver, and F. Vallentin, in *Handbook on semidefinite, conic and polynomial optimization* (Springer, 2012) pp. 219–269.

[42] GAP, *GAP – Groups, Algorithms, and Programming, Version 4.11.1*, The GAP Group (2021).

[43] N. Xu and P. Doerschuk, SIAM Journal on Scientific Computing **43**, A3657 (2021).

[44] J.-P. Serre, *Linear representations of finite groups*, Vol. 42 (Springer, 1977).

[45] H. Panagopoulos, A. Skouroupathis, and A. Tsapalis, Phys. Rev. D **73**, 054511 (2006), arXiv:hep-lat/0601009.

[46] B. Alles, A. Feo, and H. Panagopoulos, Phys. Lett. B **426**, 361 (1998), [Erratum: Phys.Lett.B 553, 337–338 (2003)], arXiv:hep-lat/9801003.

[47] J.-M. Drouffe and J.-B. Zuber, Phys. Rept. **102**, 1 (1983).

[48] D. J. Gross and E. Witten, Phys. Rev. D **21**, 446 (1980).

[49] S. R. Wadia, (2012), arXiv:1212.2906 [hep-th].

[50] V. A. Kazakov and I. K. Kostov, Phys. Lett. B **105**, 453 (1981).

[51] All the SDPs are solved by MOSEK.[52].

[52] M. ApS, *MOSEK Command Line Tools. Release 9.3.18* (2022).

Supplementary Material for "Bootstrap for Lattice Yang-Mills theory"

Vladimir Kazakov, Zechuan Zheng

A worked-out example

This section gives a step-by-step solution of $L_{\max} = 8$ bootstrap bound for 2-dimensional lattice Yang-Mills theory in the large N_c limit. For simplicity, here, we will only take into account positivity conditions from Wilson lines starting from the origin and ending at the origin. In this situation, up to rotations and reversing the line, we have only one multiplet under symmetries:
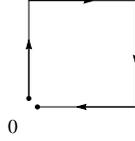
Taking the inner product between the different Wilson lines in this multiplet, we can construct the positivity matrices corresponding to Hermitian conjugation (correlation matrices) and space reflection (reflection matrices). For the correlation matrix, we have:

$$\succeq 0. \qquad (S1)$$

The row above the matrix is the Wilson lines for the inner products, and the column left to the matrix is their Hermitian conjugation. The $\mathbb{I}$ denotes the length 0 trivial Wilson line. The inner product is defined by joining the path and its Hermitian conjugation. This matrix contains six independent Wilson loops:
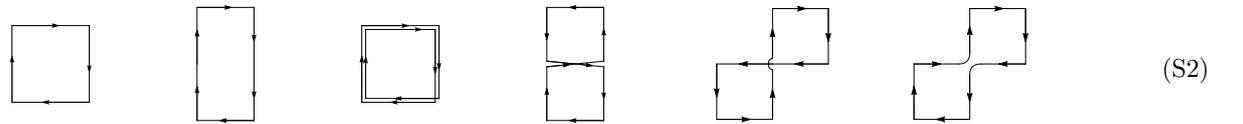
$$(S2)$$

We denote them as:

$$\mathcal{W}_1, \quad \mathcal{W}_2, \quad \mathcal{W}_3, \quad \mathcal{W}_4, \quad \mathcal{W}_5, \quad \mathcal{W}_6 \tag{S3}$$

respectively. (Here, the $\mathcal{W}_1$ is the u_P in the main text.)

We also note to the reader that although at length 8, there are Wilson loops like the 2×2 Wilson loop doesn't appear in the correlation matrix. We will also see that this is true for the loop equations and the reflection matrices, i.e., this will be an SDP with six variables.

There are two reflection matrices corresponding to site reflection and diagonal reflection. In terms of $\mathcal{W}$ variables, they read:

$$\begin{pmatrix} 1 & \mathcal{W}_1 & \mathcal{W}_1 & \mathcal{W}_1 & \mathcal{W}_1 \\ \mathcal{W}_1 & \mathcal{W}_2 & \mathcal{W}_6 & \mathcal{W}_4 & \mathcal{W}_5 \\ \mathcal{W}_1 & \mathcal{W}_6 & \mathcal{W}_2 & \mathcal{W}_5 & \mathcal{W}_4 \\ \mathcal{W}_1 & \mathcal{W}_4 & \mathcal{W}_5 & \mathcal{W}_2 & \mathcal{W}_6 \\ \mathcal{W}_1 & \mathcal{W}_5 & \mathcal{W}_4 & \mathcal{W}_6 & \mathcal{W}_2 \end{pmatrix} \text{ and } \begin{pmatrix} 1 & \mathcal{W}_1 & \mathcal{W}_1 \\ \mathcal{W}_1 & \mathcal{W}_5 & \mathcal{W}_6 \\ \mathcal{W}_1 & \mathcal{W}_6 & \mathcal{W}_5 \end{pmatrix}, \tag{S4}$$

The reflection matrix corresponds to link reflection is trivial here. Although not evident, at the present bootstrap cutoff, the positivity of reflection matrices won't improve the constraint. So we won't further discuss these matrices (including their symmetry reduction) and do the optimization only under the positivity of the correlation matrix.
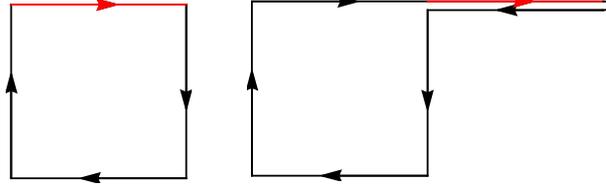
FIG. S7: Loop equations for $\Lambda = 4$.

There are two loop equations, as shown in Fig S7, the right one is a back-track loop equation. In terms of $\mathcal{W}$ variables, they read:

$$-\mathcal{W}_2 + \mathcal{W}_3 + \mathcal{W}_4 - 1 = -\lambda \mathcal{W}_1$$
$$\mathcal{W}_2 - \mathcal{W}_4 - \mathcal{W}_5 + \mathcal{W}_6 = 0 \tag{S5}$$

Finally, we do the symmetry reduction on the correlation matrix. This process will make the matrix factorize to a series of smaller matrices corresponding to each irreducible representation of the global symmetry group. We stress that this step is purely group theoretical, it doesn't change the positivity constraint itself, but it makes our algorithm orders of magnitude faster.

In our current dimension, as shown in the main text, the global symmetry is actually $B_2 \times \mathbb{Z}_2$. The B_2 group is the cubic discrete version of $O(2)$, and isomorphic to the Dihedral group D_4. The $\mathbb{Z}_2$ group corresponds to the symmetry of reversing the Wilson loop. The $\mathbb{Z}_2$ group is the Charge Conjugation symmetry on the lattice system, ensuring that all the Wilson loop averages are real numbers.

The Wilson lines above the matrix Eq S1 actually form a multiplet for the global symmetry group. We can decompose this multiplet into each irreducible component. And from the discussion in the main text, the Wilson lines in different irrep are orthogonal in the corresponding inner product.

For the group $B_2 \times \mathbb{Z}_2$, there are ten irreducible representations:

$$(A_1, +1) \qquad (A_2, +1) \qquad (B_1, +1) \qquad (B_2, +1) \qquad (E, +1) \tag{S6}$$
$$(A_1, -1) \qquad (A_2, -1) \qquad (B_1, -1) \qquad (B_2, -1) \qquad (E, -1) \tag{S7}$$

The first index is the standard notation for irreducible representation of Dihedral group $D_4 \simeq B_2$, and the second one is the parity of Charge Conjugation. Using the algorithm stated in the main text, we can project the multiplet

to different irreps:

$$
\begin{aligned}
(A_1,+1): &\; \mathbb{I}, \quad \tfrac{1}{8}\left(\;\square+\square+\square+\square+\square+\square+\square+\square\;\right) \\
(B_2,+1): &\; \tfrac{1}{8}\left(-\square-\square-\square-\square+\square+\square+\square+\square\right) \\
(E,+1): &\; \tfrac{1}{4}\left(-\square-\square+\square+\square\right) \\
(B_1,-1): &\; \tfrac{1}{8}\left(-\square-\square-\square-\square+\square+\square+\square+\square\right) \\
(A_2,-1): &\; \tfrac{1}{8}\left(-\square-\square-\square-\square+\square+\square+\square+\square\right) \\
(E,-1): &\; \tfrac{1}{4}\left(-\square-\square+\square+\square\right)
\end{aligned}
\tag{S8}
$$

We note that for the two irreps correspond to two E, there are other two vectors, but they will give the same positivity matrices. They are fully redundant. Taking the inner product between the vectors in the same irrep, we get the following positivity condition:

$$
\begin{pmatrix}
1 & \mathcal{W}_1 \\
\mathcal{W}_1 & \frac{1}{4}\mathcal{W}_2+\frac{1}{8}\mathcal{W}_3+\frac{1}{4}\mathcal{W}_4+\frac{1}{8}\mathcal{W}_5+\frac{1}{8}\mathcal{W}_6+\frac{1}{8}
\end{pmatrix} \succeq 0,
$$

$$
-\frac{1}{4}\mathcal{W}_2+\frac{1}{8}\mathcal{W}_3-\frac{1}{4}\mathcal{W}_4+\frac{1}{8}\mathcal{W}_5+\frac{1}{8}\mathcal{W}_6+\frac{1}{8} \geqslant 0,
$$

$$
-\frac{1}{4}\mathcal{W}_3+\frac{1}{4}\mathcal{W}_5-\frac{1}{4}\mathcal{W}_6+\frac{1}{4} \geqslant 0,
$$

$$
\frac{1}{4}\mathcal{W}_2-\frac{1}{8}\mathcal{W}_3-\frac{1}{4}\mathcal{W}_4-\frac{1}{8}\mathcal{W}_5+\frac{1}{8}\mathcal{W}_6+\frac{1}{8} \geqslant 0,
$$

$$
-\frac{1}{4}\mathcal{W}_2-\frac{1}{8}\mathcal{W}_3+\frac{1}{4}\mathcal{W}_4-\frac{1}{8}\mathcal{W}_5+\frac{1}{8}\mathcal{W}_6+\frac{1}{8} \geqslant 0,
$$

$$
\frac{1}{4}\mathcal{W}_3-\frac{1}{4}\mathcal{W}_5-\frac{1}{4}\mathcal{W}_6+\frac{1}{4} \geqslant 0.
\tag{S9}
$$

The reader could verify that these new positivity conditions are equivalent to the Eq S1. Still, as SDP conditions, they are much more (several orders of magnitude for higher order bootstrap problems) efficient.

By the loop equation Eq S5 and the factorized positivities Eq S9, we can maximize or minimize $\mathcal{W}_1$ to get the upper and lower bounds:

$$
0 \leqslant \mathcal{W}_1 \leqslant 0.69300 \tag{S10}
$$

We stress that all the loop equations are linear at this lowest order of bootstrap. We must implement the convex relaxation described in the main text to deal with the quadratic terms for higher order bootstrap.

Selected four-dimensional data

In this section we collect some selected data from the $4D$ bootstrap plot. Table II compares the bootstrap upper bound on u_P with the perturbation and MC data in the weak-coupling phase at several specific couplings.

λ	$u_{p,\max}$	Perturbation	Monte Carlo
0.01	0.99750	0.997498	0.9975
0.31	0.92060	0.920348	0.9212
0.51	0.86706	0.866344	0.8676
1.35913	0.60837	0.606530	0.58043063
1.37733	0.60199	0.600313	0.57087665
1.39765	0.59480	0.593336	0.55936304
1.41802	0.58752	0.586302	0.5464461
1.44202	0.57886	0.577965	0.5275951

TABLE II: Plaquette average at various 't Hooft couplings λ: bootstrap, perturbation theory and MC results.

Chapter 3

Conformal Bootstrap

1 Conformal Bootstrap for conformal correlators

The conformal bootstrap is a potent tool for investigating and constraining the properties of Conformal Field Theories (CFTs). The origins of this method can be traced back to the 1970s, stemming from the works of Polyakov, Ferrara, Gatto, Grillo, and others [Ferrara, 1973; Polyakov, 1974], who utilized the properties of operator product expansions (OPEs) and conformal symmetry to derive constraints on CFTs.

1.1 Basic Idea

The fundamental idea of the conformal bootstrap is the use of symmetries and consistency conditions to impose constraints on, or even solve, CFTs. The linchpin of this method is the crossing symmetry equation, derived from the associativity of the OPE and the invariance under the interchange of operators in the correlation function.

1.2 Core Premise

The essential premise [Rattazzi, 2008] focuses on analyzing the constraints derived from the crossing symmetric equation:

$$\sum_{\Delta,\ell} a_{\Delta,\ell} F_{\Delta,\ell}(z, \bar{z}) = 0, \tag{3.1}$$

Here, the crossing vector $F_{\Delta,\ell}(z, \bar{z})$ is determined by the crossing symmetry:

$$F_{\Delta,\ell}(z, \bar{z}) = \frac{G_{\Delta,\ell}(z, \bar{z})}{(z\bar{z})^{\Delta_\phi}} - \frac{G_{\Delta,\ell}(1-z, 1-\bar{z})}{((1-z)(1-\bar{z}))^{\Delta_\phi}} \tag{3.2}$$

To facilitate analysis, this equation is typically discretized at the crossing-symmetric point $z = \bar{z} = \frac{1}{2}$. This process employs a variety of inventive techniques to compute these derivatives efficiently [Kravchuk, 2018b; Erramilli, 2019; Kravchuk, 2018a; Karateev, 2019; Erramilli, 2021].

Post discretization, polynomial approximation transforms the equation into a standard Semidefinite Program (SDP) constraint condition. The *SDPB* solver [Simmons-Duffin, 2015] provides the solution to the corresponding SDP with arbitrary precision. With these constraints, the 'navigitor' technique [Reehorst, 2021] explores physically permissible theories within the CFT parameter space.

1.3   Challenges in Correlator Bounding

However, this established paradigm faces complications when applied to bound the correlator. When formulating the objective function to bound the correlator as follows:

$$\text{max/min:} \quad \sum_{\Delta,L} a_{\Delta,L} G_{\Delta,L}(z, \bar{z}) \tag{3.3}$$

and $(z, \bar{z})$ is not at the crossing symmetric point, the objective function and the crossing symmetry equation exhibit different exponential decay with respect to the Δ. Consequently, no valid rational approximation exists for the bootstrap formulation. To address this, the work presented here employed the continuous primal simplex algorithm [El-Showk, 2014], implemented in *JuliBoots*[Paulos, 2014].

Paper III

Bounding 3d CFT correlators

Miguel F. Paulos and Zechuan Zheng

Laboratoire de Physique de l'École Normale Supérieure
PSL University, CNRS, Sorbonne Universités, UPMC Univ. Paris 06
24 rue Lhomond, 75231 Paris Cedex 05, France

`miguel.paulos@ens.fr`, `zechuan.zheng@ens.fr`

Abstract

We consider the problem of bounding CFT correlators on the Euclidean section. By reformulating the question as an optimization problem, we construct functionals numerically which determine upper and lower bounds on correlators under several circumstances. A useful outcome of our analysis is that the gap maximization bootstrap problem can be reproduced by a numerically easier optimization problem. We find that the 3d Ising spin correlator takes the minimal possible allowed values on the Euclidean section. Turning to the maximization problem we find that for $d > 2$ there are gap-independent maximal bounds on CFT correlators. Under certain conditions we show that the maximizing correlator is given by the generalized free boson for general Euclidean kinematics. In our explorations we also uncover an intriguing 3d CFT which saturates gap, OPE maximization and correlator value bounds. Finally we comment on the relation between our functionals and the Polyakov bootstrap.
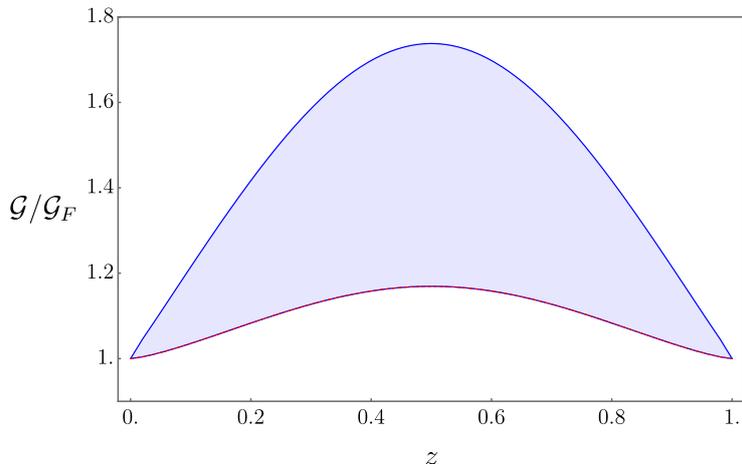
Contents

Figure 1: Upper and lower bounds on 3d CFT correlators $\mathcal{G}(z,z)$ normalized by $\mathcal{G}^F(z) = -1 + z^{-2\Delta_\phi} + (1-z)^{-2\Delta_\phi}$. Here $\Delta_\phi = \Delta_\sigma^{\text{Ising}} \sim 0.518149$. The 3d Ising spin four-point function saturates the lower bound.

1   Introduction

The last few years have taught us that CFTs and in particular the CFT data which defines correlators of local operators, such as quantum numbers and OPE coefficients, are strongly constrained [1]. These constraints imply that the CFT theory space is bounded along certain directions. More remarkably, interesting theories tend to lie at the edges of the realms of possibility [2], realms ruled by the iron fists of crossing symmetry and unitarity.

Up to now, the collective efforts of the conformal bootstrap community have explored this space by focusing on the constraints of a restricted set of four-point correlators and seeing how far one can move along two directions. In the first direction, one determines an upper bound on the scaling dimension of the first operator appearing in the OPE with certain quantum numbers - the gap maximization problem [3]. In the second one determines upper (or lower) bounds on the OPE coefficient of some particular operator appearing in these correlators [4]. The bounds are determined by constructing appropriate functionals, numerically or analytically. These two directions are like two different viewpoints on the CFT landscape.

In this paper we will introduce new ones. The idea is simple: we will determine bounds on the values of CFT correlators. This can be thought of as constraining very special infinite linear combinations of OPE coefficients. This is a very natural question which surprisingly has not been considered so far. An important motivation is the hope that with this new lens we may reach interesting and yet unseen corners of CFT space. Indeed, it is known that the analogous problem of minimizing or maximizing values of S-matrices is known to lead to bounds which can be saturated by interesting theories. This is in fact more than an analogy, since we now know that S-matrices are intimately related to (limits of) CFT correlators [5]. We will see that the corresponding CFT problem is equally interesting.

We consider CFT four-point correlators with spacelike separated operators, so that the correlator is real, and we will obtain exact and numerical bounds on its values. The exact bounds are simple consequences from recent work [6], where one of us obtained rigorous correlator bounds for the special case where these operators all lie on a line (or a circle). These bounds state that

$$
\begin{aligned}
\mathcal{G}(w,w) &\geq \mathcal{G}^F(w) \\
\mathcal{G}(w,w) &\leq \mathcal{G}^B(w)\,, \qquad \Delta_g \geq 2\Delta_\phi
\end{aligned}
\tag{1.1}
$$

where $\mathcal{G}^{B,F}(w) := \pm 1 + w^{-2\Delta_\phi} + (1-w)^{-2\Delta_\phi}$ have the interpretation of generalized free field (GFF) correlators, and the condition on the gap Δ_g is imposed across all spins. The upper bound is easily generalisable to more general Euclidean configurations. More interestingly, we can obtain bounds in Lorentzian kinematics where $w, \bar{w}$ are real and independent. In particular we will obtain that the correlator is parametrically bounded in the double lightcone limit:

$$
\begin{aligned}
\mathcal{G}(w, 1-w) &\underset{w\to 0^+}{\gtrsim} \frac{1}{w^{\Delta_\phi}} \\
\mathcal{G}(w, 1-w) &\underset{w\to 0^+}{\lesssim} \frac{1}{w^{3\Delta_\phi}}\,.
\end{aligned}
\tag{1.2}
$$

We can obtain numerical bounds by constructing appropriate linear functionals that act on the crossing equation for the correlator and satisfy appropriate positivity properties. While such bounds can be obtained for any spacelike configuration, in practice lorentzian configurations are highly sensitive to the large spin spectrum and so are difficult to study numerically. We hence focus on Euclidean configurations in this work. We will determine both upper and lower bounds for CFTs in $d = 3$. Notice that the exact lower bound above is interesting as it is saturated by the same correlator which maximizes the gap in $d = 1$. This is not an accident, and in fact we will see that under certain circumstances, the same is true in higher dimensions. In particular we will establish, numerically:

$$
\mathcal{G}(w, \bar{w}) \geq \mathcal{G}_{\text{gapmax}}(w, \bar{w})\,, \qquad \Delta_\phi \lesssim d/2
\tag{1.3}
$$

where $\mathcal{G}_{\text{gapmax}}$ stands for the correlator which maximizes the scalar gap. In particular, using the fact the the 3d Ising spin correlator maximizes the gap, we get

$$
\mathcal{G}(w, \bar{w}) \geq \mathcal{G}_{\text{Ising}}(w, \bar{w})\,, \qquad \Delta_\phi = \Delta_\sigma^{\text{Ising}} \sim 0.518149
\tag{1.4}
$$

for any 3d CFT correlator with that Δ_ϕ. An interesting outcome of this equivalence is that we can solve the gap maximization problem in terms of one of correlator minimization[1]. This has the advantage that solving the latter problem requires a single optimization step, whereas the former requires a costly binary search. In this way for instance we check that we can get in a single step the correct maximal gap to within 10^{-15}.

The maximization problem is also interesting. In $d = 3$ there is no need to impose a gap in the spectrum to obtain an upper bound on the correlator if $\Delta_\phi \leq d - 2$. We find that this

---

[1]In fact more generally it is easier to define a simpler, related problem, see section 4.

upper bound is saturated by a different CFT depending on the point at which we maximize, thereby giving us an entire family of bound saturating solutions to crossing, a family that generically contains a stress-tensor. By maximizing the correlator in the OPE limit we find a family of theories containing a protected operator of dimension 5/2. Remarkably, this family coincides with that obtained by maximizing the gap at a special point $\Delta_\phi \sim 0.505$.

If we do impose a gap, we find that the maximal correlator coincides, in a wide regime of parameters, with the correlator which maximizes the OPE coefficient of the operator at the gap. For the special value $\Delta_g = 2\Delta_\phi$ our numerical bound must match with the exact bound above, at least for 1d kinematics, since it is saturated by the generalized free boson solution which exists in any dimension. We determine that this remains unchanged in the entire Euclidean section. We also show that nearby deformations of this solution, computed by certain AdS contact interactions, also saturate this bound to leading order.

The outline of this work is as follows. Section 2 is concerned with describing general kinematics of CFT correlators as well as giving an overview of the space of such correlators and some notable points in that space. In section 3 we make some simple observations regarding what to expect for the problem of maximizing and minimizing CFT correlator values for spacelike separated operators. In particular, we show how exact results recently derived for correlators on a line can be used to obtain bounds for more general kinematics. In section 4 we show how linear optimization methods based on linear functionals can be used effectively to place both lower and upper bounds on correlators. In the process we show that the bootstrap question of maximizing a gap can be reformulated as a certain correlator minimization problem. The upshot is that this can be solved in a single optimization step. Section 5 is concerned with numerical applications and contains our main results, deriving both upper and lower bounds on 3d CFT correlators by numerically constructing appropriate functionals. We finish this paper with a short discussion and an appendix containing details of our numerical implementations.

2 Conformal correlators

2.1 Kinematics and crossing

We interested in CFT four-point correlators of identical scalar operators, which we write as as

$$\langle \phi(x_1)\phi(x_2)\phi(x_3)\phi(x_4) \rangle = \frac{\mathcal{G}(u,v)}{x_{13}^{2\Delta_\phi} x_{24}^{2\Delta_\phi}} \,, \tag{2.1}$$

with $x_{ij}^2 \equiv (x_i - x_j)^2$. The correlator depends on the two conformal cross-ratios u, v which can be written in terms of two complex variables $z, \bar{z}$, determined as

$$u \equiv z\bar{z} \equiv \frac{x_{12}^2 x_{34}^2}{x_{13}^2 x_{24}^2} \,, \qquad v \equiv (1-z)(1-\bar{z}) \equiv \frac{x_{14}^2 x_{23}^2}{x_{13}^2 x_{24}^2} \,. \tag{2.2}$$
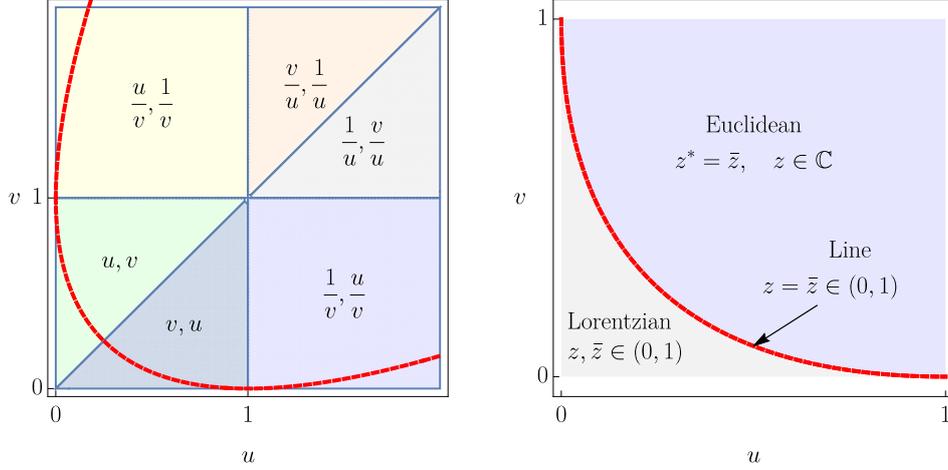
Figure 2: Cross-ratio space for spacelike separated operators. The thick red curve corresponds to operators on a line. To its right the Euclidean and to its left the Lorentzian sections. On the lefthand figure we show how this space may be split into regions mapped into each other by crossing transformation. On the righthand figure we zoom in on the region $u, v \in (0, 1)$. Our choice of fundamental domain corresponds to taking $v > u$ in that figure.

It will be also useful to consider yet a different set of coordinates, $\rho, \bar{\rho}$, defined as [7]:

$$\rho_z := \frac{1 - \sqrt{1 - z}}{1 + \sqrt{1 - z}}, \quad z = \frac{4\rho_z}{(1 + \rho_z)^2}, \qquad \text{abbreviated as} \quad \rho \equiv \rho_z, \bar{\rho} \equiv \rho_{\bar{z}}, \qquad (2.3)$$

We set $\mathcal{G}_z(z, \bar{z}) \equiv \mathcal{G}(u(z, \bar{z}), v(z, \bar{z}))$ and $\mathcal{G}_\rho(\rho, \bar{\rho}) = \mathcal{G}_z(z, \bar{z})$, but will often abuse notation and drop the subscripts.

When all operators are spacelike separated, the cross-ratios u, v can range from zero to infinity. This can be split into two regions separated by a third:

$$\begin{aligned} \text{Euclidean:} \quad & (1 + u - v)^2 > 4u \Leftrightarrow z^* = \bar{z}, \quad z \in \mathbb{C} \\ \text{Lorentzian spacelike:} \quad & (1 + u - v)^2 < 4u \Leftrightarrow (z, \bar{z}) \in (-\infty, 0)^2 \cup (0, 1)^2 \cup (1, \infty)^2 \quad (2.4) \\ \text{Line:} \quad & (1 + u - v)^2 = 4u \Leftrightarrow z = \bar{z}, \quad z \in \mathbb{R} \end{aligned}$$

Furthermore, Bose symmetry implies the invariances

$$\mathcal{G}(z, \bar{z}) = \mathcal{G}(1 - z, 1 - \bar{z}) = \frac{\mathcal{G}\left(\frac{1}{z}, \frac{1}{\bar{z}}\right)}{(z\bar{z})^{\Delta_\phi}} \qquad (2.5)$$

which are obtained by swapping $x_1 \leftrightarrow x_4$ and $x_1 \leftrightarrow x_3$. By combining these transformations we can also get

$$\mathcal{G}(z, \bar{z}) = \frac{\mathcal{G}\left(\frac{z}{z-1}, \frac{\bar{z}}{\bar{z}-1}\right)}{[(1 - z)(1 - \bar{z})]^{\Delta_\phi}} = \frac{\mathcal{G}\left(\frac{1}{1-z}, \frac{1}{1-\bar{z}}\right)}{[(1 - z)(1 - \bar{z})]^{\Delta_\phi}} = \frac{\mathcal{G}\left(\frac{z-1}{z}, \frac{\bar{z}-1}{\bar{z}}\right)}{(z\bar{z})^{\Delta_\phi}}. \qquad (2.6)$$
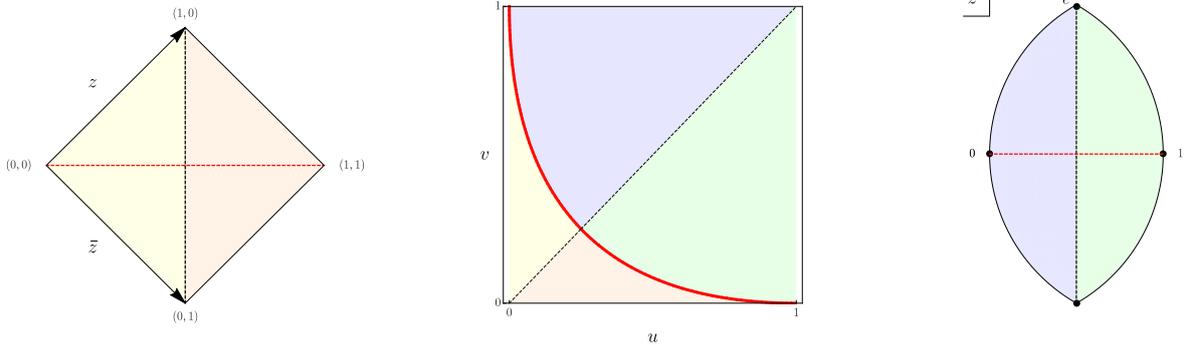
Figure 3: Fundamental domain in cross-ratio space. Our choice of fundamental domain corresponds to taking $v > u$ in the central figure. This captures both a Lorentzian spacelike and an Euclidean sections, shown on the left and right respectively. The arcs on the right lie on circles $|z| = 1$ and $|1 - z| = 1$.

This means that the spacelike region $u, v > 0$ can be divided into six subregions, each of which may be mapped into any other by one of the above transformations. We show this in figure 2.

We will be interested in studying bounds on correlation functions of spacelike operators. The identities above show that it is sufficient to restrict our attention to a particular region in cross-ratio space. We will choose this region to be the set $0 < u < v < 1$, although it is useful to keep in mind the wider region $0 < u, v < 1$. We show what this domain corresponds to in terms of the z variables in figure 3.

The correlator admits an expansion in conformal blocks, which we write as

$$\mathcal{G}(z, \bar{z}) = \frac{1}{(z\bar{z})^{\Delta_\phi}} + \sum_{\substack{\Delta \geq \Delta_u(\ell) \\ \ell = 0, 2, 4 \ldots}} a_{\Delta, \ell} \frac{G_{\Delta, \ell}(z, \bar{z})}{(z\bar{z})^{\Delta_\phi}} \,. \tag{2.7}$$

The sum ranges over the scaling dimension Δ and traceless-symmetric spin ℓ of exchanged states, which are restricted by Bose symmetry and unitarity; in particular ℓ should be even and $\Delta_u(\ell) = \frac{d-2}{1+\delta_{\ell,0}} + \ell$. We have also separated out the contribution of the identity operator. The coefficients $a_{\Delta, \ell}$ correspond to squares of OPE coefficients between the external operators and the exchanged states, viz.:

$$\phi \times \phi \sim \sum_{\mathcal{O} \in \phi \times \phi} \lambda_{\phi\phi\mathcal{O}_{\Delta, \ell}} \mathcal{O}_{\Delta, \ell} \,, \qquad a_{\Delta, \ell} := \lambda^2_{\phi\phi\mathcal{O}_{\Delta, \ell}} \,. \tag{2.8}$$

On the Euclidean section the conformal blocks satisfy

$$G_{\Delta, \ell}(z, \bar{z}) = G_{\Delta, \ell}\left(\frac{z}{z-1}, \frac{\bar{z}}{\bar{z}-1}\right) \tag{2.9}$$

96

which trivializes some of the identities in (2.6). The only independent non-trivial constraint is the crossing equation:

$$F_{0,0}(z, \bar{z}|\Delta_\phi) + \sum_{\substack{\Delta \geq \Delta_u(\ell) \\ \ell = 0,2,4\ldots}} a_{\Delta,\ell} F_{\Delta,\ell}(z, \bar{z}|\Delta_\phi) = 0 \,, \tag{2.10}$$

where we have defined the crossing vectors

$$F_{\Delta,\ell}(z, \bar{z}|\Delta_\phi) \equiv \frac{G_{\Delta,\ell}(z, \bar{z})}{(z\bar{z})^{\Delta_\phi}} - \frac{G_{\Delta,\ell}(1-z, 1-\bar{z})}{[(1-z)(1-\bar{z})]^{\Delta_\phi}} \,. \tag{2.11}$$

2.2 The space of correlators and its special points

We define the space of all consistent CFT_d four point functions of identical scalar operators with scaling dimension Δ_ϕ:

$$\mathfrak{G}^{(d)}_{\Delta_\phi} := \left\{ \textit{Identical scalar correlators } \mathcal{G} = \langle \phi\phi\phi\phi \rangle \textit{ of } CFT_d \right\} \tag{2.12}$$

By consistency here, we mean that the correlators satisfy crossing and an OPE expansion consistent with unitarity. In principle we could and should refine this by also demanding that $\mathcal{G}$ is part of a larger family of correlators involving various external operators and that the full set is consistent with all crossing symmetry constraints.

Note that since a CFT in d dimensions is also a CFT in any lower dimension, we have the inclusion relations:

$$\mathfrak{G}^{(d')}_{\Delta_\phi} \subset \mathfrak{G}^{(d)}_{\Delta_\phi}, \qquad 1 < d < d' \,. \tag{2.13}$$

The case $d = 1$ is special, since such correlators have more restricted kinematic dependence. In particular they depend on a single cross-ratio. However we can still say that

$$\mathcal{G}\big|_{z=\bar{z}} \in \mathfrak{G}^{(d=1)}_{\Delta_\phi} \qquad \text{for any} \quad \mathcal{G} \in \mathfrak{G}^{(d)}_{\Delta_\phi}\,. \tag{2.14}$$

For convenience below we will drop the subscript Δ_ϕ and the spacetime dimension, but it should be clear all statements below - where we compare values of correlators - refer to fixed choices of these parameters, so that we do not compare apples to oranges.

We will now define several quantities of interest. We begin with the *infimum correlator*:

$$\mathcal{G}_{\inf}(w, \bar{w}) := \inf \left\{ \mathcal{G}(w, \bar{w}) \quad \text{for} \quad \mathcal{G} \in \mathfrak{G} \right\} \,. \tag{2.15}$$

It is important to emphasize that the infimum correlator is actually not a physical correlator in general i.e. $\mathcal{G}_{\inf}$ itself will in general not lie in $\mathfrak{G}$. The most we can say is that for each choice of $w, \bar{w}$ there exists a *minimizing* or *minimal value* correlator at $w, \bar{w}$, denoted $\mathcal{G}_{\min;w,\bar{w}} \in \mathfrak{G}$, such that $\mathcal{G}_{\min;w,\bar{w}}(w, \bar{w}) = \mathcal{G}_{\inf}(w, \bar{w})$:

$$\mathcal{G}_{\min;w,\bar{w}} = \underset{\mathcal{G} \in \mathfrak{G}}{\arg\min} \, \mathcal{G}(w, \bar{w}) \tag{2.16}$$

We can make analogous definitions for maximization. The *supremum* correlator is:

$$\mathcal{G}_{\text{sup}}(w,\bar{w}) := \sup\{\mathcal{G}(w,\bar{w}) \quad \text{for} \quad \mathcal{G} \in \mathfrak{G}\} \tag{2.17}$$

However there is a catch: it can be the case that the result is infinite. This is essentially due to the fact that in general there are unitary solutions to the crossing equation without the identity operator. Such solutions can always be added with an arbitrarily large coefficient[2], leading to an unbounded size for the correlator. The way out is that such solutions disappear once we set a sufficiently large gap in the spectrum of operator dimensions. Defining $\Delta_g^{\mathcal{G}}$ to be the lowest non-zero scaling dimension of a scalar operator appearing in the OPE of the correlator $\mathcal{G}$, we can make the refined definition:

$$\mathcal{G}_{\text{sup}}(w,\bar{w}|\Delta_g) := \sup\{\mathcal{G}(w,\bar{w}) \quad \text{for} \quad \mathcal{G} \in \mathfrak{G} \quad \text{s.t.} \quad \Delta_g^{\mathcal{G}} \geq \Delta_g\} \tag{2.18}$$

As was the case for the minimum value correlator, it is important to emphasize the distinction between the maximal value correlator and the supremum correlators at specific points:

$$\mathcal{G}_{\text{max};w,\bar{w}}(\bullet|\Delta_g) := \underset{\mathcal{G} \in \mathfrak{G}: \Delta_g^{\mathcal{G}} \geq \Delta_g}{\arg\max} \; \mathcal{G}(w,\bar{w}) \tag{2.19}$$

We could of course refine this further by allowing for different gaps in all the various spin sectors of the spectrum, but this will do for the purposes of this work.

To conclude this section we introduce two further definitions. The first is related to the fact that for a given Δ_ϕ there is an associated maximal gap which is allowed in any given spin sector. We therefore set:

$$\mathcal{G}_{\text{gapmax}} := \underset{\mathcal{G} \in \mathfrak{G}}{\arg\max} \; \Delta_g^{\mathcal{G}} \tag{2.20}$$

The second definition is similar and related to maximizing the OPE coefficient of the operator with dimension Δ_g in the set of correlators with a $\Delta_{\mathcal{G}}^{\text{gap}} = \Delta_g$:

$$\mathcal{G}_{\text{opemax}}(\bullet|\Delta_g) := \underset{\mathcal{G} \in \mathfrak{G}: \; \Delta_{\mathcal{G}}^{\text{gap}} \geq \Delta_g}{\arg\max} \; a_{\Delta_g,0} \, . \tag{2.21}$$

As we will now discuss, the gapmax and opemax correlators can often be related to the minimal value and maximal value correlators respectively.

3 General expectations and results

3.1 Basic intuition

We would like to get some intuition on what to expect for the bounds on correlator values. For this it is useful to consider the conformal block expansion of the correlator. An important

---

[2]An equivalent way of describing the issue is that the OPE maximization problem described below can be unbounded.
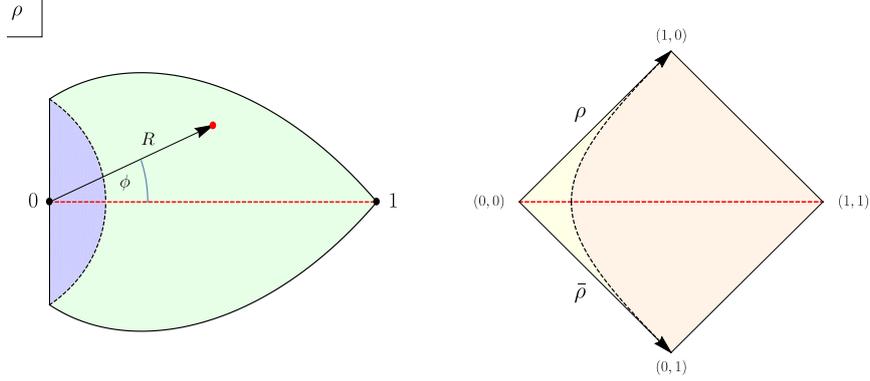
Figure 4: Fundamental domain in the ρ variable. On the left in the Euclidean section, the fundamental domain is in blue, whereas on the right in the Lorentzian spacelike it is shown in yellow. The two regions shown in each section are mapped into each other by crossing, $z, \bar{z} \to 1 - z, 1 - \bar{z}$. Inside the Euclidean fundamental domain we have that $R \leq 3 - 2\sqrt{2} \sim 0.17$ if $\phi = 0$ and $R \leq 2 - \sqrt{3} \sim 0.27$ for $\phi = \pm\pi/2$. In the Lorentzian spacelike section we have $R \leq 3 - 2\sqrt{2}$, with equality achieved along the line $\rho = \bar{\rho}$.

property of the conformal blocks is that they not only have a positive expansion in terms of the $z, \bar{z}$ cross-ratios, but also in terms of $\rho, \bar{\rho}$ [8]. That is:

$$
\begin{aligned}
G_{\Delta,\ell}(z, \bar{z}) &= r^\Delta \sum_{n=0}^{\infty} \sum_{|j-\ell| \leq 2n} c_{n,j} r^{2n} C_j^{\left(\frac{d-2}{2}\right)}(\cos\theta) \\
&= R^\Delta \sum_{n=0}^{\infty} \sum_{|j-\ell| \leq 2n} d_{n,j} R^{2n} C_j^{\left(\frac{d-2}{2}\right)}(\cos\phi)
\end{aligned}
\tag{3.1}
$$

with $c_{n,j}, d_{n,j} \geq 0$ and $z = re^{i\theta}, \rho = Re^{i\phi}$ are polar representations for z and ρ. Notice that in both cases successive terms in the power series are suppressed by the square of the radial variable. This is especially relevant if we work in the ρ variable. As shown in figure 4, in the fundamental Euclidean domain R is never larger than $2 - \sqrt{3} \sim 0.268$. It follows that everywhere inside the Euclidean fundamental domain the conformal blocks are well approximated by keeping only the leading term in the power series representation:

$$
G_{\Delta,\ell}(\rho, \bar{\rho}) \propto R^\Delta C_\ell^{\left(\frac{d-2}{2}\right)}(\cos\phi) .
\tag{3.2}
$$

In turn, the smallness of R suggests that the correlator is well approximated by keeping only the lowest dimension non-identity operator in the conformal block expansion. For definiteness we will assume this to be a scalar with dimension Δ_g. Indeed, numerical bootstrap bounds imply that at least for some range of Δ_ϕ the lowest dimension operator in a consistent CFT correlator must be a scalar. It follows then that:

$$
(z\bar{z})^{\Delta_\phi} \mathcal{G}(\rho, \bar{\rho}) \sim 1 + a_{\Delta_g,0} R^{\Delta_g} + \dots
\tag{3.3}
$$

99

At this point a clarification is in order: we are after all aiming to place bounds on the space of all consistent correlators, and an arbitrary generic correlator could have very closely space operators, or even a continuum. Who is to say we should take the above to be a good approximation? The reason is that what we are really interested in characterizing here are the properties of the maximal value or minimal value correlators, not generic ones. Since such correlators saturate bounds, they come along with associated linear functionals (i.e. they are extremal [9, 10]) and hence they must have a sparse spectrum. In particular such correlators are indeed well approximated by a relation such as the one above for sufficiently small R.

With this very simple approximation, we begin by addressing the question of an upper bound on the valueof a correlator. The approximation (3.3) teaches us several things. Firstly, since R is small in the fundamental domain, we can see that in order to maximize the value of the correlator we would do well to lower the gap as much as possible. Hence, in the set of correlators whose non-identity scalar operators all have dimensions above some Δ_g we expect that the maximal value correlator should necessarily have a scalar operator at, or very close to, the gap Δ_g. We also expect that in general lowering the gap leads to higher maximum values. Secondly, to maximize the correlator we would like to increase the OPE of that low-lying operator, $a_{\Delta_g,0}$ as much as possible. Hence we expect that:

$$\mathcal{G}_{\text{sup}}(z, \bar{z}|\Delta_g) \gtrapprox \mathcal{G}_{\text{opemax}}(z, \bar{z}|\Delta_g) \tag{3.4}$$

That is, the problems of correlator maximization and OPE maximization are related, at least for small enough values of R.

Now let us see what we can say about lower bounds on the correlator, turning again to the approximation (3.3) for guidance. In this case the logic is reversed, so that to minimize the value of the correlator it seems that we should increase Δ_g and minimize $a_{\Delta_g,0}$ as much as possible. Roughly speaking, we expect that OPE coefficients should decrease as the dimension increases, so it seems like both these effects push up the gap as much as possible. An important point is that what this argument tells us is that we expect that minimizing correlator should have a large gap *across all spin sectors*. It just so happens that there is an upper bound on the scalar gap, and for a range of Δ_ϕ this upper bound Δ_{gapmax} is smaller than the unitarity bound on the spin-2 sector $\Delta_u(2) = d$. Under these conditions, we expect

$$\mathcal{G}_{\text{inf}}(w, \bar{w}) \lessapprox \mathcal{G}_{\text{gapmax}}(w, \bar{w}), \qquad \text{as long as} \quad \Delta_{\text{gapmax}} < d. \tag{3.5}$$

So again we find a relation between the two a priori distinct problems of correlator minimization and gap maximization.

Although strictly speaking both these expectations should be borne out only for very small R, in practice we will see they are often true even for $R = O(1)$.

3.2   Exact results for $1d$ kinematics

In recent work [6], one of us has proven exact bounds on CFT correlators restricted to the line $z = \bar{z}$. Let us set $\mathcal{G}(w) \equiv \mathcal{G}(w, \bar{w})$ the line restriction of an arbitrary CFT correlator in

spacetime dimension $d \geq 1$. We can write it as:

$$\mathcal{G}(w) = \sum_{\Delta \geq 0} a_\Delta^{1d} G_\Delta(w|\Delta_\phi), \qquad G_\Delta(w|\Delta_\phi) = w^{\Delta - 2\Delta_\phi} {}_2F_1(\Delta, \Delta, 2\Delta, w). \tag{3.6}$$

We have expanded the correlator in terms of $SL(2,\mathbb{R})$ primary operators, with G_Δ an $SL(2,\mathbb{R})$ conformal block. For correlators arising from a CFT_d, this $SL(2,\mathbb{R})$ spectrum contains both higher-d primaries as well as higher-d descendant states. Accordingly there will be relations among the effective $SL(2,\mathbb{R})$ OPE coefficients, which we have denoted a_Δ^{1d}. The Polyakov bootstrap, proposed in [11–14] and proven for $d = 1$ CFTs in [15] tells us we may write

$$\mathcal{G}(w) = \sum_\Delta a_\Delta^{1d} \mathcal{P}_\Delta^B(w) \tag{3.7}$$

or alternatively

$$\mathcal{G}(w) = \sum_\Delta a_\Delta^{1d} \mathcal{P}_\Delta^F(w). \tag{3.8}$$

Here $\mathcal{P}_\Delta^B$, $\mathcal{P}_\Delta^F$ are called the bosonic and fermionic Polyakov blocks. They are crossing symmetric functions and can be obtained as certain sums of Witten exchange diagrams and contact terms for bosonic and fermionic theories in AdS_2.[3] Alternatively, the Polyakov blocks are computable from the action of certain linear functionals $\Omega_w^{B,F}$, called master functionals in [6]:

$$\pm \mathcal{P}_\Delta^{B,F}(w) = \Omega_w^{B,F}[F_\Delta] - G_\Delta(w|\Delta_\phi) \tag{3.9}$$

where $F_\Delta(w) \equiv G_\Delta(w|\Delta_\phi) - G_\Delta(1 - w|\Delta_\phi)$. This representation of the Polyakov blocks leads to the following expressions:

$$\mathcal{P}_\Delta^B(w) = -\sin^2\left[\frac{\pi}{2}(\Delta - 2\Delta_\phi)\right] \int_0^1 dz\, g_w^B(z) G_\Delta(z|\Delta_\phi), \qquad \Delta > 2\Delta_\phi$$

$$\mathcal{P}_\Delta^F(w) = +\cos^2\left[\frac{\pi}{2}(\Delta - 2\Delta_\phi)\right] \int_0^1 dz\, g_w^F(z) G_\Delta(z|\Delta_\phi), \qquad \Delta > 2\Delta_\phi - 1 \tag{3.10}$$

where crucially, the master functional kernels $g_w^F(z)$ and $g_w^B(z)$ are positive for $w, z \in (0, 1)$. Since the SL(2,$\mathbb{R}$) blocks are also positive in that range, the Polyakov bootstrap together with the above establishes the bounds:

$$\overline{\mathcal{G}}(w) := \mathcal{G}(w) - \sum_{0 \leq \Delta \leq 2\Delta_\phi} a_\Delta^{1d} \mathcal{P}_\Delta^B(w) \leq 0,$$

$$\underline{\mathcal{G}}(w) := \mathcal{G}(w) - \sum_{0 \leq \Delta \leq 2\Delta_\phi - 1} a_\Delta^{1d} \mathcal{P}_\Delta^F(w) \geq 0 \tag{3.11}$$

---

[3]It is important however that the above are rigorous identities that must hold for any unitary CFT, and in this sense have nothing to do with holography or perturbation theory.

valid for $w \in (0,1)$. In particular the identity Polyakov blocks, which always appear in the subtractions above, are computable as:

$$\mathcal{P}_\Delta^B(w) = \mathcal{G}^B(w) \equiv \frac{1}{w^{2\Delta_\phi}} + \frac{1}{(1-w)^{2\Delta_\phi}} + 1$$

$$\mathcal{P}_\Delta^F(w) = \mathcal{G}^F(w) \equiv \frac{1}{w^{2\Delta_\phi}} + \frac{1}{(1-w)^{2\Delta_\phi}} - 1 \tag{3.12}$$

which are bosonic / fermionic generalized free field correlators, respectively. The fermionic correlator makes sense only for $d = 1$ as it cannot be extended for $z \neq \bar{z}$. However the bosonic can:

$$\mathcal{G}^B(w) = \mathcal{G}^B(w, \bar{w})\Big|_{w=\bar{w}}, \qquad \mathcal{G}^B(w, \bar{w}) = \frac{1}{(w\bar{w})^{\Delta_\phi}} + \frac{1}{[(1-w)(1-\bar{w})]^{\Delta_\phi}} + 1. \tag{3.13}$$

Finally, although it is not guaranteed by the above, by an examination of the master functional action it was observed that

$$\mathcal{P}_\Delta^B(w) \geq 0, \qquad 0 \leq \Delta \leq 2\Delta_\phi$$

$$\mathcal{P}_\Delta^F(w) \geq 0, \qquad 0 \leq \Delta \leq 2\Delta_\phi - 1 \tag{3.14}$$

Putting everything together we get:

$$\mathcal{G}(w) \equiv \mathcal{G}(w, w) \geq \mathcal{G}^F(w)$$

$$\mathcal{G}(w) \equiv \mathcal{G}(w, w) \leq \mathcal{G}^B(w), \qquad \text{if} \quad \Delta_g \geq 2\Delta_\phi. \tag{3.15}$$

As a couple of comments, notice that interestingly for $d = 1$ the expectations (3.5) (3.4) quoted above are actually exact statements for any w, i.e.:

$$\mathcal{G}_{\text{inf}}^{(1d)}(w) = \mathcal{G}_{\text{gapmax}}^{(1d)}(w) = \mathcal{G}^F(w), \qquad \mathcal{G}_{\text{sup}}^{(1d)}(w|2\Delta_\phi) = \mathcal{G}_{\text{opemax}}^{(1d)}(w|2\Delta_\phi) = \mathcal{G}^B(w) \tag{3.16}$$

The second comment is that since the generalized free boson is a good solution to crossing in arbitrary spacetime dimension, the upper bound quoted above is actually optimal. Although it is restricted to the line, we will give numerical evidence that it holds throughout the Euclidean section. Analytically though, we can only obtain a weaker result, as we now demonstrate.

The positivity properties of expansion (3.1) imply

$$G_{\Delta,\ell}(\rho, \bar{\rho}) \leq G_{\Delta,\ell}(R, R). \tag{3.17}$$

Let us set

$$\mathcal{G}_\rho(R, R) = \mathcal{G}_z(z_{\text{eff}}, z_{\text{eff}}), \qquad \text{with} \quad z_{\text{eff}} \equiv \frac{4R}{(1+R)^2} \tag{3.18}$$

This implies:

$$\mathcal{G}(\rho, \bar{\rho}) = \frac{\sum_{\Delta,\ell} a_{\Delta,\ell} G_{\Delta,\ell}(\rho, \bar{\rho})}{(z\bar{z})^{\Delta_\phi}} \leq \frac{\sum_{\Delta,\ell} a_{\Delta,\ell} G_{\Delta,\ell}(R, R)}{(z\bar{z})^{\Delta_\phi}}$$

$$= \left[1 - z_{\text{eff}} \sin^2\left(\tfrac{\phi}{2}\right)\right]^{2\Delta_\phi} \mathcal{G}(R, R). \tag{3.19}$$

This is better than the coarser $\mathcal{G}(\rho, \bar{\rho}) \leq \mathcal{G}(R, R)$ which follows from the Cauchy-Schwarz inequality for the correlator. Altogether this implies

$$\mathcal{G}(\rho, \bar{\rho}) \leq \left[1 - z_{\text{eff}} \sin^2\left(\tfrac{\phi}{2}\right)\right]^{2\Delta_\phi} \left(1 + \frac{1}{z_{\text{eff}}^{2\Delta_\phi}} + \frac{1}{(1 - z_{\text{eff}})^{2\Delta_\phi}}\right), \qquad \text{if} \quad \Delta_{\mathcal{G}}^{\text{gap}} \geq 2\Delta_\phi \quad (3.20)$$

with the bound being optimal for $\phi = 0$. A caveat is that the bound holds only if there is a gap on the full set of $\text{SL}(2,\mathbb{R})$ primaries. This means that for higher-d CFT correlators restricted to the line the gap must be imposed uniformly across all spins. In particular the bound is less interesting when $\Delta_\phi > d/2$ as it would rule out CFT correlators with a stress-tensor.

3.3   Lorentzian kinematics

We now discuss the case where we have spacelike separated operators but we are not in the Euclidean section, so that $z, \bar{z}$ are both real and independent variables in the fundamental domain where $z, \bar{z} \in (0, 1) \times (0, 1)$. This regime corresponds to taking imaginary angle in the polar representations of section 3.1, so that e.g. $\rho = Re^{-\phi}$ with real ϕ. In particular the argument of the Gegenbauer polynomials in (3.1) becomes $\cosh\phi$. This means then that our basic approximation (3.3) is in general not valid. This is because although the radius R remains small inside the fundamental domain, the Gegenbauer polynomials are now exponentially growing in spin and this may compensate the exponential suppression with respect to R. The only way to guarantee this does not occur is to keep both ρ and $\bar{\rho}$ small and $\rho \sim \bar{\rho}$. In this regime our expectations for correlator minimization and maximization are the same as our discussion in the Euclidean regime.

The more interesting case corresponds to taking one of the cross-ratios to be relatively large, i.e. approaching one. Notice that inside the fundamental domain this necessarily means that the other must be small, since e.g. $\sqrt{\rho\bar{\rho}} \leq 3 - 2\sqrt{2}$ inside this region. In this case it is better to use a different series expansion for the conformal block:

$$G_{\Delta,\ell}(z, \bar{z}) = z^{\Delta-\ell}\bar{z}^{\Delta-\ell} \sum_{n,m=0}^{\infty} c_{n,m} z^n \bar{z}^m, \qquad c_{n,m} \geq 0, \qquad (3.21)$$

where $c_{n,m} \geq 0$ follows from unitarity [8]. In particular, for small z we have

$$G_{\Delta,\ell}(z, \bar{z}) \sim c_{0,2\ell} z^{\Delta-\ell}\bar{z}^{\Delta+\ell} \, {}_2F_1\left(\frac{\Delta+\ell}{2}, \frac{\Delta+\ell}{2}, \Delta+\ell, \bar{z}\right) \qquad (3.22)$$

so that in this regime, $z \ll \bar{z} \sim 1$, the parameter controlling the operators which give dominant contributions to the correlator is the twist $\Delta - \ell$.

Let us suppose firstly that $d \geq 3$. In this case unitarity allows in principle for scalar operators to dominate since the lowest allowed twists are $\frac{d-2}{2}$ and $d - 2$ for spin zero and greater than zero respectively. In particular, if we consider the correlator maximization problem with a scalar gap Δ_g which is not too close to $d - 2$, we expect that the result

should be essentially the same as in the Euclidean case: the maximal value correlator should essentially be the same as the opemax correlator for an operator which sits at the gap. If in contrast $d = 2$, or if we choose to set the gap above $d - 2$ then in principle the only thing we can say is that correlator maximization should involve minimizing the twist gap across all spins, and secondly maximizing their overall contribution, by increasing their OPE coefficients, but unfortunately we cannot make any general statement.

The same logic applies to correlator minimization. In this case the gapmax correlator always has a scalar operator whose twist is above $d-2$ (for instance when $\Delta_\phi = \frac{d-2}{2}$ the gap sits at $d-2$ and is saturated by free theory). Hence for this problem we always expect that the solution will involve increasing the overall twist gap across all spins but not necessarily uniformly across spins.

After these general remarks, we will now establish rigorous bounds on the correlator in the Lorentzian regime in terms of those in $d = 1$. This can be done quite trivially given expansion (3.21) since it implies

$$G_{\Delta,\ell}(z_m, z_m) \leq G_{\Delta,\ell}(z, \bar{z}) \leq G_{\Delta,\ell}(z_M, z_M), \qquad z_m = \min\{z, \bar{z}\}, \quad z_M = \max\{z, \bar{z}\} \quad (3.23)$$

and therefore

$$z_m^{2\Delta_\phi} \mathcal{G}(z_m, z_m) \leq (z\bar{z})^{\Delta_\phi} \mathcal{G}(z, \bar{z}) \leq z_M^{2\Delta_\phi} \mathcal{G}(z_M, z_M). \qquad (3.24)$$

Using the $d = 1$ bounds we find for $z, \bar{z} \in (0, 1)$:

$$\mathcal{G}(z, \bar{z}) \geq \left(\frac{z_m}{z_M}\right)^{\Delta_\phi} \mathcal{G}_{\inf}^{(d)}(z_m, z_m) \geq \left(\frac{z_m}{z_M}\right)^{\Delta_\phi} \mathcal{G}^F(z_m)$$

$$\mathcal{G}(z, \bar{z}) \leq \left(\frac{z_M}{z_m}\right)^{\Delta_\phi} \mathcal{G}_{\sup}^{(d)}(z_M, z_M | \Delta_g) \leq \left(\frac{z_M}{z_m}\right)^{\Delta_\phi} \mathcal{G}_{\sup}^{(d=1)}(z_M | \Delta_g) \qquad \Delta_g^{\mathcal{G}} \geq \Delta_g$$

(3.25)

Using these we can study the double lightcone limit, where $z \to 0$ and $\bar{z} \to 1$ at the same rate. In this case we write $z_m = z, z_M = 1 - z$ and take the limit where $z \to 0$. Then we can find

$$z^{\Delta_\phi} \mathcal{G}(z, 1 - z) \underset{z \to 0^+}{\geq} 1$$

$$z^{3\Delta_\phi} \mathcal{G}(z, 1 - z) \underset{z \to 0^+}{\leq} 1$$

(3.26)

The lower bound cannot be parametrically improved, since it is satisfied by generalized free fields. As for the upper bound, notice that it holds independently of the choice of gap (as long as the maximal value correlator exists, i.e. it is not infinite). We believe however that in this case it can be parametrically improved to $\mathcal{G}(z, 1 - z) = O(z^{-2\Delta_\phi})$, which holds for $d = 2$ CFTs [6, 16].

4 Correlator bounds from linear optimization

4.1 Formulation of the linear programming problems

Consider conformal correlators admitting an expansion of the following form:

$$\mathcal{G}(w, \bar{w}) = \frac{1}{(w\bar{w})^{\Delta_\phi}} + \sum_{\Delta, \ell \in \mathcal{S}} a_{\Delta, \ell} G_{\Delta, \ell}(w, \bar{w} | \Delta_\phi) \tag{4.1}$$

with corresponding crossing equation

$$F_{0,0}(w, \bar{w}) + \sum_{\Delta, \ell \in \mathcal{S}} a_{\Delta, \ell} F_{\Delta, \ell}(w, \bar{w} | \Delta_\phi) = 0 \,. \tag{4.2}$$

The first term stands for the identity contribution which we have singled out. The set $\mathcal{S}$ should be some subset of $\mathcal{U}$, the set of those quantum numbers Δ, ℓ allowed by unitarity, namely:

$$\mathcal{U} = \left\{ (\Delta, \ell) : \begin{array}{ll} \ell = 0 : & \Delta \geq \frac{d-2}{2} \\ \ell \in 2\mathbb{N} : & \Delta \geq d - 2 + \ell \end{array} \right\} \tag{4.3}$$

Often we will simply set $\mathcal{S} = \mathcal{U}$, othertimes we will impose additional gaps in Δ.

We will consider both minimization and maximization problems so as to get lower and upper bounds on values of correlators on the Euclidean section. Such bounds can be obtained by constructing linear functionals that act on the crossing equation (4.2), satisfying suitable properties. We will denote functionals providing upper/lower bounds at a given point $w, \bar{w}$ as $\overline{\Lambda}_{w, \bar{w}}$ and $\underline{\Lambda}_{w, \bar{w}}$. The action of such a functional on a crossing vector $F_{\Delta, \ell}$ is denoted for instance $\overline{\Lambda}_{w, \bar{w}}(\Delta, \ell)$. The conditions to be imposed are simply

$$\underline{\Lambda}_{w, \bar{w}}(\Delta, \ell) \geq -G_{\Delta, \ell}(w, \bar{w} | \Delta_\phi) \qquad \overline{\Lambda}_{w, \bar{w}} \geq G_{\Delta, \ell}(w, \bar{w} | \Delta_\phi) \,, \qquad \text{for all} \quad \Delta, \ell \in \mathcal{S} \,. \tag{4.4}$$

Acting with these functionals on the crossing equation we find:

$$\begin{aligned} \underline{\Lambda}_{w, \bar{w}}(0, 0) &= -\sum_{\Delta, \ell \in \mathcal{S}} a_{\Delta, \ell} \underline{\Lambda}_{w, \bar{w}}(\Delta, \ell) \leq \mathcal{G}(w, \bar{w}) - \frac{1}{(w\bar{w})^{\Delta_\phi}} \\ -\overline{\Lambda}_{w, \bar{w}}(0, 0) &= +\sum_{\Delta, \ell \in \mathcal{S}} a_{\Delta, \ell} \overline{\Lambda}_{w, \bar{w}}(\Delta, \ell) \geq \mathcal{G}(w, \bar{w}) - \frac{1}{(w\bar{w})^{\Delta_\phi}} \,. \end{aligned} \tag{4.5}$$

This implies:

$$\frac{1}{(w\bar{w})^{\Delta_\phi}} + \underline{\Lambda}_{w, \bar{w}}(0, 0) \leq \mathcal{G}(w, \bar{w}) \leq \frac{1}{(w\bar{w})^{\Delta_\phi}} - \overline{\Lambda}_{w, \bar{w}}(0, 0) \,. \tag{4.6}$$

We are now ready to formulate our optimization problems:

Correlator minimization:

$$\max_{\underline{\Lambda}_{w, \bar{w}} \in \mathcal{L}} \underline{\Lambda}_{w, \bar{w}}(0, 0) \quad \text{s.t.} \quad \underline{\Lambda}_{w, \bar{w}}(\Delta, \ell) \geq -G_{\Delta, \ell}(w, \bar{w} | \Delta_\phi) \quad \text{for all } (\Delta, \ell) \in \mathcal{S} \tag{4.7}$$

Correlator maximization:

$$\max_{\overline{\Lambda}_{w,\bar{w}} \in \mathcal{L}} \overline{\Lambda}_{w,\bar{w}}(0,0) \quad \text{s.t.} \quad \overline{\Lambda}_{w,\bar{w}}(\Delta,\ell) \geq G_{\Delta,\ell}(w,\bar{w}|\Delta_\phi) \quad \text{for all } (\Delta,\ell) \in \mathcal{S} \tag{4.8}$$

In the above the set $\mathcal{L}$ is typically some finite dimensional but large search space of elementary basis functionals. The idea therefore is to look for functionals satisfying the right positivity conditions inside $\mathcal{L}$, choosing the one whose action on the identity is the largest. In section 5 below we use the tried and tested approach of choosing $\mathcal{L}$ to be a finite set of derivatives at the crossing-symmetric point $z = \bar{z} = \frac{1}{2}$, leaving an exploration of better functional bases [15, 17–20] for the future.

Let us obtain some basic bounds following this logic. Consider first minimization. A simple functional satisfying all the desired conditions is simply

$$\underline{\Lambda}_{w,\bar{w}}[F_{\Delta,\ell}] = -F_{\Delta,\ell}(w,\bar{w}) = G_{\Delta,\ell}(1-w,1-\bar{w}) - G_{\Delta,\ell}(w,w|\Delta_\phi) \tag{4.9}$$

which leads to the (trivial) bound

$$\mathcal{G}(w,\bar{w}) \geq \max\left\{ \frac{1}{(w\bar{w})^{\Delta_\phi}}, \frac{1}{[(1-w)(1-\bar{w})]^{\Delta_\phi}}, 1 \right\} \tag{4.10}$$

where in passing we have used crossing symmetry to get better bounds for all $w, \bar{w}$ where the correlator is real-valued. This bound follows simply from the statement that the correlator is the sum of the identity block in some OPE channel plus positive contributions.

To get an upper bound we have to work slightly harder. Let us obtain a bound at the crossing symmetric point $w = \bar{w} = \frac{1}{2}$, choosing:

$$\overline{\Lambda}_{\frac{1}{2},\frac{1}{2}}[F_{\Delta,\ell}] = \frac{\lambda}{2}\partial_z F_{\Delta,\ell}(z,z)\Big|_{z=\frac{1}{2}} = \lambda\partial_z G_{\Delta,\ell}(z,z)\Big|_{z=\frac{1}{2}} \tag{4.11}$$

It can be checked that in general this will only satisfy the required constraints above some gap depending on λ. This is in line with our expectations that we do not expect a bound to exist for general Δ_ϕ unless we set a gap in the spectrum. To get a nice result let us work in the limit of large Δ_ϕ, where conformal blocks at large Δ take the form

$$G_{\Delta,\ell}(w,\bar{w}|\Delta_\phi) \underset{\Delta,\Delta_\phi\to\infty}{\sim} \frac{(4\rho)^\Delta}{z^{2\Delta_\phi}}g_\ell(w,\bar{w}) \tag{4.12}$$

where $g_\ell(w,\bar{w})$ does not vary exponentially with Δ. Let us demand that our functional provides a bound on correlators for which the gap satisfies $\Delta_g \geq \alpha\Delta_\phi$. The optimal such functional will satisfy

$$\overline{\Lambda}_{\frac{1}{2},\frac{1}{2}}(\Delta_g,\ell) = G_{\Delta_g,\ell}(\tfrac{1}{2},\tfrac{1}{2}|\Delta_\phi) \tag{4.13}$$

i.e. the positivity constraints will be saturated at the gap value. Note that the value of ℓ is irrelevant in the above, since g_ℓ is independent of ℓ when $w = \bar{w}$ in the large Δ limit. We can use this to fix λ:

$$\lambda = \frac{1}{2\sqrt{2}\Delta_\phi}\frac{1}{\alpha - \sqrt{2}} \tag{4.14}$$

106

One can check that the functional will satisfy the right positivity conditions above the gap, but only if $\alpha > \sqrt{2}$. From this we get the bound

$$\mathcal{G}(\tfrac{1}{2}, \tfrac{1}{2}) \underset{\Delta_\phi \to \infty}{\leq} 2^{2\Delta_\phi} \left(1 + \frac{\sqrt{2}}{\alpha - \sqrt{2}} \right), \qquad \Delta_g^{\mathcal{G}} \geq \alpha \Delta_\phi > \sqrt{2} \Delta_\phi \qquad (4.15)$$

As an example, setting $\alpha = 2$ we know the optimal bound correspond to the generalized free boson solution, which scales as $2^{2\Delta_\phi} \times 2$. The above is parametrically as good as the optimal bound, scaling $2^{2\Delta_\phi} \times (2 + \sqrt{2})$. This result does not give us any bound if the gap is smaller than $\sqrt{2}\Delta_\phi$. Could this be improved? We believe the answer is no. Firstly, it can be checked that including an arbitrary number of derivatives (but smaller than Δ_ϕ) won't change this conclusion. Secondly, the analytic functionals and corresponding bounds on OPE coefficients determined in [17] also precisely break down at that point. So it is rather nice that such a simple functional already correctly captures this feature.

4.2   Aside: reformulating the gap maximization problem

Let us make contact with our expectation that the correlator minimization problem is related to gap maximization. A similar argument to the one below can be made for the relation between correlator maximization and OPE maximization.

Suppose one wanted to prove a bound on the leading scaling dimension in the spin channel $\ell = \ell_0$. One can do this by constructing a functional, β, inside some finite dimensional search space $\mathcal{L}$, satisfying the constraints:

$$\begin{aligned}
\beta(0,0) &= 0, & \partial_\Delta \beta(\Delta_g, \ell_0) &= 1, \\
\beta(\Delta, \ell_0) &\geq 0 & \text{for} \quad \Delta &> \Delta_g \\
\beta(\Delta, \ell) &\geq 0 & \text{for} \quad (\Delta, \ell) &\in \mathcal{S}, \quad \ell \neq \ell_0
\end{aligned} \qquad (4.16)$$

If such a functional can be found, it is easily seen (by acting with β on the crossing equation) that it establishes an upper bound on the dimension equal to Δ_g. For each choice of Δ_g, finding whether the corresponding β exists is an optimization problem. In practice, one must fix Δ_g, check if such a functional exists, lather, rinse, repeat, until one finds the smallest such Δ_g possible. We denote the lowest such Δ_g by Δ_{gapmax}: it is the best possible bound available on the gap, given the constraints in set $\mathcal{L}$.

Fortunately, there is a better way. Consider the correlator minimization functional. At optimality we have

$$\frac{1}{(w\bar{w})^{\Delta_\phi}} + \underline{\Lambda}_{w,\bar{w}}(0,0) = \mathcal{G}_{\min;w,\bar{w}}(w, \bar{w}) \qquad (4.17)$$

Let us assume that the lowest dimension, non-identity operator in $\mathcal{G}_{\min;w,\bar{w}}(w, \bar{w})$ is a scalar of dimension Δ_g^r, with $r = \sqrt{w\bar{w}}$. In the limit where $r \to 0$ we get

$$\begin{aligned}
\underline{\Lambda}_{w,\bar{w}}(0,0) &\underset{r\to 0}{\sim} a_{\Delta_g^r,0}\, r^{\Delta_g^r - 2\Delta_\phi} \\
\underline{\Lambda}_{w,\bar{w}}(\Delta, \ell) &\underset{r\to 0}{\geq} -r^{\Delta - 2\Delta_\phi} C_\ell^{\left(\frac{d-2}{2}\right)}(\cos\theta)
\end{aligned} \qquad (4.18)$$

with the inequality being saturated at $\Delta = \Delta_g^r$. It follows that the functional

$$\beta \equiv \lim_{r \to 0} \frac{\Lambda_{w,\bar{w}}}{\partial_\Delta \Lambda_{w,\bar{w}}(\Delta_g^r, 0)} \tag{4.19}$$

satisfies

$$\beta(0,0) = 0\,, \quad \partial_\Delta \beta(\lim_{r \to 0} \Delta_g^r, 0) = 1\,, \quad \beta(\Delta, \ell) \geq 0\,, \quad \text{for} \quad \Delta > \lim_{r \to 0} \Delta_g^r \tag{4.20}$$

Hence β is a valid gap maximization functional, and leads to:

$$\Delta_{\text{gapmax}} = \lim_{r \to 0} \Delta_g^r \tag{4.21}$$

The conclusion is that minimizing the correlator for $r \to 0$ is the same as gap maximization as long as the leading operator is a scalar. We will see direct evidence for this in the numeric applications of section 5.

This result also suggests a new way to maximize the gap by a single optimization step. It is not really necessary to minimize the full correlator, since the important point really is to introduce constraints that decay sufficiently fast with Δ. It is also possible to do away with the restriction that the correlator minimization agrees with gap maximization only when the leading operator is a scalar, and to be able to maximize the gap in other spin sectors. To do this consider then the following optimization problem:

$$\max_{\omega \in \mathcal{L}} \omega(0,0) \quad \text{s.t.} \quad \begin{aligned} \omega(\Delta, \ell_0) &\geq -c(\Delta)\,, & \Delta > \Delta_0 \\ \omega(\Delta, \ell) &\geq 0 & \text{for} \quad (\Delta, \ell) \in U, \quad \ell \neq \ell_0 \end{aligned} \tag{4.22}$$

Here $c(\Delta)$ should be a non-negative function which should decay quickly with Δ and be positive at least in some range where the maximal gap is expected to occur. Good choices are for instance:

$$\begin{aligned} \text{Exponential:} &\quad c(\Delta) = \epsilon^\Delta\,, & \epsilon \ll 1 \\ \text{Power law:} &\quad c(\Delta) = \frac{1}{(\Delta - \Delta_0)^p} \end{aligned} \tag{4.23}$$

The optimal value for this optimization problem will be given by a functional ω^{opt} dual to an approximate solution to crossing. This solution minimizes the cost in the following dual problem:

$$\min_{a_{\Delta,\ell}} \sum_{\Delta > \Delta_0} a_{\Delta,\ell_0} c(\Delta) \quad \text{s.t.} \quad \sum_{\substack{\ell \neq \ell_0 : (\Delta, \ell) \in \mathcal{U} \\ \ell = \ell_0 : \Delta > \Delta_0}} a_{\Delta,\ell}\, \omega(\Delta, \ell) = 0 \quad \text{for all} \quad \omega \in \mathcal{L} \tag{4.24}$$

From this latter perspective it is clear that the outcome of the problem is a solution with as large a gap as possible while remaining consistent with the functional constraints. Denoting $\Delta_g^{\min}$ the leading scaling dimension (in channel ℓ_0) of the solution to this problem, it is clear that

$$\Delta_g^{\min} \sim \Delta_{\text{gapmax}} \tag{4.25}$$

108

Depending on our choice $c(\Delta)$ we can get an arbitrarily good estimate for Δ_{gapmax}. This is achieved by setting $\epsilon \ll 1$ in the exponential ansatz, or $p \gg 1$ and Δ_0 as close as possible to the expected maximal gap. Once we have such an estimate, we can then simply check that a functional β exists for $\Delta_g = \Delta_g^{\min} + \eta$, for small η. This can be done very efficiently since we can "hotstart" the search for the β functional with ω^{opt}. Alternatively, we can simply "flow" from the above problem to the gap maximization problem [10]: essentially, the β functional can be immediately constructed merely from knowledge of the solution to the dual problem, without any new optimization required to be solved.

These approaches are all equivalent, and all lead to an extremal functional β with the correct properties establishing indeed that $\Delta_g^{\min} = \Delta_{\text{gapmax}}$ to any desired accuracy. We have tested this procedure using both an exponential cost function as well as a power law of high degree. For instance, setting $\epsilon = 10^{-150}$ we obtained a $\Delta_{\text{gapmax}} - \Delta_g^{\min} < 10^{-15}$, which we checked by explicitly constructing a gapmax functional after obtaining the initial estimate. We believe this method will be useful for future numerical bootstrap applications.

5 Numerical applications

In this section we present numerical bounds on 3d CFT correlators. The bounds are obtained by applying the logic of the previous section, constructing suitable functionals inside some search space using the `JuliBootS` package [21]. Further details on the numerical implementation are relegated to appendix A.

5.1 Summary

Our numerical results are summarized in figure 5, which shows the allowed range of values of the four-point correlator at the crossing symmetric point $z = \bar{z} = \frac{1}{2}$ as a function of Δ_ϕ, and figure 6, which shows upper and lower bounds along the line $z = \bar{z}$ for various values of Δ_ϕ. There are several interesting features in these plots, so let us discuss them in turn.

Beginning from the top of figure 5, we see that there is an upper bound on the correlator, at least in some range of Δ_ϕ. This bound is valid without any particular assumptions on the spectrum. In the figure we also show the effect of imposing various gaps in the scalar sector, leading to stronger bound curves. The upper bound assuming a gap of $2\Delta_\phi$ is closely saturated by the exact generalized free boson correlator, in agreement with the exact bound reviewed in section 3.2. In the absence of an assumption in the gap, the upper bound diverges in the vicinity of $\Delta_\phi = 1$. This can be understood from the fact that there is a unitary solution to the crossing equation without identity for $\Delta_\phi \geq d - 2$, namely

$$\mathcal{G}_C(u,v) = (uv)^{-\frac{\Delta_\phi}{2}} + u^{-\frac{\Delta_\phi}{2}} + v^{-\frac{\Delta_\phi}{2}} \tag{5.1}$$

This correlator arises in the computation of the ϕ^2 4-point function in the generalized free CFT. One can check by direct expansion that unitarity of this solution is violated unless $\Delta_\phi \geq d - 2$. Since this solution may be added to any given correlator with an arbitrarily
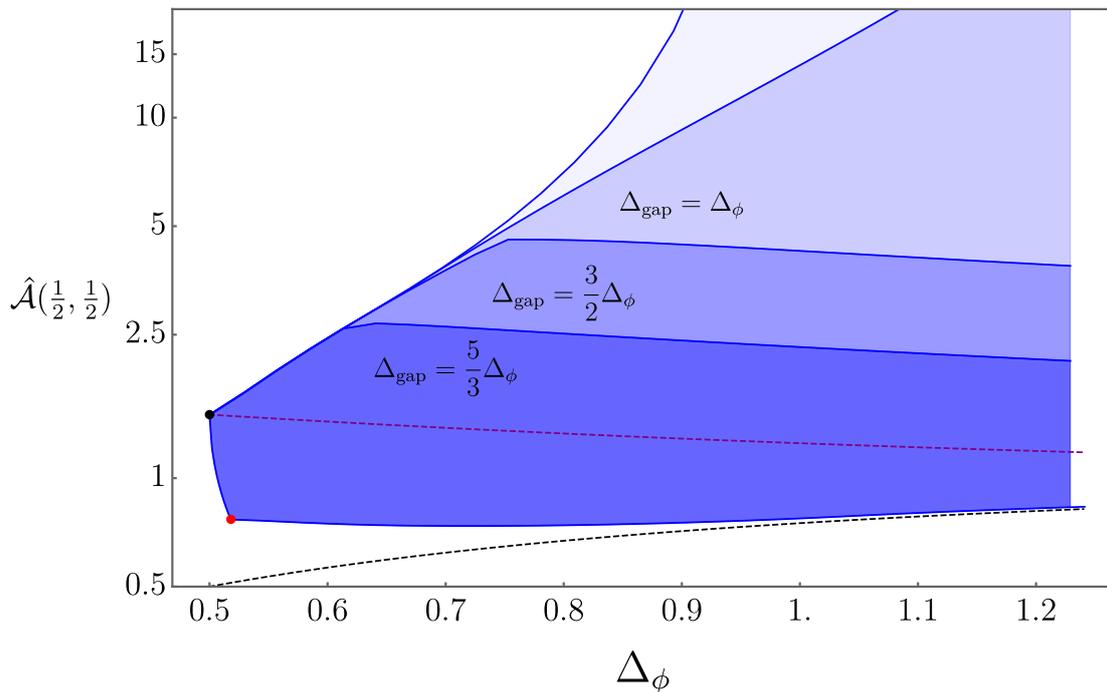
Figure 5: Bounds on 3d CFT correlator values, with $\hat{\mathcal{A}}(z, \bar{z}) = (z\bar{z})^{2\Delta_\phi}\mathcal{G}(z, \bar{z}) - 1$. The shaded region represents the values such a correlator may take at the crossing symmetric point $z = \bar{z} = \frac{1}{2}$. The dashed lines inside the allowed region correspond to maximal allowed values assuming a gap. The upper bound goes to ∞ close to $\Delta_\phi = 1$. The dashed line outside the allowed region is the 1d generalized free fermion correlator, which provides a (suboptimal) lower bound. The dashed line inside the allowed region is the generalized free boson correlator, which provides an upper bound for $\Delta_{\text{gap}} = 2\Delta_\phi$. The black and red dots are the free theory and 3d Ising values respectively.

large coefficient, there can be no bound without assuming a gap in the spectrum for such values of Δ_ϕ. In particular the gap Δ_g must be necessarily larger than $\Delta_\phi/2$.

As we move towards the left along the top curve we hit a kink which occurs at the free theory point, where $\Delta_\phi = 1/2$. The upper and lower bounds reassuringly coincide both with each other and the free theory value, as the only CFT correlator with that dimension should be the free one. Continuing now below and to the right, we have a lower bound on the correlator. It is compatible with the exact lower bound on the correlator determined by the 1d generalized free fermion solution reviewed in section 3.2. Although our bound is stronger since it takes into account constraints from the full 3d crossing equation, nevertheless, it seems to rapidly approach the 1d bound for moderate values of Δ_ϕ.

The lower bound has a distinctive kink at $\Delta_\phi \sim 0.518149$, which is the dimension of the spin field in the 3d Ising CFT. This is not an accident. Indeed, in figure 6 we see that at that particular value of Δ_ϕ the infimum correlator actually matches the 3d Ising correlator [22] extremely accurately. This is in perfect agreement with our argument that correlator minimization is closely related to gap maximization, since gap maximization
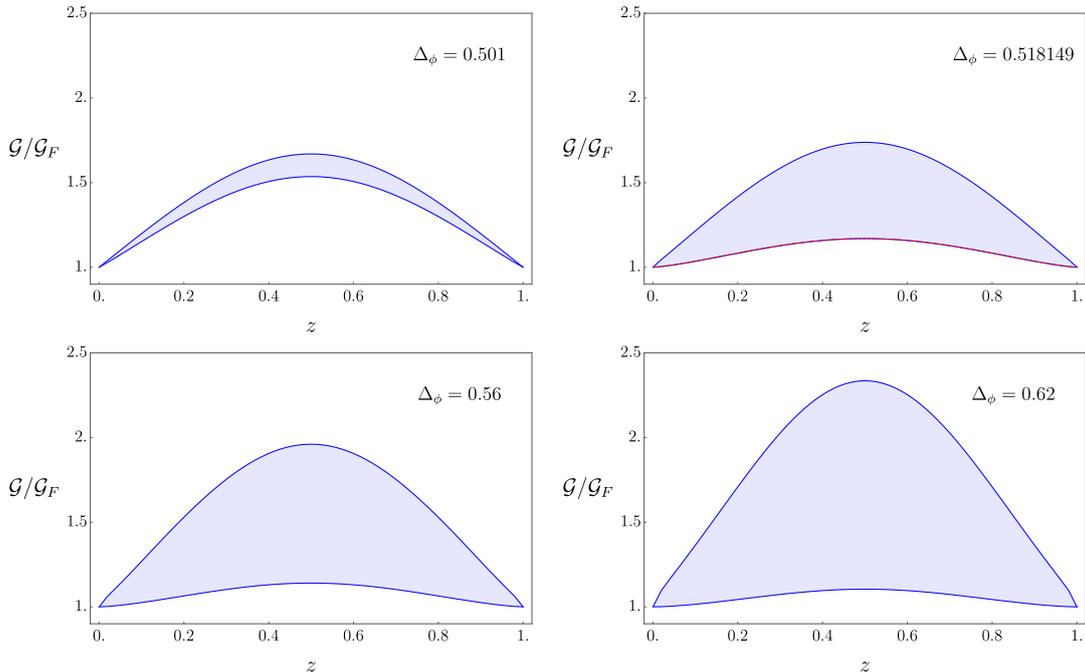
110

Figure 6: Allowed values for CFT correlators on the line $z = \bar{z}$, for various values of Δ_ϕ, normalized by the 1d generalized free fermion correlator. The 3d Ising correlator matches the lower bound for $\Delta_\phi = \Delta_\sigma^{\text{Ising}} \sim 0.518149$.

indeed leads to the 3d Ising model at the correct value of Δ_ϕ [2]. We will further confirm this below by a comparison of the leading scalar dimension in gap maximization versus correlator minimization.

5.2   Minimization

We now take a closer look at the spectra of the minimizing correlators. Figure 7 show the dimension of the leading scalar operator in $\mathcal{G}_{\min;z,\bar{z}}$ as functions of Δ_ϕ, depending on the choice of minimization point. We find that to very high accuracy the minimization problem is saturated by the same correlator (i.e. the same solution to crossing) independently of the choice of point on the Euclidean section, as long as $\Delta_\phi \lesssim 1$. That is, in this region the infimum correlator $\mathcal{G}_{\inf}$ is an actual correlator. Furthermore, in this region the full spectrum very closely matches the spectrum of the gap maximizing correlator, i.e.

$$\mathcal{G}_{\inf} \sim \mathcal{G}_{\text{gapmax}}\,, \qquad \Delta_\phi \lesssim 1\,. \tag{5.2}$$

In particular it matches that of the critical 3d Ising model when $\Delta_\phi = 0.518149$. Checking this to high precision is difficult for higher dimensional search spaces, since gap maximization requires a costly bissection procedure[4], but to the extent we were able to do it we found very close agreement. As a proxy measure for how close, consider figure 8, which shows

---

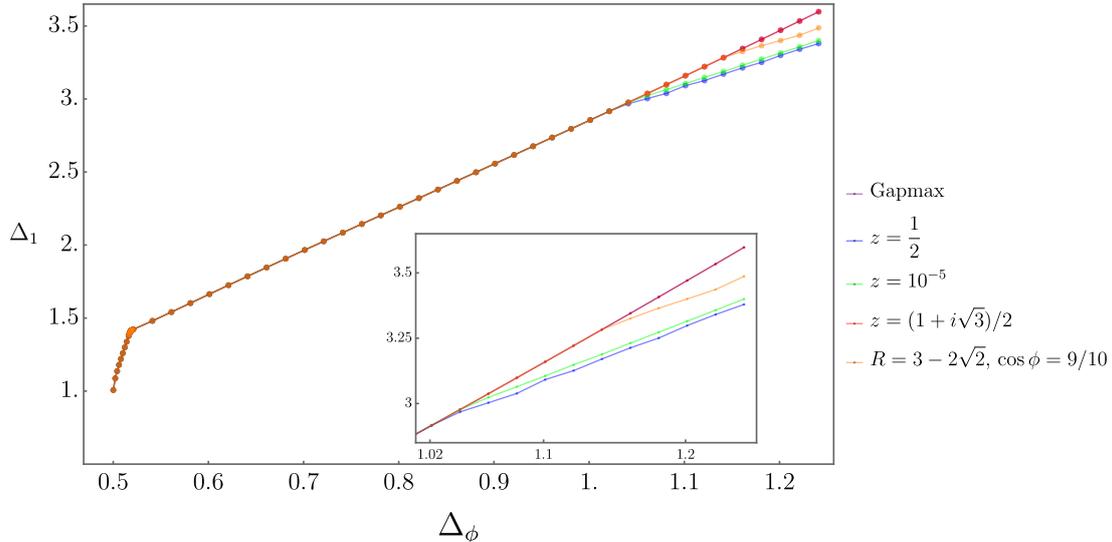[4]An improved way to search for the boundary of the allowed region has been recently proposed [23].

Figure 7: Leading scalar operator in the infimum correlator for different points on the Euclidean section as a function of Δ_ϕ. Shown is also is an upper bound on the maximal scalar gap. All curves closely overlap until about $\Delta_\phi \sim 1$ where the gap bound crosses $\Delta_1 \sim d$.

the difference between spectra obtained by minimizing the full correlator or just minimizing contributions to the correlator from spin-0. The latter should be closer to the result of gap maximization in that channel. The figure reveals a very small difference for minimization at $z = \bar{z} = \frac{1}{2}$, which further shrinks as we make this value smaller.

The observation that minimization yields the same correlator almost independently of the choice of minimization point can be understood from our discussion in section 3: as long as the scalar gap is far from the spin-2 unitarity bound, the correlator is dominated for small values of $z, \bar{z}$ by the leading scalar, angle independent, contribution, which is minimized by maximizing the gap. However, as the dimension of the leading scalar approaches $3 = d$, i.e. the unitarity bound in the spin-2 channel, we start to see an interplay between the contributions of the leading scalar and spin-2 operators, since now the value of the full correlator can be made smaller by pushing up the gaps in both these spin channels. Indeed, in this region the correlator is now approximately given by

$$(z\bar{z})^{\Delta_\phi} \mathcal{G}(\rho, \bar{\rho}) \sim 1 + a_g R^{\Delta_g} + a_T R^{\Delta_T} C_{\ell=2}^{(\frac{d-2}{2})}(\cos\phi) + \dots. \tag{5.3}$$

Minimization at different points $(z, \bar{z})$ on the Euclidean section will lead to distinct minimal correlators $\mathcal{G}_{\min;z,\bar{z}}$ depending on the detailed contributions of each opeartor.

We demonstrate this interplay in figure 9. On the left, we show the leading operators in the scalar and spin-2 channel in the vicinity of the cross-over point where the gap bound hits d. For some R dependent value of Δ_ϕ, it becomes favourable to increase the gap in both sectors. In the limit where $R \to 0$ we expect the matching between gap maximization and correlator minimization to stop precisely for that value of Δ_ϕ where $\Delta_{\text{gapmax}} = d = 3$. On the righthand figure we consider a specific $\Delta_\phi > 1$ (i.e. beyond the cross-over) and
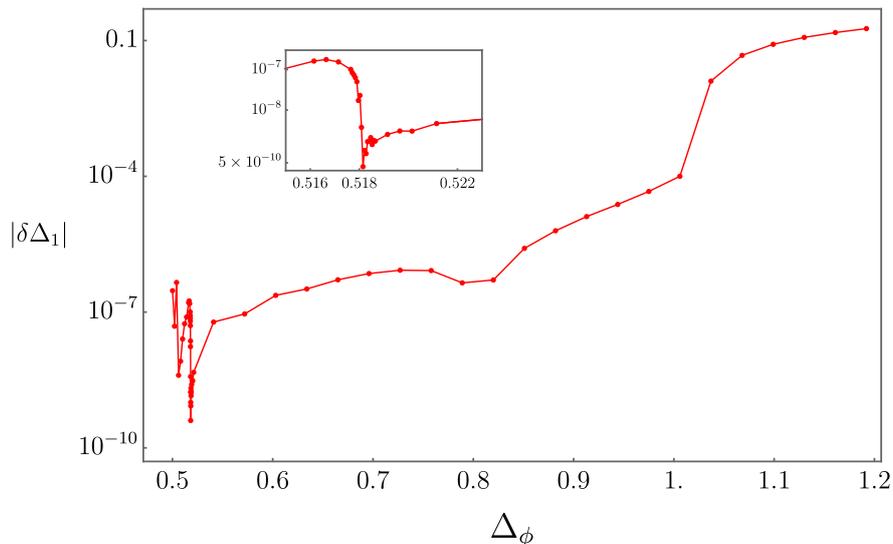
Figure 8:   Difference in dimension of leading scalar operator between full correlator minimization and scalar channel correlator minimization.

minimize the correlator for fixed R but varying angle. As we move away from the forward limit, the scalar operator moves up until it hits the corresponding upper bound for that Δ_ϕ. This can be understood from our simple approximation above, as increasing the angle makes the spin-2 contribution smaller. In fact, it can even become negative, which then favours pushing down the dimension of the T operator to the unitarity bound.

5.3   Maximization: no gap

Let us now turn to a closer look into the upper bounds on correlator values. Figure 10 shows the upper bound $\mathcal{G}_{\mathrm{sup}}(z, \bar{z})$ on the correlator along the line $z = \bar{z}$. The bound $\mathcal{G}_{\mathrm{sup}}$ is the envelope of distinct maximizing correlators at distinct points, $\mathcal{G}_{\mathrm{max}, z_i, \bar{z}_i}(z, \bar{z})$. Hence the maximization problem generically leads to a continuous family of correlators labeled by the maximizing point.

We can understand this by going back to the small R approximation of the correlator,

$$(z\bar{z})^{\Delta_\phi} \mathcal{G}(R) \sim 1 + a_g R^{\Delta_g} + \dots \tag{5.4}$$

where Δ_g is the dimension of the leading (scalar) operator, which we don't know a priori. Since we are not imposing any gap, maximizing the correlator at a fixed value of R would tentatively place an operator at the lowest possible value of scaling dimension, namely the scalar unitarity bound, and maximize its OPE coefficient. However there is a snag, since a free field cannot appear in the OPE of two identical scalars. As we lower the scaling dimension towards unitarity, the conformal block for such an operator diverges, and this divergence must be cancelled by a vanishing OPE coefficient. In practice then we have a competition between wanting to lower the gap and keeping the OPE coefficient large.
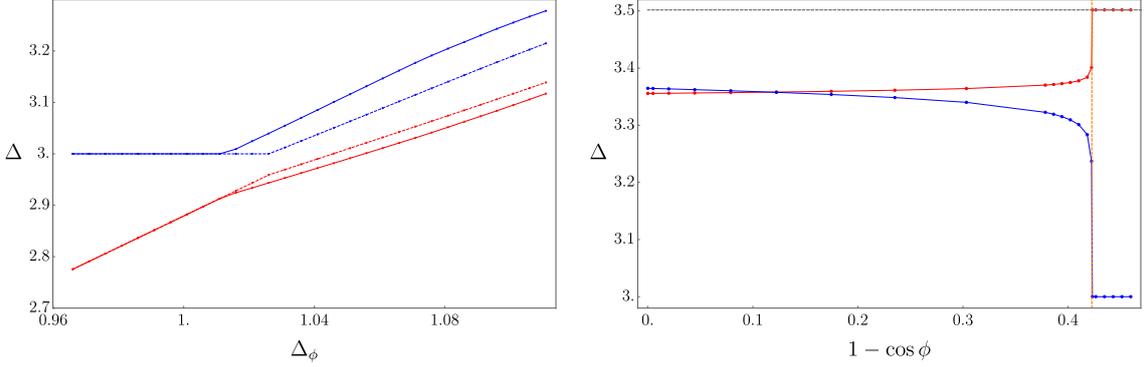
Figure 9: Correlator spectra in the cross-over region. Left: dimensions of leading scalar and spin-2 operators, shown in red and blue respectively, in the spectrum of $\mathcal{G}_{\min,R}$. The solid lines correspond to spectra for $R = 3 - 2\sqrt{2} \sim 0.17$, and dashed lines for $R = 5 \times 10^{-3}$. Right: the same operators when minimizing for $R = 3 - 2\sqrt{2}$ and different choices of the angle ϕ. For $\cos\phi > 1/\sqrt{3}$ the spin-2 Gegenbauer polynomial becomes negative and T gets pushed down to unitarity.
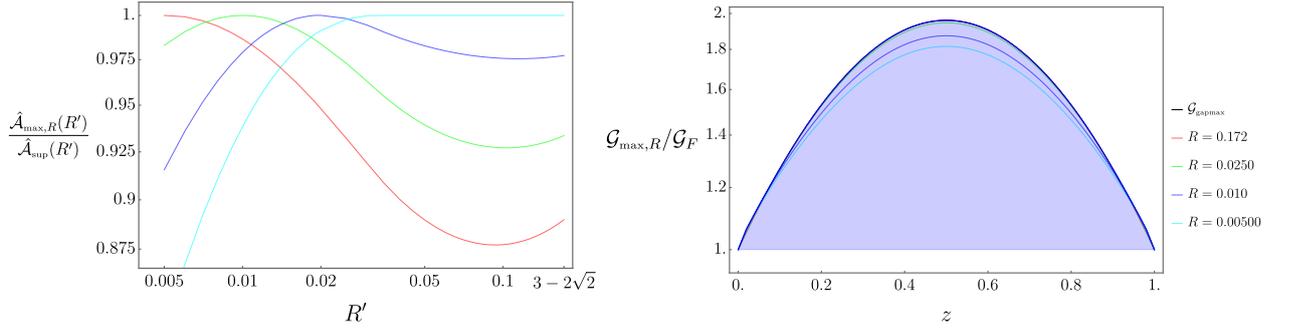

Figure 10: Upper bound on correlator. On the right we plot $\mathcal{G}_{\max,R}(z)$ for various values of R. Their envelope defines $\mathcal{G}_{\sup}(z)$. This is seen more clearly in the lefthand figure.

Writing $a_g \sim (\Delta_g - 1/2)\hat{a}_g$ the correlator value at R is maximized when

$$\partial_{\Delta_g}\left(a_g R^{\Delta_g}\right) = 0 \Leftrightarrow \Delta_g - \frac{1}{2} \sim \frac{1}{-\log(R)} \tag{5.5}$$

Hence we see that the maximizing correlator will indeed depend on the value of R. This is visible in figure 11 where we show the spectrum of the maximal correlator as a function of R.

Something very interesting happens in the limit where $R \to 0$. In this case the dimension of the leading operator in $\mathcal{G}_{\max,R}$ goes towards unitarity, and hence its OPE coefficient becomes vanishing, according to our reasoning above. This happens in such a way that the contribution of this operator still dominates the overall size of the correlator when we evaluate it close to the maximizing point. However, evaluating this correlator at some other value of the cross-ratio, i.e. $\mathcal{G}_{\max,R}(R')$ with $R \ll 1$ but R' fixed, then the contribution of this operator will generically not be the dominant one. Since the corresponding OPE
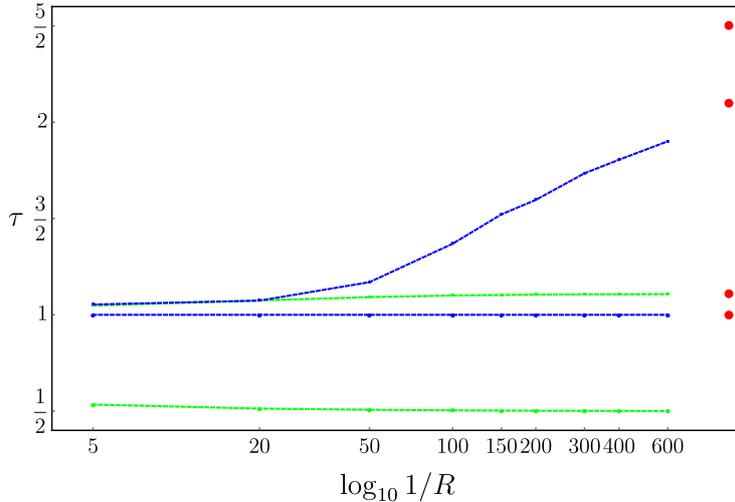
114

Figure 11: Twist spectrum of $\mathcal{G}_R$ as R goes to zero. In green/blue $\ell = 0/2$ operators. In the limit where $R \to 0$ the contribution of the operator at unitarity mimics that of an operator with $\Delta = 5/2$, and the full spectrum matches that of OPE maximization at shown as the red dots. See the main text for further details.

coefficient is going to zero we can use the identity

$$\lim_{\Delta \to \frac{1}{2}} (\Delta - \frac{1}{2}) G_{\Delta,0}(z, \bar{z}) \propto G_{5/2,0}(z, \bar{z}) \,. \tag{5.6}$$

and so the contribution of that operator becomes equivalent to that of an operator of dimension $5/2$.

In other words, the family of maximal correlators labeled by R tends to a universal correlator when $R \to 0$, although it does so non-uniformly as a function of the cross-ratio. Let us therefore set:

$$\mathcal{G}_{\text{max},0}(R') \equiv \lim_{R \to 0} \mathcal{G}_{\text{max},R}(R') \,. \tag{5.7}$$

Let us comment on what we know about the properties of the spectrum of $\mathcal{G}_{\text{max},0}$. Firstly, the leading operator in $\mathcal{G}_{\text{max},0}(R')$ is now the ($R \to 0$ limit of) the subleading operator in the family $\mathcal{G}_{\text{max},R}$, and it will have some scaling dimension which we denote Δ_g^0. Secondly, the correlator will contain a scalar operator of dimension $5/2$. Furthermore, because of the way in which this operator arose, we expect that its OPE coefficient should be quite large. In fact, it is reasonable to expect that it should be as large as possible, so that $\mathcal{G}_{\text{max},0}$ should actually be closely related to that correlator which maximizes the OPE coefficient of the operator at $\Delta = 5/2$ *without assumptions on the gap*:[5]

$$\mathcal{G}_{\text{max},0}(z, \bar{z}) \overset{?}{=} \mathcal{G}_{\text{opemax},\Delta=5/2} \tag{5.9}$$

---

[5]In the notation of section 2.2, this correlator is given by:

$$\mathcal{G}_{\text{opemax},\Delta=5/2} = \underset{\mathcal{G} \in \mathfrak{G}}{\arg\max} \quad a_{5/2,0} \,. \tag{5.8}$$

We compare the spectrum of $\mathcal{G}_{\mathrm{max},0}$ against that of $\mathcal{G}_{\mathrm{opemax},\Delta=5/2}$ in figure 12 (see also figure 11). We can see that up to the mapping between the two scalar operators at unitarity and $\Delta = 5/2$, the spectra indeed closely match.
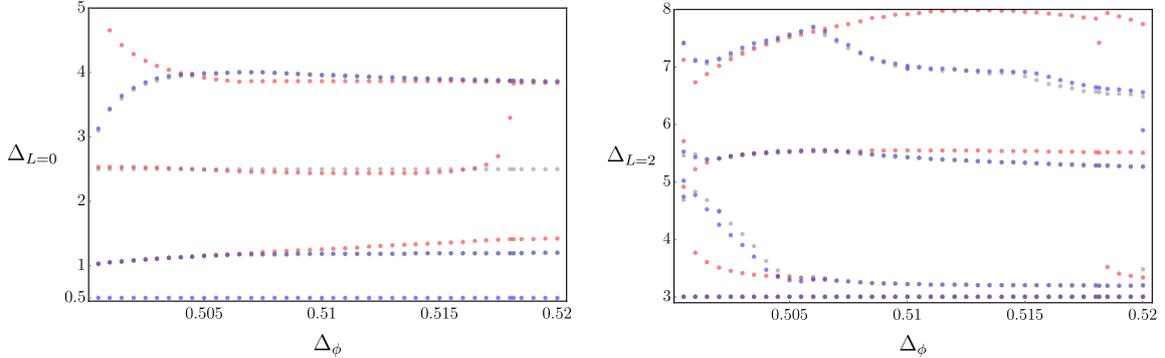

Figure 12: Extremal correlator spectra. The blue dots correspond to correlator maximization at $R = 10^{-600}$, the gray dots to OPE maximization at $\Delta = 5/2$. The spectra closely match, once we identify the scalar at unitarity in the former to the $\Delta = 5/2$ scalar in the latter. The red dots correspond to gap maximization. All three spectra closely match around $\Delta_\phi \sim 0.505$.

However, we also find a surprise. In the same plot we show the spectrum of the gap maximization correlator $\mathcal{G}_{\mathrm{gapmax}}$. Recall that we had found that this closely matches that of correlator *minimization*. Remarkably, it appears that around some critical value $\Delta_\phi \sim 0.505$, the three correlators actually match! In fact, the subleading scalar operator in $\mathcal{G}_{\mathrm{gapmax}}$, which corresponds to ϵ' in the 3d Ising model with $\Delta \sim 3.84$, comes down with decreasing Δ_ϕ and becomes the $5/2$ operator. This suggests that at this point could sit an interesting CFT, one which would be characterized by the existence of a protected operator of dimension $5/2$. This CFT is singled out by simultaneously satisfying an OPE maximization bound on this operator and saturating a bound on the maximal gap. It would be interesting to extend our analysis of this theory further by considering a multiple correlator setup.

5.4   Maximization: with a gap

Let us now discuss correlator maximization assuming a gap in the spectrum of scalar operators.

In figure 13 we show the upper bound for the value of the correlator at the crossing symmetric point as a function of the gap at a specific value of Δ_ϕ. Other choices lead to similar looking figures. For large enough gaps, we find that the maximizing correlator is independent of the precise maximizing point, so that the supremum correlator $\mathcal{G}_{\mathrm{sup}}$ is physical. Indeed, in this case the bound is very closely saturated by the correlator saturating OPE maximization with the same gap. There are minute differences between the two, which seemingly get stamped out as we decrease r, similarly to what we saw for gapmax versus
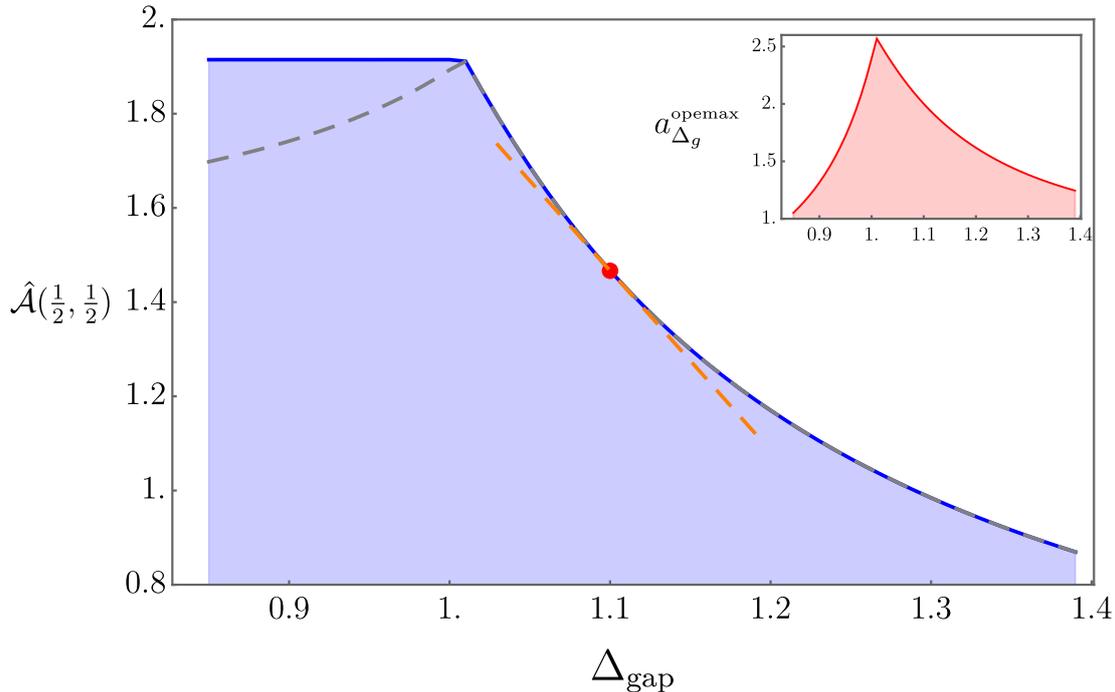
116

Figure 13: Correlator maximization at the crossing symmetric point as a function of the gap. The resulting correlator matches the OPE maximization correlator (shown as a gray dashed line) above a certain critical gap. Both correlators agree with the generalized free boson at a gap $\Delta_g = 2\Delta_\phi$ shown by the red dot. The dashed orange line which is tangent to the bound curve at the GFF point represents the leading correction to the correlator from an AdS$_4$ contact interaction. The inset shows a bound on the OPE coefficient $a_{\Delta_g}^{\text{opemax}}$ as a function on the gap. It shows a maximum at the point below which correlator maximization and OPE maximization give different results.

correlator minimization. A particularly interesting point is where we set the gap to be equal to $2\Delta_\phi$. In this case, the 1d functionals discussed in section 3.2 imply that the optimal OPE and correlator maximization bounds should not only match, but should correspond to the generalized free boson correlator. Our numerical results agree with this and we've checked the result is unchanged by moving away from the line $z = \bar{z}$.

As we lower the gap, we eventually reach a critical value Δ_g^c, which is approximately equal to one in a wide range of Δ_ϕ, where the OPE max correlator $\mathcal{G}_{\text{opemax}}$ and $\mathcal{G}_{\text{sup}}$ stop matching. Also, if we lower the gap further, the value of the correlator varies very little. This can be understood by a closer examination of the OPE maximization problem. Indeed, as shown in the inset of the figure, the maximal value of the OPE coefficient as a function of the gap, peaks at about $\Delta_g \sim \Delta_g^c$. So, for gaps lower than this, the maximizing correlator can now benefit from a tradeoff between having an operator at a dimension larger than the gap but with larger OPE coefficient.

The region where both OPE and correlator maximization agree is very interesting. Zooming in to the vicinity of the generalized free field point, we have verified that the

117

maximal solution is well approximated by the boundary correlator of a weakly coupled field Φ in AdS$_4$ with a Φ^4 contact interaction:

$$\mathcal{G}_{\text{sup}}(z, \bar{z}|\Delta_g) \underset{\Delta_g \sim 2\Delta_\phi}{\sim} \mathcal{G}^B(z, \bar{z}) + \frac{(\Delta_g - 2\Delta_\phi)}{2} D_{\Delta_\phi}(z, \bar{z}) \tag{5.10}$$

where the crossing symmetric D function is the overlap of four bulk-to-boundary propagators in AdS [24–26], with conformal block expansion

$$D_{\Delta_\phi}(z, \bar{z}) = \sum_{n=0}^{\infty} \left[a_n^{(1)} G_{\Delta_n, 0}(z, \bar{z}) + a_{n,0}^{\text{gff}} \gamma_{n,0} \partial_\Delta G_{\Delta_n, 0}(z, \bar{z}) \right] \tag{5.11}$$

where

$$\begin{aligned}
a_n^{(1)} &= \frac{1}{2} \partial_n \left(a_{n,0}^{\text{gff}} \gamma_{n,0} \right) \\
a_{n,0}^{\text{gff}} \gamma_{n,0} &= \frac{2^{1-2n} \Gamma\left(\Delta_\phi + \frac{1}{2}\right) \Gamma(\Delta_\phi + n)^3 \Gamma\left(2\Delta_\phi - \frac{d}{2} + n\right)^2}{(n!)^2 \Gamma(\Delta_\phi)^3 \Gamma\left(2\Delta_\phi - \frac{d}{2}\right) \Gamma\left(\Delta_\phi + n + \frac{1}{2}\right) \Gamma\left(2\Delta_\phi - \frac{d}{2} + 2n\right)}
\end{aligned} \tag{5.12}$$

For instance we have verified that close to the GFF point the spectrum of the solution is well described by the GFF one plus corrections to the scalar operators controlled by $\gamma_{n,0}$. This suggests that the line of solutions running from Δ_g^c and Δ_{gapmax} is related to a scalar theory in AdS$_4$, whose dynamics at small coupling is described by a simple contact interaction. A similar line of solutions had been observed in $d = 1$ CFTs where in fact it was checked the agreement extended to $O(g^3)$ with $g = \Delta_g - 2\Delta_\phi$ the effective coupling. It would be interesting to investigate what happens here where the contact interaction in AdS$_4$ is classically marginal. Increasing the coupling, making the interaction more attractive, lowers the energy of states and the gap goes down. However there seems to a limit for doing this, since when we hit $\Delta_g = \Delta_g^c$ we must move on to a very different branch of solutions; for instance we find that the stress-tensor becomes a part of the spectrum for gaps lower than Δ_g^c. Conversely making the interaction repulsive increases the energy. We cannot do this indefinitely however: at some point we reach the maximal allowed value of the gap. This is interesting: were we to sit at $\Delta_\phi = \Delta_\sigma^{\text{Ising}}$ (say by tuning the AdS mass), we know that the maximal gap is achieved by the 3d Ising correlator, which is also described by a scalar field with a quartic interaction, but of course on the *boundary* of AdS. The transition from the family of theories labeled by the gap to the Ising solution is therefore most likely discontinuous, since the latter is local (it contains a stress tensor), whereas our family does not (as we've checked). This is what happens in the $d = 1$ case where the gap max solution is a free fermion.[6] It would be very interesting to understand this family of solutions better, and how it links with yet another family of solutions linking 3d Ising and generalized free fields, namely the long-range Ising family [27–30].

---

[6]In that case there is an order of limits issue: for any solution with Δ_g strictly smaller than Δ_{gapmax}, its spectrum is always different from that of the gap max solution at sufficiently high energies.
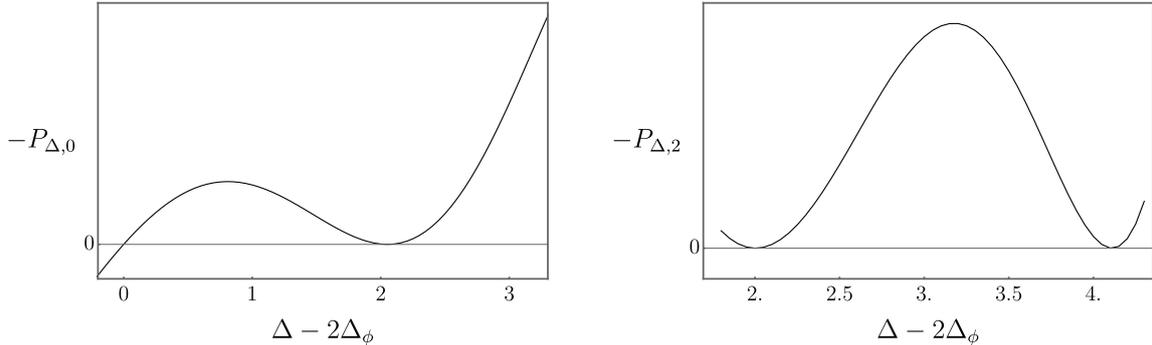
Figure 14: Polyakov blocks from numerical results. They are defined by $-P_{\Delta,\ell}(z,\bar{z}) := \Omega_{z,\bar{z}}(\Delta,\ell) - G_{\Delta,\ell}(z,\bar{z}|\Delta_\phi)$. Here we evaluate them in the case where Ω is the functional establishing an upper bound on th correlator at the crossing symmetric point and in the presence of a gap $\Delta_g \geq 2\Delta_\phi$. The spin-2 Polyakov block is non-negative for all Δ above the unitarity bound.

6 Discussion

In this paper we have initiated an exploration of the CFT landscape from a new perspective: that of optimization of correlator values. We have found that in some circumstances, this new viewpoint coincides or closely matches with more familiar ones of OPE maximization or gap maximization, in others it leads to new extremal solutions that would be difficult to find otherwise. An example is the gap maximizing correlator around $\Delta_\phi = 0.505$ which has an operator of dimension $\Delta = 5/2$. It would be very interesting to try to isolate this theory as an island in a multiple correlator setup and to try to understand theoretically how such a protected operator can arise. Another example is the fact that the GFF solution and its nearby deformations in AdS saturate an OPE/correlator maximization bound. This immediately implies that in the vicinity of $\Delta_\phi = d/4$ the long-range Ising model family also saturates this bound. It is likely this fact can be used to isolate the theory. We hope to report on this in the near future.

There are several obvious generalizations of our work, such as different spacetime dimensionality, including global symmetries and so forth. It could also be interesting to consider different optimization problems, where instead of optimizing over correlator values we would optimize over value variations, e.g. derivatives of the correlator. There is some motivation for doing this from the analogy with the S-matrix bootstrap, where this would correspond to optimizing over couplings to resonances. It might also be interesting to consider non-linear optimization targets in the multiple correlator bootstrap. For instance, is the determinant of the matrix of correlators involving σ and ϵ for the 3d Ising model the minimal possible for all CFTs?

We have obtained bounds by constructing functionals numerically. These functionals constitute approximations to master functionals [6, 31] which encode higher dimensional versions of Polyakov blocks [11–15]. We can plot them numerically (they are simply the functional actions) and see that they have nice positivity properties. In particular, for the

maximization problem with gap $2\Delta_\phi$, where the blocks have GFF spectra, they cannot and do not match those of the Polyakov-Regge expansion of the works [20, 31]. For instance our functionals do not have any nice structure in the odd-spin sector, and they are positive below twist $2\Delta_\phi$ for all $\ell > 0$. It would be very interesting to investigate if instead they could be matched to the fully crossing-symmetric Polyakov blocks defined in [32].

Acknowledgments

A   Numerical parameters

All computations done in this work used the the `JuliBootS` package [21]. The table below specifies the parameters in our numerical calculations. When mmax = 1, nmax is equivalent to the usual Λ used in SDPB [33] by $\Lambda = 2\text{nmax} + 1$. For almost all the plots, we used using the parameters No.1. The Fig 11 and Fig 12 correspond parameters No.2. Fig 9 left and right correspond to parameters No.3 and No.4. The Fig 7 and Fig 13 correspond to parameters No.5.

No.	nmax	mmax	Spins
1	11	1	$\{0, 2, ..., 28\} \cup \{46, 48, 50\}$
2	20	1	$\{0, 2, ..., 40\} \cup \{64, 66, 68, 70\}$
3	10	1	$\{0, 2, ..., 40\} \cup \{64, 66, 68, 70\}$
4	10	1	$\{0, 2, ..., 28\} \cup \{46, 48, 50\}$
5	13	1	$\{0, 2, ..., 40\} \cup \{58, 60, 76, 78, 96, 98, 100\}$

Table 1: Parameters used in numerical computations.

References

[1] D. Poland, S. Rychkov, and A. Vichi, *The Conformal Bootstrap: Theory, Numerical Techniques, and Applications*, Rev. Mod. Phys. **91** (2019) 015002, [arXiv:1805.04405].

[2] S. El-Showk, M. F. Paulos, D. Poland, S. Rychkov, D. Simmons-Duffin, and A. Vichi, *Solving the 3D Ising Model with the Conformal Bootstrap*, Phys. Rev. D **86** (2012) 025022, [arXiv:1203.6064].

[3] R. Rattazzi, V. S. Rychkov, E. Tonni, and A. Vichi, *Bounding scalar operator dimensions in 4D CFT*, JHEP **12** (2008) 031, [arXiv:0807.0004].

[4] R. Rattazzi, S. Rychkov, and A. Vichi, *Central Charge Bounds in 4D Conformal Field Theory*, Phys. Rev. D **83** (2011) 046011, [arXiv:1009.2725].

[5] M. F. Paulos, J. Penedones, J. Toledo, B. C. van Rees, and P. Vieira, *The S-matrix bootstrap. Part I: QFT in AdS*, JHEP **11** (2017) 133, [arXiv:1607.06109].

[6] M. F. Paulos, *Dispersion relations and exact bounds on CFT correlators*, arXiv:2012.10454.

[7] M. Hogervorst and S. Rychkov, *Radial Coordinates for Conformal Blocks*, Phys. Rev. D **87** (2013) 106004, [arXiv:1303.1111].

[8] D. Pappadopulo, S. Rychkov, J. Espin, and R. Rattazzi, *OPE Convergence in Conformal Field Theory*, Phys. Rev. D **86** (2012) 105043, [arXiv:1208.6449].

[9] S. El-Showk and M. F. Paulos, *Bootstrapping Conformal Field Theories with the Extremal Functional Method*, Phys. Rev. Lett. **111** (2013), no. 24 241601, [arXiv:1211.2810].

[10] S. El-Showk and M. F. Paulos, *Extremal bootstrapping: go with the flow*, JHEP **03** (2018) 148, [arXiv:1605.08087].

[11] K. Sen and A. Sinha, *On critical exponents without Feynman diagrams*, *J. Phys. A* **49** (2016), no. 44 445401, [arXiv:1510.07770].

[12] R. Gopakumar, A. Kaviraj, K. Sen, and A. Sinha, *Conformal Bootstrap in Mellin Space*, *Phys. Rev. Lett.* **118** (2017), no. 8 081601, [arXiv:1609.00572].

[13] R. Gopakumar, A. Kaviraj, K. Sen, and A. Sinha, *A Mellin space approach to the conformal bootstrap*, *JHEP* **05** (2017) 027, [arXiv:1611.08407].

[14] R. Gopakumar and A. Sinha, *On the Polyakov-Mellin bootstrap*, *JHEP* **12** (2018) 040, [arXiv:1809.10975].

[15] D. Mazac and M. F. Paulos, *The analytic functional bootstrap. Part II. Natural bases for the crossing equation*, *JHEP* **02** (2019) 163, [arXiv:1811.10646].

[16] S. Collier, Y. Gobeil, H. Maxfield, and E. Perlmutter, *Quantum Regge Trajectories and the Virasoro Analytic Bootstrap*, *JHEP* **05** (2019) 212, [arXiv:1811.05710].

[17] D. Mazac and M. F. Paulos, *The analytic functional bootstrap. Part I: 1D CFTs and 2D S-matrices*, *JHEP* **02** (2019) 162, [arXiv:1803.10233].

[18] M. F. Paulos, *Analytic functional bootstrap for CFTs in $d > 1$*, *JHEP* **04** (2020) 093, [arXiv:1910.08563].

[19] M. F. Paulos and B. Zan, *A functional approach to the numerical conformal bootstrap*, *JHEP* **09** (2020) 006, [arXiv:1904.03193].

[20] D. Mazáč, L. Rastelli, and X. Zhou, *A Basis of Analytic Functionals for CFTs in General Dimension*, arXiv:1910.12855.

[21] M. F. Paulos, *JuliBootS: a hands-on guide to the conformal bootstrap*, arXiv:1412.4127.

[22] D. Simmons-Duffin, *The Lightcone Bootstrap and the Spectrum of the 3d Ising CFT*, *JHEP* **03** (2017) 086, [arXiv:1612.08471].

[23] M. Reehorst, S. Rychkov, D. Simmons-Duffin, B. Sirois, N. Su, and B. Van Rees, *Navigator Function for the Conformal Bootstrap*, arXiv:2104.09518.

[24] D. Z. Freedman, S. D. Mathur, A. Matusis, and L. Rastelli, *Comments on 4 point functions in the CFT / AdS correspondence*, *Phys. Lett. B* **452** (1999) 61–68, [hep-th/9808006].

[25] E. D'Hoker, S. D. Mathur, A. Matusis, and L. Rastelli, *The Operator product expansion of N=4 SYM and the 4 point functions of supergravity*, *Nucl. Phys. B* **589** (2000) 38–74, [hep-th/9911222].

[26] E. Hijano, P. Kraus, E. Perlmutter, and R. Snively, *Witten Diagrams Revisited: The AdS Geometry of Conformal Blocks*, *JHEP* **01** (2016) 146, [arXiv:1508.00501].

[27] M. F. Paulos, S. Rychkov, B. C. van Rees, and B. Zan, *Conformal Invariance in the Long-Range Ising Model*, *Nucl. Phys. B* **902** (2016) 246–291, [arXiv:1509.00008].

[28] C. Behan, L. Rastelli, S. Rychkov, and B. Zan, *Long-range critical exponents near the short-range crossover*, *Phys. Rev. Lett.* **118** (2017), no. 24 241601, [arXiv:1703.03430].

[29] C. Behan, L. Rastelli, S. Rychkov, and B. Zan, *A scaling theory for the long-range to short-range crossover and an infrared duality*, *J. Phys. A* **50** (2017), no. 35 354002, [arXiv:1703.05325].

[30] C. Behan, *Bootstrapping the long-range Ising model in three dimensions*, *J. Phys. A* **52** (2019), no. 7 075401, [arXiv:1810.07199].

[31] S. Caron-Huot, D. Mazac, L. Rastelli, and D. Simmons-Duffin, *Dispersive CFT Sum Rules*, *JHEP* **05** (2021) 243, [arXiv:2008.04931].

[32] R. Gopakumar, A. Sinha, and A. Zahed, *Crossing Symmetric Dispersion Relations for Mellin Amplitudes*, *Phys. Rev. Lett.* **126** (2021), no. 21 211602, [arXiv:2101.09017].

[33] D. Simmons-Duffin, *A Semidefinite Program Solver for the Conformal Bootstrap*, *JHEP* **06** (2015) 174, [arXiv:1502.02033].

Conclusion and Prospects

This dissertation has thoroughly explored the application of the bootstrap method to matrix models, Yang-Mills theory, and conformal field theory. We have underscored the potency and versatility of the bootstrap method as an optimization-based approach to problem-solving in the contemporary physical landscape, often yielding precise numerical bounds and deep theoretical insights.

We proposed an enhanced relaxation bootstrap method to numerically solve multi-matrix models in the large N limit. We showed that this method offers robust inequalities on the single trace moments of the matrices up to a specified "cutoff" order of the moments. Our demonstration of the method's numerical efficiency is made evident through the successful resolution of the analytically "unsolvable" two-matrix model with $\text{tr}[A, B]^2$ interaction and quartic potentials.

The extension of our study to lattice Yang-Mills theory in dimensions 2, 3, and 4 using the numerical bootstrap method has yielded promising outcomes. The combination of loop equations with a cutoff on the maximal length of loops and positivity conditions on specific matrices of Wilson loop averages has demonstrated that this approach could present a tangible alternative to the predominant Monte Carlo approach.

Our investigation into bounding CFT correlators in the Euclidean section elucidates a remarkable connection between optimization problems and the determination of upper and lower bounds on correlators. Our work suggests that the 3d Ising correlator occupies the minimal possible allowed values on the Euclidean section. We have also unveiled a peculiar 3d CFT that saturates gap, OPE maximization, and correlator value bounds.

In conclusion, this thesis has deepened our understanding of the power and versatility of the bootstrap method in dealing with complex problems in contemporary physics. The results obtained in matrix models, Yang-Mills theory, and conformal field theory demonstrate the considerable promise of this approach, and we anticipate that further exploration will continue to yield valuable insights into the fundamental nature of these systems. The journey of discovery using the bootstrap method is far from complete, and the results of this dissertation provide a strong foundation for future explorations and advancements.

Despite the promising direction, the bootstrap method is still in its early stages and is open to significant improvements. The following improvements are proposed to achieve the ambitious goals outlined:

- The establishment of a general method to bootstrap the long-range/asymptotic behavior

of lattice systems. The existing lattice bootstrap results [Kazakov, 2023; Cho, 2022] primarily focus on the correlators localized in small regions. A comprehensive method to bootstrap long-range behavior of correlators is required, which will encapsulate the information in the IR of the lattice theories.

• Parallelization. The current algorithm, albeit accurate, is essentially sequential. Notably, most algorithm components can be readily parallelized. Employing MPI or CUDA libraries for complete parallelization of the algorithm would markedly enhance computational efficiency.

The bootstrap method studied in this thesis, in its nascent stages, has already demonstrated its capacity to yield highly accurate numerical results with 100% error control. This thesis asserts the high potentiality of the bootstrap method in numerous areas of physics. This document delineates several anticipated applications and goals for this method.

1 Lattice Field Theory

Lattice Quantum Chromodynamics (QCD) is an instrumental framework in comprehending the non-perturbative aspects of QCD. Despite its successes, the standard numerical method for Lattice QCD - the Monte Carlo (MC) method, faces inherent limitations. These include statistical errors, finite lattice size, computational burdens for dynamic quark inclusion, challenges in addressing finite baryon density, and real-time dynamics.

Our recent result [Kazakov, 2023] suggests the bootstrap approach could provide a viable alternative or even pose competition for the MC method. An immediate and significant research direction is to generalize large N bootstrap settings to finite color numbers, with a particular interest in $N_c = 3$. Potential quantities like quark condensation $\langle \bar{\psi}(0)\psi(0) \rangle$ [Cvetic, 1999] are already available for comparison in the pure gauge sector.

We believe another bootstrap candidate is the glueball spectrum [Athenodorou, 2021]. The bootstrap method can offer rigorous results for the asymptotic region, surpassing traditional numerical methods without necessitating extrapolation, as demonstrated in the large N limit [Kazakov, 2022]. We posit that the bootstrap method can also compute glueball masses, which are asymptotic quantities in the large volume limit.

Furthermore, the bootstrap method can be applied to finite temperature lattice QCD, with an aim to establish rigorous bounds on quantities like the Polyakov loop, which could shed light on the confinement phenomenon in QCD.

In addition, there is potential for a bootstrap formulation of the (renormalizable) quantum field theory. While lattice field theory is one of the potential regularizations of UV physics, the bootstrap method's efficiency is closely tied with symmetries. Consequently, lattice regularization, which disrupts the original symmetries of the quantum field theory, may not be optimal. It would be of significant interest to generalize this bootstrap method to alternative regularizations that conserve the original symmetries of quantum field theory.

2 Quantum Systems on the Lattice

For certain problems in condensed matter physics, there is an acute need for reliable numerical tools to understand the model's ground state characterizations and phase diagrams.

Consider the Hubbard model in $d \geq 2$. This model is believed to exhibit fascinating physical phenomena like superconductivity [Arovas, 2021], but its phase diagram remains elusive.

A similar case is the $2d$ quantum Heisenberg model on the kagome lattice. Previous studies suggested that its ground state could be a gapped $\mathbb{Z}_2$ spin liquid [Yan, 2011]. However, recent numerical evidence supports the ground state realization as a gapless $U(1)$ Dirac spin liquid [He, 2017]. An efficient numerical approach with rigorous error control will unquestionably deepen our understanding of these models.

Résumé en Français

1 Contexte

Dans le domaine de la théorie quantique des champs (TQC) moderne, l'importance de la symétrie est indiscutable. Notre compréhension progressive de la TQC a toujours été associée aux connaissances acquises grâce aux symétries, qu'elles soient supposées (comme la symétrie de Poincaré et le pouvoir contraignant des anomalies) ou brisées spontanément.
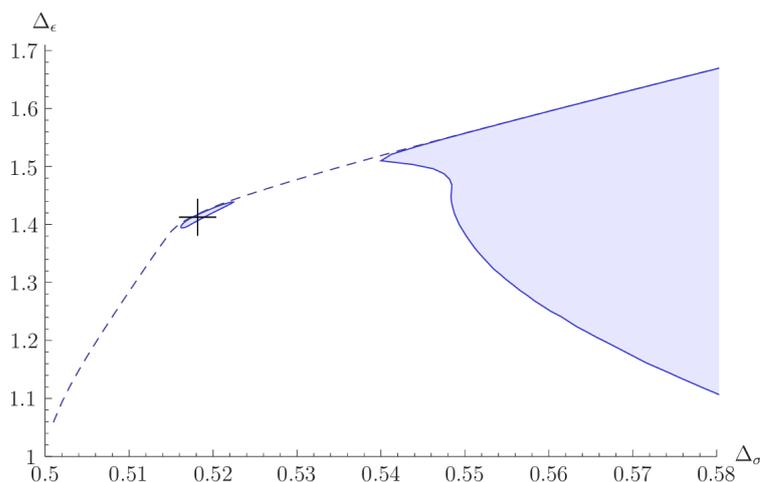

Figure 5.1: La région représentée correspond à l'espace des paramètres autorisé par le modèle Ising en $3d$. Elle est définie par les contraintes de trois corrélateurs à quatre points distincts, en supposant qu'il n'y a qu'un seul opérateur pertinent $\mathbb{Z}_2$-impair présent. Le graphique a été adapté du travail de Kos et al. [Kos, 2014].

La philosophie du bootstrap en physique incarne une méthodologie qui vise à exploiter la puissance potentielle de la symétrie à son maximum. L'approche cherche à résoudre les problèmes principalement en utilisant l'hypothèse de symétrie, avec d'autres contraintes génériques comme l'unitarité et la localité. Cette méthode évite de s'appuyer sur les détails microscopiques du problème en question. Bien que cette perspective ait été initialement proposée dans les années 1960 dans le contexte de la S-matrice [Chew, 1961], elle a été largement éclipsée par les succès ultérieurs en Chromodynamique Quantique (CDQ).

Le premier résultat significatif suivant la philosophie du bootstrap n'a pas vu le jour avant les années 1980, lorsque Belavin, Polyakov et Zamolodchikov (BPZ) ont utilisé le "bootstrap

conforme" pour résoudre des modèles minimaux avec $c < 1$ [Belavin, 1984]. Leur solution reposait fortement sur les symétries infinies présentes dans la théorie des champs conformes en $2d$, une caractéristique absente dans d'autres dimensions.

Le 21ème siècle a connu une augmentation sans précédent du développement de la théorie de l'optimisation mathématique, largement stimulée par l'expansion rapide de l'industrie de l'apprentissage automatique, qui a connu une percée significative en 2006 [Hinton, 2006]. À peu près à la même période, un travail fondateur a émergé, utilisant la théorie de l'optimisation pour limiter la dynamique de la théorie des champs conformes en $4d$ (TCC) [Rattazzi, 2008]. Cette méthode, connue sous le nom de "méthode bootstrap", a suscité un intérêt renouvelé pour l'application de la théorie de l'optimisation pour aborder les problèmes en physique théorique [Ferrara, 1973; Polyakov, 1974]. Malgré sa nature numérique, la méthode bootstrap s'est avérée efficace pour générer des limites rigoureuses pour les quantités dynamiques. L'approche a connu un succès particulièrement remarquable dans le contexte de la TCC [1], démontrant que des résultats numériques très précis peuvent être obtenus uniquement à partir des axiomes de la TCC, de l'unitarité et des symétries globales.

L'invariance conforme et l'expansion du produit d'opérateurs ont conduit à l'équation dite de bootstrap :

$$\sum_{\Delta} a_{\Delta}^2 F_{\Delta}(z, \bar{z}) = 0, \quad (z, \bar{z}) \in (\mathbb{C}\backslash(-\infty, 0) \cup (1, \infty))^2 \tag{5.4}$$

Ici, l'invariance conforme nous aide à déterminer $F_{\Delta}[z, \bar{z}]$ (soit analytiquement soit numériquement), et l'unitarité nous donne la réalité et la région potentielle Δ dans l'Eq. (5.4).

La situation mentionnée représente une généralisation infinie de la programmation linéaire. À partir de cela, nous pouvons obtenir des limites pour des quantités dynamiques intrigantes comme l'écart de dimension au-dessus de l'opérateur d'identité. Par exemple, considérez une fonctionnelle Λ agissant sur F_{Δ}, où $\Lambda(F_{\Delta}) \geq 0$ pour $\Delta \geq \Delta_{\text{gap}}$ et $\Lambda(F_0) > 0$. L'existence d'une telle fonctionnelle, couplée à l'Eq. (5.4), implique qu'il doit y avoir au moins un opérateur dans la région $0 < \Delta < \Delta_{\text{gap}}$. En recherchant Λ sur tous les Δ_{gap} possibles, nous pouvons obtenir une limite optimale pour l'écart de dimension.

De nombreuses études ultérieures utilisant l'approche bootstrap ont produit des résultats convaincants, montrant l'efficacité de cette méthodologie. L'un des réalisations les plus significatives dans cette veine a été la détermination des dimensions d'opérateur dans le modèle Ising Critique 3D avec une précision sans précédent [El-Showk, 2012; El-Showk, 2014; Kos, 2014]. Comme représenté sur la Fig. 5.1, le modèle Ising critique en $3d$, tel que déterminé par le bootstrap conforme, réside dans une minuscule île de l'espace des paramètres.

L'exécution réussie de la méthode bootstrap, illustrée sur la Figure 5.2, témoigne de l'interaction essentielle entre la physique, les mathématiques et l'informatique :

- Sur le front de la physique, une compréhension complète des principes sous-jacents est essentielle pour concevoir des contraintes efficaces. Des exemples notables de ceci incluent l'application de l'expansion du bloc conforme[Dolan, 2004] du corrélateur à quatre points

---

[1] Des revues complètes de ces avancées peuvent être trouvées dans [Poland, 2019; Bissi, 2022]. Voir aussi [Poland, 2022; Hartman, 2022] pour des mises à jour plus récentes.
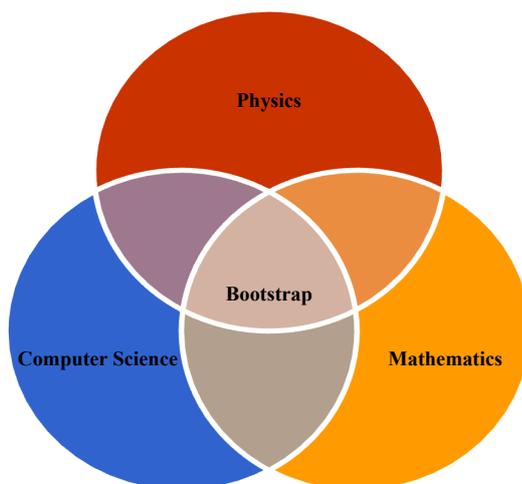
Figure 5.2: La méthode bootstrap.

en théorie des champs conformes, et l'utilisation des équations de boucle de Makeenko-Migdal[Makeenko, 1979] en théorie de jauge comme contraintes non triviales dans les calculs de bootstrap.

- Les mathématiques fournissent l'ensemble d'outils nécessaires pour interpréter et valider les contraintes associées au modèle physique. Par exemple, une solide analyse mathématique est requise pour vérifier la véracité numérique du bootstrap conforme [Pappadopulo, 2012].

- Dans le domaine de l'informatique, des techniques robustes sont essentielles pour la mise en œuvre pratique de la méthode bootstrap. Une maîtrise de la programmation est nécessaire pour le développement de solveurs d'optimisation spécialisés, tels que *SDPB* [Simmons-Duffin, 2015; Reehorst, 2021; Liu, 2023], *JuliBoots* [Paulos, 2014], *PyCFTBoot*[Behan, 2017] et *FunBoot* [Ghosh, 2023b], spécifiquement conçus pour résoudre les problèmes de bootstrap. Il est également à noter que d'importants résultats numériques issus de la méthode bootstrap sont généralement générés à l'aide de ressources de supercalcul [Chester, 2020].

Malgré les avancées impressionnantes dans le bootstrap conforme, l'application de la méthode bootstrap à des systèmes dépourvus de l'avantage de la symétrie conforme reste un problème difficile. Un domaine potentiel d'exploration est le bootstrap de la S-matrice [Homrich, 2019; Kruczenski, 2022; Paulos, 2017a; Paulos, 2017b; Paulos, 2019], où l'auteur s'est lancé dans une enquête préliminaire dans ce domaine pendant ses études de master [Paulos, 2020c]. Cependant, les progrès dans le domaine du bootstrap de la S-matrice ont été largement limités à l'établissement de limites générales sur les paramètres de la théorie. À l'heure actuelle, il n'est pas possible d'intégrer efficacement les informations ou les contraintes dérivées de la théorie ultraviolette (UV) dans le cadre du bootstrap de la S-matrice.

À la lumière des avancées récentes [Anderson, 2017; Lin, 2020; Han, 2020b], une nouvelle approche bootstrap est apparue pour étudier les modèles matriciels. Cette méthode est car-

actérisée non seulement par l'adhésion à des hypothèses générales telles que l'unitarité et les symétries globales, mais aussi par l'intégration des relations entre les observables physiques imposées par les équations du mouvement.[2] Son applicabilité a été rapidement démontrée dans les théories des champs sur réseau [Anderson, 2017; Anderson, 2018; Cho, 2022; Kazakov, 2023], les modèles matriciels [Han, 2020b; Jevicki, 1983; Jevicki, 1984; Koch, 2022; Lin, 2020; Lin, 2023; Mathaba, 2023], les systèmes quantiques[Aikawa, 2022a; Aikawa, 2022b; Bai, 2022; Berenstein, 2021; Berenstein, 2022b; Berenstein, 2023b; Berenstein, 2022a; Berenstein, 2023a; Bhattacharya, 2021; Blacker, 2022; Ding, 2023; Du, 2022; Eisert, 2023; Fawzi, 2023; Han, 2020a; Hastings, 2022b; Hastings, 2022a; Hessam, 2022; Hu, 2022; Khan, 2022; Kull, 2022; Li, 2022; Li, 2023b; Morita, 2023; Nakayama, 2022; Nancarrow, 2022; Tavakoli, 2023; Tchoumakov, 2021; Fan, 2023b; Fan, 2023a; John, 2023; Li, 2023a; Zeng, 2023], et même les systèmes dynamiques classiques [Goluskin, 2018; Goluskin, 2020; Tobasco, 2018; Cho, 2023a].

La première partie de cette thèse discute de notre application de cette nouvelle méthode bootstrap aux modèles matriciels [Kazakov, 2022] et aux théories de jauge de grande N sur réseau [Kazakov, 2023]. Dans notre première publication, nous avons justifié rigoureusement l'approche bootstrap dans le contexte d'un modèle à une matrice et introduit un assouplissement sur les termes quadratiques dans les équations de boucle, atteignant ainsi une précision sans précédent dans un modèle à deux matrices insoluble. Dans notre seconde publication, nous avons étendu l'application de cette méthode bootstrap (avec l'assouplissement pertinent) à la théorie de jauge de grande N sur réseau. De manière remarquable, cette approche a donné d'excellents résultats dans l'estimation (ou plus précisément, la délimitation) de la moyenne des plaquettes de la théorie de jauge sur réseau.

La dernière partie de cette thèse aborde le travail collaboratif de l'auteur avec Miguel Paulos, axé sur la délimitation des fonctions de corrélation via le bootstrap conforme[Paulos, 2022]. Étant donné le comportement exponentiel unique de la fonction cible dans ce problème bootstrap spécifique, l'approximation polynomiale traditionnelle utilisée dans $SDPB$[Simmons-Duffin, 2015] est inadaptée. Nous avons démontré que la solution pour maximiser l'écart sature généralement la minimisation du corrélateur. En même temps, la maximisation du corrélateur, soumise à des contraintes supplémentaires, reproduit efficacement la théorie du champ moyen.

Dans le dernier chapitre de cette thèse, nous consolidons nos découvertes, offrant un résumé concis et les implications de notre travail. De plus, nous suggérons une variété de directions prometteuses pour la recherche et l'exploration futures.

2 Principaux résultats

2.1 Bootstrap matriciel

Une grande partie de mon programme de recherche tourne autour du bootstrap matriciel [Kazakov, 2022]. Cette entreprise comprend deux composants cruciaux : une solide justification de la méthode bootstrap pour le modèle à une matrice en utilisant les résultats du problème du

---

[2]Pour une étude détaillée sur les convergences mathématiques de cette méthode, les lecteurs sont dirigés vers [Guionnet, 2022; Kazakov, 2022; Cho, 2023b].

moment de Hamburger, et une avancée notable de cette méthode pour bootstrapper les modèles matriciels de grande N via relaxation convexe.

Plus précisément, le processus de justification, s'appuyant sur les résultats du problème du moment de Hamburger, affirme rigoureusement que la positivité de la matrice de corrélation implique la positivité du résolvant, et vice versa :

$$\text{Positivité de la matrice de corrélation} \Leftrightarrow \text{Positivité du Résolvant} \tag{5.5}$$

Cette équivalence a été utilisée en conjonction avec les équations de boucle pour catégoriser analytiquement et exhaustivement les solutions du modèle matriciel de grande N spécifié ci-dessous :

$$Z_N = \int d^{N^2} M \, e^{-N\text{tr}V(M)}, \quad V(x) = \frac{1}{2}\mu x^2 + \frac{1}{4}g x^4 \tag{5.6}$$

La seconde moitié de l'article se concentre sur la résolution du modèle suivant :

$$Z = \lim_{N \to \infty} \int d^{N^2} A, d^{N^2} B, e^{-N\text{tr}\left(-h[A,B]^2/2 + A^2/2 + gA^4/4 + B^2/2 + gB^4/4\right)} \tag{5.7}$$

Avec nos méthodologies existantes, ce modèle n'a pas de solution analytique. Pour bootstrapper ce modèle, nous avons utilisé une méthode de relaxation comme suit :

$$Q = xx^{\text{T}} \Rightarrow \mathcal{R} = \begin{pmatrix} 1 & x^{\text{T}} \\ x & Q \end{pmatrix} \succeq 0. \tag{5.8}$$

Dans ce qui précède, Q représente les termes quadratiques dans les équations de boucle, dérivés de la factorisation de grande N. Le vecteur x fait référence au vecteur colonne des variables de trace unique. Les résultats obtenus à partir du problème de bootstrap relaxé surpassent considérablement la précision et l'efficacité de la méthode numérique conventionnelle pour les modèles matriciels de grande N, la méthode Monte Carlo (MC) [Jha, 2022]. Pour $g = h = 1$, nous avons obtenu un résultat de précision à 6 chiffres :

$$\begin{cases} 0.421783612 \leq t_2 \leq 0.421784687 \\ 0.333341358 \leq t_4 \leq 0.333342131 \end{cases} \tag{5.9}$$

L'illustration de la contraction du domaine admissible en fonction du cutoff bootstrap correspondant est visuellement démontrée dans la Figure 5.3.

2.2 Bootstrap de la théorie de Yang-Mills sur réseau

Un autre projet [Kazakov, 2023] a consisté à utiliser cette méthode pour bootstrap la boucle de Wilson à une plaquette moyenne dans la théorie Yang-Mills sur réseau de grande N.[3] Les

---

[3] Pour d'autres études de bootstrap de la théorie de jauge ou QCD, le lecteur peut se référer à [Nakayama, 2015; Albert, 2022; Albert, 2023; Fernandez, 2023; Guerrieri, 2019; He, 2023; Caron-Huot, 2023b; Ma, 2023]. Il est largement admis que le Yang-Mills de grande N est équivalent au QCD de grande N en raison de la suppression de la composante fermionique à la limite planaire. Cependant, des preuves récentes suggèrent que cette hypothèse pourrait être plus nuancée [Cherman, 2023].
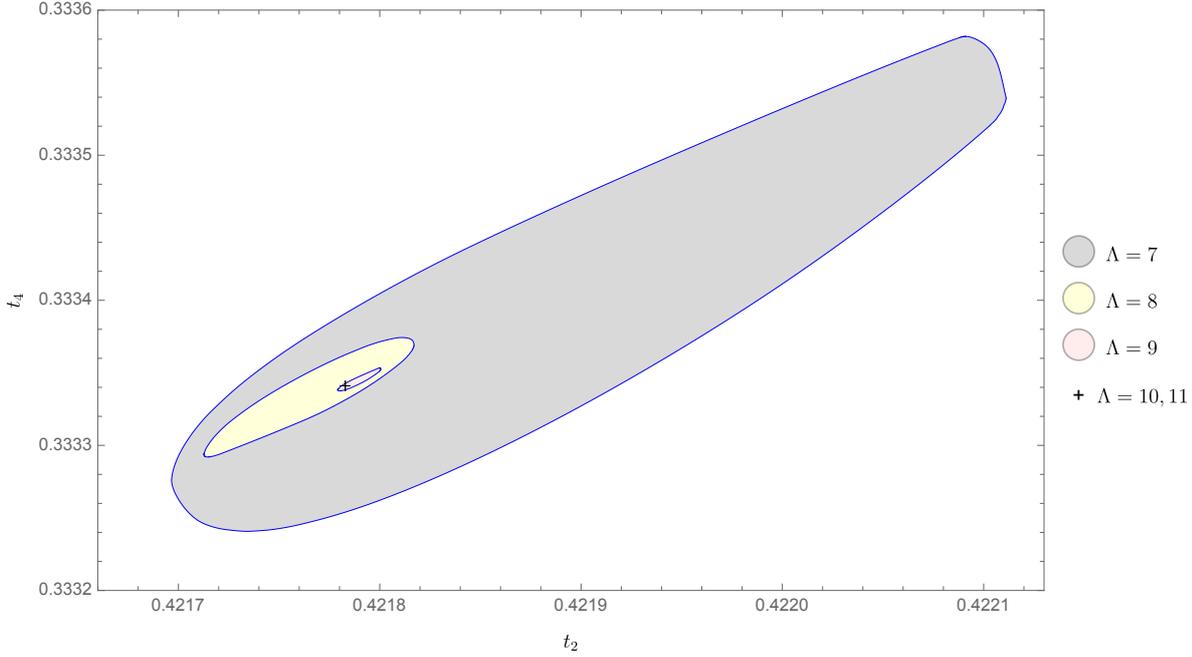
Figure 5.3: La région autorisée de $t_2 - t_4$ du modèle (5.7) avec le paramètre $g = 1, h = 1$ pour le cutoff $\Lambda = 7, 8, 9, 10, 11$. Nous rappelons la définition de Λ : les opérateurs les plus longs dans la matrice de corrélation et dans les équations de boucle ont la longueur 2Λ.

résultats sont encourageants par rapport à la méthode MC, surtout si l'on considère que la méthode MC pour le QCD sur réseau a fait l'objet d'intenses recherches pendant plusieurs décennies.

Nous analysons la Théorie de la Grande Jauge basée sur l'action de Wilson (LGT) [Wilson, 1974] représentée par $S = -\frac{N_c}{\lambda} \sum_P \operatorname{Re} \operatorname{tr} U_P$, avec U_P désignant le produit de quatre variables de lien unitaires autour de la plaquette P. En considérant la limite 't Hooft ($N_c \to \infty$), l'accent principal est mis sur les Moyennes de Boucle de Wilson (WAs) : $W[C] = \langle \frac{\operatorname{tr}}{N_c} \prod_{l \in C} U_l \rangle$, où le produit matriciel traverse les variables de lien à l'intérieur de la boucle de réseau C. Les WAs adhèrent aux Équations de Boucle Makeenko-Migdal (LEs)[Makeenko, 1979], ou équations Schwinger-Dyson, qui englobent l'invariance de mesure par rapport aux décalages de groupe, de sorte que $U_l \to U_l(1 + i\epsilon)$.[4] Les LEs sont représentées schématiquement :

$$\sum_{\nu \perp \mu} \left(W[C_{l_\mu} \cdot \overrightarrow{\delta C_{l_\mu}^\nu}] - W[C_{l_\mu} \cdot \overleftarrow{\delta C_{l_\mu}^\nu}] \right) = \lambda \sum_{\substack{l' \in C \\ l' \sim l}} \epsilon_{ll'} W[C_{ll'}] \, W[C_{l'l}] \tag{5.10}$$

avec le LHS indiquant l'action de l'opérateur de boucle sur le lien l_μ, et le RHS signifiant la division du contour $C \to C_{ll'} \cdot C_{l'l}$, comme le montre la Figure 5.4.

Dans la plupart des cas, le système d'équations de boucle (5.10) donne plus de variables de boucle que d'équations de boucle indépendantes. Comme le suggèrent Anderson et al. [Anderson, 2017], la positivité de $\langle \mathcal{O}^\dagger \mathcal{O} \rangle$ peut être utilisée pour contraindre les quantités dynamiques

---

[4]L'avancement récent implique l'utilisation des équations de boucle pour traiter les problèmes de turbulence.[Migdal, 2023a; Migdal, 2023b]
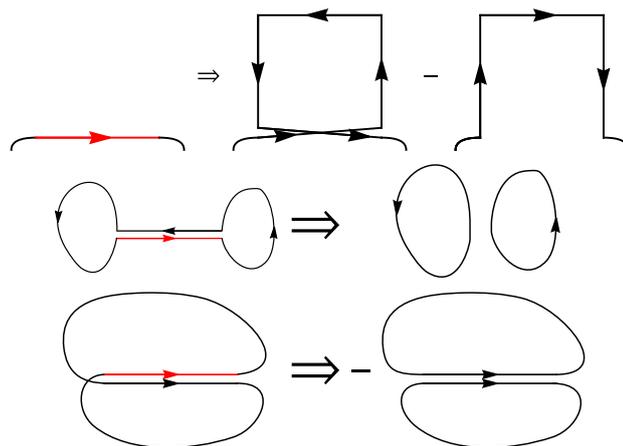
Figure 5.4: Représentation schématique des LEs : La première ligne montre la variation d'un lien de boucle de Wilson dans le LHS de l'Eq.(5.10). Les 2ème et 3ème lignes montrent la division du contour le long de la ligne variée en deux sous-contours, pour deux orientations différentes des liens coïncidant dans le RHS de l'Eq.(5.10).

pertinentes. Nous avons considérablement avancé cette méthode en intégrant les améliorations suivantes :

1. Nous prenons en compte les équations de boucle Back-track, qui seront discutées plus en détail ultérieurement.

2. La positivité de la réflexion du système de réseau est considérée.

3. La symétrie de réseau est utilisée pour réduire les conditions de positivité.

4. Nous employons la méthode de relaxation de grande N proposée par les résultats précédents [Kazakov, 2022].

Ces améliorations nous ont permis de dériver une limite numérique impressionnante sur la moyenne d'une plaquette $u_P = \frac{1}{N_c}\langle \mathrm{tr} U_P \rangle$. Comme le montre la Fig. 5.5, les limites de bootstrap pour u_P pour $L_{\max} = 8, 12, 16$ montrent un raffinement rapide à mesure que les coupures augmentent. La limite supérieure encapsule efficacement la phase de boucle de Wilson physiquement significative et reproduit de manière fiable la Théorie de Perturbation à 3 boucles sur une vaste plage de couplage, dépassant même le point de transition de phase. Une comparaison avec les données de Monte Carlo, cependant, indique une marge d'amélioration, notamment dans l'intervalle (2.4, 2.8) où les données divergent de la Théorie de Perturbation. Cet intervalle, provenant de [Athenodorou, 2021], a été utilisé pour calculer les masses et la tension de la corde. Une amélioration notable est attendue en atteignant $L_{\max} = 20$ ou 24, bien que cela nécessitera d'importantes ressources informatiques.

2.3 Bootstrap conforme

Les recherches académiques de l'auteur pendant sa thèse de doctorat se sont également étendues au bootstrap conforme.
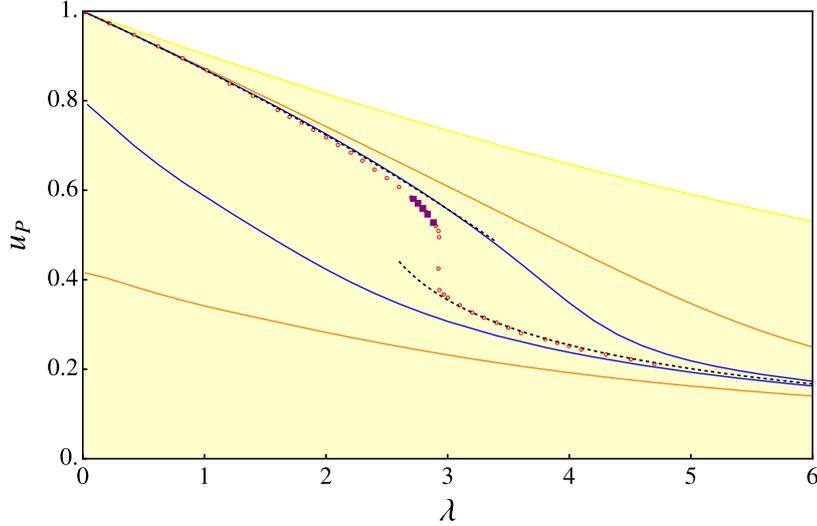
Figure 5.5: La figure présente nos résultats de bootstrap pour les limites supérieures et inférieures de la moyenne de plaquette en $4D$ LGT. Les domaines pour $L_{\max} = 8, 12, 16$ sont respectivement représentés en jaune, orange et bleu. Les cercles rouges représentent les données de Monte Carlo (MC) pour $SU(10)$ LGT, avec 5 carrés violets indiquant les résultats pour $SU(12)$. Les lignes en pointillés supérieure et inférieure signifient respectivement la théorie de perturbation à 3 boucles [Alles, 1998] et l'expansion de couplage fort [Drouffe, 1983].

Des études récentes ont souligné les contraintes strictes que les données CFT, définissant les corrélateurs d'opérateurs locaux, doivent respecter [Poland, 2019]. Ces restrictions ne se limitent pas à encadrer l'espace théorique CFT, mais positionnent également de manière intrigante des théories saillantes à la lisière du domaine autorisé [El-Showk, 2012]. La communauté du bootstrap conforme a jusqu'à présent enquêté sur cet espace, explorant principalement deux directions de contraintes sur un ensemble spécifique de corrélateurs à quatre points. Premièrement, nous maximisons l'écart dans les dimensions d'échelle du premier opérateur dans l'Expansion du Produit d'Opérateur (OPE) [Rattazzi, 2008]. Deuxièmement, nous limitons le coefficient OPE d'opérateurs spécifiques au sein de ces corrélateurs [Rattazzi, 2011]. Ces limites sont établies à l'aide de fonctionnels numériques ou analytiques, offrant des perspectives doubles sur le paysage CFT. Ce travail a proposé de nouvelles directions en limitant les valeurs des corrélateurs CFT, un problème naturel mais inexploré. Cette approche, similaire à la méthode de minimisation ou de maximisation des valeurs de la matrice S, devrait révéler des territoires inconnus dans l'espace CFT. Le problème de la matrice S, connu pour produire des limites saturables par des théories passionnantes, est étroitement lié aux corrélateurs CFT (ou à leurs limites) [Paulos, 2017b], suggérant un potentiel équivalent pour le problème CFT correspondant.

Nos résultats numériques, illustrés dans la Figure 5.6, montrent la plage autorisée du corrélateur à quatre points au point de symétrie de croisement $z = \bar{z} = \frac{1}{2}$ en fonction de Δ_ϕ, et les limites le long de $z = \bar{z}$ pour différentes valeurs de Δ_ϕ.

La Figure 5.6 révèle une limite supérieure du corrélateur pour certaines gammes de Δ_ϕ, indépendamment des hypothèses de spectre. Imposer des écarts dans le secteur scalaire affine cette limite, le corrélateur de bosons libres généralisés se rapprochant étroitement de la limite
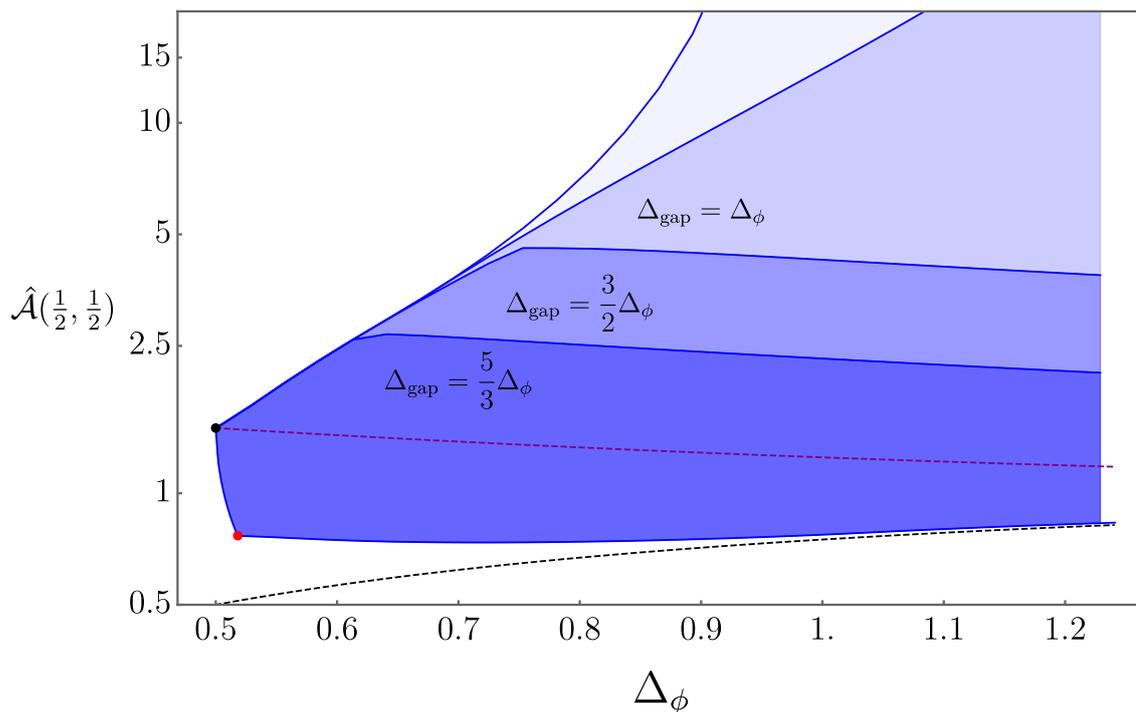
Figure 5.6: Limites sur les valeurs des corrélateurs CFT 3d, avec $\hat{\mathcal{A}}(z, \bar{z}) = (z\bar{z})^{\Delta_\phi} \mathcal{G}(z, \bar{z}) - 1$. La région ombragée représente les valeurs qu'un tel corrélateur peut prendre au point symétrique de croisement $z = \bar{z} = \frac{1}{2}$. Les lignes en pointillés à l'intérieur de la région autorisée correspondent aux valeurs maximales autorisées en supposant un écart. La limite supérieure tend vers ∞ près de $\Delta_\phi = 1$. La ligne en pointillés à l'extérieur de la région autorisée est le corrélateur de fermions libres généralisés 1d, qui fournit une limite inférieure (non optimale). La ligne en pointillés à l'intérieur de la région autorisée est le corrélateur de bosons libres généralisés, qui fournit une limite supérieure pour $\Delta_{\text{gap}} = 2\Delta_\phi$. Les points noirs et rouges sont respectivement les valeurs de la théorie libre et du modèle d'Ising 3d.

supérieure pour un écart de $2\Delta_\phi$, en accord avec la limite exacte dans [Paulos, 2021][5]. Pour $\Delta_\phi = 1$, la limite diverge en raison de la solution de l'équation de croisement unitaire dépourvue d'identité pour $\Delta_\phi \geq d - 2$. Cela conduit à l'absence de limite sans une hypothèse d'écart de spectre, nécessitant l'écart $\Delta_g > \Delta_\phi / 2$.

À $\Delta_\phi = 1/2$, le point de théorie libre, les limites supérieure et inférieure convergent avec la valeur de la théorie libre, comme on pouvait s'y attendre pour le seul corrélateur CFT avec cette dimension. La limite inférieure est également congruente avec la limite exacte déterminée par la solution de fermion libre généralisé 1d, bien que plus forte en raison des contraintes de l'équation de croisement 3d.

La limite inférieure affiche une cassure prononcée à $\Delta_\phi \sim 0.518149$, la dimension du champ de spin dans le CFT d'Ising 3d. Cela renforce notre argument reliant la minimisation du corrélateur

---

[5]L'argument s'appuie sur le fonctionnel analytique, une construction théorique spécifique en théorie des champs conformes avec une base historique étendue [Afkhami-Jeddi, 2020; Carmi, 2020; Caron-Huot, 2021; Caron-Huot, 2023a; Dey, 2017; Dey, 2018; El-Showk, 2013; El-Showk, 2018; Ferrero, 2020; Ghosh, 2021; Ghosh, 2023a; Ghosh, 2023b; Giombi, 2020; Gopakumar, 2017a; Gopakumar, 2017b; Gopakumar, 2021; Hartman, 2019; Hartman, 2022; Kaviraj, 2020; Kaviraj, 2022; Li, 2023c; Mazac, 2017; Mazáč, 2019; Mazac, 2019a; Mazac, 2019b; Mazáč, 2021; Paulos, 2020b; Paulos, 2020a; Paulos, 2021; Qiao, 2017; Trinh, 2022].

à la maximisation de l'écart, car ce dernier conduit au modèle d'Ising 3d à la valeur précise de Δ_ϕ :

$$\Delta_g^{\min} \sim \Delta_{\mathrm{gapmax}} \tag{5.11}$$

Reference

[t Hooft, 1974]   Gerard 't Hooft. "A Planar Diagram Theory for Strong Interactions". *Nucl. Phys. B* 72 (1974). Ed. by J. C. Taylor, p. 461 (cit. on p. 10).

[Afkhami-Jeddi, 2020]   Nima Afkhami-Jeddi, Henry Cohn, Thomas Hartman, David de Laat, and Amirhossein Tajdini. "High-Dimensional Sphere Packing and the Modular Bootstrap". *JHEP* 12 (2020), p. 066. arXiv: `2006.02560 [hep-th]` (cit. on pp. 9, 135).

[Aikawa, 2022a]   Yu Aikawa, Takeshi Morita, and Kota Yoshimura. "Application of Bootstrap to a \ensuremath-þeta Term". *Phys. Rev. D* 105.8 (2022), p. 085017. arXiv: `2109.02701 [hep-th]` (cit. on pp. 4, 130).

[Aikawa, 2022b]   Yu Aikawa, Takeshi Morita, and Kota Yoshimura. "Bootstrap Method in Harmonic Oscillator". *Phys. Lett. B* 833 (2022), p. 137305. arXiv: `2109.08033 [hep-th]` (cit. on pp. 4, 130).

[Albert, 2022]   Jan Albert and Leonardo Rastelli. "Bootstrapping Pions at Large N". *JHEP* 08 (2022), p. 151. arXiv: `2203.11950 [hep-th]` (cit. on pp. 6, 131).

[Albert, 2023]   Jan Albert and Leonardo Rastelli. "Bootstrapping Pions at Large N. Part II: Background Gauge Fields and the Chiral Anomaly". *arXiv:2307.01246 [hep-th]* (2023). arXiv: `2307.01246 [hep-th]` (cit. on pp. 6, 131).

[Alles, 1998]   B. Alles, A. Feo, and H. Panagopoulos. "Asymptotic scaling corrections in QCD with Wilson fermions from the three loop average plaquette". *Phys. Lett. B* 426 (1998), pp. 361–366. arXiv: `hep-lat/9801003` (cit. on pp. 7, 134).

[Anderson, 2018]   Peter Anderson and Martin Kruczenski. "Loop Equation in Lattice Gauge Theories and Bootstrap Methods". *EPJ Web Conf.* 175 (2018). Ed. by M. Della Morte, P. Fritzsch, E. Gámiz Sánchez, and C. Pena Ruano, p. 11011 (cit. on pp. 4, 130).

[Anderson, 2017]   Peter D. Anderson and Martin Kruczenski. "Loop Equations and bootstrap methods in the lattice". *Nucl. Phys. B* 921 (2017), pp. 702–726. arXiv: `1612.08140 [hep-th]` (cit. on pp. 3, 4, 7, 129, 130, 132).

[Arovas, 2021]   Daniel P. Arovas, Erez Berg, Steven Kivelson, and Srinivas Raghu. "The Hubbard Model". *arXiv e-prints*, arXiv:2103.12097 (2021), arXiv:2103.12097. arXiv: `2103.12097 [cond-mat.str-el]` (cit. on p. 126).

[Athenodorou, 2021]   Andreas Athenodorou and Michael Teper. "SU(N) gauge theories in 3+1 dimensions: glueball spectrum, string tensions and topology". *JHEP* 12 (2021), p. 082. arXiv: `2106.00364 [hep-lat]` (cit. on pp. 7, 125, 133).

[Bai, 2022]   Dong Bai. "Bootstrapping the Deuteron". *arXiv:2201.00551 [nucl-th]* (2022). arXiv: `2201.00551 [nucl-th]` (cit. on pp. 4, 130).

[Behan, 2017]   Connor Behan. "PyCFTBoot: A flexible interface for the conformal bootstrap". *Commun. Comput. Phys.* 22.1 (2017), pp. 1–38. arXiv: `1602.02810 [hep-th]` (cit. on pp. 3, 129).

[Belavin, 1984]   AA Belavin, AM Polyakov, and AB Zamolodchikov. "Infinite conformal symmetry in two-dimensional quantum field theory". *Nuclear Physics B* 241 (1984), pp. 333–380 (cit. on pp. 2, 128).

[Berenstein, 2021]   David Berenstein and George Hulsey. "Bootstrapping Simple QM Systems". *arXiv:2108.08757 [hep-th]* (2021). arXiv: `2108.08757 [hep-th]` (cit. on pp. 4, 130).

[Berenstein, 2022a]   David Berenstein and George Hulsey. "Anomalous Bootstrap on the Half-Line". *Phys. Rev. D* 106.4 (2022), p. 045029. arXiv: `2206.01765 [hep-th]` (cit. on pp. 4, 130).

[Berenstein, 2022b]   David Berenstein and George Hulsey. "Bootstrapping More QM Systems". *J. Phys. A* 55.27 (2022), p. 275304. arXiv: `2109.06251 [hep-th]` (cit. on pp. 4, 130).

[Berenstein, 2023a] David Berenstein and George Hulsey. "One-Dimensional Reflection in the Quantum Mechanical Bootstrap". *arXiv:2307.11724 [hep-th]* (2023). arXiv: 2307.11724 [hep-th] (cit. on pp. 4, 130).

[Berenstein, 2023b] David Berenstein and George Hulsey. "Semidefinite Programming Algorithm for the Quantum Mechanical Bootstrap". *Phys. Rev. E* 107.5 (2023), p. L053301. arXiv: 2209.14332 [hep-th] (cit. on pp. 4, 130).

[Bhanot, 1982] Gyan Bhanot, Urs M. Heller, and Herbert Neuberger. "The Quenched Eguchi-Kawai Model". *Phys. Lett. B* 113 (1982), pp. 47–50 (cit. on p. 12).

[Bhattacharya, 2021] Jyotirmoy Bhattacharya, Diptarka Das, Sayan Kumar Das, Ankit Kumar Jha, and Moulindu Kundu. "Numerical Bootstrap in Quantum Mechanics". *Phys. Lett. B* 823 (2021), p. 136785. arXiv: 2108.11416 [hep-th] (cit. on pp. 4, 130).

[Bissi, 2022] Agnese Bissi, Aninda Sinha, and Xinan Zhou. "Selected topics in analytic conformal bootstrap: A guided journey". *Phys. Rept.* 991 (2022), pp. 1–89. arXiv: 2202.08475 [hep-th] (cit. on pp. 2, 128).

[Blacker, 2022] Matthew J. Blacker, Arpan Bhattacharyya, and Aritra Banerjee. "Bootstrapping the Kronig-Penney Model". *Phys. Rev. D* 106.11 (2022), p. 116008. arXiv: 2209.09919 [quant-ph] (cit. on pp. 4, 130).

[Bohigas, 1984] O. Bohigas, M. J. Giannoni, and C. Schmit. "Characterization of Chaotic Quantum Spectra and Universality of Level Fluctuation Laws". *Phys. Rev. Lett.* 52 (1 1984), pp. 1–4 (cit. on p. 10).

[Brezin, 1978] E. Brezin, C. Itzykson, G. Parisi, and J. B. Zuber. "Planar Diagrams". *Commun. Math. Phys.* 59 (1978), p. 35 (cit. on p. 11).

[Cao, 2023] Sky Cao, Minjae Park, and Scott Sheffield. "Random surfaces and lattice Yang-Mills" (2023). arXiv: 2307.06790 [math.PR] (cit. on p. 12).

[Carmi, 2020] Dean Carmi and Simon Caron-Huot. "A Conformal Dispersion Relation: Correlations from Absorption". *JHEP* 09 (2020), p. 009. arXiv: 1910.12123 [hep-th] (cit. on pp. 9, 135).

[Caron-Huot, 2023a] Simon Caron-Huot, Frank Coronado, Anh-Khoi Trinh, and Zahra Zahraee. "Bootstrapping \mathcalN = 4 sYM Correlators Using Integrability". *JHEP* 02 (2023), p. 083. arXiv: 2207.01615 [hep-th] (cit. on pp. 9, 135).

[Caron-Huot, 2021] Simon Caron-Huot, Dalimil Mazac, Leonardo Rastelli, and David Simmons-Duffin. "Dispersive CFT Sum Rules". *JHEP* 05 (2021), p. 243. arXiv: 2008.04931 [hep-th] (cit. on pp. 9, 135).

[Caron-Huot, 2023b] Simon Caron-Huot, Andrzej Pokraka, and Zahra Zahraee. "Two-point sum-rules in three-dimensional Yang-Mills theory" (2023). arXiv: 2309.04472 [hep-th] (cit. on pp. 6, 131).

[Cherman, 2023] Aleksey Cherman, Theodore Jacobson, and Maria Neuzil. "1-form symmetry versus large N QCD". *JHEP* 02 (2023), p. 192. arXiv: 2209.00027 [hep-th] (cit. on pp. 6, 131).

[Chester, 2020] Shai M. Chester, Walter Landry, Junyu Liu, David Poland, David Simmons-Duffin, Ning Su, et al. "Carving out OPE space and precise $O(2)$ model critical exponents". *JHEP* 06 (2020), p. 142. arXiv: 1912.03324 [hep-th] (cit. on pp. 3, 129).

[Chew, 1961] Geoffrey Foucar Chew. *S-matrix theory of strong interactions: lecture note*. Frontiers in Physics. New York, NY: Benjamin, 1961 (cit. on pp. 1, 127).

[Cho, 2023a] Minjae Cho. "Bootstrapping the Stochastic Resonance" (2023). arXiv: 2309.06464 [math.DS] (cit. on pp. 4, 130).

[Cho, 2022] Minjae Cho, Barak Gabai, Ying-Hsuan Lin, Victor A. Rodriguez, Joshua Sandor, and Xi Yin. "Bootstrapping the Ising Model on the Lattice" (2022). arXiv: 2206.12538 [hep-th] (cit. on pp. 4, 125, 130).

[Cho, 2023b] Minjae Cho and Xin Sun. "Bootstrap, Markov Chain Monte Carlo, and LP/SDP Hierarchy for the Lattice Ising Model" (2023). arXiv: 2309.01016 [hep-th] (cit. on pp. 4, 130).

[Creutz, 1980] M. Creutz. "Monte Carlo Study of Quantized SU(2) Gauge Theory". *Phys. Rev. D* 21 (1980), pp. 2308–2315 (cit. on p. 12).

[Cvetic, 1999] G. Cvetic. "Top quark condensation". *Rev. Mod. Phys.* 71 (1999), pp. 513–574. arXiv: hep-ph/9702381 (cit. on p. 125).

[David, 1985] F. David. "Planar Diagrams, Two-Dimensional Lattice Gravity and Surface Models". *Nucl. Phys. B* 257 (1985). Ed. by E. Brezin and S. R. Wadia, p. 45 (cit. on p. 10).

[Dey, 2018] Parijat Dey, Kausik Ghosh, and Aninda Sinha. "Simplifying Large Spin Bootstrap in Mellin Space". *JHEP* 01 (2018), p. 152. arXiv: 1709.06110 [hep-th] (cit. on pp. 9, 135).

[Dey, 2017] Parijat Dey, Apratim Kaviraj, and Aninda Sinha. "Mellin Space Bootstrap for Global Symmetry". *JHEP* 07 (2017), p. 019. arXiv: 1612.05032 [hep-th] (cit. on pp. 9, 135).

[Dijkgraaf, 2003]   Robbert Dijkgraaf, Sergei Gukov, Vladimir A. Kazakov, and Cumrun Vafa. "Perturbative analysis of gauged matrix models". *Phys. Rev. D* 68 (2003), p. 045007. arXiv: `hep-th/0210238` (cit. on p. 10).

[Dijkgraaf, 2002]   Robbert Dijkgraaf and Cumrun Vafa. "Matrix models, topological strings, and supersymmetric gauge theories". *Nucl. Phys. B* 644 (2002), pp. 3–20. arXiv: `hep-th/0206255` (cit. on p. 10).

[Ding, 2023]   Wenxin Ding. "Variational Equations-of-States for Interacting Quantum Hamiltonians". *arXiv:2307.00812 [cond-mat.str-el]* (2023). arXiv: `2307.00812 [cond-mat.str-el]` (cit. on pp. 4, 130).

[Dolan, 2004]   F. A. Dolan and H. Osborn. "Conformal partial waves and the operator product expansion". *Nucl. Phys. B* 678 (2004), pp. 491–507. arXiv: `hep-th/0309180` (cit. on pp. 2, 128).

[Drouffe, 1983]   Jean-Michel Drouffe and Jean-Bernard Zuber. "Strong Coupling and Mean Field Methods in Lattice Gauge Theories". *Phys. Rept.* 102 (1983), p. 1 (cit. on pp. 7, 134).

[Du, 2022]   Bao-ning Du, Min-xin Huang, and Pei-xuan Zeng. "Bootstrapping Calabi–Yau Quantum Mechanics". *Commun. Theor. Phys.* 74.9 (2022), p. 095801. arXiv: `2111.08442 [hep-th]` (cit. on pp. 4, 130).

[Eguchi, 1982]   Tohru Eguchi and Hikaru Kawai. "Reduction of Dynamical Degrees of Freedom in the Large N Gauge Theory". *Phys. Rev. Lett.* 48 (1982), p. 1063 (cit. on p. 12).

[Eisert, 2023]   J. Eisert. "A Note on Lower Bounds to Variational Problems with Guarantees". *arXiv:2301.06142 [quant-ph]* (2023). arXiv: `2301.06142 [quant-ph]` (cit. on pp. 4, 130).

[Erramilli, 2019]   Rajeev S. Erramilli, Luca V. Iliesiu, and Petr Kravchuk. "Recursion relation for general 3d blocks". *JHEP* 12 (2019), p. 116. arXiv: `1907.11247 [hep-th]` (cit. on p. 87).

[Erramilli, 2021]   Rajeev S. Erramilli, Luca V. Iliesiu, Petr Kravchuk, Walter Landry, David Poland, and David Simmons-Duffin. "blocks_3d: software for general 3d conformal blocks". *JHEP* 11 (2021), p. 006. arXiv: `2011.01959 [hep-th]` (cit. on p. 87).

[Eynard, 2007]   Bertrand Eynard and Nicolas Orantin. "Invariants of algebraic curves and topological expansion". *Commun. Num. Theor. Phys.* 1 (2007), pp. 347–452. arXiv: `math-ph/0702045` (cit. on p. 10).

[Fan, 2023a]   Wei Fan and Huipen Zhang. "A non-perturbative formula unifying double-wells and anharmonic oscillators under the numerical bootstrap approach" (2023). arXiv: `2309.09269 [quant-ph]` (cit. on pp. 4, 130).

[Fan, 2023b]   Wei Fan and Huipeng Zhang. "Non-perturbative instanton effects in the quartic and the sextic double-well potential by the numerical bootstrap approach" (2023). arXiv: `2308.11516 [hep-th]` (cit. on pp. 4, 130).

[Fawzi, 2023]   Hamza Fawzi, Omar Fawzi, and Samuel O. Scalet. "Entropy Constraints for Ground Energy Optimization". *arXiv:2305.06855 [quant-ph]* (2023). arXiv: `2305.06855 [quant-ph]` (cit. on pp. 4, 130).

[Fernandez, 2023]   Clara Fernandez, Alex Pomarol, Francesco Riva, and Francesco Sciotti. "Cornering Large-N_c QCD with Positivity Bounds". *JHEP* 06 (2023), p. 094. arXiv: `2211.12488 [hep-th]` (cit. on pp. 6, 131).

[Ferrara, 1973]   S. Ferrara, A. F. Grillo, and R. Gatto. "Tensor representations of conformal algebra and conformally covariant operator product expansion". *Annals Phys.* 76 (1973), pp. 161–188 (cit. on pp. 2, 87, 128).

[Ferrero, 2020]   Pietro Ferrero, Kausik Ghosh, Aninda Sinha, and Ahmadullah Zahed. "Crossing Symmetry, Transcendentality and the Regge Behaviour of 1d CFTs". *JHEP* 07 (2020), p. 170. arXiv: `1911.12388 [hep-th]` (cit. on pp. 9, 135).

[Ghosh, 2021]   Kausik Ghosh, Apratim Kaviraj, and Miguel F. Paulos. "Charging up the Functional Bootstrap". *JHEP* 10 (2021), p. 116. arXiv: `2107.00041 [hep-th]` (cit. on pp. 9, 135).

[Ghosh, 2023a]   Kausik Ghosh, Apratim Kaviraj, and Miguel F. Paulos. "Polyakov Blocks for the 1D CFT Mixed Correlator Bootstrap". *arXiv:2307.01257 [hep-th]* (2023). arXiv: `2307.01257 [hep-th]` (cit. on pp. 9, 135).

[Ghosh, 2023b]   Kausik Ghosh and Zechuan Zheng. "Numerical Conformal bootstrap with Analytic Functionals and Outer Approximation" (2023). arXiv: `2307.11144 [hep-th]` (cit. on pp. 3, 9, 129, 135).

[Giombi, 2020]   Simone Giombi, Himanshu Khanchandani, and Xinan Zhou. "Aspects of CFTs on Real Projective Space". *J. Phys. A* 54.2 (2020), p. 024003. arXiv: `2009.03290 [hep-th]` (cit. on pp. 9, 135).

[Goluskin, 2018]   David Goluskin. "Bounding Averages Rigorously Using Semidefinite Programming: Mean Moments of the Lorenz System". *J Nonlinear Sci* 28.2 (2018), pp. 621–651. arXiv: `1610.05335 [nlin]` (cit. on pp. 4, 130).

[Goluskin, 2020]   David Goluskin. "Bounding Extrema over Global Attractors Using Polynomial Optimisation". *Nonlinearity* 33.9 (2020), pp. 4878–4899. arXiv: `1807.09814 [nlin]` (cit. on pp. 4, 130).

[Gonzalez-Arroyo, 2010]   Antonio Gonzalez-Arroyo and Masanori Okawa. "Large N Reduction with the Twisted Eguchi-Kawai Model". *JHEP* 07 (2010), p. 043. arXiv: `1005.1981 [hep-th]` (cit. on p. 12).

[Gopakumar, 1995]   Rajesh Gopakumar and David J. Gross. "Mastering the master field". *Nucl. Phys. B* 451 (1995), pp. 379–415. arXiv: `hep-th/9411021` (cit. on p. 12).

[Gopakumar, 2017a]   Rajesh Gopakumar, Apratim Kaviraj, Kallol Sen, and Aninda Sinha. "A Mellin Space Approach to the Conformal Bootstrap". *JHEP* 05 (2017), p. 027. arXiv: `1611.08407 [hep-th]` (cit. on pp. 9, 135).

[Gopakumar, 2017b]   Rajesh Gopakumar, Apratim Kaviraj, Kallol Sen, and Aninda Sinha. "Conformal Bootstrap in Mellin Space". *Phys. Rev. Lett.* 118.8 (2017), p. 081601. arXiv: `1609.00572 [hep-th]` (cit. on pp. 9, 135).

[Gopakumar, 2021]   Rajesh Gopakumar, Aninda Sinha, and Ahmadullah Zahed. "Crossing Symmetric Dispersion Relations for Mellin Amplitudes". *Phys. Rev. Lett.* 126.21 (2021), p. 211602. arXiv: `2101.09017 [hep-th]` (cit. on pp. 9, 135).

[Guerrieri, 2019]   Andrea L. Guerrieri, Joao Penedones, and Pedro Vieira. "Bootstrapping QCD Using Pion Scattering Amplitudes". *Phys. Rev. Lett.* 122.24 (2019), p. 241604. arXiv: `1810.12849 [hep-th]` (cit. on pp. 6, 131).

[Guionnet, 2022]   Alice Guionnet and Édouard Maurel-Segala. "Matrix models at low temperature". *arXiv e-prints*, arXiv:2210.05239 (2022), arXiv:2210.05239. arXiv: `2210.05239 [math.PR]` (cit. on pp. 3, 130).

[Han, 2020a]   Xizhi Han. *Quantum Many-body Bootstrap*. 2020. arXiv: `2006.06002 [cond-mat]` (cit. on pp. 4, 130).

[Han, 2020b]   Xizhi Han, Sean A. Hartnoll, and Jorrit Kruthoff. "Bootstrapping Matrix Quantum Mechanics". *Phys. Rev. Lett.* 125.4 (2020), p. 041601. arXiv: `2004.10212 [hep-th]` (cit. on pp. 3, 4, 129, 130).

[Hartman, 2022]   Thomas Hartman, Dalimil Mazac, David Simmons-Duffin, and Alexander Zhiboedov. "Snowmass White Paper: The Analytic Conformal Bootstrap". *Snowmass 2021*. 2022. arXiv: `2202.11012 [hep-th]` (cit. on pp. 2, 9, 128, 135).

[Hartman, 2019]   Thomas Hartman, Dalimil Mazáč, and Leonardo Rastelli. "Sphere Packing and Quantum Gravity". *JHEP* 12 (2019), p. 048. arXiv: `1905.01319 [hep-th]` (cit. on pp. 9, 135).

[Hastings, 2022a]   Matthew B. Hastings. "Perturbation Theory and the Sum of Squares". *arXiv:2205.12325 [cond-mat.str-el]* (2022). arXiv: `2205.12325 [cond-mat.str-el]` (cit. on pp. 4, 130).

[Hastings, 2022b]   Matthew B. Hastings and Ryan O'Donnell. "Optimizing Strongly Interacting Fermionic Hamiltonians". *arXiv:2110.10701 [quant-ph]* (2022). arXiv: `2110.10701 [quant-ph]` (cit. on pp. 4, 130).

[He, 2023]   Yifei He and Martin Kruczenski. "Bootstrapping Gauge Theories". *arXiv:2309.12402 [hep-th]* (2023). arXiv: `2309.12402 [hep-th]` (cit. on pp. 6, 131).

[He, 2017]   Yin-Chen He, Michael P. Zaletel, Masaki Oshikawa, and Frank Pollmann. "Signatures of Dirac Cones in a DMRG Study of the Kagome Heisenberg Model". *Physical Review X* 7.3, 031020 (2017), p. 031020. arXiv: `1611.06238 [cond-mat.str-el]` (cit. on p. 126).

[Hessam, 2022]   Hamed Hessam, Masoud Khalkhali, and Nathan Pagliaroli. "Bootstrapping Dirac Ensembles". *J. Phys. A* 55.33 (2022), p. 335204. arXiv: `2107.10333 [hep-th]` (cit. on pp. 4, 130).

[Hinton, 2006]   Geoffrey E. Hinton, Simon Osindero, and Yee-Whye Teh. "A Fast Learning Algorithm for Deep Belief Nets". *Neural Computation* 18.7 (2006), pp. 1527–1554 (cit. on pp. 2, 128).

[Homrich, 2019]   Alexandre Homrich, João Penedones, Jonathan Toledo, Balt C. van Rees, and Pedro Vieira. "The S-matrix Bootstrap IV: Multiple Amplitudes". *JHEP* 11 (2019), p. 076. arXiv: `1905.06905 [hep-th]` (cit. on pp. 3, 129).

[Hu, 2022]   Xihe Hu. "Different Bootstrap Matrices in Many QM Systems". *arXiv:2206.00767 [quant-ph]* (2022). arXiv: `2206.00767 [quant-ph]` (cit. on pp. 4, 130).

[Jevicki, 1984]   A. Jevicki, O. Karim, J. P. Rodrigues, and H. Levine. "Loop-Space Hamiltonians and Numerical Methods for Large-N Gauge Theories (II)". *Nucl. Phys. B* 230.3 (1984), pp. 299–316 (cit. on pp. 4, 130).

[Jevicki, 1983]   A. Jevicki, O. Karim, J.P. Rodrigues, and H. Levine. "Loop Space Hamiltonians and Numerical Methods for Large-N Gauge Theories". *Nucl. Phys. B* 213.1 (1983), pp. 169–188 (cit. on pp. 4, 130).

[Jha, 2022]   Raghav Govind Jha. "Introduction to Monte Carlo for matrix models". *SciPost Phys. Lect. Notes* 46 (2022), p. 1. arXiv: `2111.02410 [hep-th]` (cit. on pp. 5, 131).

[John, 2023]   Renjan Rajan John and Krishna Priya R. "Anharmonic oscillators and the null bootstrap" (2023). arXiv: `2309.06381 [quant-ph]` (cit. on pp. 4, 130).

[Karateev, 2019]   Denis Karateev, Petr Kravchuk, and David Simmons-Duffin. "Harmonic Analysis and Mean Field Theory". *JHEP* 10 (2019), p. 217. arXiv: `1809.05111 [hep-th]` (cit. on p. 87).

[Kaviraj, 2022]   Apratim Kaviraj. "Crossing Antisymmetric Polyakov Blocks + Dispersion Relation". *JHEP* 01 (2022), p. 005. arXiv: 2109.02658 [hep-th] (cit. on pp. 9, 135).

[Kaviraj, 2020]   Apratim Kaviraj and Miguel F. Paulos. "The Functional Bootstrap for Boundary CFT". *JHEP* 04 (2020), p. 135. arXiv: 1812.04034 [hep-th] (cit. on pp. 9, 135).

[Kazakov, 1985a]   V. A. Kazakov. "Bilocal Regularization of Models of Random Surfaces". *Phys. Lett. B* 150 (1985), pp. 282–284 (cit. on p. 10).

[Kazakov, 1987]   V. A. Kazakov. "EXACTLY SOLVABLE POTTS MODELS, BOND AND TREE LIKE PER-COLATION ON DYNAMICAL (RANDOM) PLANAR". *International Symposium on Field Theory of the Lattice.* 1987 (cit. on p. 10).

[Kazakov, 1985b]   V. A. Kazakov, Alexander A. Migdal, and I. K. Kostov. "Critical Properties of Randomly Triangulated Planar Random Surfaces". *Phys. Lett. B* 157 (1985), pp. 295–300 (cit. on p. 10).

[Kazakov, 2022]   Vladimir Kazakov and Zechuan Zheng. "Analytic and numerical bootstrap for one-matrix model and "unsolvable" two-matrix model". *JHEP* 06 (2022), p. 030. arXiv: 2108.04830 [hep-th] (cit. on pp. 4, 7, 125, 130, 133).

[Kazakov, 2023]   Vladimir Kazakov and Zechuan Zheng. "Bootstrap for lattice Yang-Mills theory". *Phys. Rev. D* 107.5 (2023), p. L051501. arXiv: 2203.11360 [hep-th] (cit. on pp. 4, 6, 125, 130, 131).

[Khan, 2022]   Sakil Khan, Yuv Agarwal, Devjyoti Tripathy, and Sachin Jain. "Bootstrapping PT Symmetric Quantum Mechanics". *Phys. Lett. B* 834 (2022), p. 137445. arXiv: 2202.05351 [quant-ph] (cit. on pp. 4, 130).

[Koch, 2022]   Robert de Mello Koch, Antal Jevicki, Xianlong Liu, Kagiso Mathaba, and João P. Rodrigues. "Large N Optimization for Multi-Matrix Systems". *JHEP* 01.1 (2022), p. 168. arXiv: 2108.08803 [hep-th] (cit. on pp. 4, 130).

[Kontsevich, 1992]   M. Kontsevich. "Intersection theory on the moduli space of curves and the matrix Airy function". *Commun. Math. Phys.* 147 (1992), pp. 1–23 (cit. on p. 10).

[Kos, 2014]   Filip Kos, David Poland, and David Simmons-Duffin. "Bootstrapping Mixed Correlators in the 3D Ising Model". *JHEP* 11 (2014), p. 109. arXiv: 1406.4858 [hep-th] (cit. on pp. 1, 2, 127, 128).

[Kravchuk, 2018a]   Petr Kravchuk. "Casimir recursion relations for general conformal blocks". *JHEP* 02 (2018), p. 011. arXiv: 1709.05347 [hep-th] (cit. on p. 87).

[Kravchuk, 2018b]   Petr Kravchuk and David Simmons-Duffin. "Counting Conformal Correlators". *JHEP* 02 (2018), p. 096. arXiv: 1612.08987 [hep-th] (cit. on p. 87).

[Kruczenski, 2022]   Martin Kruczenski, Joao Penedones, and Balt C. van Rees. "Snowmass White Paper: S-matrix Bootstrap". *arXiv:2203.02421 [hep-th]* (2022). arXiv: 2203.02421 [hep-th] (cit. on pp. 3, 129).

[Kull, 2022]   Ilya Kull, Norbert Schuch, Ben Dive, and Miguel Navascués. "Lower Bounding Ground-State Energies of Local Hamiltonians Through the Renormalization Group". *arXiv:2212.03014 [quant-ph]* (2022). arXiv: 2212.03014 [quant-ph] (cit. on pp. 4, 130).

[Li, 2022]   Wenliang Li. "Null bootstrap for non-Hermitian Hamiltonians". *Phys. Rev. D* 106.12 (2022), p. 125021. arXiv: 2202.04334 [hep-th] (cit. on pp. 4, 130).

[Li, 2023a]   Wenliang Li. "Principle of minimal singularity for Green's functions" (2023). arXiv: 2309.02201 [hep-th] (cit. on pp. 4, 130).

[Li, 2023b]   Wenliang Li. "Solving Anharmonic Oscillator with Null States: Hamiltonian Bootstrap and Dyson-Schwinger Equations". *Phys. Rev. Lett.* 131.3 (2023), p. 031603. arXiv: 2303.10978 [hep-th] (cit. on pp. 4, 130).

[Li, 2023c]   Zhijin Li. "Large N Analytical Functional Bootstrap. Part I. 1D CFTs and Total Positivity". *JHEP* 07 (2023), p. 167. arXiv: 2301.01311 [hep-th] (cit. on pp. 9, 135).

[Lin, 2020]   Henry W. Lin. "Bootstraps to strings: solving random matrix models with positivity". *JHEP* 06 (2020), p. 090. arXiv: 2002.08387 [hep-th] (cit. on pp. 3, 4, 129, 130).

[Lin, 2023]   Henry W. Lin. "Bootstrap Bounds on D0-brane Quantum Mechanics". *JHEP* 06 (2023), p. 038. arXiv: 2302.04416 [hep-th] (cit. on pp. 4, 130).

[Liu, 2023]   Aike Liu, David Simmons-Duffin, Ning Su, and Balt C. van Rees. "Skydiving to Bootstrap Islands" (2023). arXiv: 2307.13046 [hep-th] (cit. on pp. 3, 129).

[Ma, 2023]   Teng Ma, Alex Pomarol, and Francesco Sciotti. "Bootstrapping the Chiral Anomaly at Large N_c". *arXiv:2307.04729 [hep-th]* (2023). arXiv: 2307.04729 [hep-th] (cit. on pp. 6, 131).

[Makeenko, 1979]   Yu. M. Makeenko and Alexander A. Migdal. "Exact Equation for the Loop Average in Multicolor QCD". *Phys. Lett. B* 88 (1979), p. 135 (cit. on pp. 3, 6, 129, 132).

[Mathaba, 2023]   Kagiso Mathaba, Mbavhalelo Mulokwe, and João P. Rodrigues. "Large N Master Field Optimization: The Quantum Mechanics of Two Yang-Mills Coupled Matrices". *arXiv:2306.00935 [hep-th]* (2023). arXiv: 2306.00935 [hep-th] (cit. on pp. 4, 130).

[Mazac, 2017]   Dalimil Mazac. "Analytic Bounds and Emergence of AdS$_2$ Physics from the Conformal Bootstrap". *JHEP* 04 (2017), p. 146. arXiv: 1611.10060 [hep-th] (cit. on pp. 9, 135).

[Mazac, 2019a]   Dalimil Mazac and Miguel F. Paulos. "The Analytic Functional Bootstrap. Part I: 1D CFTs and 2D S-matrices". *JHEP* 02 (2019), p. 162. arXiv: 1803.10233 [hep-th] (cit. on pp. 9, 135).

[Mazac, 2019b]   Dalimil Mazac and Miguel F. Paulos. "The Analytic Functional Bootstrap. Part II. Natural Bases for the Crossing Equation". *JHEP* 02 (2019), p. 163. arXiv: 1811.10646 [hep-th] (cit. on pp. 9, 135).

[Mazáč, 2019]   Dalimil Mazáč, Leonardo Rastelli, and Xinan Zhou. "An Analytic Approach to BCFT$_d$". *JHEP* 12 (2019), p. 004. arXiv: 1812.09314 [hep-th] (cit. on pp. 9, 135).

[Mazáč, 2021]   Dalimil Mazáč, Leonardo Rastelli, and Xinan Zhou. "A Basis of Analytic Functionals for CFTs in General Dimension". *JHEP* 08 (2021), p. 140. arXiv: 1910.12855 [hep-th] (cit. on pp. 9, 135).

[Migdal, 2023a]   Alexander Migdal. "Statistical Equilibrium of Circulating Fluids". *Phys. Rept.* 1011 (2023), p. 2257. arXiv: 2209.12312 [physics.flu-dyn] (cit. on pp. 6, 132).

[Migdal, 2023b]   Alexander Migdal. "To the Theory of Decaying Turbulence". *Fractal Fract.* 7 (2023), p. 754. arXiv: 2304.13719 [physics.flu-dyn] (cit. on pp. 6, 132).

[Migdal, 1983]   Alexander A. Migdal. "Loop Equations and 1/N Expansion". *Phys. Rept.* 102 (1983), pp. 199–290 (cit. on p. 10).

[Montgomery, 1973]   Hugh L Montgomery. "The pair correlation of zeros of the zeta function". *Proc. Symp. Pure Math.* Vol. 24. 1973, pp. 181–193 (cit. on p. 10).

[Morita, 2023]   Takeshi Morita. "Universal Bounds on Quantum Mechanics through Energy Conservation and the Bootstrap Method". *PTEP* 2023.2 (2023), 023A01. arXiv: 2208.09370 [hep-th] (cit. on pp. 4, 130).

[Nakayama, 2022]   Yu Nakayama. "Bootstrapping Microcanonical Ensemble in Classical System". *Mod. Phys. Lett. A* 37.09 (2022), p. 2250054. arXiv: 2201.04316 [hep-th] (cit. on pp. 4, 130).

[Nakayama, 2015]   Yu Nakayama and Tomoki Ohtsuki. "Bootstrapping phase transitions in QCD and frustrated spin systems". *Phys. Rev. D* 91.2 (2015), p. 021901. arXiv: 1407.6195 [hep-th] (cit. on pp. 6, 131).

[Nancarrow, 2022]   Colin Oscar Nancarrow and Yuan Xin. "Bootstrapping the Gap in Quantum Spin Systems". *arXiv:2211.03819 [hep-th]* (2022). arXiv: 2211.03819 [hep-th] (cit. on pp. 4, 130).

[Pappadopulo, 2012]   Duccio Pappadopulo, Slava Rychkov, Johnny Espin, and Riccardo Rattazzi. "OPE Convergence in Conformal Field Theory". *Phys. Rev. D* 86 (2012), p. 105043. arXiv: 1208.6449 [hep-th] (cit. on pp. 3, 129).

[Paulos, 2014]   Miguel F. Paulos. "JuliBootS: a hands-on guide to the conformal bootstrap". *arXiv e-prints*, arXiv:1412.4127 (2014), arXiv:1412.4127. arXiv: 1412.4127 [hep-th] (cit. on pp. 3, 88, 129).

[Paulos, 2020a]   Miguel F. Paulos. "Analytic Functional Bootstrap for CFTs in d > 1". *JHEP* 04 (2020), p. 093. arXiv: 1910.08563 [hep-th] (cit. on pp. 9, 135).

[Paulos, 2021]   Miguel F. Paulos. "Dispersion Relations and Exact Bounds on CFT Correlators". *JHEP* 08 (2021), p. 166. arXiv: 2012.10454 [hep-th] (cit. on pp. 9, 135).

[Paulos, 2017a]   Miguel F. Paulos, Joao Penedones, Jonathan Toledo, Balt C. van Rees, and Pedro Vieira. "The S-matrix Bootstrap II: Two Dimensional Amplitudes". *JHEP* 11.CERN-TH-2016-163 (2017), p. 143. arXiv: 1607.06110 [hep-th] (cit. on pp. 3, 129).

[Paulos, 2017b]   Miguel F. Paulos, Joao Penedones, Jonathan Toledo, Balt C. van Rees, and Pedro Vieira. "The S-matrix Bootstrap. Part I: QFT in AdS". *JHEP* 11.CERN-TH-2016-162 (2017), p. 133. arXiv: 1607.06109 [hep-th] (cit. on pp. 3, 8, 129, 134).

[Paulos, 2019]   Miguel F. Paulos, Joao Penedones, Jonathan Toledo, Balt C. van Rees, and Pedro Vieira. "The S-matrix Bootstrap. Part III: Higher Dimensional Amplitudes". *JHEP* 12.CERN-TH-2017-162 (2019), p. 040. arXiv: 1708.06765 [hep-th] (cit. on pp. 3, 129).

[Paulos, 2020b]   Miguel F. Paulos and Bernardo Zan. "A Functional Approach to the Numerical Conformal Bootstrap". *JHEP* 09 (2020), p. 006. arXiv: 1904.03193 [hep-th] (cit. on pp. 9, 135).

[Paulos, 2020c]   Miguel F. Paulos and Zechuan Zheng. "Bounding scattering of charged particles in $1+1$ dimensions". *JHEP* 05 (2020), p. 145. arXiv: 1805.11429 [hep-th] (cit. on pp. 3, 129).

[Paulos, 2022]   Miguel F. Paulos and Zechuan Zheng. "Bounding 3d CFT correlators". *JHEP* 04 (2022), p. 102. arXiv: 2107.01215 [hep-th] (cit. on pp. 4, 130).

[Poland, 2019]   David Poland, Slava Rychkov, and Alessandro Vichi. "The Conformal Bootstrap: Theory, Numerical Techniques, and Applications". *Rev. Mod. Phys.* 91 (2019), p. 015002. arXiv: 1805.04405 [hep-th] (cit. on pp. 2, 8, 128, 134).

[Poland, 2022]   David Poland and David Simmons-Duffin. "Snowmass White Paper: The Numerical Conformal Bootstrap". *Snowmass 2021*. 2022. arXiv: 2203.08117 [hep-th] (cit. on pp. 2, 128).

[Polyakov, 1974]   A. M. Polyakov. "Non-Hamiltonian approach to conformal quantum field theory". *Soviet Journal of Experimental and Theoretical Physics* 39 (1974), p. 10 (cit. on pp. 2, 87, 128).

[Qiao, 2017]   Jiaxin Qiao and Slava Rychkov. "Cut-Touching Linear Functionals in the Conformal Bootstrap". *JHEP* 06 (2017), p. 076. arXiv: 1705.01357 [hep-th] (cit. on pp. 9, 135).

[Rattazzi, 2011]   Riccardo Rattazzi, Slava Rychkov, and Alessandro Vichi. "Central Charge Bounds in 4D Conformal Field Theory". *Phys. Rev. D* 83 (2011), p. 046011. arXiv: 1009.2725 [hep-th] (cit. on pp. 8, 134).

[Rattazzi, 2008]   Riccardo Rattazzi, Vyacheslav S. Rychkov, Erik Tonni, and Alessandro Vichi. "Bounding scalar operator dimensions in 4D CFT". *JHEP* 12 (2008), p. 031. arXiv: 0807.0004 [hep-th] (cit. on pp. 2, 8, 87, 128, 134).

[Reehorst, 2021]   Marten Reehorst, Slava Rychkov, David Simmons-Duffin, Benoit Sirois, Ning Su, and Balt van Rees. "Navigator Function for the Conformal Bootstrap". *SciPost Phys.* 11 (2021), p. 072. arXiv: 2104.09518 [hep-th] (cit. on pp. 3, 88, 129).

[El-Showk, 2013]   Sheer El-Showk and Miguel F. Paulos. "Bootstrapping Conformal Field Theories with the Extremal Functional Method". *Phys. Rev. Lett.* 111.24 (2013), p. 241601. arXiv: 1211.2810 [hep-th] (cit. on pp. 9, 135).

[El-Showk, 2018]   Sheer El-Showk and Miguel F. Paulos. "Extremal Bootstrapping: Go with the Flow". *JHEP* 03 (2018), p. 148. arXiv: 1605.08087 [hep-th] (cit. on pp. 9, 135).

[El-Showk, 2012]   Sheer El-Showk, Miguel F. Paulos, David Poland, Slava Rychkov, David Simmons-Duffin, and Alessandro Vichi. "Solving the 3D Ising Model with the Conformal Bootstrap". *Phys. Rev. D* 86 (2012), p. 025022. arXiv: 1203.6064 [hep-th] (cit. on pp. 2, 8, 128, 134).

[El-Showk, 2014]   Sheer El-Showk, Miguel F. Paulos, David Poland, Slava Rychkov, David Simmons-Duffin, and Alessandro Vichi. "Solving the 3d Ising Model with the Conformal Bootstrap II. c-Minimization and Precise Critical Exponents". *J. Stat. Phys.* 157 (2014), p. 869. arXiv: 1403.4545 [hep-th] (cit. on pp. 2, 88, 128).

[Simmons-Duffin, 2015]   David Simmons-Duffin. "A Semidefinite Program Solver for the Conformal Bootstrap". *JHEP* 06 (2015), p. 174. arXiv: 1502.02033 [hep-th] (cit. on pp. 3, 4, 88, 129, 130).

[Tavakoli, 2023]   Armin Tavakoli, Alejandro Pozas-Kerstjens, Peter Brown, and Mateus Araújo. "Semidefinite Programming Relaxations for Quantum Correlations". *arXiv:2307.02551 [quant-ph]* (2023). arXiv: 2307.02551 [quant-ph] (cit. on pp. 4, 130).

[Tchoumakov, 2021]   Serguei Tchoumakov and Serge Florens. "Bootstrapping Bloch Bands". *J. Phys. A* 55.1 (2021), p. 015203. arXiv: 2109.06600 [cond-mat.mes-hall] (cit. on pp. 4, 130).

[Tobasco, 2018]   Ian Tobasco, David Goluskin, and Charles R. Doering. "Optimal Bounds and Extremal Trajectories for Time Averages in Nonlinear Dynamical Systems". *Physics Letters A* 382.6 (2018), pp. 382–386. arXiv: 1705.07096 [nlin] (cit. on pp. 4, 130).

[Trinh, 2022]   Anh-Khoi Trinh. "Mixed Correlator Dispersive CFT Sum Rules". *JHEP* 03 (2022), p. 032. arXiv: 2111.14731 [hep-th] (cit. on pp. 9, 135).

[Wilson, 1974]   Kenneth G. Wilson. "Confinement of Quarks". *Phys. Rev. D* 10 (1974). Ed. by J. C. Taylor, pp. 2445–2459 (cit. on pp. 6, 12, 132).

[Yan, 2011]   Simeng Yan, David A. Huse, and Steven R. White. "Spin-Liquid Ground State of the S = 1/2 Kagome Heisenberg Antiferromagnet". *Science* 332.6034 (2011), p. 1173. arXiv: 1011.6114 [cond-mat.str-el] (cit. on p. 126).

[Zeng, 2023]   Mao Zeng. "Feynman integrals from positivity constraints". *JHEP* 09 (2023), p. 042. arXiv: 2303.15624 [hep-ph] (cit. on pp. 4, 130).

RÉSUMÉ

Dans le domaine de la physique contemporaine, la méthode bootstrap est généralement associée à une approche basée sur l'optimisation pour résoudre des problèmes. Cette méthode exploite notre compréhension d'un problème physique spécifique, utilisée comme les contraintes pour le problème d'optimisation, afin de délimiter la région autorisée de notre théorie physique. Notamment, cette méthode donne souvent non seulement des limites numériques précises pour les quantités physiques mais offre également des perspectives théoriques sur la nature du problème en question. La méth- ode numérique bootstrap moderne a connu son plus grand succès dans les domaines de la théorie des champs con- formes (via le bootstrap conforme) et de l'amplitude de dispersion (à travers le bootstrap de la matrice S). Cette thèse présente l'application de la méthode bootstrap aux modèles matriciels (matrices aléatoires), à la théorie de Yang-Mills et à la théorie des champs conformes. Nous commencerons par un examen des éléments fondamentaux de ces théories. Ensuite, nous nous plongerons dans les études bootstrap de ces modèles.

Nous proposons une méthode bootstrap de relaxation améliorée pour la résolution numérique de modèles multi-matriciels à la limite de N grand. Cette méthode fournit des inégalités rigoureuses sur les moments de trace simple des matrices jusqu'à un ordre "coupure" spécifié des moments. Nous avons une preuve rigoureuse de l'applicabilité de cette méthode dans le cas du modèle à une matrice. Nous démontrons l'efficacité numérique de notre méthode en résolvant le modèle à deux matrices analytiquement "insolvable" avec une interaction tr[A, B]2 et des potentiels quartiques. Nous étendons ensuite notre étude à la théorie de Yang-Mills sur réseau aux dimensions 2, 3 et 4 en utilisant la méthode numérique bootstrap. Notre approche combine des équations de boucle, avec une coupure sur la longueur maximale des boucles, et des conditions de positivité sur certaines matrices de moyennes de boucles de Wilson. Nos résultats suggèrent que cette approche bootstrap peut offrir une alternative tangible à l'approche de Monte Carlo, jusqu'à présent incontestée.

Nous explorons le problème de la mise en limite des corrélateurs CFT dans la section euclidienne. En reformulant la question comme un problème d'optimisation, nous construisons numériquement des fonctionnelles qui déterminent des limites supérieures et inférieures sur les corrélateurs dans plusieurs circonstances. Notre analyse révèle que le corrélateur d'Ising 3d prend les valeurs minimales possibles autorisées dans la section euclidienne. Nous découvrons également un intrigant CFT 3d qui sature les limites de l'écart, de la maximisation OPE et des valeurs des corrélateurs.

MOTS CLÉS

Méthode bootstrap, Modeles des matrices, Théorie des champs conforme

ABSTRACT

In the realm of contemporary physics, the bootstrap method is typically associated with an optimization-based approach to problem-solving. This method leverages our understanding of a specific physical problem, which is used as the constraints for the optimization problem, to carve out the allowed region of our physical theory. Notably, this method often yields not only precise numerical bounds for physical quantities but also offers theoretical insights into the nature of the problem at hand. The modern numerical bootstrap method has seen its greatest success in the fields of conformal field theory (via the conformal bootstrap) and Scattering amplitude (through the S-matrix bootstrap). This dissertation presents the application of the bootstrap method to matrix models (random matrices), Yang-Mills theory, and conformal field theory. We will commence with a review of the fundamental elements of these theories. Following this, we will delve into the bootstrap studies of these models.

We propose an enhanced relaxation bootstrap method for the numerical resolution of multi-matrix models in the large N limit. This method provides rigorous inequalities on the single trace moments of the matrices up to a specified "cutoff" order of the moments. We have rigorous proof of the applicability of this method in the case of the one-matrix model. We demonstrate the numerical efficiency of our method by solving the analytically "unsolvable" two-matrix model with tr[A, B]2 interaction and quartic potentials. We further extend our study to the lattice Yang-Mills theory at dimensions 2, 3, and 4 using the numerical bootstrap method. Our approach combines loop equations, with a cutoff on the maximal length of loops, and positivity conditions on certain matrices of Wilson loop averages. Our results suggest that this bootstrap approach can provide a tangible alternative to the, so far uncontested, Monte Carlo approach.

We explore the problem of bounding CFT correlators in the Euclidean section. By reformulating the question as an optimization problem, we construct functionals numerically which determine upper and lower bounds on correlators under several circumstances. Our analysis reveals that the 3d Ising correlator takes the minimal possible allowed values on the Euclidean section. We also uncover an intriguing 3d CFT that saturates gap, OPE maximization, and correlator value bounds.

KEYWORDS

Bootstrap Method, Matrix models, Conformal field thoery